HAWAII GEOTHERMAL PROJECT

ENGINEERING PROGRAM

PHASE I REPORT

JANUARY, 1975

Prepared Under

NATIONAL SCIENCE FOUNDATION

RESEARCH GRANT NO. GI-38319

By

Hi Chang Chai
Bill Chen
Ping Cheng
James Chou
Deane Kihara
Kah Hie Lau
L. Stephen Lau
Patrick Takahashi
Paul Yuen

Hilo College
University of Hawaii
Hilo, Hawaii 96720

College of Engineering
University of Hawaii
Honolulu, Hawaii 96822

TABLE OF CONTENTS

HAWAII GEOTHERMAL PROJECT

ENGINEERING PROGRAM

The principal objectives of the Engineering Program are 1) to solve important problems related to the extraction of energy from geothermal resources (Task 3.1), and 2) to plan and design an environmentally-acceptable geothermal power plant suitable for Hawaiian geothermal reservoirs (Task 3.6). Research during the past period has been devoted primarily to the theoretical and physical modelling of geothermal reservoirs, preparation for the engineering testing of wells to be drilled on the island of Hawaii, and studies of various methods of converting the heat energy in a geothermal reservoir to electrical energy. Results of the research effort have been reported in five quarterly progress reports and the following technical memorandums and reports:

1. "Modelling of Hawaiian Geothermal Resources," Technical Report No. 1, by P. Cheng and P. Takahashi, January 1974.

2. "Warm Water Wells on the Island of Hawaii," Technical Memorandum No. 1, by S. Shito, January 1974.

3. "Steady State Free Convection in an Unconfined Geothermal Reservoir," Technical Report No. 2, by P. Cheng and K.H. Lau, March 15, 1974. Published in *Journal of Geophysical Research*, Vol. 79, No. 29, October 10, 1974.

4. "Geothermal Reservoir Engineering: State-of-the-Art," Technical Report No. 3, by P. Takahashi, B. Chen, K. Mashima, and A. Seki, March 15, 1974. Submitted for publication in *American Society of Civil Engineers, Power Division.*

5. "Regenerative Vapor-Turbine Cycle for Geothermal Power Plant," by J.C.S. Chou. Published in *Geothermal Energy*, Vol. 2, No. 6, June 1974.

6. "Regenerative Vapor Cycle with Isobutane as Working Fluid," Technical Report No. 4, by J.C.S. Chou, R. Ahluwalia, and E. Woo, June 10, 1974. Published in *Geothermics*, Vol. 3, No. 3, September 1974.

7. "Geothermal Reservoir and Well Test Analysis: A Literature Survey," Technical Memorandum No. 2, by B. Chen, September 1974.

8. "A Parametric Study of a Vertical Heat Exchanger Designed for Geothermal Power Plant Application," Technical Report No. 5, by G. Shimozono, H.C. Chai, and D. Kihara, September 1974.

9. "Characteristics of Vapor Flashing Geothermal Plants," Technical Report No. 6, by R. Ahluwalia and J.C.S. Chou, November 15, 1974.

10. "The Effect of Dike Intrusion on Free Convection in Geothermal Reservoirs," Technical Report No. 7, by K.H. Lau and P. Cheng, December 1, 1974. Accepted for publication in *International Journal of Heat and Mass Transfer*.

Summaries of the research results follow.

TASK 3.1 GEOTHERMAL RESERVOIR ENGINEERING

INTRODUCTION

The geothermal reservoir engineering research effort, as shown in Fig. 3.1-0, has three subtask groups: computer modelling, physical modelling, and geothermal well testing/analysis. All three subtasks have the ultimate goal of predicting the performance of producing geothermal fields. The computer modelling group will use a mathematical model approach, the physical modelling group will scale model a geothermal system, and the testing/analysis group will evaluate existing geothermal and petroleum/gas hardware and software techniques with the aim of synthesizing optimal measurement and prediction alternatives.

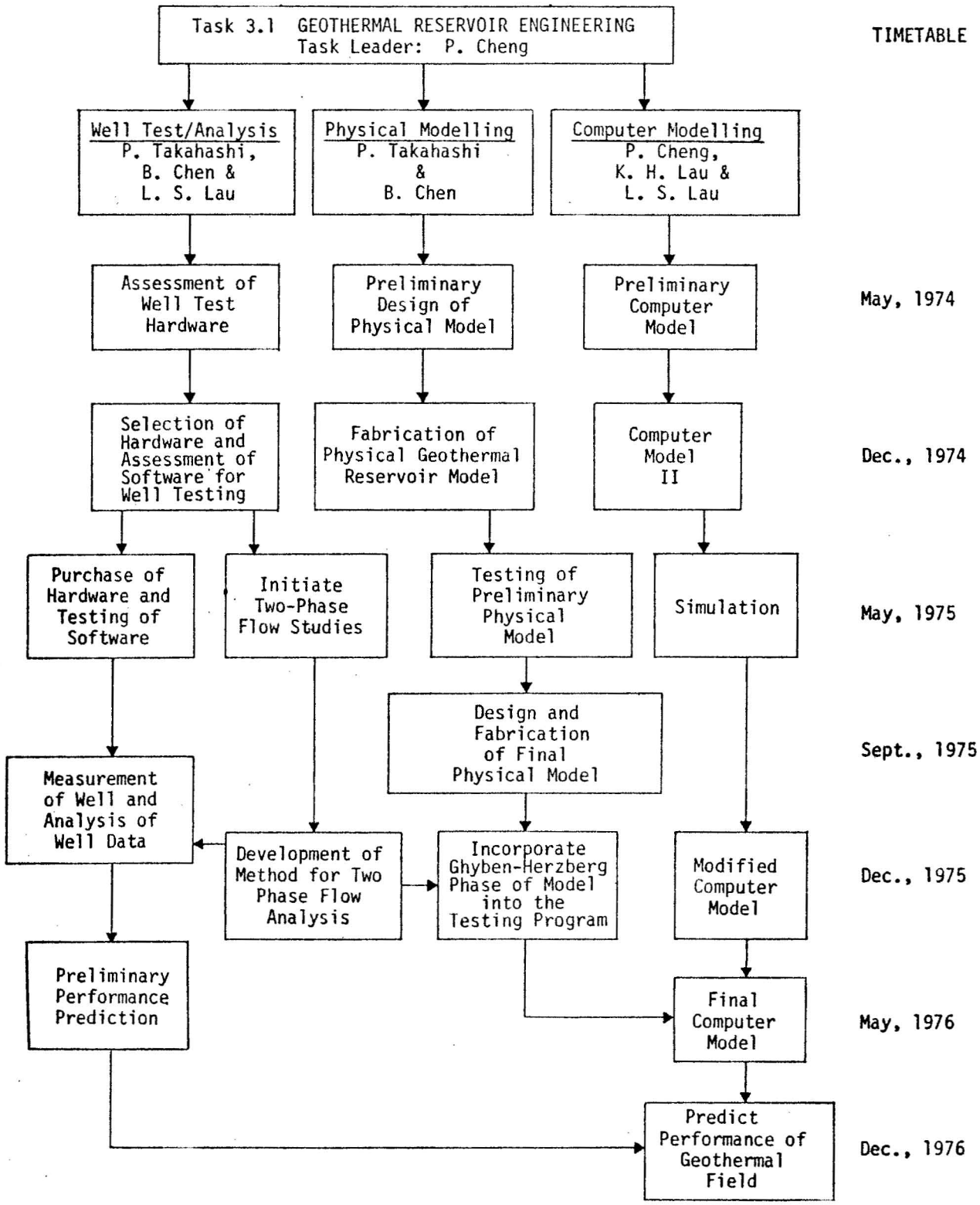

FIG. 3.1-0 ORGANIZATIONAL PLAN FOR THE TASK ON GEOTHERMAL RESERVOIR ENGINEERING

I. Numerical Modelling of Geothermal Reservoirs

Investigators: P. Cheng, K. H. Lau, & L. S. Lau

The primary objectives of the numerical modelling are to predict the performance of geothermal wells under different conditions and to study the environmental impact of the geothermal system, especially the stability of the Ghyben-Herzberg lens when perturbed by the extraction of a fluid from a well below the lens. The results of these studies will aid in the selection of a viable well-site. Specific topics to be investigated are:

1. temperature distribution, heat transfer and fluid flow characteristics of geothermal systems on the island of Hawaii,
2. capacity of a geothermal well,
3. expected life span of a geothermal well under different operating and resource conditions,
4. minimum depth required for a geothermal well so that fresh water will not cone downwards to the well bottom as water is pumped out, and
5. effect of fluid recharge on the performance of a geothermal well.

A realistic simulation of Hawaii geothermal reservoirs must take into consideration the anisotropic property of rock formation; the irregular geometry of boundaries; the dynamics of the Ghyben-Herzberg lens; and the effects of pumping, reinjection, and freshwater recharging. Mathematically, the problem is very complicated since it involves the solution of a set of highly non-linear partial differential equations with non-linear boundary conditions at the water table where its position is unknown. The strategy adopted by the numerical simulation group has been to study simplified situations during the initial phase of the work. These simplified models, which consider different effects one at a time, will aid in a qualitative understanding of the physical processes involved. Furthermore, since the numerical solutions for a more realistic model will probably involve iteration, the results of the simplified models can be used as input data for the first iteration to guarantee convergence of the iteration process. After maturity and expertise have been developed, more realistic models will be considered. The research work will then culminate in the development of a general computer code capable of predicting the performance of a specific geothermal reservoir. During Phase I we have completed the investigation of three important problems and these are discussed next.

1. Steady Free Convection in an Unconfined Rectangular Geothermal Reservoir

A parametric study has been completed which investigates the effects of geothermal heating from below on the movement of seawater, the upwelling of water table, and the pressure and temperature distribution in a rectangular two-dimensional geothermal reservoir. This work is published in the *Journal of Geophysical Research* [1]. The following is a brief discussion on the formulation and the numerical results of the problem.

The Hawaii geothermal reservoir (Fig. 3.1-1A) is idealized as a two-dimensional porous medium bounded on the bottom by a horizontal impermeable wall and on the vertical sides by the ocean (Fig. 3.1-1B). The shape of the water table is not known a priori and must be determined from the solution. To simplify the mathematical formulation of the problem, the following assumptions are made:

A. The flow field is steady and two-dimensional.

B. The temperature of the fluid is everywhere below boiling for the pressure at that depth.

C. The Boussinesq approximation is employed; i.e., density is assumed to be constant except in the buoyancy force term.

D. There is no accretion at the water table; namely, no rainfall.

E. Fluid properties such as thermal conductivity, specific heat, kinematic viscosity, and permeability are assumed to be constant.

F. Ocean is at rest; i.e., the effects of tides are neglected.

With these approximations, the governing equations in terms of dimensionless variables are

$$\frac{\partial^2 P}{\partial X^2} + \frac{\partial^2 P}{\partial Y^2} = \varepsilon \frac{\partial \theta}{\partial Y} , \tag{1}$$

and

$$\frac{\partial^2 \Theta}{\partial X^2} + \frac{\partial^2 \Theta}{\partial Y^2} + D \left[\frac{\partial P}{\partial X} \frac{\partial \Theta}{\partial X} + \frac{\partial P}{\partial Y} \frac{\partial \Theta}{\partial Y} + [1 - \varepsilon\Theta] \frac{\partial \Theta}{\partial Y} \right] = 0 , \tag{2}$$

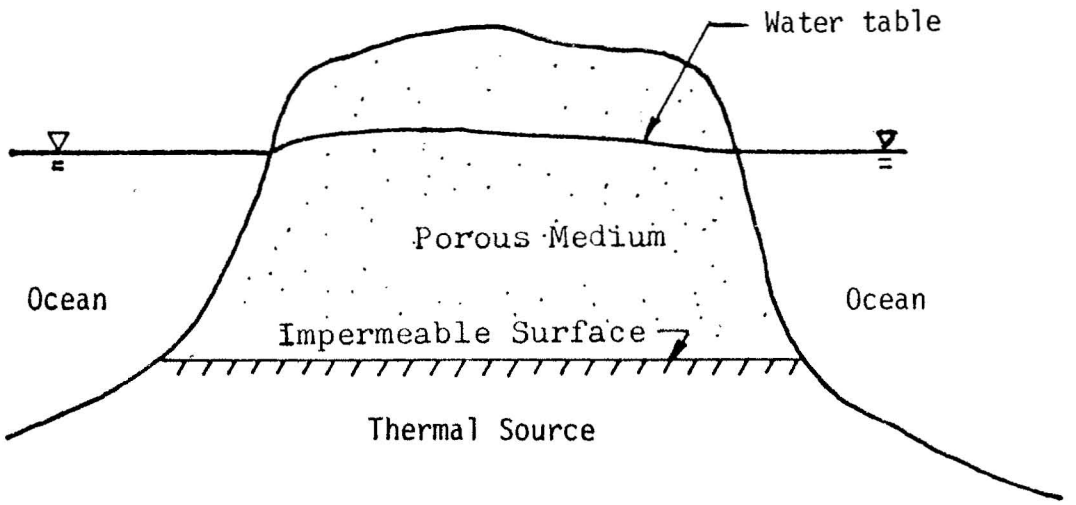

FIG. 3.1-1A UNCONFINED AQUIFER WITH THERMAL SOURCE

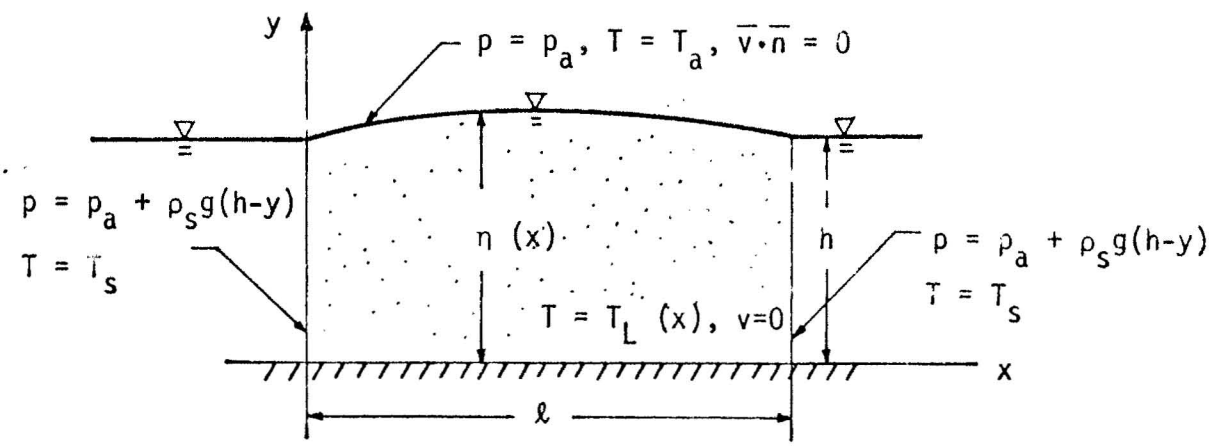

FIG. 3.1-1B RECTANGULAR MODEL OF AQUIFER

where

$$P \equiv \frac{p - p_a}{\rho_s g h}, \quad \Theta \equiv \frac{T - T_s}{T_c - T_s}, \quad \bar{\eta} \equiv \frac{\eta}{h}, \quad X \equiv \frac{x}{h}, \tag{3}$$

$$Y \equiv \frac{y}{h}, \quad L \equiv \frac{\ell}{h}, \quad \varepsilon \equiv \beta(T_c - T_s), \text{ and } D \equiv \frac{\rho_s K g h}{\alpha \mu}$$

with p, T, ρ, and μ denoting the pressure, temperature, density, viscosity; α and K denoting the thermal diffusivity and permeability of the medium; g and η denoting the gravitational acceleration and the height of the water table; T_c denoting the maximum temperature of the impermeable surface, and the subscript "s" denoting the condition in the ocean; ε and D are dimensionless parameters.

The boundary conditions along the ocean are given by

$$P(0, Y) = 1 - Y, \tag{4a}$$

$$P(L, Y) = 1 - Y, \tag{4b}$$

$$\Theta(L, Y) = 0, \tag{5a}$$

$$\Theta(0, Y) = 0. \tag{5b}$$

Along the impermeable surface, the boundary conditions are

$$\frac{\partial P}{\partial Y}(X, 0) = -1 + \varepsilon \Theta_L(X), \tag{6a}$$

$$\Theta(X, 0) = \Theta_L(X), \tag{6b}$$

$$\text{where} \quad \Theta_L(X) \equiv \frac{T_L(X) - T_s}{T_c - T_s} \quad \text{with } T_L(X) \text{ prescribed.} \tag{6c}$$

Along the free surface, the boundary conditions are

$$\frac{\partial \bar{\eta}}{\partial X}\frac{\partial P}{\partial X}(X, \bar{\eta}) - \left[\frac{\partial P}{\partial Y}(X, \bar{\eta}) + 1 - \varepsilon \Theta_a\right] = 0, \tag{7a}$$

$$P(X, \bar{\eta}) = 0, \tag{7b}$$

$$\Theta(X, \bar{\eta}) = \Theta_a, \tag{7c}$$

where $\Theta_a \equiv \frac{T_a - T_s}{T_c - T_s}$ with T_a denoting the atmospheric temperature, and $Y = \bar{\eta}(X)$ is the shape of the water table, which is not known a priori, and must be determined from the solution. Since the value of ε in Eqs. (1-7) is small, the mathematical problem can be simplified based on perturbation method. For this purpose, we now assume that dependent variables be expanded in a power series of ε. Thus we have

$$P(X, Y) = \sum_{m=0}^{\infty} \varepsilon^m P_m(X, Y), \tag{8a}$$

$$\Theta(X, Y) = \sum_{m=0}^{\infty} \varepsilon^m \Theta_m(X, Y), \tag{8b}$$

$$\bar{\eta}(X) = 1 + \sum_{m=0}^{\infty} \varepsilon^m \eta_m(X), \tag{8c}$$

where $P_m(X, Y)$, $\Theta_m(X, Y)$ and $\eta_m(X)$ are perturbation functions to be determined. Substituting Eqs. (8) into Eqs. (1-7), making a Taylor's series expansion on boundary conditions (7), and collecting terms of like power in ε, we have a set of linear subproblems.

The governing equations for the zero-order and the first-order problems are respectively the Laplace equation and Poisson equation with nonhomogeneous boundary conditions. In principle they can be solved in closed form by the classical method of separation of variables. However, the numerical evaluation of the resultant expressions in terms of many double and triple Fourier series will be of dubious value because of its slow convergent rate. For this reason we resort to the numerical solution of these linear problems by the finite difference method.

The parameters for the present problem are L the aspect ratio, D the discharge number, and ε the perturbation parameter. Grid values of pressure, temperature, and stream function are computed for L=4, ε=0.1 with D=50, and 500 for the following three temperature distributions of the impermeable surface:

(1) $\Theta_L = \exp\left[-\left(\frac{X - 2.0}{0.5}\right)^2\right]$,

with a maximum temperature at X=2.0,

(2) $\Theta_L = \exp\left[-\left(\frac{X - 0.5}{0.5}\right)^2\right]$,

with a maximum temperature at X=0.5,

(3) $\Theta_L = \exp\left[-\left(\frac{X - 0.5}{0.1}\right)^2\right]$,

with a maximum temperature at X=0.5.

Comparison of the numerical results for Cases 1 and 2 will show the effect of the location of heat source whereas the comparison of results for Case 2 (a broad heat source) and Case 3 (a narrow heat source) will show the effect of the size of the heat source.

Fig. 3.1-2 shows the contour of the first-order perturbation of stream function, ψ_1, for Case 1. As is shown in the figure, the fluid particles begin to rise as they approach the point of maximum surface temperature. This is because the density of the fluid becomes smaller as its temperature rises. As the fluid particles rise to a colder region they begin to lose heat and will begin their descending paths when the density becomes the same as that of the surrounding fluid. Fig. 3.1-3 shows the pressure contours for Case 1 with $\varepsilon = 0.1$ and for all values of D. The fact that the pressure contours are almost horizontal indicates that the pressure in an unconfined geothermal reservoir can be approximated by hydrostatic pressure. The effect of discharge number on temperature contours for Case 1 is shown in Fig. 3.1-4. D = 50 corresponds to the case where heat transfer by conduction is predominant whereas D = 500 corresponds to the case where convection heat transfer cannot be neglected. The effect of discharge number on vertical temperature profiles is shown in Fig. 3.1-5. For locations directly above the point of maximum surface temperature (i.e., at X = 2), temperature is higher for higher value of D. Similar behavior exists

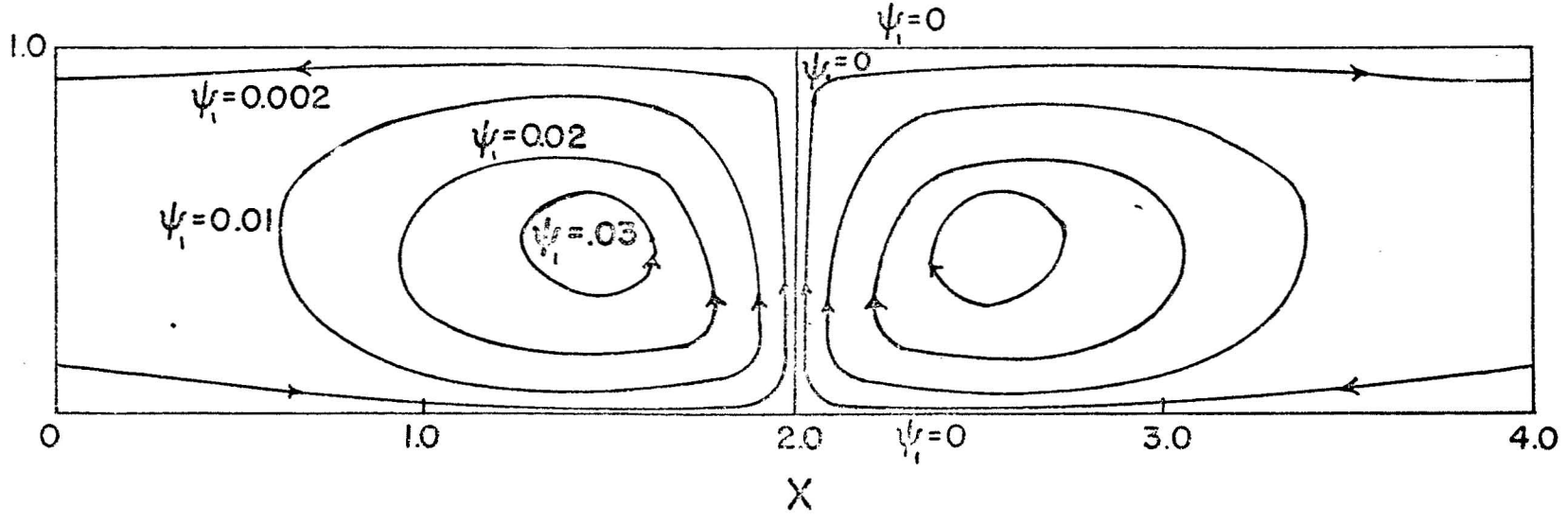

FIG. 3.1-2 CONTOURS OF FIRST-ORDER PERTURBATION FOR STREAM FUNCTION

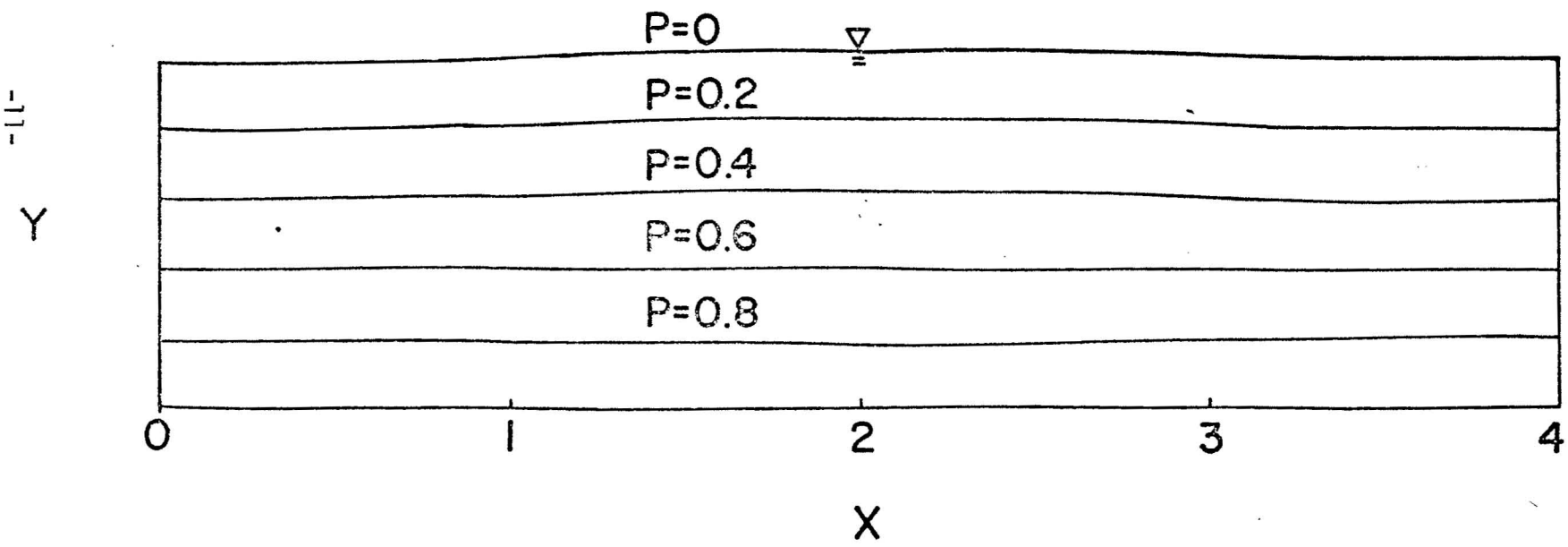

FIG. 3.1-3 PRESSURE CONTOURS FOR CASE 1

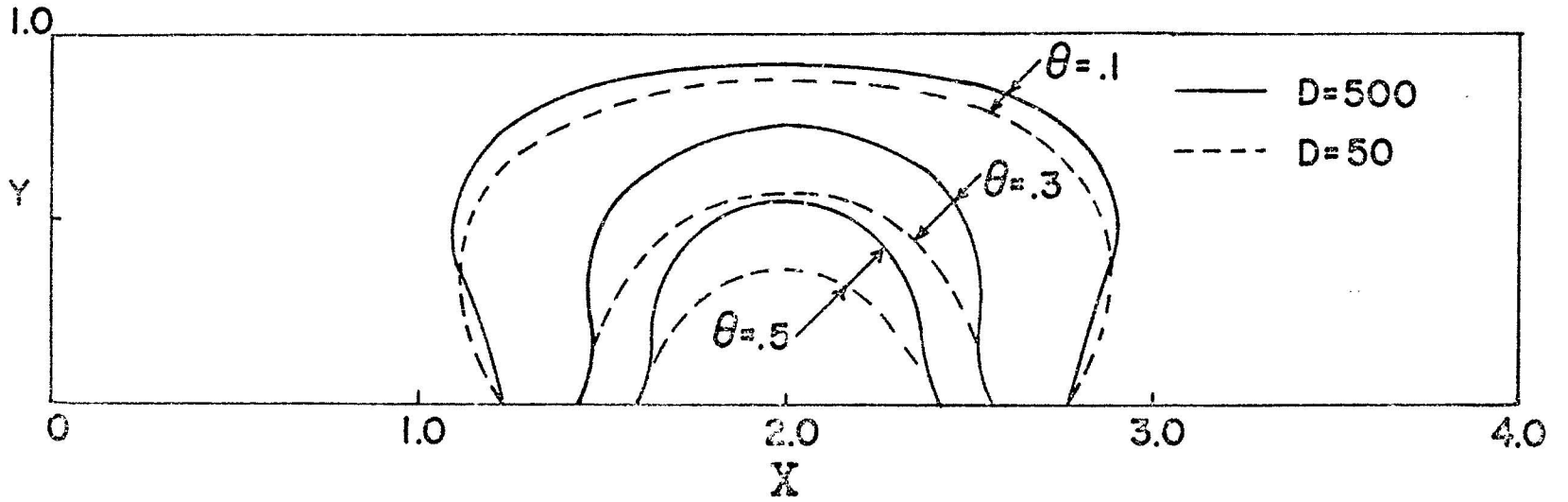

FIG. 3.1-4 EFFECT OF DISCHARGE NUMBER ON TEMPERATURE CONTOURS FOR CASE 1

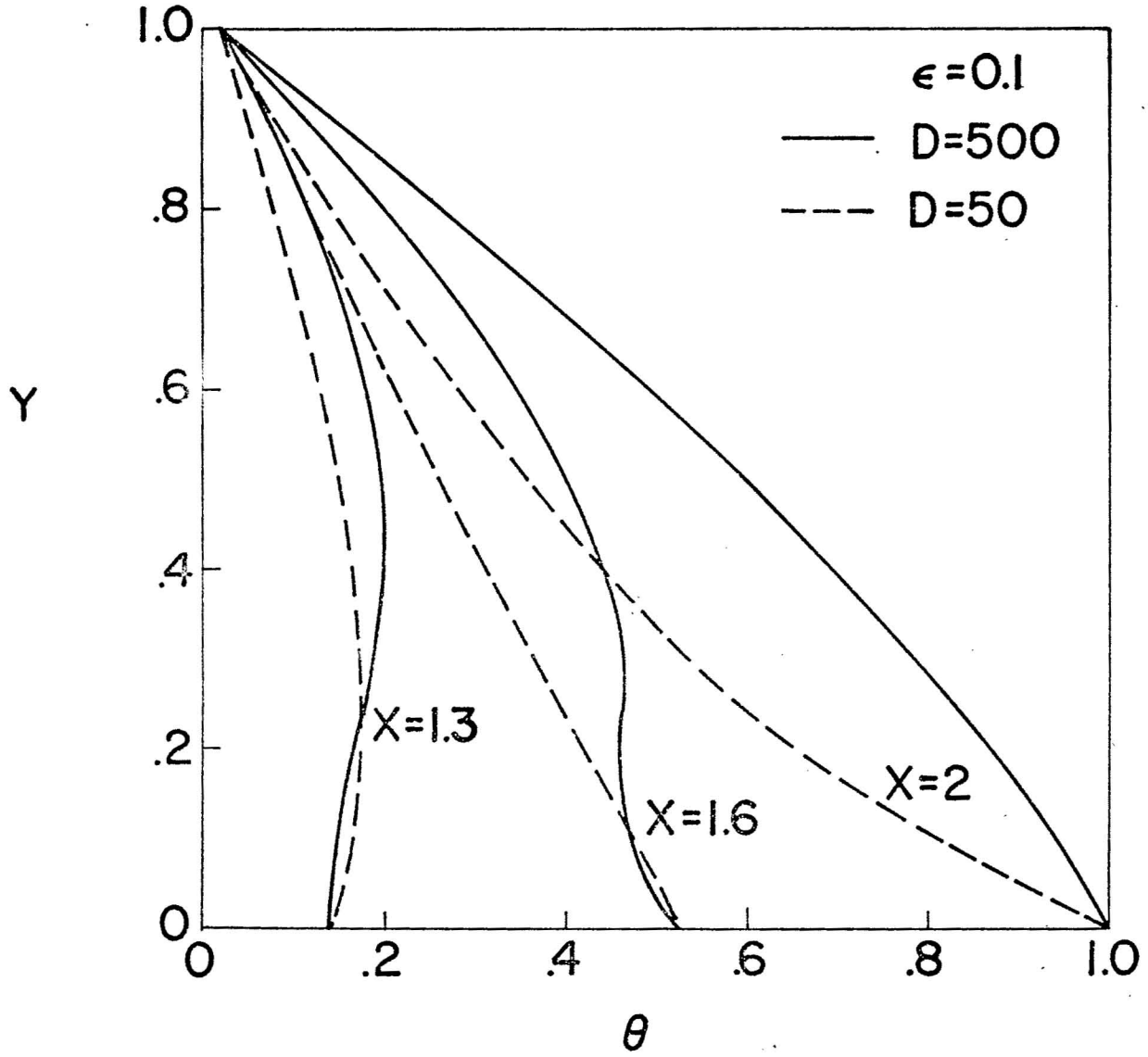

FIG. 3.1-5 EFFECT OF DISCHARGE NUMBER ON VERTICAL TEMPERATURE PROFILES FOR CASE 1

in the upper portion of the aquifer. However, in the lower portion of the aquifer, temperature decreases as the value of D is increased. This is due to the inflow of colder seawater in the lower portion of the aquifer and the outflow of warmer seawater in the upper portion of the aquifer.

Figs. 3.1-6A and 3.1-6B show the effect of location and the size of heat source on η_1, the first-order perturbation function for the shape of water table. To the first-order approximation the upwelling of water table is given by $\varepsilon\eta_1$, and is independent of D. The amount of upwelling depends on the vertical temperature gradient of the porous medium and the temperature distribution of the impermeable surface. The size and the location of the heat source have a strong influence on the amount of upwelling of water table. The maximum value of η_1 is approximately 0.08 at X = 2 for Case 1 (Fig. 3.1-6A). For a heat source near the ocean (Fig. 3.1-6B), it is interesting to note that the location of maximum water table height is not necessarily located directly above the point of maximum temperature of the impermeable surface. In fact, the position of maximum value of η_1 moves inland as the size of the heat source is increased.

It is estimated that the value of D for Hawaii geothermal reservoirs will probably be much higher than D = 500. Consequently, the numerical results do not really correspond to a realistic situation. However, since temperature distribution increases as D increases, the numerical results do give a qualitative, and yet conservative estimation. Thus, it can be concluded that (1) for a geothermal reservoir 1 mile deep with a heat source at 800°F and half mile in diameter, hot brine at 400°F can be found at half a mile below sea level if the drilling site is at the top of the heat source, (2) while the size of the heat source has an important effect on the temperature distribution in the reservoir, the location of the heat source has a small effect on the temperature distribution, (3) as a result of geothermal heating, cold seawater moves inland from the lower portion of the reservoir and warm water flows into the ocean from the upper portion of the reservoir, (4) heat transfer by convection is important in geothermal reservoirs. Thus the prediction of temperature distribution based on heat conduction

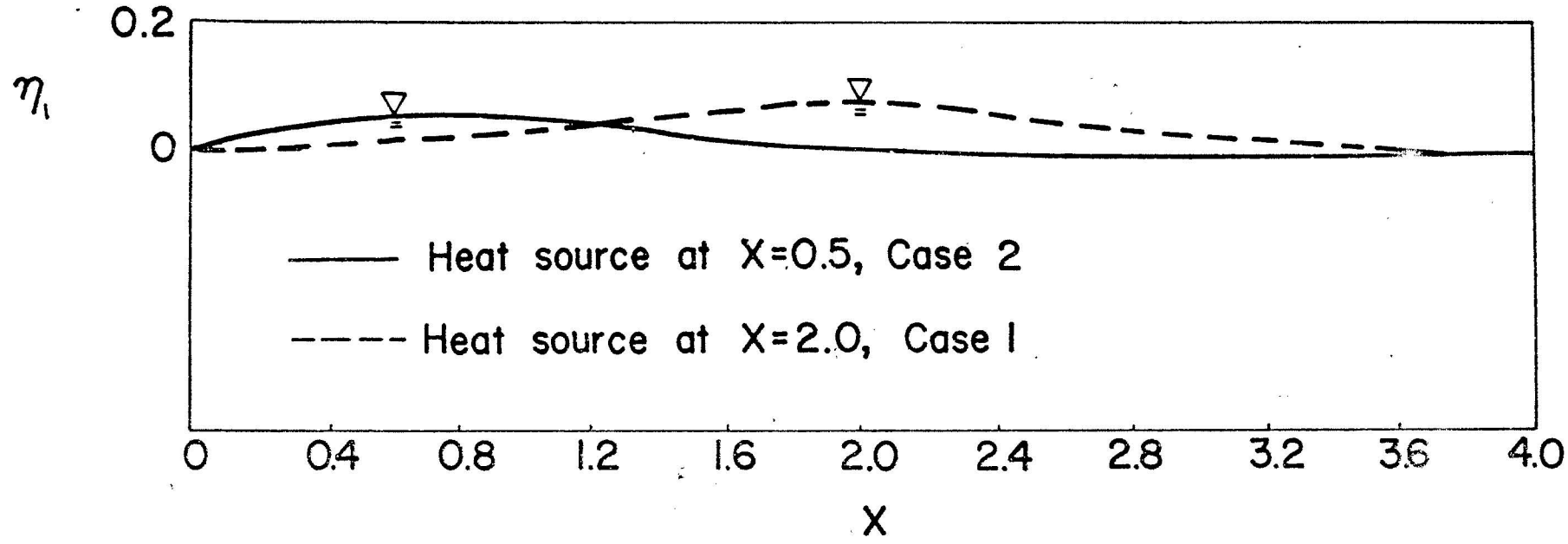

FIG. 3.1-6A EFFECT OF THE LOCATION OF HEAT SOURCE ON THE FIRST-ORDER PERTURBATION FUNCTION FOR THE UPWELLING OF WATER TABLE

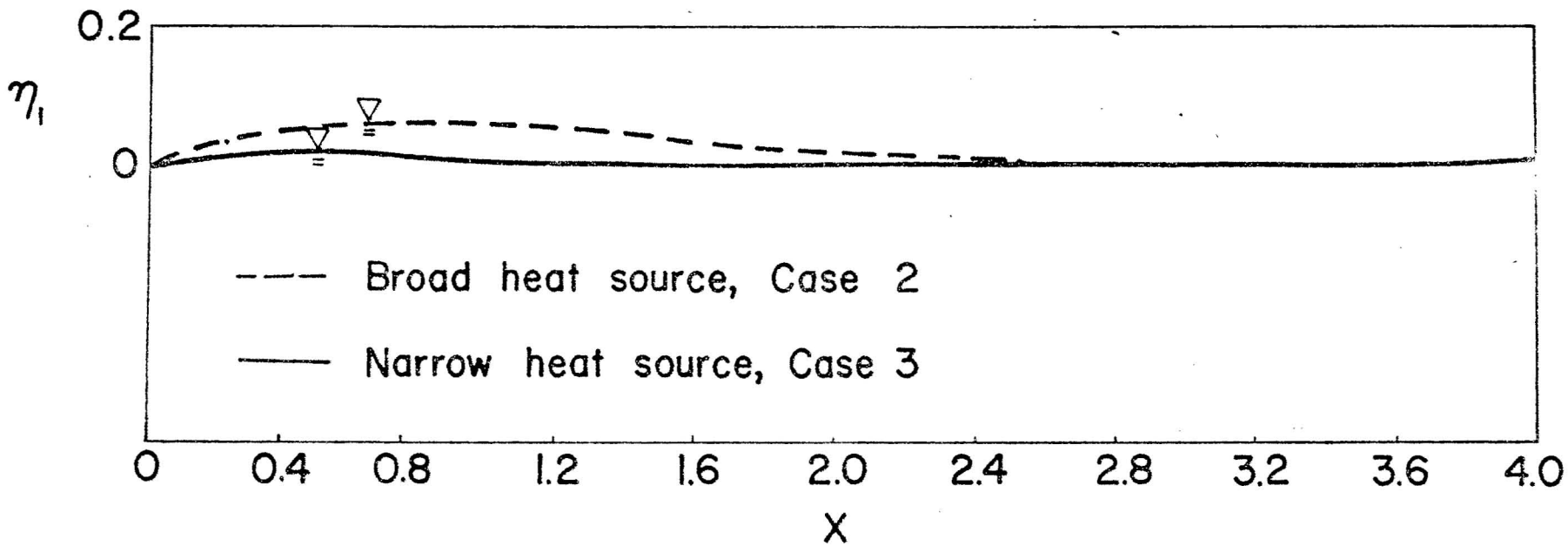

FIG. 3.1-6B EFFECT OF THE SIZE OF THE HEAT SOURCE ON THE FIRST-ORDER PERTURBATION FUNCTION FOR THE UPWELLING OF WATER TABLE

will be in serious error, (5) the convection of heat is more efficient vertically than horizontally. This implies that the drilling site must be within the maximum temperature zone of the hot rock, (6) pressure in unconfined geothermal reservoirs can be estimated based on hydrostatic pressure, and (7) the upwelling of the water table is in the order of 100 feet for a reservoir one mile in depth. The upwelling of water table as a result of geothermal heating is predicted analytically for the first time.

The perturbation method is used in the present analysis. The major advantages of the application of the method to the present problem are (1) the problem becomes linear and the difficulty in the non-convergence of iteration associated with the numerical solution of non-linear finite difference equations does not exist, (2) the unknown position of the water table is explicitly determined from the first-order problem, thus the usual practice of the iteration of position of water table is avoided, and (3) a clearer physical picture emerged with regard to the driving forces and the role played by various parameters in heat transfer and fluid flow characteristics in a geothermal reservoir.

2. The Effects of Vertical Heat Sources on the Upwelling of Water Table

The perturbation approach discussed earlier was extended to investigate the effect of vertical heat sources on the upwelling of water table. The purpose of the analysis is to assess in a qualitative manner whether the upwelling of water table of 2000 feet above sea level reported by Keller [private communication] is due to vertical heat sources.

Suppose a dike exists in the reservoir as shown in Fig. 3.1-7A with the idealized situation shown in Fig. 3.1-7B. The governing equations are given by Eqs. (1-2). In addition to boundary conditions given by Eqs. (4-7), the boundary conditions on the dike are

$$\theta(X_1, Y) = \theta_d, \qquad Y \leq Y_1 \tag{9a}$$

$$\theta(X_2, Y) = \theta_d, \qquad Y \leq Y_1 \tag{9b}$$

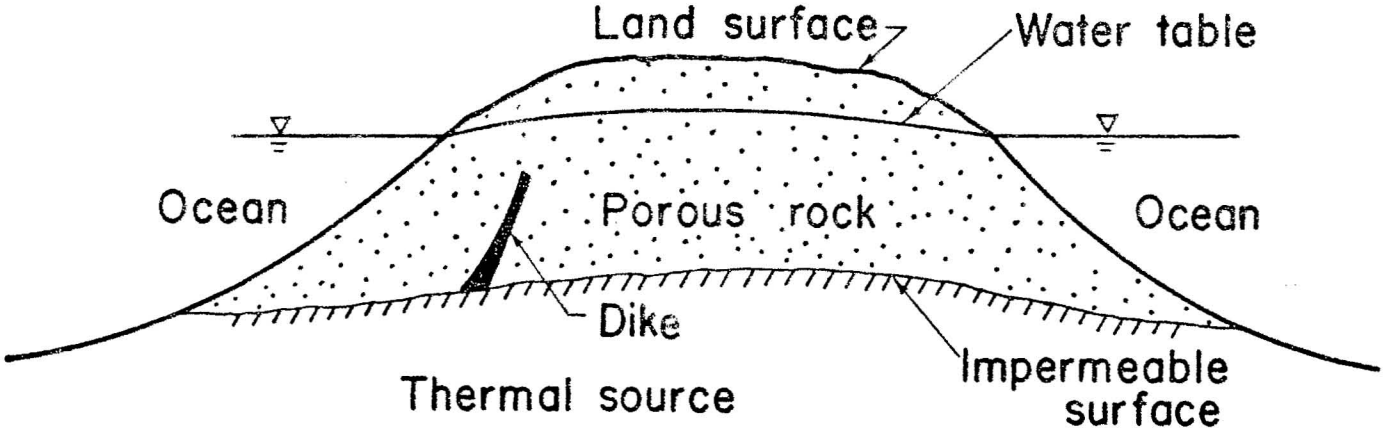

FIG. 3.1-7A AN UNCONFINED AQUIFER IN A VOLCANIC ISLAND WITH DIKE INTRUSION

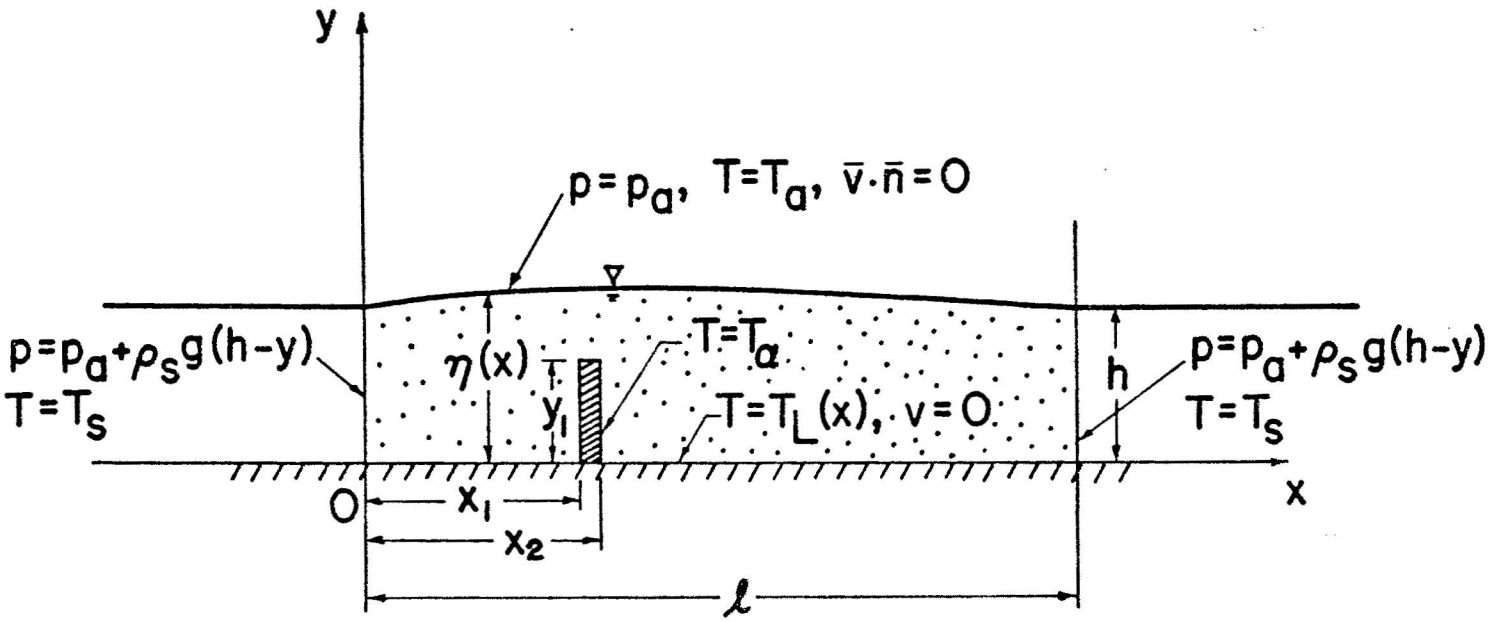

FIG. 3.1-7B IDEALIZED MODEL OF A GEOTHERMAL RESERVOIR WITH DIKE INTRUSION

$$\frac{\partial P}{\partial X}(X_1, Y) = 0, \qquad Y \leq Y_1 \tag{9c}$$

$$\frac{\partial P}{\partial X}(X, Y_1) = -1 + \varepsilon v_d, \qquad X_1 \leq X \leq X_2 \tag{9d}$$

$$\theta(X, Y_1) = \theta_d, \qquad X_1 \leq X \leq X_2 \tag{9e}$$

where θ_d is the prescribed dimensionless temperature of the dike. As a result of the perturbation technique described earlier, a set of linear equations is obtained. The resultant equations can then be solved numerically based on the finite difference method. Computations were carried out up to the second-order approximation for D = 500 (upper bound for which the perturbation method is valid) with L = 4, ε = 0.1, and θ_a = 0.02 for the following five cases with different prescribed temperatures of θ_d and θ_L.

Case A. One vertical heat source. For the problem of geothermal heating due to a hot dike 0.5 unit in height and 2 units in width located at the center of the aquifer with a cold impermeable surface at the bottom, the prescribed temperatures are

$$\theta_d = 1 \quad , \qquad 1.9 \leq X \leq 2.1 \text{ and } 0 \leq Y \leq 0.5$$

$$\theta_L(X) = 0 \quad , \qquad 0 \leq X \leq 1.9 \text{ and } 2.1 \leq X \leq 4.$$

Case B. One horizontal heat source. For comparison, computations were also carried out for a geothermal reservoir without a dike, but with geothermal heating from the bottom impermeable surface having the following prescribed temperature

$$\theta_L(X) = \exp\left[-\left(\frac{X-2}{0.5}\right)^2\right].$$

Case C. Combined vertical and horizontal heat sources. Heating in this case is due to the combination of a vertical dike located at the center of the reservoir as in Case A, and the hot impermeable surface as in Case B. The prescribed temperatures for the heat sources are

$$\theta_d = 1 \quad , \qquad 1.9 \leq X \leq 2.1 \text{ and } 0 \leq Y \leq 0.5$$

$$\theta_L(X) = \exp\left[-\left(\frac{X-2}{0.5}\right)^2\right] , \qquad 0 \leq X \leq 1.9 \text{ and } 2.1 \leq X \leq 4.0$$

Case D. Two vertical heat sources. Computations were also carried out for two hot dikes at the same temperature with a cold impermeable bottom surface. The two dikes are of the same thickness (2 units in width) but with different heights where the left dike (at $1.4 \leq X \leq 1.5$) is 0.6 unit in height while the right dike (at $2.5 \leq X \leq 2.6$) is 0.3 unit in height. The prescribed temperatures are

$$\theta_d = 1 \text{ , for } \quad 1.4 \leq X \leq 1.5 \text{ and } 0 \leq Y \leq 0.6$$

$$\theta_d = 1 \text{ , for } \quad 2.5 \leq X \leq 2.6 \text{ and } 0 \leq Y \leq 0.3$$

with $\theta_L = 0$ elsewhere on the bottom impermeable surface.

Case E. Two horizontal heat sources. Computations for this case were carried out so that results can be compared with Case D. There are no dikes existing in Case E and the heating is due to the hot bottom impermeable surface with two relatively maximum temperatures located at X = 1.45 and X = 2.55 corresponding to the locations of the dikes in Case D. The prescribed temperatures are

$$\theta_L = \exp\left[-\left(\frac{X-1.45}{0.5}\right)^2\right] , \qquad X \leq 2.0$$

$$\theta_L = \exp\left[-\left(\frac{X-2.55}{0.5}\right)^2\right] , \qquad X > 2.0 .$$

Results of Cases A, B, and C are plotted in Figs. 3.1-8 to 3.1-12. Both the flow pattern and temperature contours are symmetric with respect to X = 2. For clarity, however, only $\psi = 0.001$ and $\psi = 0.0004$ are plotted in either side of the aquifer as shown in Fig. 3.1-8. The streamlines for the three cases exhibit similar behavior with cold water moving inland in the lower portion of the island aquifer and warm water discharging into the ocean in the

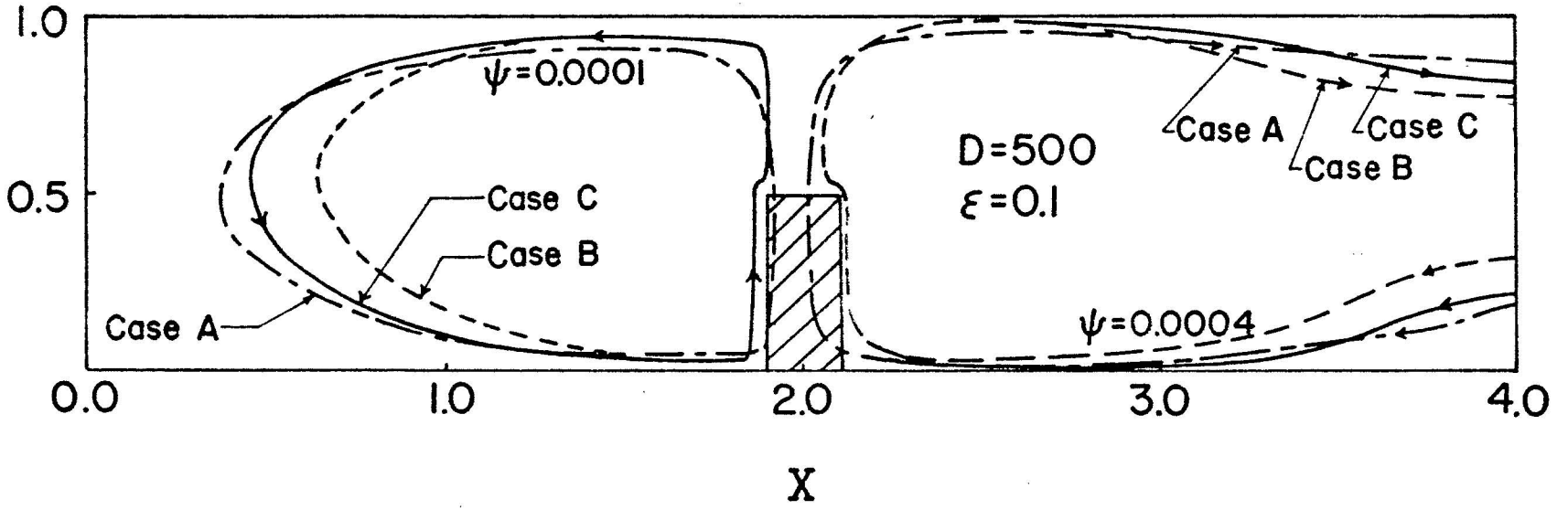

FIG. 3.1-8 EFFECTS OF VERTICAL AND HORIZONTAL HEATING ON STREAMLINES IN UNCONFINED GEOTHERMAL RESERVOIRS

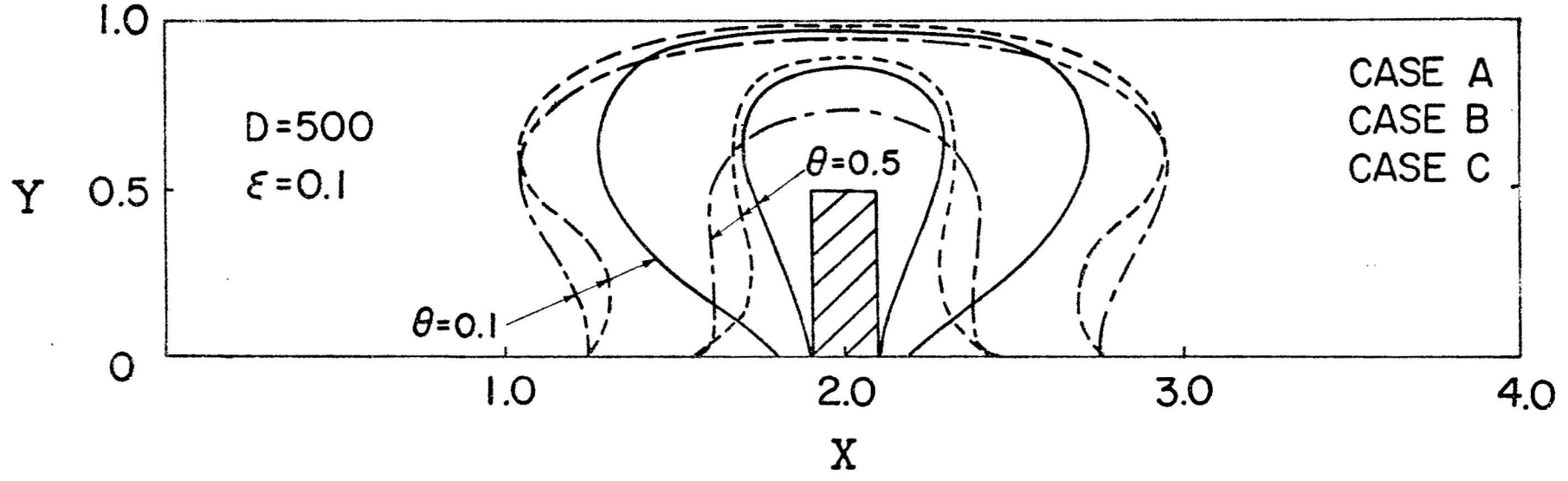

FIG. 3.1-9 EFFECTS OF VERTICAL AND HORIZONTAL HEATING ON TEMPERATURE CONTOURS IN UNCONFINED GEOTHERMAL RESERVOIRS

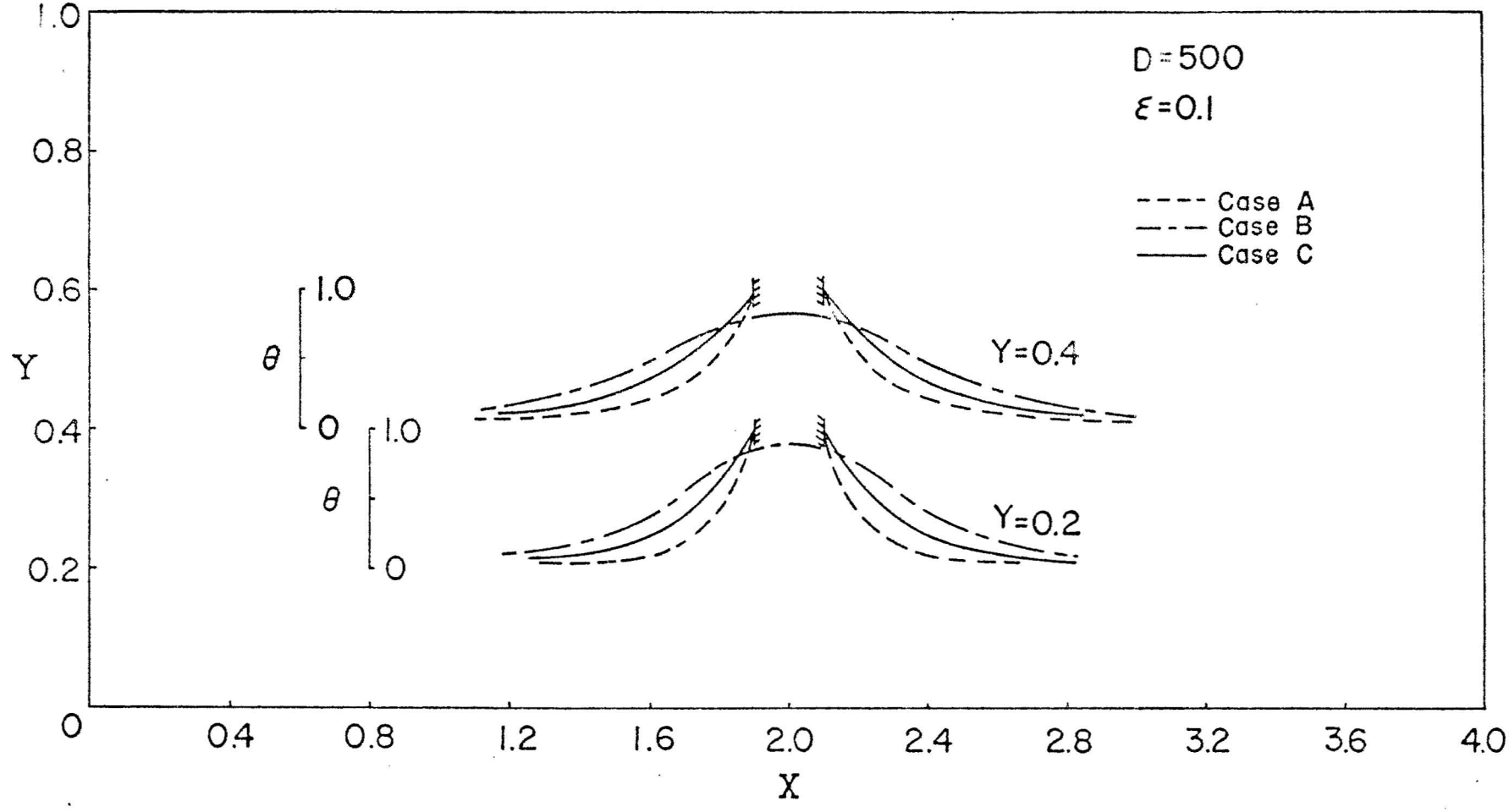

FIG. 3.1-10 HORIZONTAL TEMPERATURE DISTRIBUTION FOR CASES A, B, and C

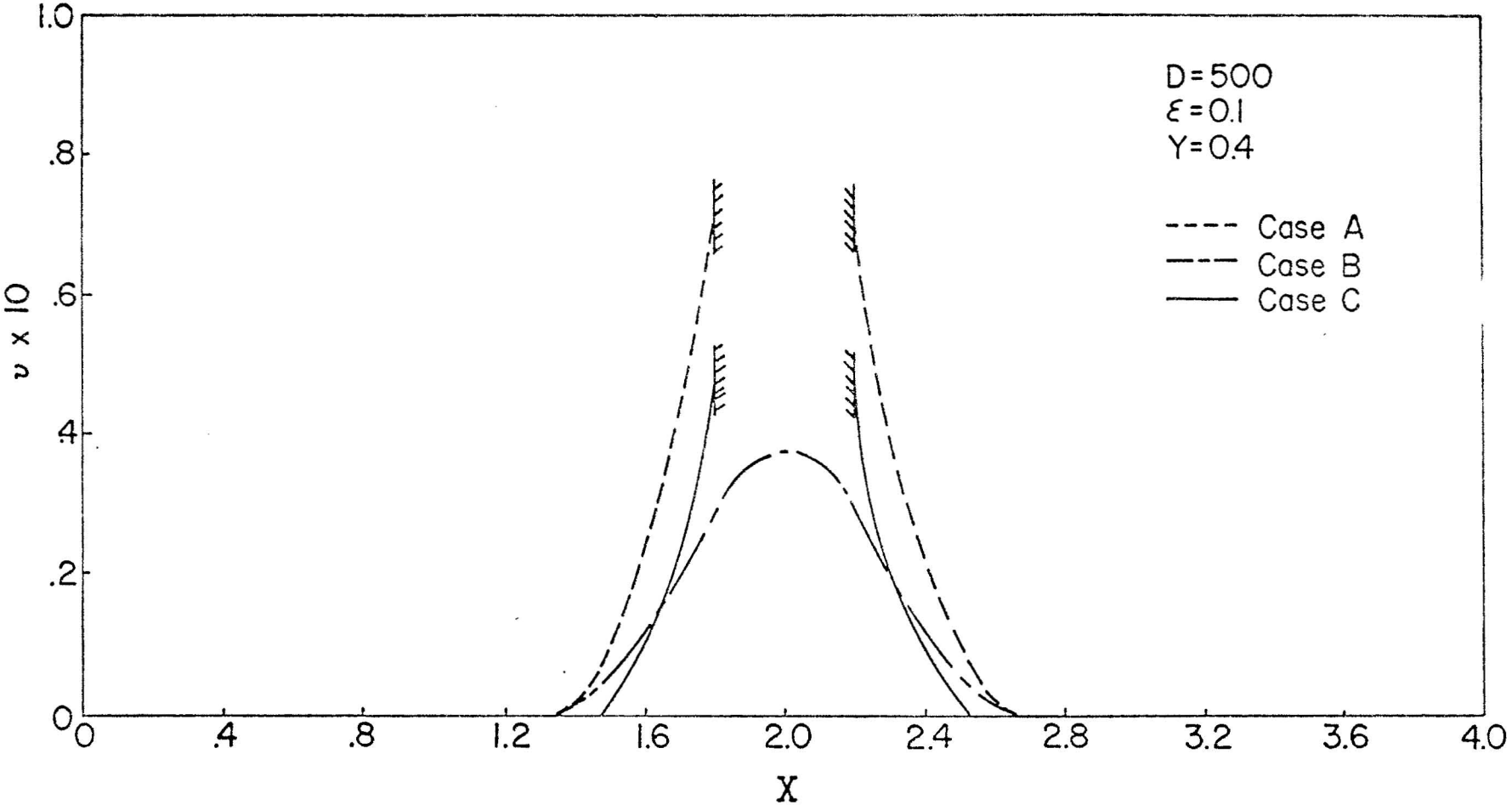

FIG. 3.1-11 VERTICAL VELOCITY PROFILES AT Y = 0.4 for CASES A, B, and C

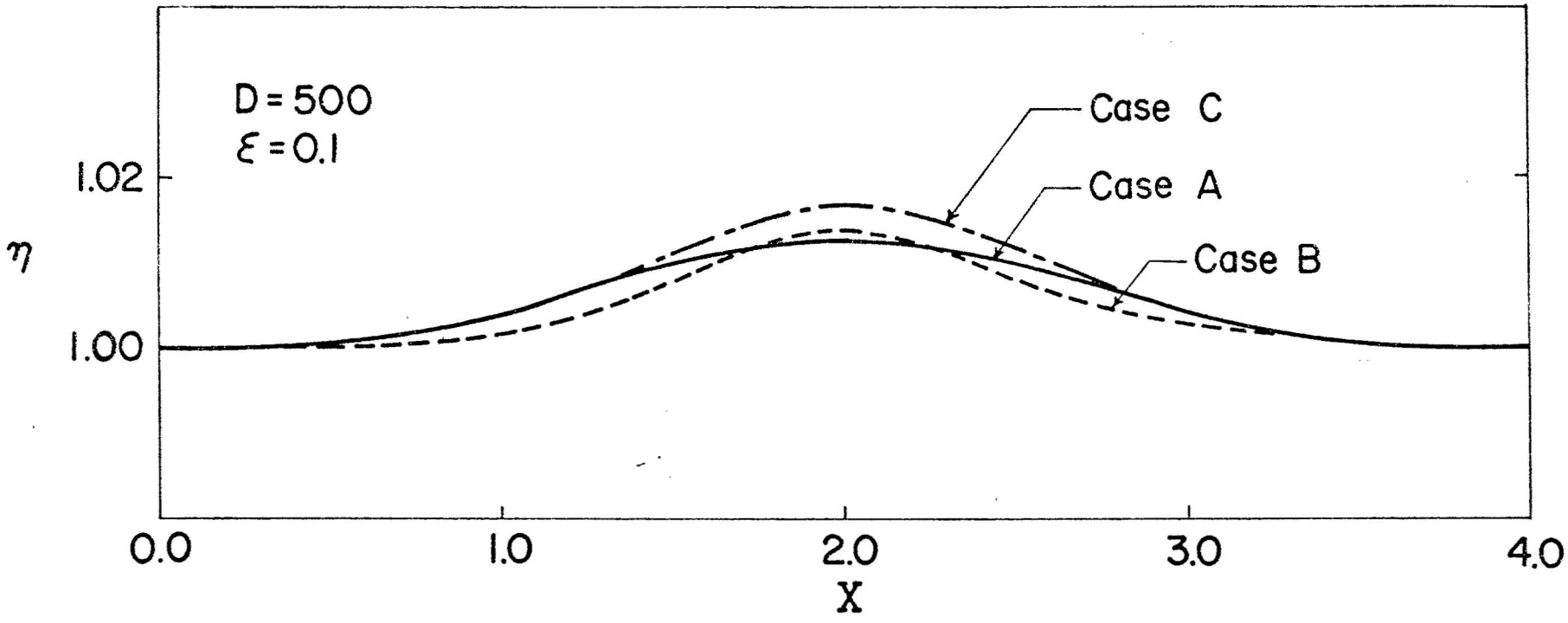

FIG. 3.1-12 EFFECTS OF HEAT SOURCES ON THE UPWELLING OF WATER TABLE FOR CASES A, B, AND C

upper portion of the aquifer. Near the heat sources, a column of hot fluid rises rapidly which induces two convective cells on either side of the heat sources. When a hot dike exists in the reservoir, the heat source becomes relatively close to the water table. This, plus the fact that the dike provides a larger area for heat transfer, makes it a possibility that hot water can be found at shallow depths, as is shown in Fig. 3.1-9. The horizontal temperature distributions at Y = 0.2 and Y = 0.4 for Cases A, B, and C are plotted in Fig. 3.1-10, where it is shown that the rate of change in temperature is rapid at the region near the heat source. This boundary layer behavior in temperature distribution is most pronounced for Case A. It is of interest to note that the vertical velocity distribution (Fig. 3.1-11) has the same shape as the temperature distribution (Fig. 3.1-10), and that "velocity slip" occurs on the impermeable surface. The effects of vertical and horizontal heating on the amount of upwelling of water table are shown in Fig. 3.1-12 -- it can be seen here that upwelling of water table increases if a hot dike exists.

Results of Cases D and E are plotted in Fig. 3.1-13 to Fig. 3.1-15. The streamlines for Cases D and E are shown in Figs. 3.1-13A and 3.1-13B where it is noted that the convective pattern in the region left of X = 1.55 (i.e., at the point of maximum heating) for both cases are similar qualitatively. In both of these cases, a column of hot fluid near X = 1.55 rises all the way up to the top of the water table and then moves either to the right or left and discharges into the ocean. Consequently, cold water entering from the left of the aquifer does not mix with those from the right, and vice versa. A comparison of Figs. 3.1-13A and 3.1-13B shows that the convective pattern in the region to the right of X = 1.55 is different for Cases D and E. Of particular interest is the region between the two dikes in Fig. 3.1-13A. It is noted that, although the dikes are only 0.6 and 0.3 units in height, they act as a complete barrier for the movement of ground water, thus sealing off the seepage from the ocean. On the other hand, without a dike at X = 2.55, groundwater moves freely as is shown in Fig. 3.1-13B. Figs. 3.1-14 and 3.1-15 show the temperature contours and the upwelling of water table for Cases D and E. Again, it is shown that warm water at shallow depth is possible and that the amount of upwelling of water table increases, whenever there is a dike.

The details of the analysis are described in Technical Report No. 7 [2]. A manuscript based on this work will be submitted for publication shortly.

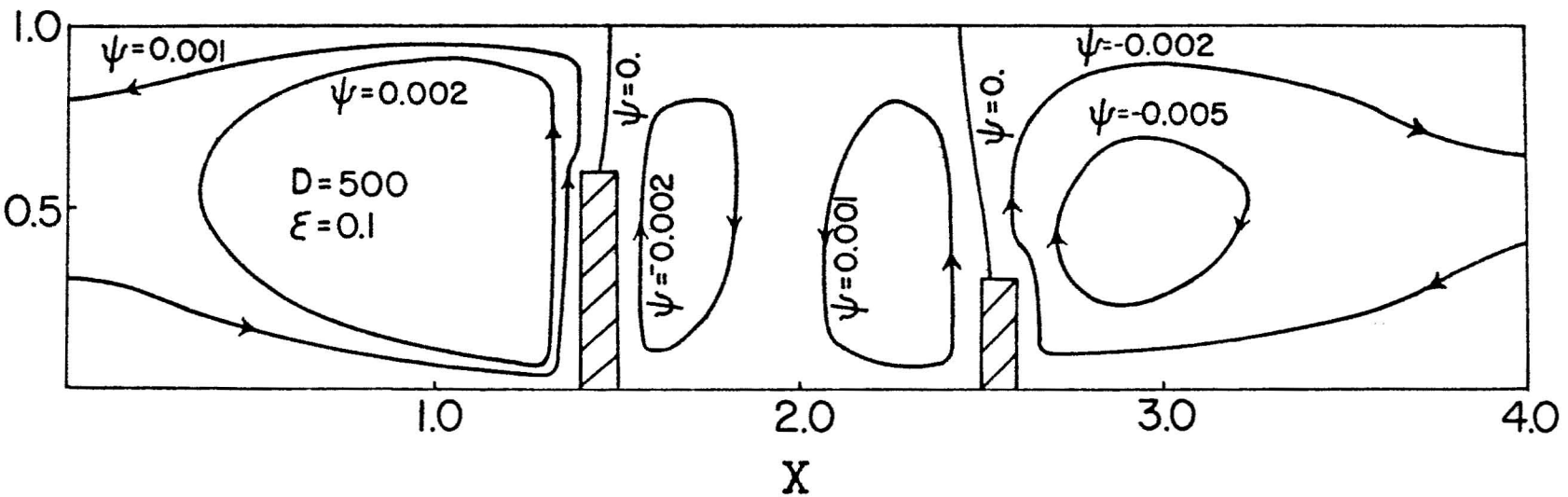

FIG. 3.1-13A CONVECTIVE PATTERN FOR CASE D

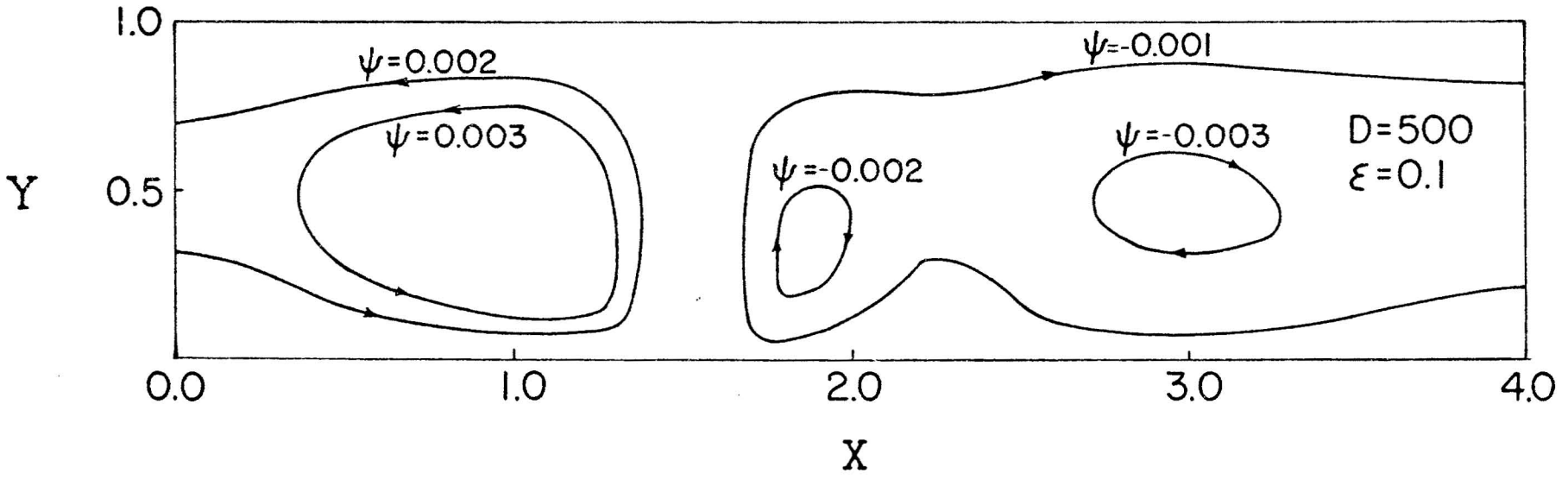

FIG. 3.1-13B CONVECTIVE PATTERN FOR CASE E

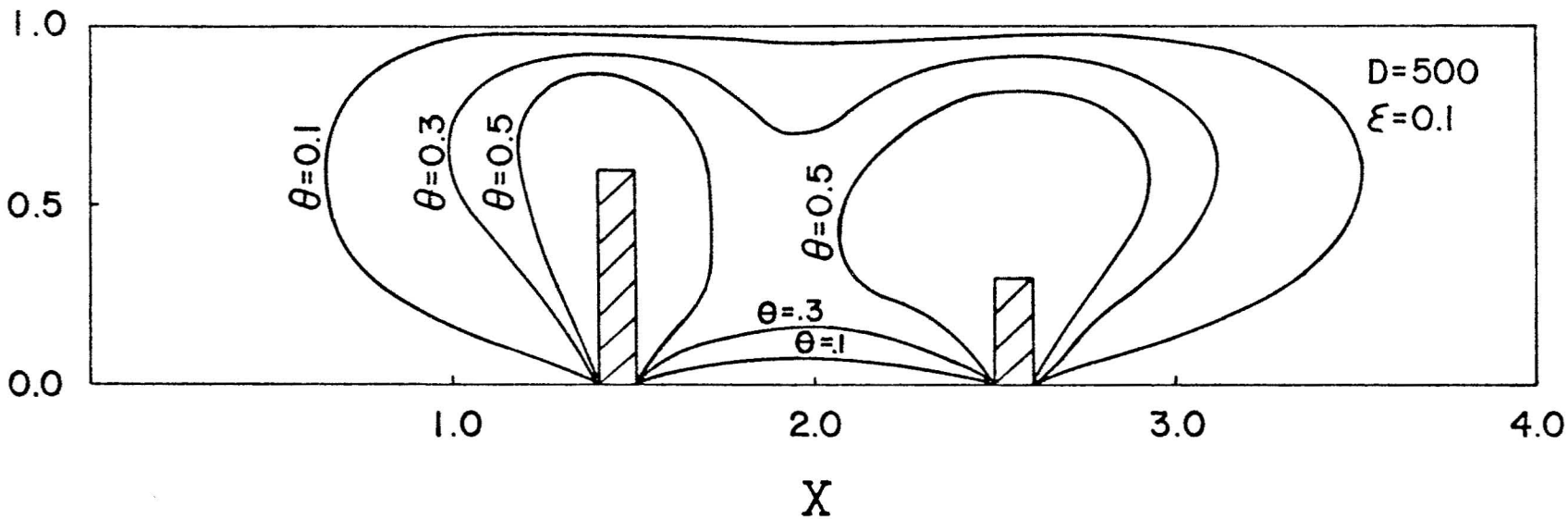

FIG. 3.1-14A TEMPERATURE CONTOURS FOR CASE D

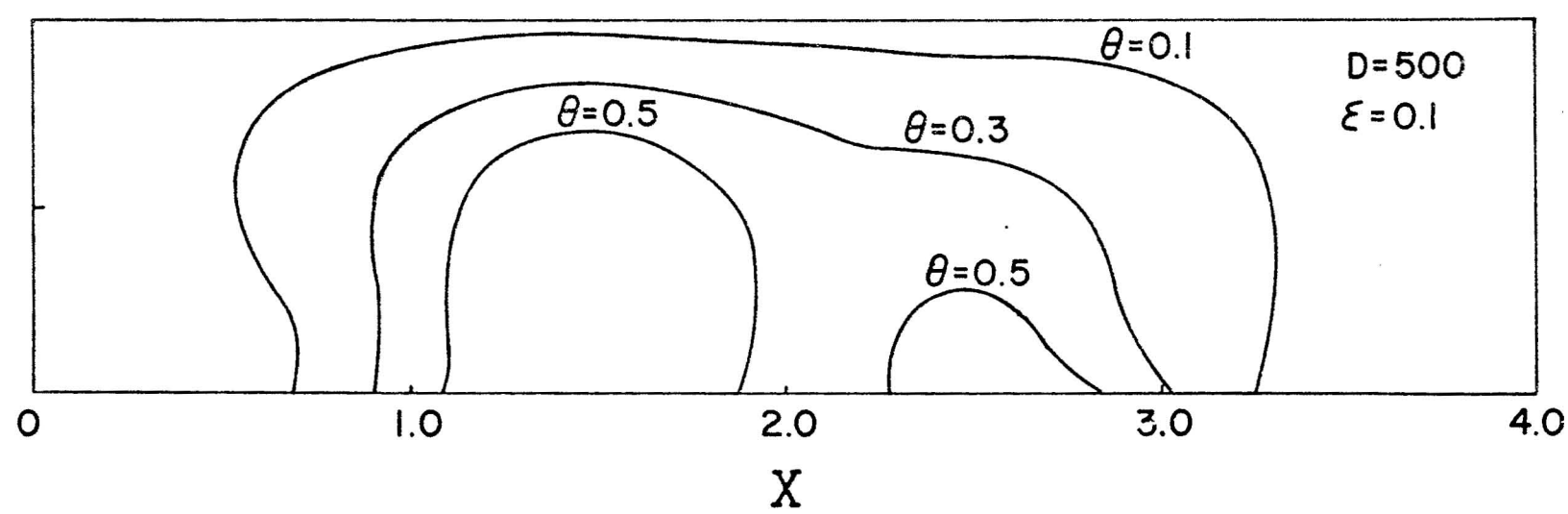

FIG. 3.1-14B TEMPERATURE CONTOURS FOR CASE E

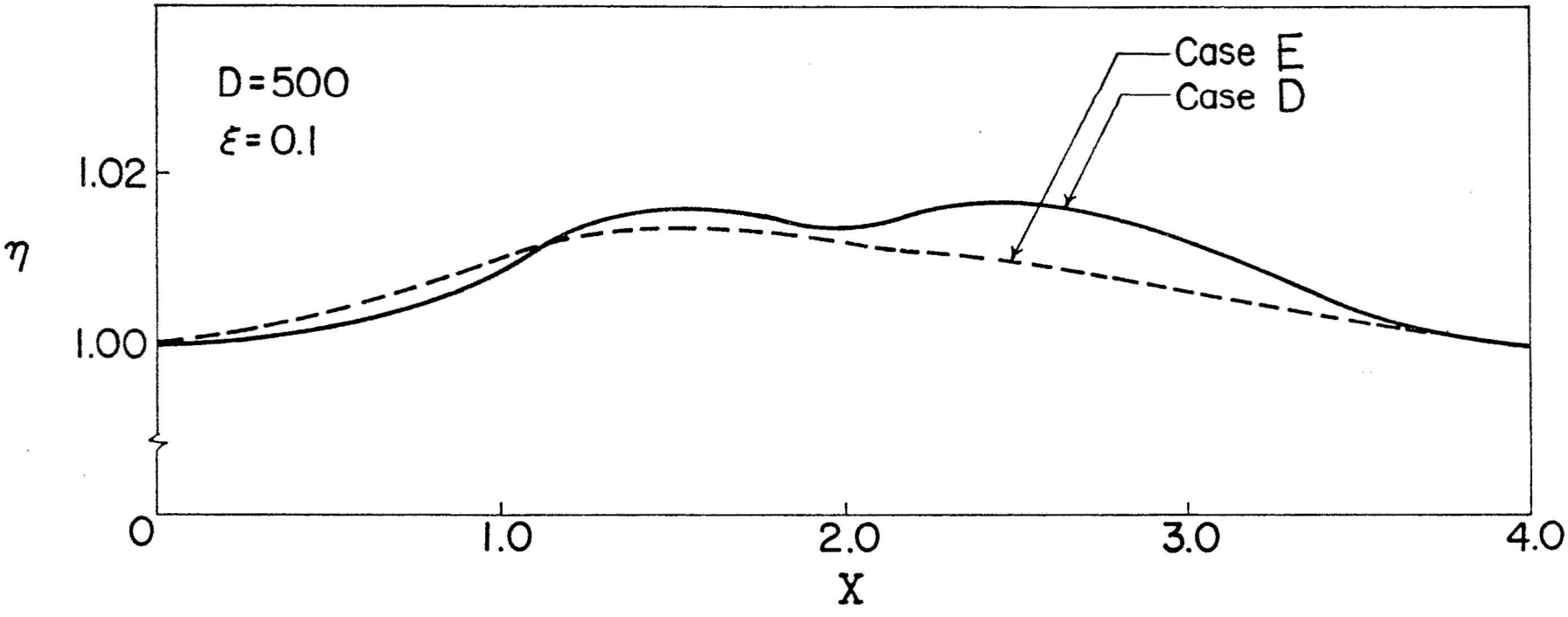

FIG. 3.1-15 EFFECTS OF HEAT SOURCES ON THE UPWELLING OF WATER TABLE FOR CASES D AND E

3. Free Convection at High Rayleigh Number in Confined Geothermal Reservoirs

The perturbation method used in the previous two problems is valid for small ε and for small and moderate values of D. Thus, the method is applicable for reservoirs with low permeability. In the present study, we shall focus our attention to reservoirs with high permeability. For this purpose it is convenient to express the governing equations in terms of dimensionless stream function ($\Psi = \frac{\mu\psi}{\rho_s ghK}$, where μ, the viscosity of the fluid, ρ_s, the density of the fluid at some reference condition, g, the gravitational acceleration, h, the depth of the reservoir, and K, the permeability of the aquifer) and dimensionless temperature ($\theta \equiv \frac{T-T_s}{T_c-T_s}$ where T_s is the temperature at some reference condition and T_c is the maximum temperature at the impermeable surface). The resultant set of non-linear partial differential equations are of elliptic type that can be approximated by a set of non-linear, algebraic equations by the finite difference method. The parameters in the equations are the aspect ratio L, and the Rayleigh number Ra where $Ra \equiv K\rho_s gh\beta \frac{(T_c-T_s)}{\mu\alpha} \equiv \varepsilon D$ with β and α denoting the coefficient of thermal expansion and the diffusivity of the saturated porous medium. To insure convergence at large Rayleigh numbers, the standard finite difference method is modified with the procedures discussed by Greenspan [4] to convert into a resultant set of diagonally dominant linear algebraic equations. Over-relaxation method is used to accelerate the iteration process. Numerical solutions are found to be convergent for all values of parameters involved.

Computations were carried out for L = 4 and for Ra from 0 to 2,000 with the following three different boundary conditions.

Case 1. Cylindrical and rectangular island aquifers with caprock temperature specified. Consider an island aquifer bounded by ocean on the sides, confined by caprock at the top, and heated by a horizontal impermeable surface at the bottom (Fig. 3.1-16A). The temperature of the ocean and the caprock are given by $\theta_s = 0$ and $\theta_a = 0.02$, and that of the heated surface is given by

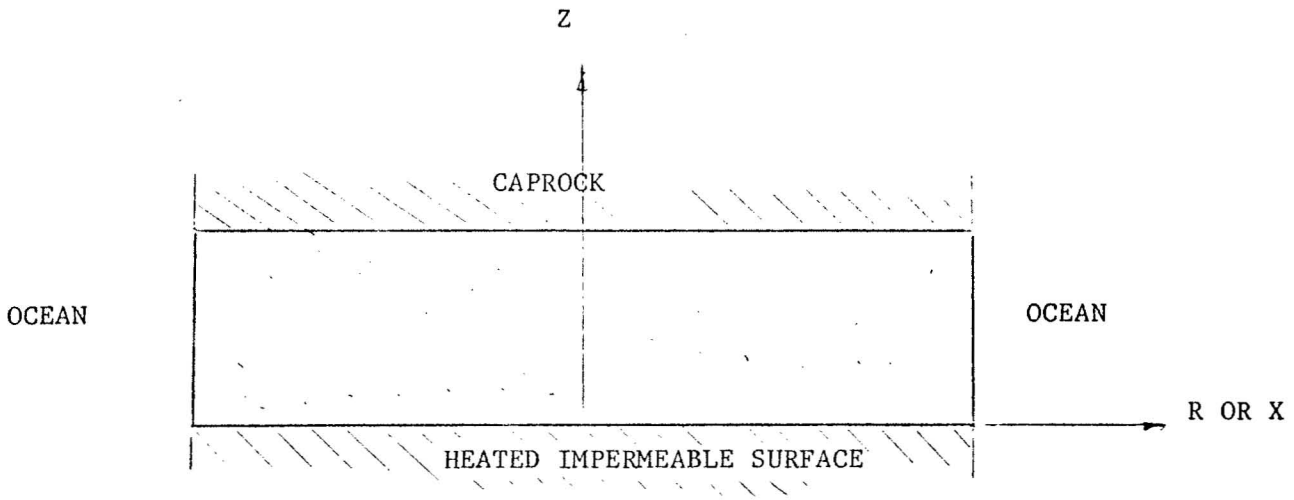

FIG. 3.1-16A ISLAND AQUIFER HEATED FROM BELOW

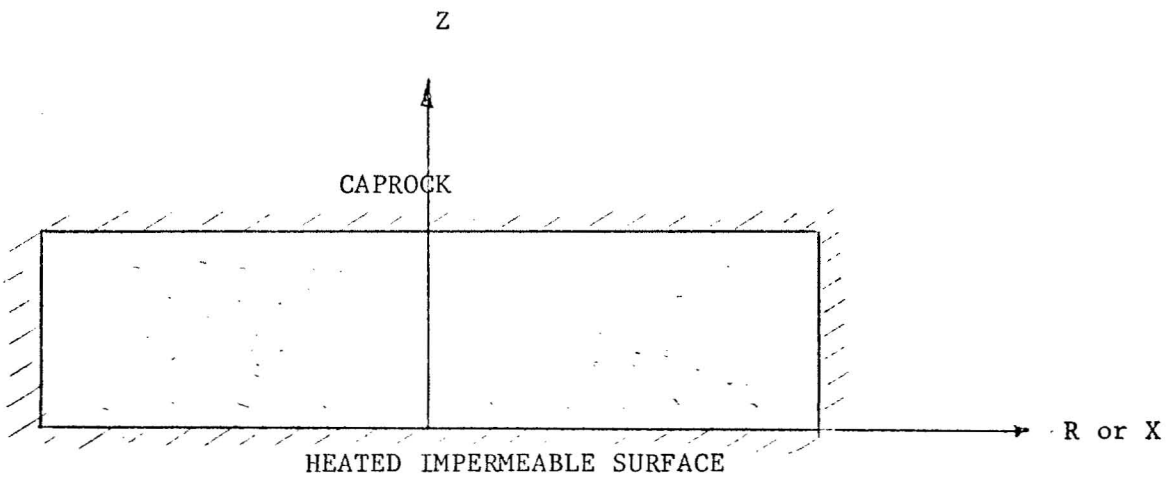

FIG. 3.1-16B BOUNDED AQUIFER HEATED FROM BELOW

$$\theta = \exp\left[-\left(\frac{R}{0.5}\right)^2\right] \quad \text{for cylindrical reservoirs,}$$

and $$\theta = \exp\left[-\left(\frac{X}{0.5}\right)^2\right] \quad \text{for rectangular reservoirs,}$$

where R and X are dimensionless coordinates given by $R \equiv r/h$ and $X = x/h$.

Fig. 3.1-17 shows the convective pattern in a cylindrical aquifer for two values of Ra. In both of these figures, cold water moves inland along the lower portion of the aquifer and is gradually being heated by the impermeable surface. Near the point of maximum heating, the fluid rises all the way to the top. Since the aquifer is confined at the top, the warm water is spread around the caprock and is finally discharged into the ocean in the upper portion of the aquifer. A comparison of Figs. 3.1-17A and 3.1-17B shows that the convective cells in Fig. 3.1-17A are absent in Fig. 3.1-17B. The temperature contours in a cylindrical island aquifer are shown in Fig. 3.1-18. For small values of Ra (Ra = 50, for example), the temperature contours are similar to those by conduction. As the value of Ra is increased, temperature contours develop into mushroom shapes. The results have important implications on the selection of a drilling site. It indicates that for a reservoir at a large value of Ra and having a hot heat source, a large amount of hot water is indeed available at shallow depths. The effects of Ra on horizontal temperature distribution at Y = 0.2, 0.4, 0.6, and 0.8 are plotted in Fig. 3.1-19 where it is shown that the horizontal temperature distribution exhibits a bell shape with a maximum value at the center of the aquifer. The rate of increase in temperature in the region near the center is rapid for large Ra, indicating a boundary layer behavior. The same data for Fig. 3.1-19 is replotted in Fig. 3.1-20 to show the vertical temperature profiles in a cylindrical island aquifer. At the location directly above the heat source (R = 0), temperature increases rapidly from nearly zero at the caprock to almost unity at a small vertical distance from the caprock. The vertical temperature profile at R = 0 is dramatically different from the rest of the profiles which have a temperature reversal at a vertical distance not too far from the caprock. It is worth mentioning that the temperature reversal occurs because of the discharge of warm water toward the ocean. The behavior of temperature reversal is most pronounced for large Ra at a horizontal distance near the heat source.

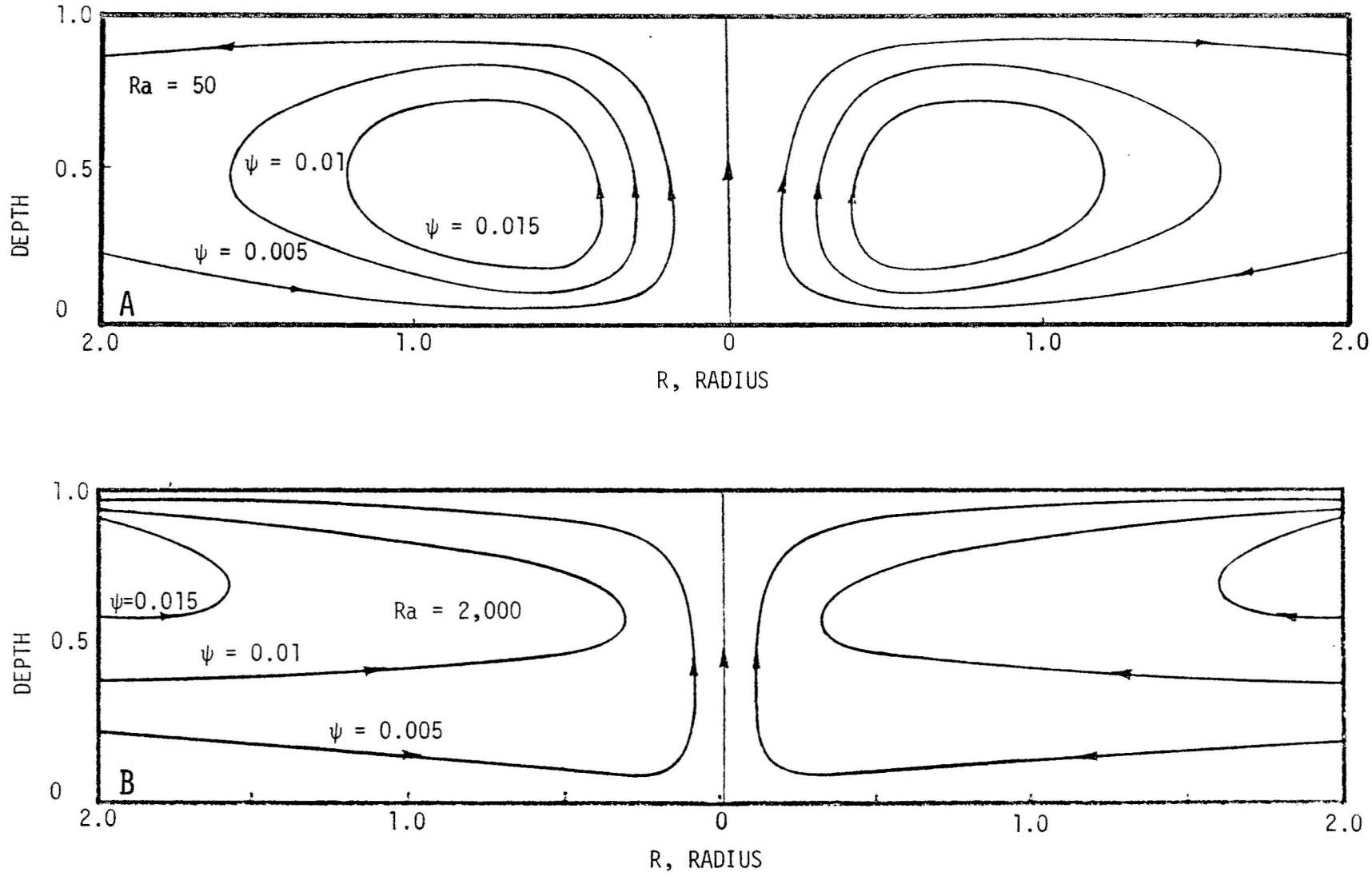

FIG. 3.1-17 STREAMLINES FOR A CYLINDRICAL ISLAND AQUIFER

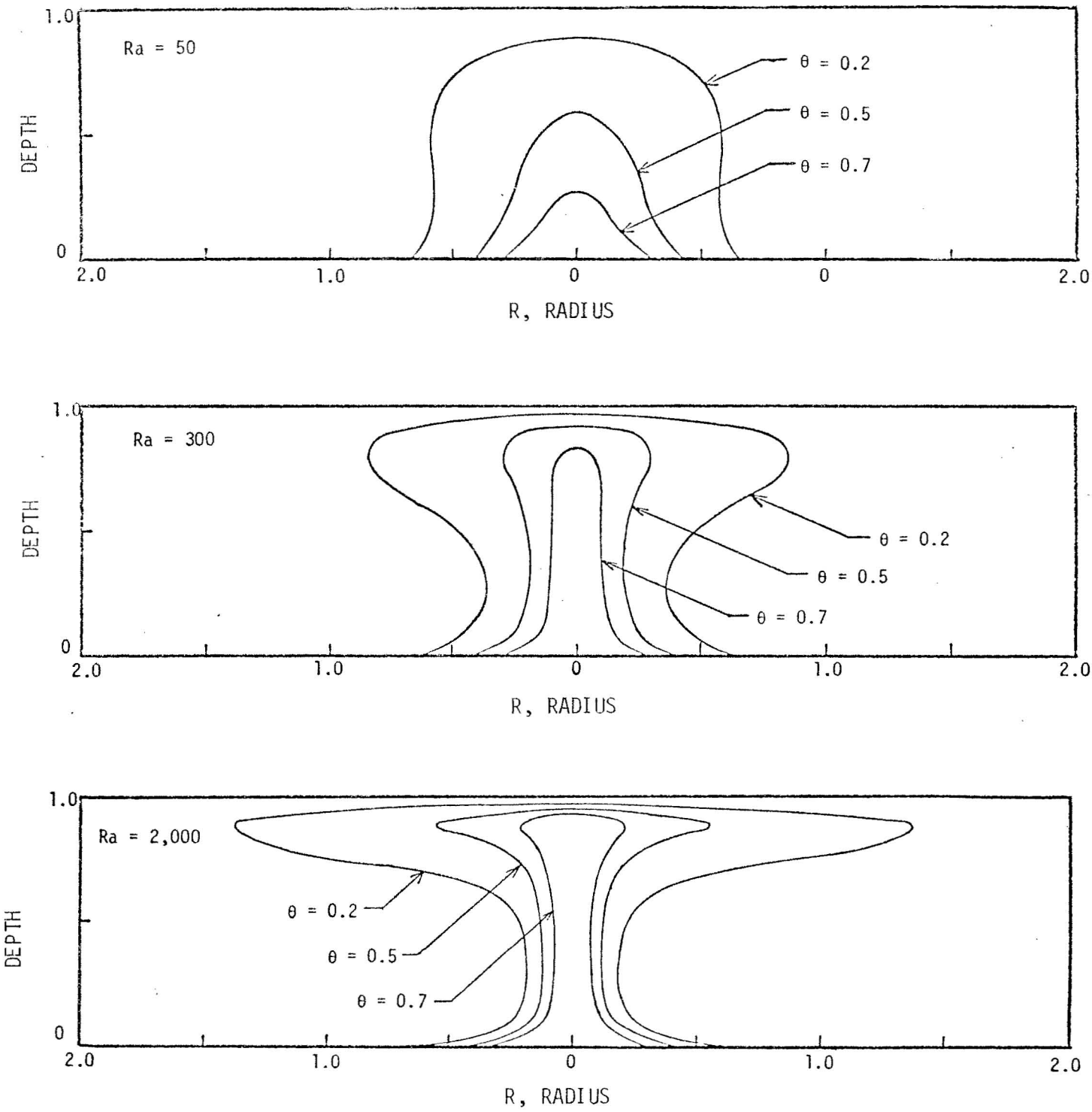

FIG. 3.1-18 TEMPERATURE CONTOURS IN A CYLINDRICAL ISLAND AQUIFER WITH CAPROCK TEMPERATURE SPECIFIED

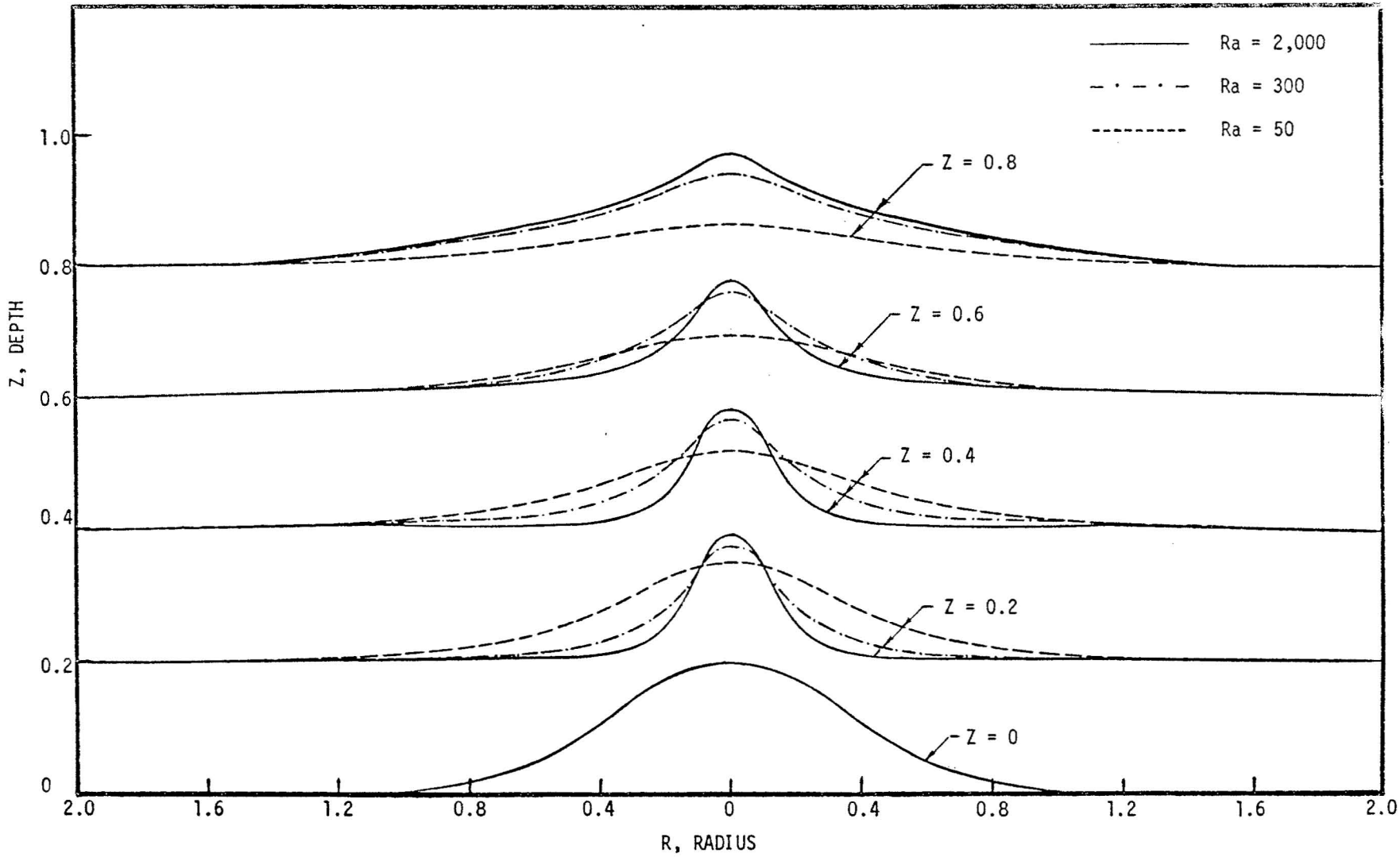

FIG. 3.1-19 HORIZONTAL TEMPERATURE DISTRIBUTION IN A CYLINDRICAL ISLAND AQUIFER WITH CAPROCK TEMPERATURE SPECIFIED

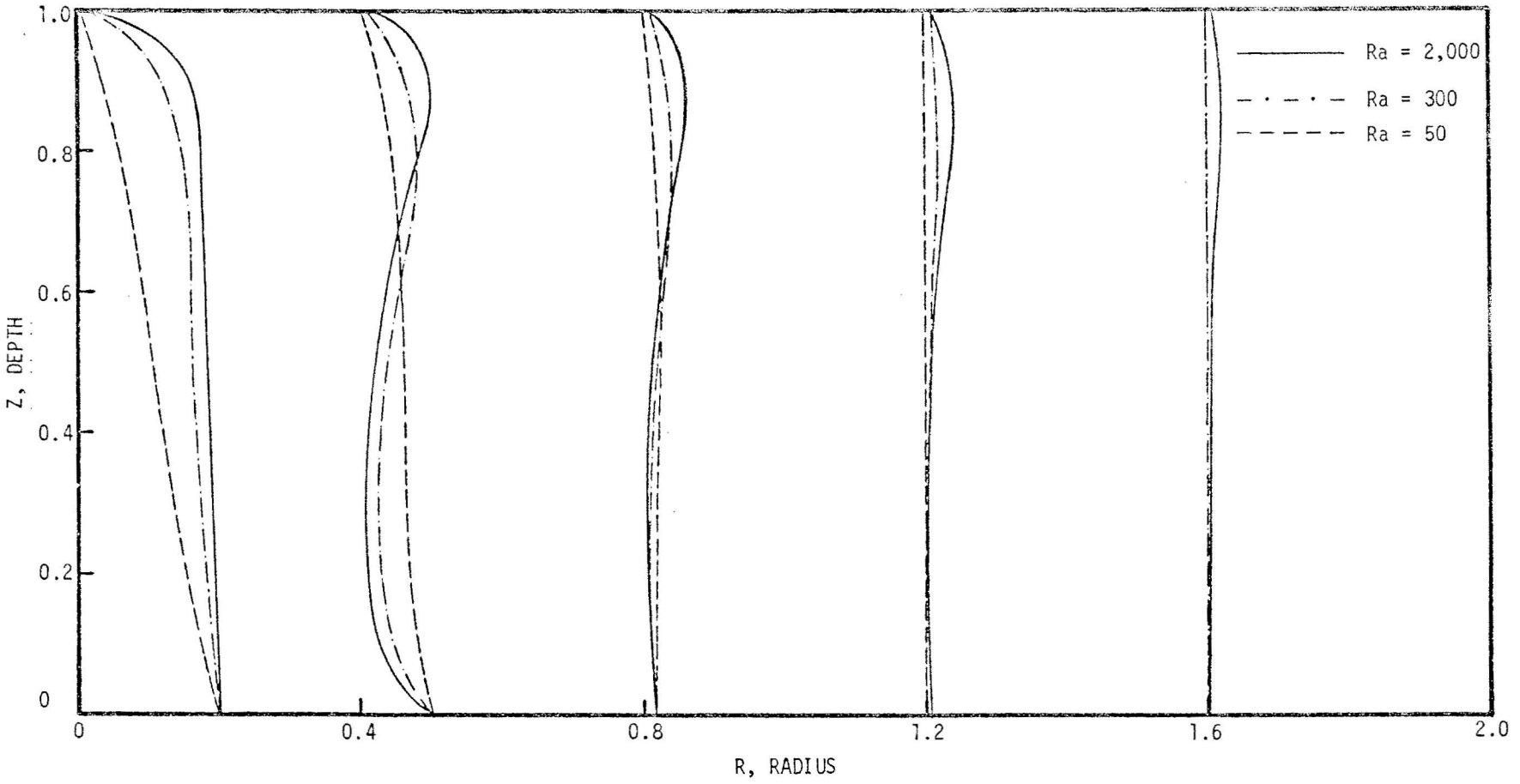

FIG. 3.1-20 VERTICAL TEMPERATURE PROFILES IN A CYLINDRICAL ISLAND AQUIFER WITH CAPROCK TEMPERATURE SPECIFIED

It is interesting to note that temperature vs. depth measurements obtained by G. Keller [3] show also a temperature reversal behavior (Fig. 3.1-21). A comparison between theory and measurements shows a striking similarity (Fig. 3.1-22), although the island of Hawaii is supposed to be an unconfined aquifer. The comparison of temperature distribution between a cylindrical and a rectangular island aquifer with caprock temperature specified is shown in Figs. 3.1-23A and 3.1-23B. Here it is seen that temperature distribution in a cylindrical aquifer is everywhere below that of a rectangular aquifer because of the three-dimensional effect of the seepage.

Case 2. Cylindrical and rectangular island aquifer with nonheat conducting caprock. The geometry is similar to Case 1 except the thermal boundary condition of the caprock is changed to an adiabatic surface.

The convective pattern for a cylindrical island aquifer with nonheat conducting caprock is very similar to Fig. 3.1-17. The corresponding temperature contours are plotted in Fig. 3.1-24. A comparison of Fig. 3.1-24 and Fig. 3.1-18 shows that a substantially larger amount of hot water at shallow depth is available for Case 2 because of the nonheat conducting caprock. The data for Fig. 3.1-24 is replotted in Figs. 3.1-25 and 3.1-26 to show the effect of Ra on the horizontal and vertical temperature distribution. Again, the boundary layer behavior is pronounced for large Ra. As in Case 1, temperature distribution in a cylindrical island aquifer is everywhere lower than that in a rectangular island aquifer (Figs. 3.1-27A and 3.1-27B).

Effects of thermal boundary conditions on the caprock can be shown by comparing Case 1 and Case 2, as is shown in Figs. 3.1-28A and 3.1-28B. As is expected, temperature distribution everywhere in the reservoir with a nonheat conducting caprock is higher than that of a heat conducting caprock. However, the increase in temperature is most significant in the region adjacent to the caprock. The larger the value of Ra, the smaller the region in which temperature is affected. In other words, for large value of Ra, the effect of thermal boundary condition on the caprock would influence temperature distribution in a small region adjacent to the caprock; for the temperature distribution in the rest of the reservoir it is unaffected by the thermal condition at the caprock.

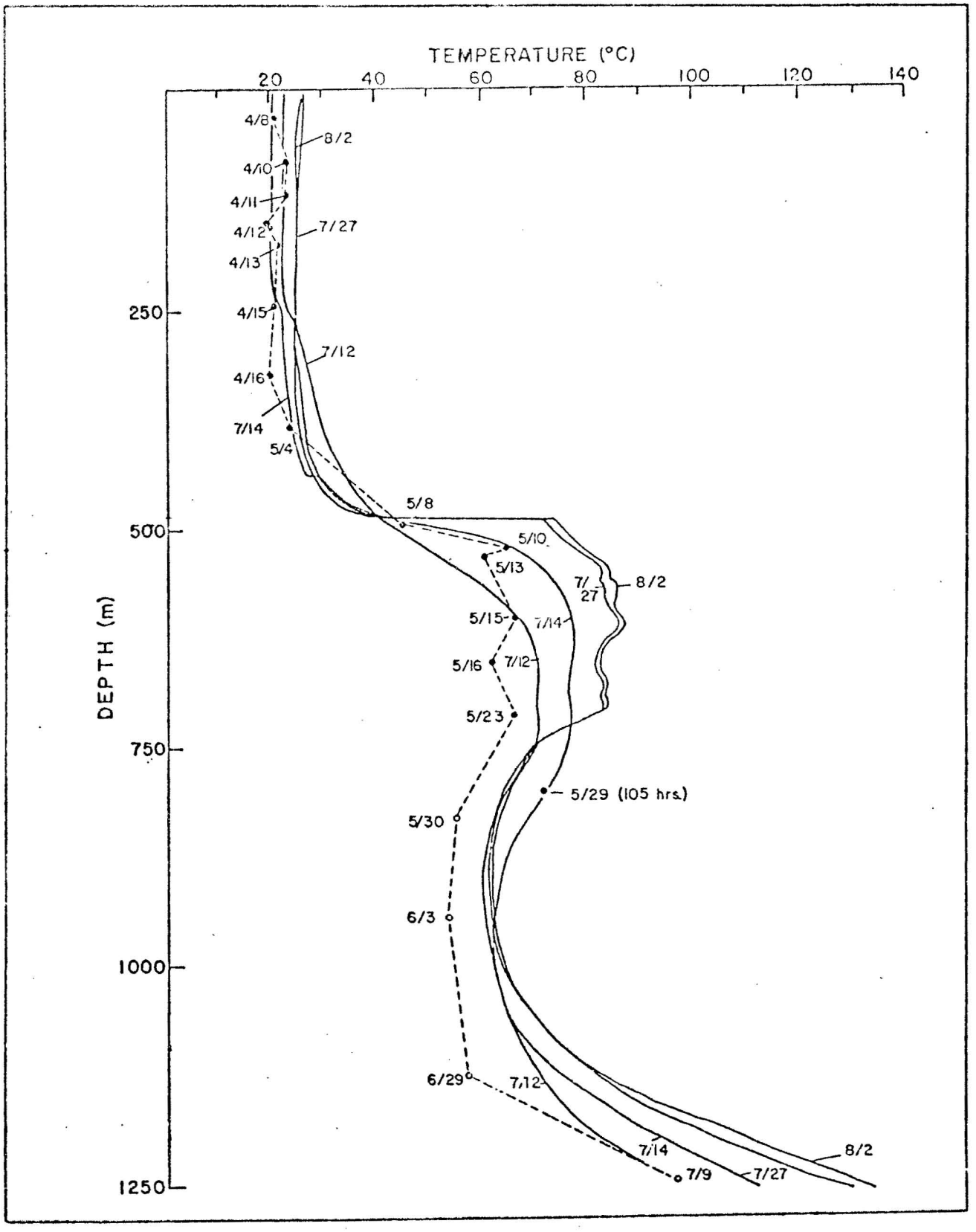

FIG. 3.1-21 TEMPERATURE PROFILES IN THE KILAUEA DRILL HOLE MEASURED BY KELLER

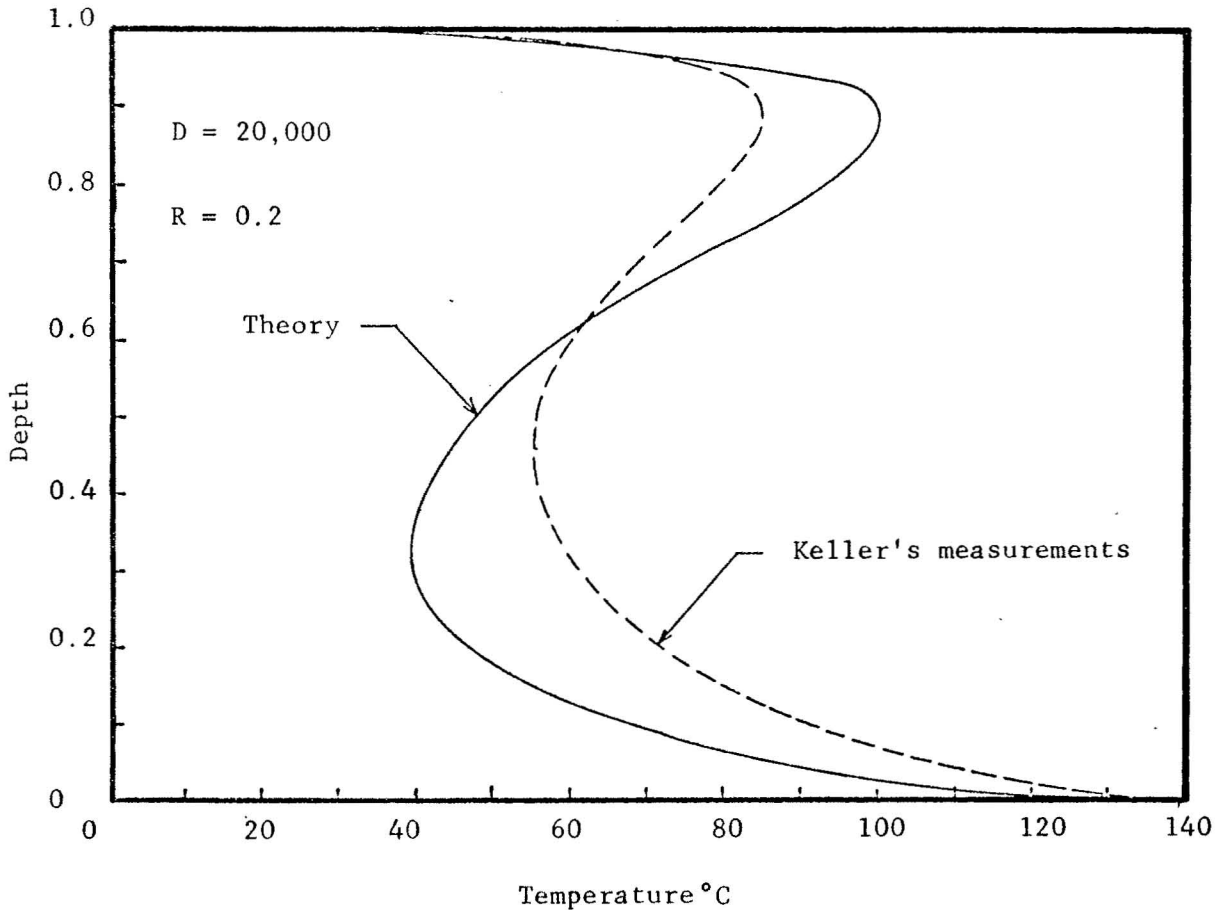

FIG. 3.1-22 COMPARISON OF THEORY AND MEASUREMENTS

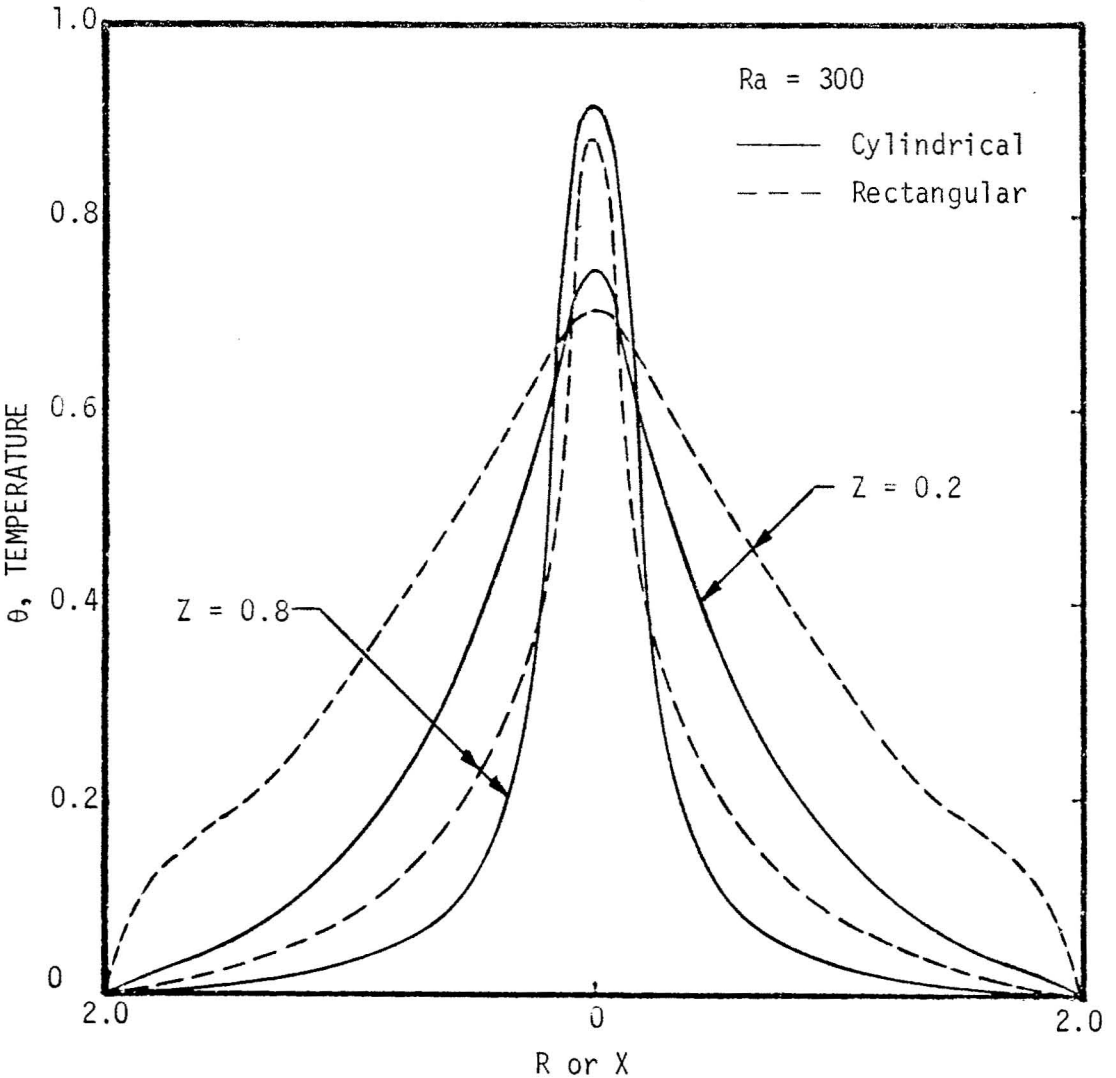

FIG. 3.1-23A COMPARISON OF HORIZONTAL TEMPERATURE DISTRIBUTION IN A CYLINDRICAL AND A RECTANGULAR ISLAND AQUIFER WITH CAPROCK TEMPERATURE SPECIFIED

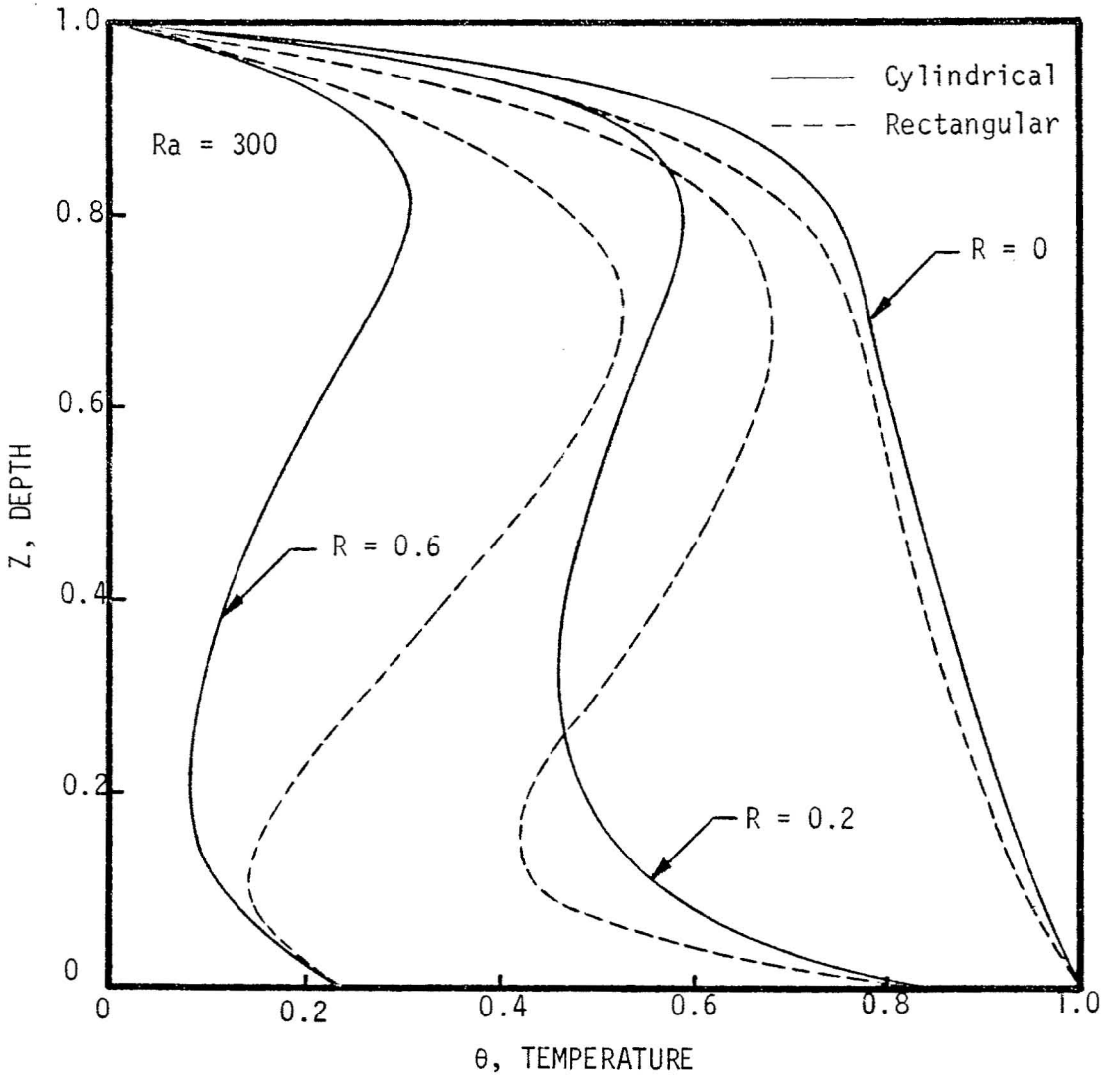

FIG. 3.1-23B COMPARISON OF VERTICAL TEMPERATURE PROFILES IN A CYLINDRICAL AND A RECTANGULAR ISLAND AQUIFER WITH CAPROCK TEMPERATURE SPECIFIED

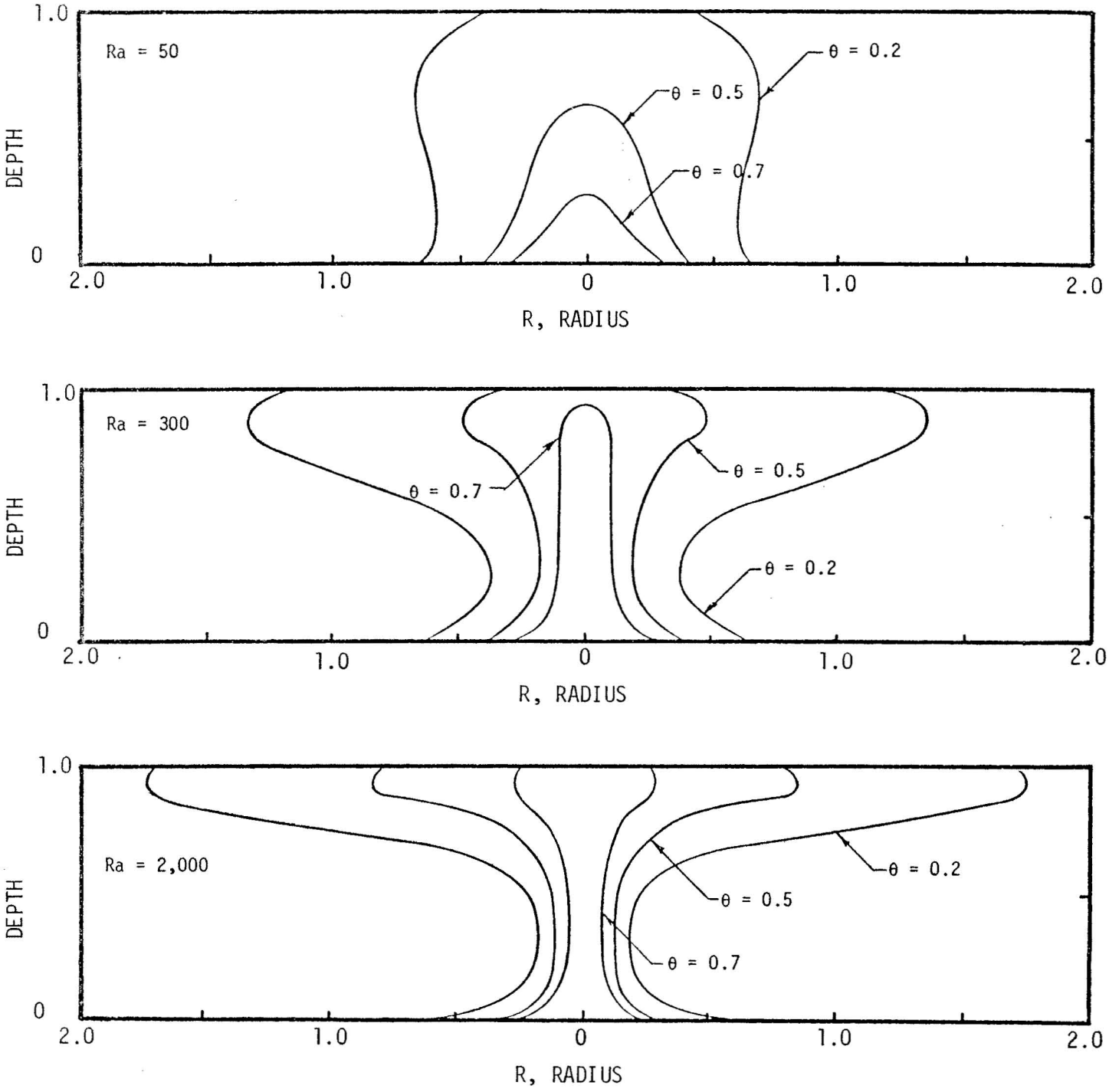

FIG. 3.1-24 TEMPERATURE CONTOURS IN A CYLINDRICAL ISLAND AQUIFER WITH ADIABATIC CAPROCK

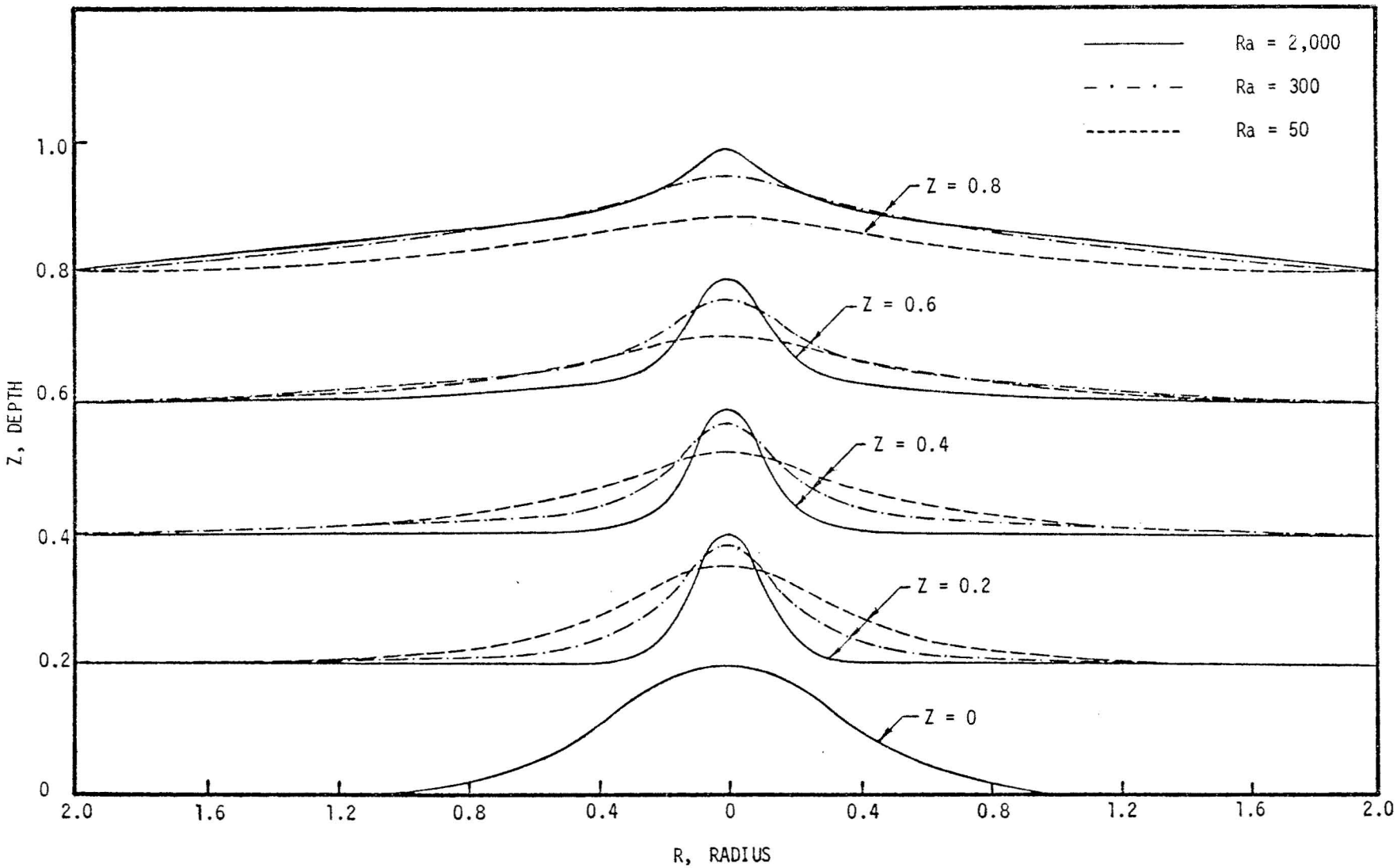

FIG. 3.1-25 HORIZONTAL TEMPERATURE DISTRIBUTION IN A CYLINDRICAL ISLAND AQUIFER WITH NON-HEAT CONDUCTING CAPROCK

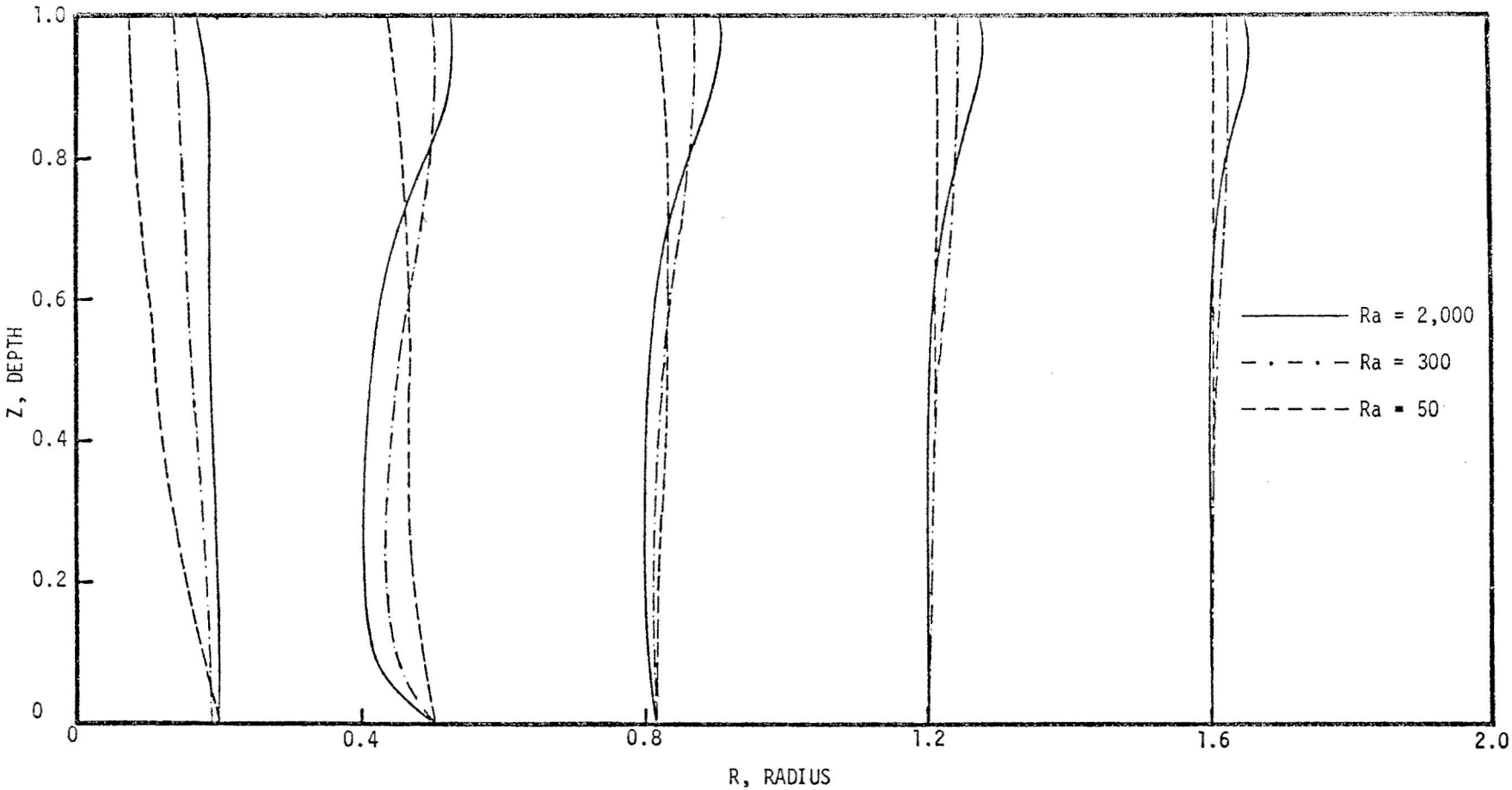

FIG. 3.1-26 VERTICAL TEMPERATURE PROFILES IN A CYLINDRICAL ISLAND AQUIFER WITH NON-HEAT CONDUCTING CAPROCK

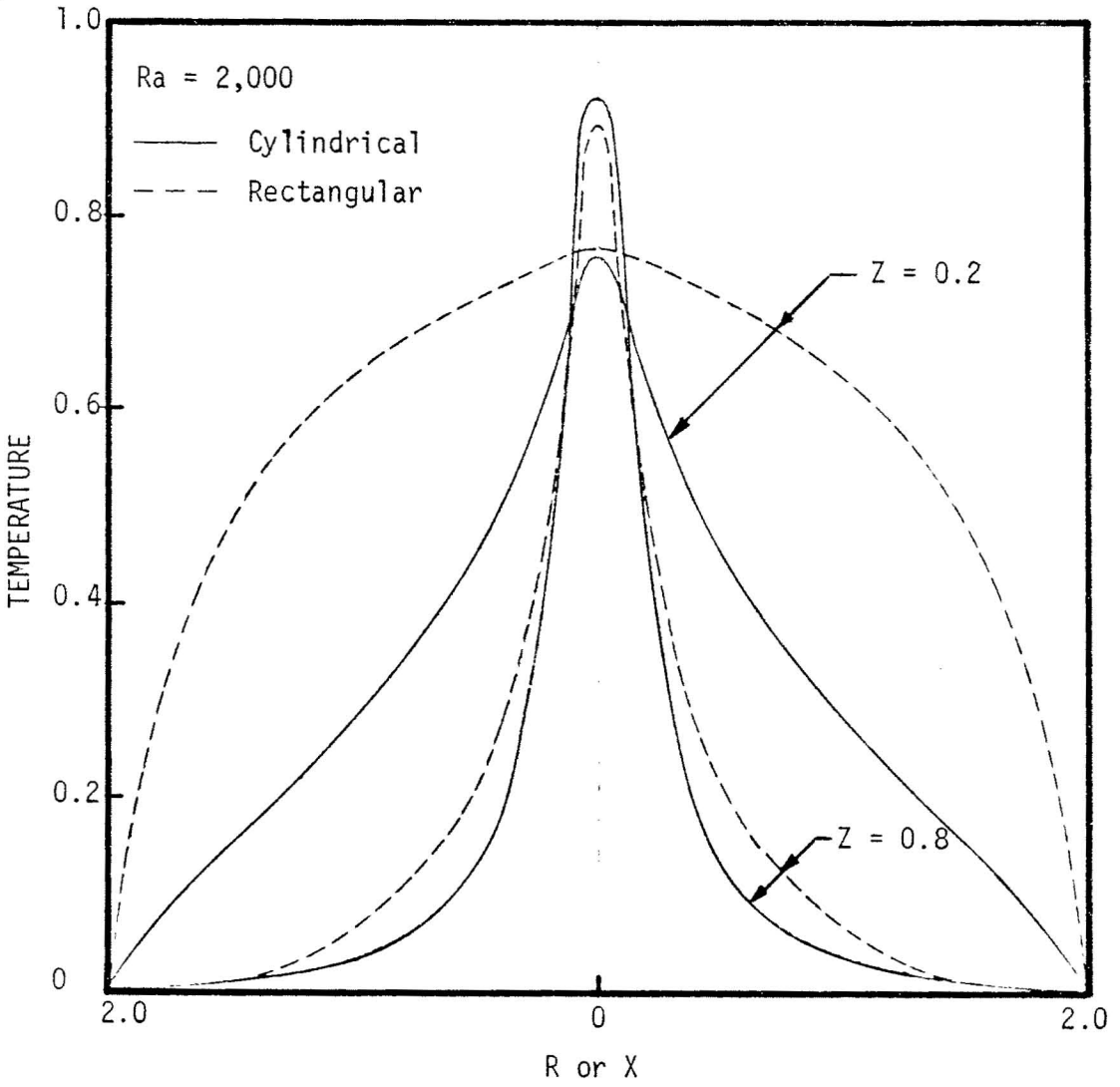

FIG. 3.1-27A COMPARISON OF HORIZONTAL TEMPERATURE DISTRIBUTION IN A CYLINDRICAL AND A RECTANGULAR ISLAND AQUIFER WITH ADIABATIC CAPROCK

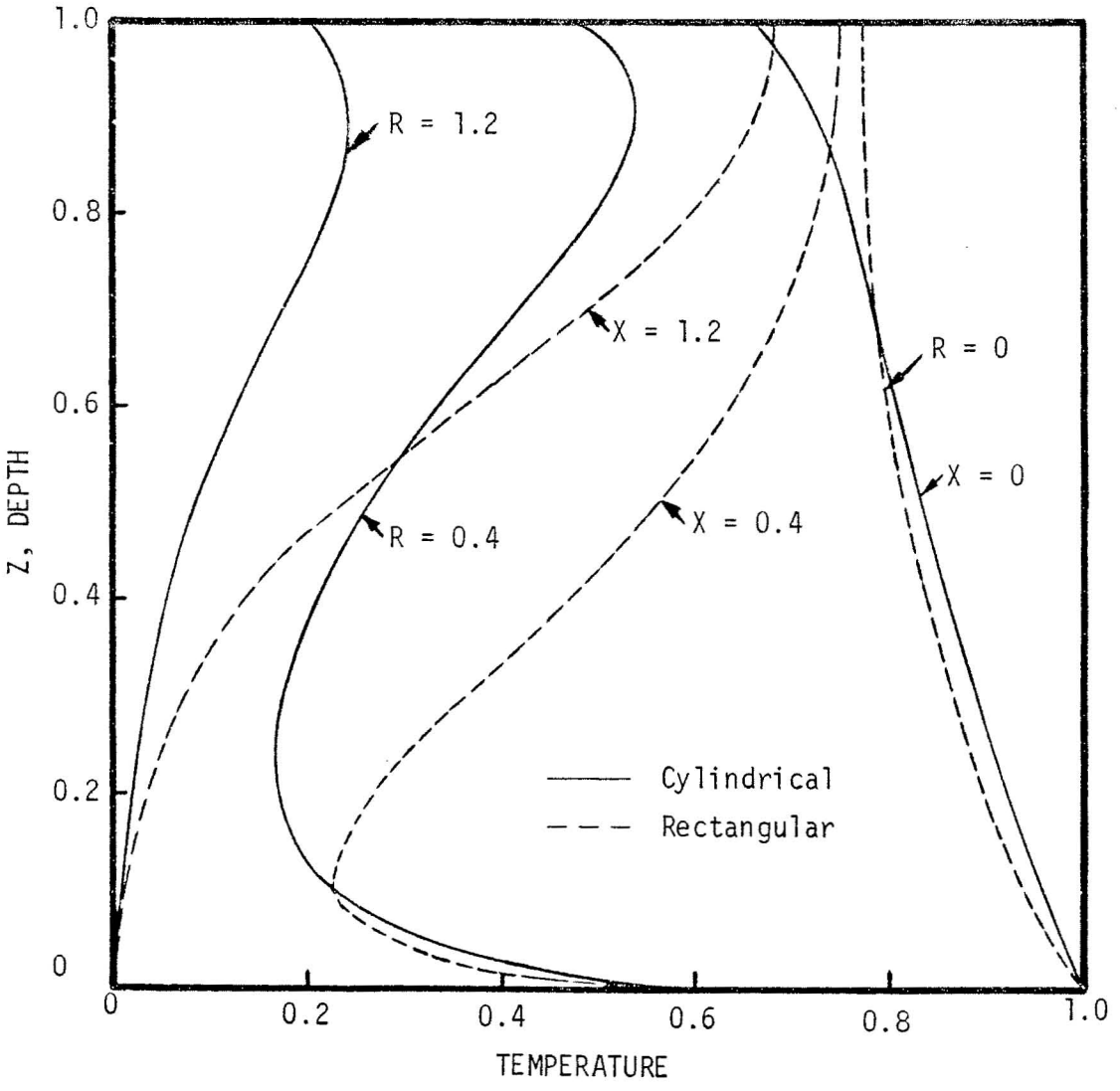

FIG. 3.1-27B COMPARISON OF VERTICAL TEMPERATURE PROFILES IN A CYLINDRICAL AND A RECTANGULAR ISLAND AQUIFER WITH ADIABATIC CAPROCK

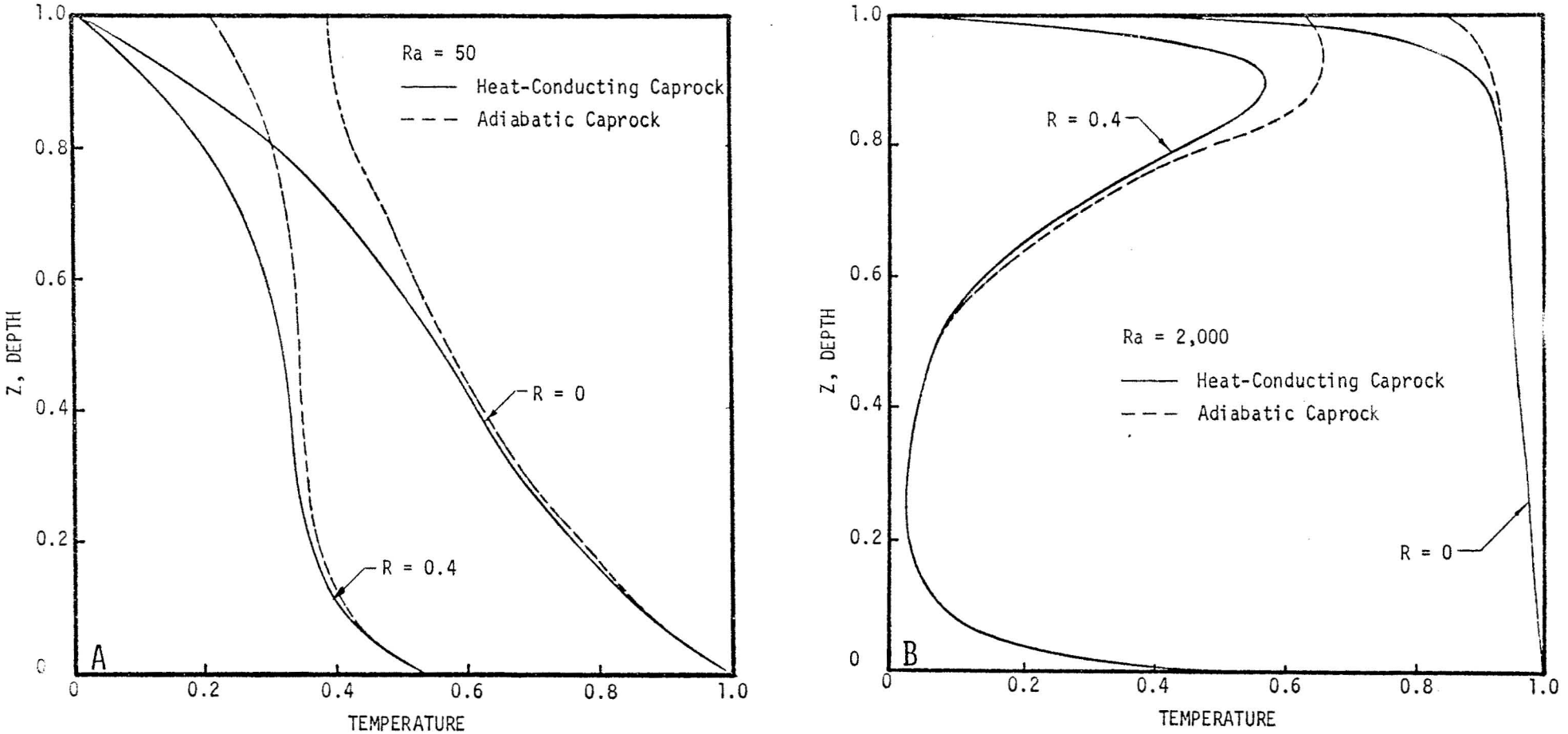

FIG. 3.1-28 EFFECT OF THERMAL BOUNDARY CONDITION OF THE CAPROCK ON THE VERTICAL TEMPERATURE PROFILES IN A CYLINDRICAL ISLAND AQUIFER

Case 3. Cylindrical and rectangular bounded aquifer with boundary temperatures specified. The geometry of this case is shown in Fig. 3.1-16B where the reservoir is bounded by impermeable surfaces. Temperature on the bottom impermeable surface is similar to Case 1. Temperatures on the rest of the impermeable surfaces are at zero.

The convective pattern for a cylindrical bounded aquifer with zero temperatures on the top and on the sides and heated from below is shown in Fig. 3.1-29. Here it is shown that two convective cells exist on either side of the heat source. Temperature distribution for this case is very similar to that of Case 1.

A manuscript covering this work is now under preparation for publication.

II. Well Testing and Analysis

Investigators: P. Takahashi, B. Chen, & L. S. Lau

The following section will report on the activities of the well testing/analysis subtasks. The report will be in five parts:

1. History of reservoir engineering.
2. Nature of a geothermal reservoir.
3. The international questionnaire (TABLE 2).
4. What is a geothermal reservoir engineer?
5. Geothermal reservoir engineering--measurement and methods of analysis.

HISTORY OF RESERVOIR ENGINEERING

The history of geothermal reservoir engineering really goes back to the beginnings of petroleum and gas reservoir engineering. Although reservoir evaluation undoubtedly first began with Drake's oil well in 1859, it is only during the last quarter century--December, 1949, to be exact, when the *JOURNAL OF PETROLEUM TECHNOLOGY* was born with van Everdingen and Hurst's classic paper entitled, "The Application of the Laplace Transformation to Flow Problems in Reservoirs"--that the science of reservoir engineering has developed. Twenty-five years ago a conformance of 50 to 70 percent was the best that could be

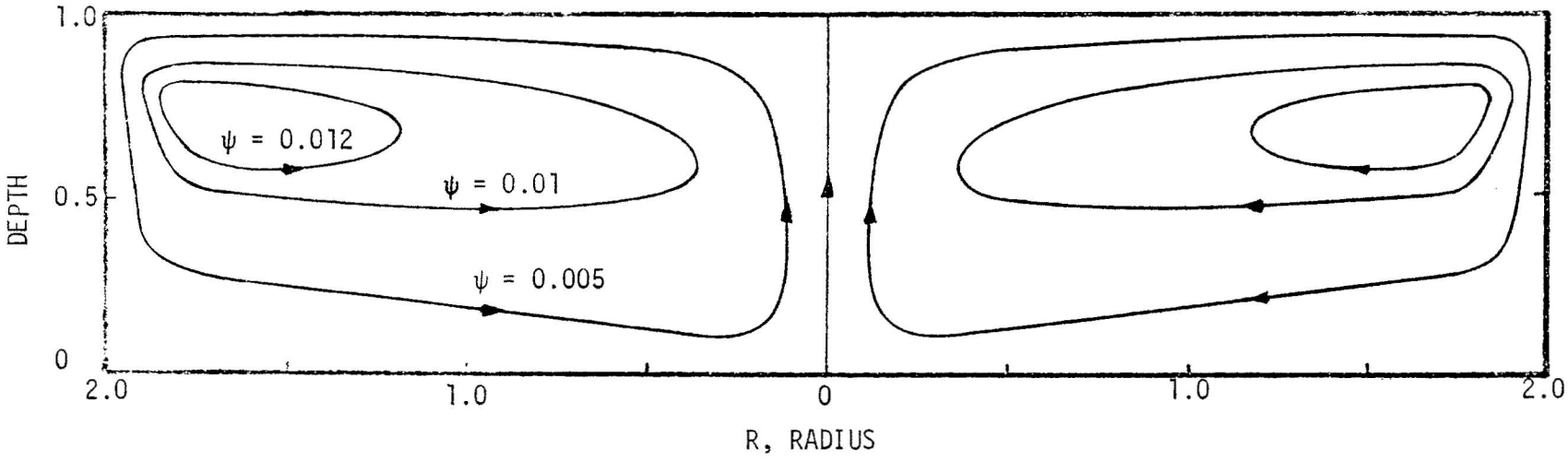

FIG. 3.1-29 STREAMLINES FOR A BOUNDED CYLINDRICAL RESERVOIR

accomplished in matching actual reservoir behavior and calculated prediction. Today, a conformance exceeding 90% is commmonplace in the petroleum industry.

The art of geothermal reservoir engineering can thus equivalently be placed somewhere before 1949. There are definite reasons why this state-of-the-art is relatively undeveloped:

1. Geothermal energy exploitation is in its infancy. Remember that almost a century elapsed before the science of petroleum reservoir engineering began to show progress. Although the first geothermal well began producing 70 years ago, it is only during the past 15 years that active evaluative efforts have been attempted.
2. There has been minimal interchange of ideas and methods--a carryover from the general secrecy practiced by the petroleum industry.
3. Geothermal reservoirs are complicated by the parameter temperature. Although petroleum can have at least three different substances--gas, petroleum, and water to contend with--the dominant factor, temperature, in geothermal wells, alters the situation significantly enough so as to change the rules of the game. Hardware problems are encountered at high temperatures and software packages must incorporate temperature and its effects.

The "state-of-the-art" in geothermal reservoir engineering is in the most part formative. Four groups in particular, though, have contributed well: New Zealand, the Bureau of Reclamation, the U. S. Geological Survey, and Stanford University. Also available are some individual investigations, as for example, Robert Whiting's reservoir engineering study of Wairakei [5].

The primary reason why the literature is relatively sparse is that private companies treat geothermal well testing, the data, and methods of anlaysis as proprietary. Certain legal restrictions furthermore tend to preserve this form of classification. Fortunately, there appears to be an increasing international spirit of cooperation. The United Nations has done a remarkable job in attempting to get the world together.

THE NATURE OF A GEOTHERMAL RESERVOIR

Speculations on the nature of geothermal reservoirs can be found in the literature. Legally, in the United States, the U. S. Geological Survey defines a geothermal reservoir to be contained in either a known geothermal resource

area (KGRA) or a potential geothermal resource area (PGRA). Geothermal reservoirs can be characterized in several other ways:

1. Depletable (self-sealed) or regenerative (recharged),
2. Physical state: vapor-steam, liquid-hot-water (normally two-phased at wellhead), solid-hot rock, liquid magma,
3. Physical condition: temperature/pressure, size/depth, production rate,
4. Degree of dissolved solid content.

In California, vapor-dominated wells are considered to be depletable. A tax allowance is permitted under this classification. A decision has not yet been made on other types of wells. There is some reason to believe that all wells are at least partially regenerative because of the meteoric (rainwater) origin of geothermal fluids [6]. Furthermore, reports of measurable pressure drops in steam-dominated geothermal fields seen after rainfall lead one to suspect that perhaps fluid recharge could be significant.

Although vapor-dominated geothermal wells are generally contaminated with CO_2 (primarily) and H_2S, there is little dissolved solid content. On the other hand, some of the hot water well samples in the Imperial Valley have shown as much as 30% dissolved solids by weight.

There seems to be no clear-cut answer to a universal definition of a geothermal reservoir. A geothermal reservoir generally requires: heat source (magma or geopressure); to be confined in an aquifer, although non-permeable hot rocks can be transformed into an aquifer through hydrofracturing/thermal cracking and the addition of water; and caprock--to hold the hot fluid in place . . . although the latter requirement is controversial. Speculations on geothermal reservoirs have been advanced by White and Muffler [6], U.S.; Facca [7], Italy; Elder [8], New Zealand; and Hayashida [9], Japan.

For the island of Hawaii, it is generally believed that the system is self-sealed and liquid-dominated. Figs. 3.1-30 & 3.1-31 are conceptualizations of the expected system for Hawaii. Fig. 3.1-30 is a macro-view of the total underground system and Fig. 3.1-31 is a possible self-sealed system. It should be noted that magma is generated at the crust-mantle interface. For the Hawaiian Islands, there is belief that the production of magma could be as close as 20 miles from the surface of the earth [10, 11].

George Keller, discussing results of his drilling program at Kilauea Volcano, [12] concluded that evidence favored the existence of hydrothermal convection cells and, most importantly, suggested the action of self-sealing

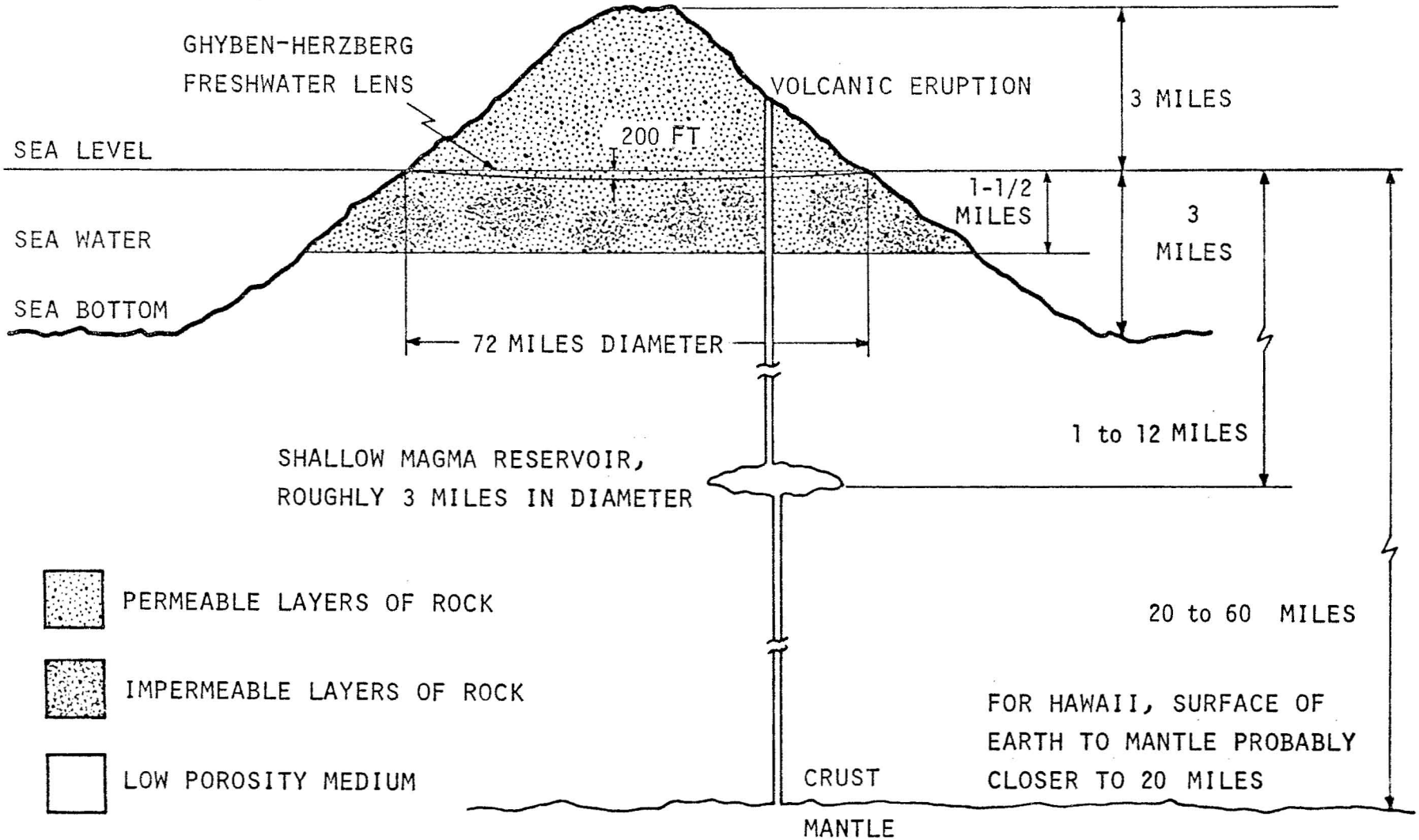

FIG. 3.1-30 SPECULATIVE CROSS-SECTIONAL VIEW OF THE ISLAND OF HAWAII

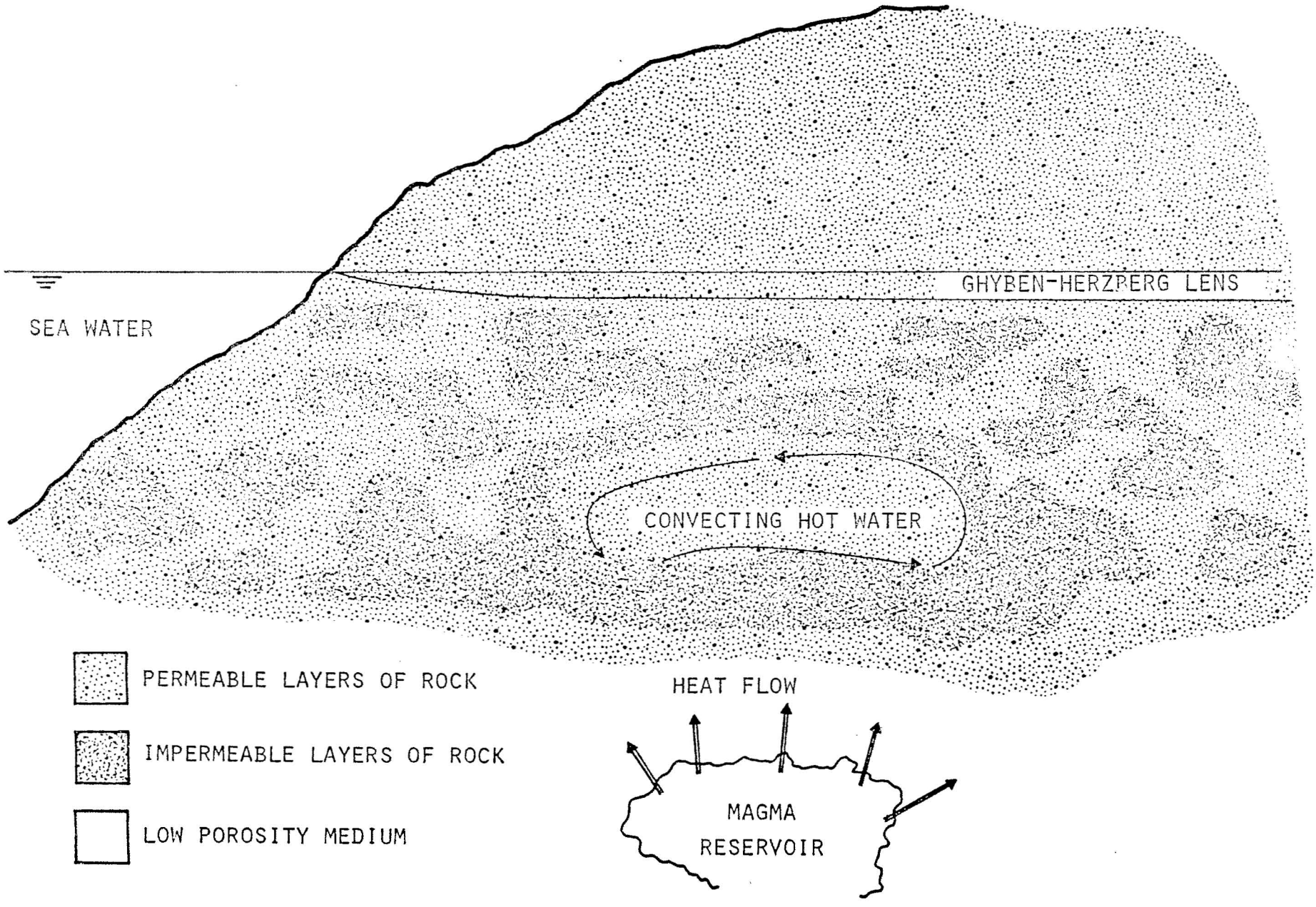

FIG. 3.1-31 SELF-SEALED / DEPLETABLE GEOTHERMAL RESERVOIR

within the porous island medium. The supposition advanced, therefore, is that Hawaiian geothermal reservoirs resemble Fig. 3.1-31 with the heat source being magma at depth, which with time either: 1) induced abnormally high circulation rates resulting in flashing or thermal deposition, effectively capping the reservoir, perhaps even above sea level; or 2) intruded above the magma chamber and released energy to the surrounding aquifer, in effect forming a system composed of a cooling, vertical dike surrounded by hot fluid, which through the physical phenomenon as described in "1" has been capped into a self-sealed reservoir. In the latter case, Fig. 3.1-31 needs to be modified to show a vertical low permeability formation within the convecting geothermal fluid.

Although it has been reported that hot water reservoirs are twenty times more prevalent than vapor-dominated ones [13], technical difficulties in the former have resulted in considerably more production from the latter. Table 3.1-1 shows that five vapor, eleven hot water, and two binary cycle plants are either operating or close to completion. The hot rock concept is undergoing investigation by researchers from the Los Alamos Scientific Laboratory (for New Mexico). Finally, a fourth concept, direct utilization of magma, was originally advanced by George Kennedy and David Griggs in 1960 [14]. A recent conference on volcano energy supported the reasonability of this latter scheme [15]. Some preliminary work, mostly in the proposal stage, is being advanced by researchers from Sandia (New Mexico), Lawrence Livermore Laboratory, and the University of Hawaii.

When calculating the usable energy in a geothermal reservoir, one should be aware that only 1% of the total available energy can be converted to electrical energy from a hot-water reservoir using present proven technology. The equivalent figure from a vapor-dominated reservoir is 2-5% [6]. It should nevertheless be realized that on an absolute energy scale, a self-sealed liquid-dominated reservoir, per cubic foot of reservoir, will produce more energy than a vapor-dominated one. A quick comparison of water and steam densities bears this out. Secondly, the thermal conductivity of rock precludes conduction as a mechanism for regenerating a geothermal well. For example, H. Ramey has reported that the net heat recharge rate in the Big Geysers is less than 0.6% [16]. However, the possibility of extraordinary fluid convection through porous media as driven by circulating magma should not be discounted--thermal cracking of the receding,

TABLE 3.1-1 GEOTHERMAL PLANTS

DRY STEAM PLANTS	MW CAPACITY	INITIAL OPERATIONS
Italy		
Lardarello	380	1904
Monte Amiata	26	1967
U.S.A.		
Geysers, California	502	1960
Japan		
Matsukawa	20	1966
Hachimantai	10	1975

FLASHED STEAM PLANTS	MW CAPACITY	INITIAL OPERATIONS
New Zealand		
Wairakei	192	1958
Kawerau	10	1969
Japan		
Otake	13	1967
Hatchobaru	50	late 1970's
Mexico		
Pathe	3.5	1958
Cerro Prieto	75	1973
Iceland		
Namafjall	3	1969
Hengrill	13-32	late 1970's
Philippines		
Tiwi	10	1969
USSR		
Pauzhetsk	6	1967
El Salvador		
Ahuachapan Field	30	1975

BINARY CYCLE PLANTS	MW CAPACITY	INITIAL OPERATIONS
USSR		
Paratunka	1	1967
U.S.A.		
Imperial Valley, California	10-50	1975-1980

cooled magma can possibly result in high permeability. Unfortunately, unless the magma chamber is extremely large or self-sealing occurs, this energy will quickly dissipate with recharging meteoric water.

Under present economic and technical conditions a viable geothermal reservoir is generally one which: Has a minimum temperature of 356°F (180°C)--to conform to current steam turbine design, is located within 10,000 feet (3,050 m) from the surface, and can produce steam at a minimum rate of 40,000 lb/hr (18,120 kg/hr) with a 9-5/8 inch (24.4 cm) diameter hole. Geothermal wells not quite satisfying the above criteria can nevertheless be used for special applications, as for example, the 158°F (70°C) binary system in the U.S.S.R. Furthermore, there is every reason to believe that wells exceeding 10,000 feet (3,050 m) will, with improved drilling technology and increasing energy fuel prices, become economically feasible.

The general nature of a geothermal reservoir is contentious. The question of its being self-sealed or regenerative has not been completely answered.

INTERNATIONAL QUESTIONNAIRE

A questionnaire on the nature of geothermal reservoirs and well testing and analysis was sent to a number of workers in the field. Over twenty replies were received from companies, institutions, and government agencies from all of the prominent geothermal energy nations. While some of the responses were received through oral communication, the majority of them were in the form of personal written correspondence. Many of the individuals chose to answer the questions by citing published technical literature. All responses were evaluated and the most appropriate ones were tabulated in a matrix arrangement as shown in Table 3.1-2. This table should be a convenient guide for quick reference to geothermal reservoir engineering.

WHAT IS A GEOTHERMAL RESERVOIR ENGINEER?

To obtain an appreciation of the field of geothermal reservoir engineering, a quick attempt at defining what is a geothermal reservoir engineer (GRE) is appropriate. The diversity of functions the GRE is expected to perform makes it imperative that he has a multi-disciplinary background. As the GRE will be working with geologists, geophysicists, geochemists, drilling engineers, hydrologists, thermodynamicists, fluid dynamicists, mathematicians, lawyers, computer scientists, and economists, it is important that the GRE has an acquaintance with each field so that he can better communicate with these

TABLE 3.1-2 RESPONSES TO INTERNATIONAL QUESTIONNAIRE

NAME AND AFFILIATION	WHAT IS THE NATURE OF A GEOTHERMAL RESERVOIR	WELL TESTING AND ANALYSIS HARDWARE	SOFTWARE
B. C. McCabe Magma Power Company USA	In geothermal reservoir engineering, the theoretical information to determine the size or longevity of a geothermal field is a very inexact science. For steam and hot water reservoirs, no one knows what the % of replaceable heat is coming into the reservoir in proportion to the amount being withdrawn. Probably, the replacement heat is much greater than it is generally imagined.	No reply	No reply
W. K. Summers New Mexico Bureau of Mines USA	Geothermal fluids consist of two components: 1) meteoric water and 2) gases (H_2S and CO_2), rising from great depths. The mixture of the components occur in fractures. If the fractures are sufficiently close together, a well will produce routinely. Otherwise, only occasional wells will produce.	Petroleum or groundwater hydrology equipment can be used, as modified to incorporate temperature.	Computer technology is generally adequate, but software is dependent on adequate sampling of the flow continuum and the proper incorporation of the parameter temperature.
Giancarlo E. Facca Registered geologist Italy and USA	Geothermal fields are composed of: 1) a deep sequence of layers, heated by an underlying magmatic stock and which, in turn, heats the overlying porous strata, and 2) a very permeable layer with thickness, porosity and permeability of such an order as to allow the formation and the permanence of a system of convection currents in the water filling the pores of the rock, and 3) an impermeable layer over the reservoir.	Refer to United Nations and UNESCO publications [28, 29, 30, 31, 32].	Refer to United Nations and UNESCO publications [28, 29, 32, 33, 34, 35].

TABLE 3.1-2 (CONTINUED)

W. E. Allen Oil and Gas Conservation Commission (Arizona) USA	References 28 - 38.	References 28 - 38.	For the purpose of predicting well performance, there are no marketing companies in Arizona.
Robin Kingston Kingston, Reynolds, Thom, and Allardice, Ltd., New Zealand	Refer to United Nations publications in References 28 - 38.	Refer to articles by D.K. Wainwright [36] and A.M. Hunt [29].	Prediction of well performance is a composition of permeability, temperature, reservoir capacity, and rate of flow. Permeability in geothermal terms depends on fracture zones much more than on porosity. Oil reservoir assessment techniques can in some applications be modified for geothermal applications.
Enrico Barbier International Institute for Geothermal Research Italy	Refer to United Nations and UNESCO publications [37, 38].	Equipment and other hardware are generally not avaialble.	The evaluation of the quality of a geothermal well is uncertain. Analogies are generally made with existing wells.
J. L. Guiza Geothermal Resources Cerro Prieto Mexico	Geothermal fields are classified into two major groups: 1) sedimentary fields and 2) volcanic fields. In a sedimentary field the productive strata is a permeable sandstone interbedded by impermeable clay layers. The sandstone is saturated with meteoric water, and the heat flow is due to the faults and fissures of the granitic basement. In volcanic fields the possible production mechanism is due to the water flow through fissures in the volcanic rocks being heated by a cooling magmatic body.	For the determination of reservoir parameters such as permeability index and porosity, the synergetic log named SARABAND is used. For temperature, pressure, and flow measurements the conventional systems (Kuster RPG and KTG instruments) are employed.	The performance in a well can be predicted by means of a hydrologic model modified by the temperature effect and taking into account the physical characteristics of the productive sandstone as well as the physical-chemical properties of the geothermal fluids. For the purpose of optimizing well locations, computer programs are used to simulate field production.

specialists, better understand the interrelationships and complexities, and know when to consult them. As an example, the GRE must develop the geologist's cognizance of sediments and other underground conditions--the chemist's knowledge of chemical properties and electrical conductivity--the mechanical engineer's grasp of the associated hardware--the chemical engineer's familiarity with reservoirs--the civil engineer's competence at analyzing porous media--the mathematician's flexibility with numerical analysis and computer programming--the lawyer's understanding of certain statutes--the economist's overview of the financial implications.

A GRE must be trained. The ideal starting point is an engineer who has had exposure to petroleum well testing and analysis. If reservoir experience has been nil, a reasonable training program would involve several short courses on reservoir engineering and well test analysis combined with on-the-job experience at a geothermal well site. Hands-on training is essential.

In preparation for the above training, the prospective GRE should acquaint himself with the following publications:

1. Joseph Barnea, "Geothermal Power," *SCIENTIFIC AMERICAN*, Vol. 226, January, 1972.
2. H. Cristopher Armstead, Editor, *GEOTHERMAL ENERGY*, UNESCO, Paris, 1973.
3. Paul Kruger and Carel Otte, *GEOTHERMAL ENERGY*, Stanford Press, 1973.
4. B.C. Craft and M.F. Hawkins, *PETROLEUM RESERVOIR ENGINEERING*, Prentice-Hall, 1959.
5. C.S. Matthews and D.B. Russell, *PRESSURE BUILDUP AND FLOW TESTS IN WELLS*, Society of Petroleum Engineers of AIME, 1967.
6. *NEW SOURCES OF ENERGY, PROCEEDINGS OF THE CONFERENCE*, Rome, 21-31 August, 1961, Vol. 2 and 3.
7. *GEOTHERMICS* (All proceedings and regular publications).
8. American Petroleum Institute, *WELL TESTING*.
9. American Petroleum Institute, *WIRELINE OPERATIONS AND PROCEDURES*.

If a more comprehensive formal course on geothermics is desired, Japan has a three-month course and Italy has one that lasts for nine months. Both courses are taught in English.

So what is a geothermal reservoir engineer? He is many things at once and never everything he might want to be. The field is so multidisciplinary that the ideal GRE is one who always knows less than the individual specialists on a given

topic, but because he can bring perspective into the picture, he is a necessary interfacer, integrator, and synthesizer.

GEOTHERMAL RESERVOIR ENGINEERING: WELL MEASUREMENT AND ANALYSIS

Geothermal reservoir engineering begins with exploration and progresses through stages of drilling, well testing, analysis and performance prediction. Investigators in the engineering phase of the program have worked closely with the geophysical effort in activities that impact engineering. The "well test analysis" team has progressed in two well-defined but closely interrelated sequential areas. Close to completion is a master's thesis on formation evaluation, the interface region connecting geophysics and engineering. This initial probe has categorized the various techniques utilized in geophysical exploratory programs, especially with respect to engineering relevant data. All activities in the region of the geothermal well, from speculations into most probable reservoir configurations to fluid flow properties in the well itself, to measurement of the necessary parameters, have been considered. Study #2, well test analysis, logically extends the first. Methods used by the petroleum industry have been studied for adaptation to geothermal fluids.

The purpose of a reservoir engineering study is to collect enough information to reveal the nature of the reservoir and to determine the pertinent physical parameters which control the behavior of fluids in the reservoir. Some of the questions that need to be asked are:

What are the temperature and pressure ranges of the fluid?

What is the nature of the fluid; i.e., vapor, liquid or a mixture of both?

What is the chemical composition of the fluid?

What is the expected production rate and expected life of the reservoir?

After the geologists and geophysicists have decided on the drill site and drilling has commenced, a reservoir testing program should be outlined. Well tests are performed in two phases. In the first phase tests are performed during open-hole drilling operations. They consist of fluid temperature measurement, fluid sampling, core analysis, and formation logging. After completion, the producing well must undergo a second phase of tests to determine the thermodynamic condition of the fluid and the adequacy of the reservoir. Measurements are taken both at the wellhead and downhole.

1. Hardware

The following list outlines the hardware to adequately measure a geothermal reservoir [14, 17-21].

A. Subsurface formation condition

Permeability: resistivity logs, core sampling.

Porosity: resistivity logs, core sampling, density logs, neutron logs, sonic logs.

Water saturation: resistivity logs, porosity measurements.

B. Evaluation of well casing: inclination for deviation survey, wellbore calipering, casing condition.

C. Downhole fluid condition

Pressure: Amerada-Kuster RPG-3 gauge, pressure transducer, gas purge tube with pressure element.

Temperature: expansion thermometer, resistance thermometer thermocouple, geothermograph, maximum registering thermometer, temperature sensitive paint, metal, and ceramic pellets.

Flow rate: mechanical spinner, electronic flowmeter.

Fluid sampling: Kuster sampler, Schlumberger sampler, gas purge tube with fluid sampler.

D. Surface fluid condition

Pressure: aneroid barometer, mercury column, glass manometer, pressure recorder.

Temperature: filled thermal measuring systems, resistance bulbs, thermocouples.

Flow rate (and enthalpy): separator, orifices, and weirs for separate vapor and liquid flow, beta ray, gas method, magnesium sulfate injection, critical lip pressure, conductivity, calorimetry.

In fluid measurement the data obtained from one particular downhole instrument are not always reliable due to its operational characteristics. Combined readings from two or more instruments for a certain parameter are desirable to predict a specific subsurface condition. Data generated from these measuring devices are cross-verified to determine the probable downhole condition.

A study was made on the costs involved in well parameter measurement. Table 3.1-3 lists the equipment required for a simple temperature/pressure/flow program. For comparison purposes, the bottom half of Table 3.1-3 reveals the contract cost of a typical comprehensive testing program. Initially,

TABLE 3.1-3 EQUIPMENT COST

KUSTER SUBSURFACE INSTRUMENTS

1	KPG pressure gage, complete, clock, tools, charts, calibration table	$ 1,575.00
1	KTG temperature gage, complete, clock, tools, charts, calibration table	1,675.00
1	2-way chart reader, complete	1,146.00
1	Sampler, complete	≃ 1,000.00
1	Spinner gage	≃ 1,000.00
1	Measuring line reels (hoists)	≃ 2,000.00
	Accessories and spares:	
2	Spare clocks	800.00
100	O-rings, high temperature	40.00
5	Thread lubricant	7.50
20	Filters	15.00
10	Maximum registering thermometers	188.50
	Total	≃ $ 9,447.00

FORMATION LOGGING (APPROXIMATE TOTAL COST FOR A TWO KILOMETER DEEP BOREHOLE CAN BE AS HIGH AS $112,000.)

Induction log

Lateral log

Spontaneous potential

Sonic log

Gamma density log

Neutron density log

well testing will be contracted out to a company such as Schlumberger or Rogers Engineering. These companies have the equipment and know-how to run a thorough measurement and analysis program. Eventually, as testing becomes routine, equipment should be purchased to locally run temperature/flow tests.

A comparison was made of the measurement techniques used by Keller at Kilauea and the Schlumberger Company at Test Well Mesa. Table 3.1-4 summarizes this comparison.

2. Analysis

Although the two types of analyses to be described are closely related, they are being separated because part "a" is the classical method used by geologists and petroleum engineers. This technique has an empirical foundation and is not conducive to the analytical/computer solutions to be developed in part "b."

a. Formation Evaluation

The proper interpretation of data from well tests will determine the feasibility of utilizing a geothermal well. Both open-hole non-flowing and cased-hole production tests are used to aid in characterizing a reservoir. The required data includes formation thickness, permeability, porosity, water saturation, viscosity, compressibility, fluid and rock density, temperature and formation fluid pressures. The values for these parameters can be obtained in different ways depending upon the developmental phase of the well. For practical purposes, it is important to understand the ways in which these values are obtained.

The most common parameters calculated in formation evaluation are porosity, water saturation and permeability. The equations used below have been developed mainly for oil-field interpretation where NaCl is generally the dominant salt in the solution. As it is assumed that the formation fluid on the island of Hawaii is brackish, these equations should be valid.

Water saturation, S_w, in terms of resistivities can be expressed by the Archie [20] formula, as

$$S_w = \frac{R_i/R_t}{R_z/R_w} \qquad (1)$$

TABLE 3.1-4 COMPARISON OF WELL TEST METHODS

Hardware and Method		Measured Parameter
Hawaii	Imperial Valley	
1. Spontaneous Potential (SP) 2. Induction Log (IL) 3. Lateral Log (LL)	1. Dual Induction Laterol Log (combination of SP, IL & LL)	Formation Resistivities
1. Sonic 2. Gamma Density 3. Neutron Density	1. Sonic 2. Gamma Density 3. Neutron Density	Formation Porosities
1. Thermistor Probe 2. Maximum Registering Mercury Thermometer 3. Wireline RTG Temperature Gage (Kuster)	1. Maximum Registering Mercury Thermometer 2. Wireline Amerada RTG Gage	Formation Temperature
1. Wireline RPG Pressure Gage	1. Wireline Amerada RPG Gage	Formation Pressure

where R_t is obtained from a deep-investigation device such as a lateral log; R_i is taken as the resistivity from a shallow-investigation device such as an induction log; R_w is taken as the resistivity from a spontaneous potential device and R_z is equal to $\frac{R_w R_{mf}}{ZR_{mf} + (1-Z)R_w}$. R_{mf} is obtained from a regular induction tool. Z is the fraction of invaded zone pore water that is formation water, and 1-Z is the fraction that is mud filtrate. For normal cases of invasion Z is taken as 0.075. If the formation is deeply invaded a value of 0.035 is preferred.

Water saturation can be applied to determine the fraction of pore volume occupied by formation water. If S_w approaches 1.0, the formation is completely saturated with water. Equation (1) and the resistivity relations have been incorporated into a chart by the Schlumberger Company [20] as shown in Fig. 3.1-32.

Porosity can be calculated from the following relation

$$\phi = \left(\frac{a}{F}\right)^{\frac{1}{m}} = \left(\frac{aR_w}{R_t S_w^2}\right)^{\frac{1}{m}} \qquad (2)$$

This formula was again proposed by Archie [20] where ϕ is fractional porosity and m and a are constants depending upon the type of formation.

For Hawaii, Keller[12] suggests that the constants in equation (2) are, a = 18 and m = 1.05. The relation is shown in chart form in Fig. 3.1-33. A sample calculation is helpful in illustrating the use of both charts.

The following resistivities were obtained at Kilauea Summit at a depth of about 1600 ft.

R_{mf} = 0.2 Ohm-meter
R_w = 0.08 "
R_i = 48.0
R_t = 80.0 "

Since mud infiltration was moderate, a Z value of 0.075 is assumed. Then R_i/R_t = 48.0/80.0 = 0.6 and R_{mf}/R_w = 0.2/0.08 = 2.5. From Fig. 3.1-32 S_w is approximately equal to 30%. Using this water saturation value and R_t/R_w = 80.0/0.08 = 1000, we obtain a porosity of 21.6% from Fig. 3.1-33.

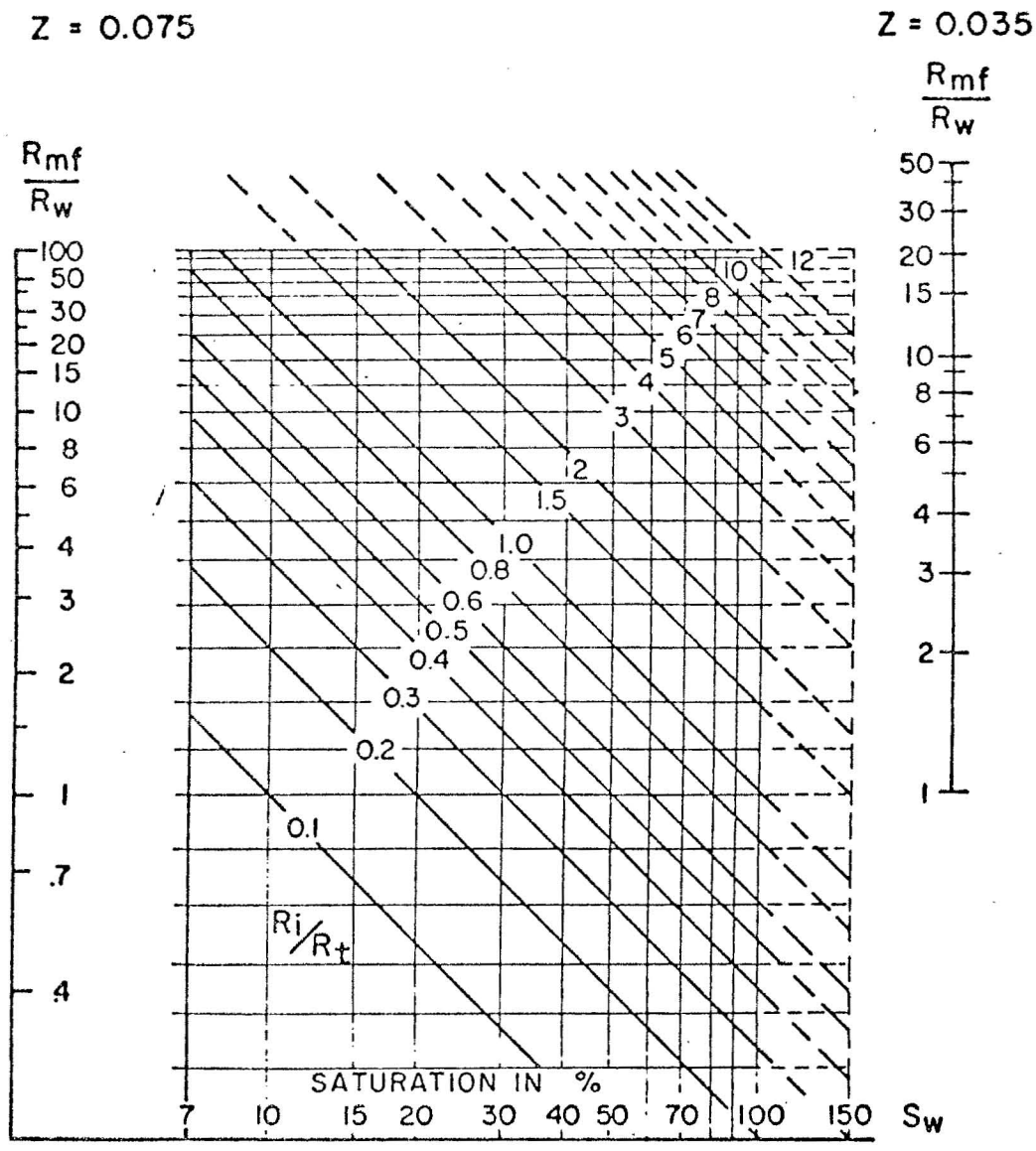

FIG. 3.1-32 RESISTIVITY RATIO CHART TO DETERMINE WATER SATURATION
REF. [20]

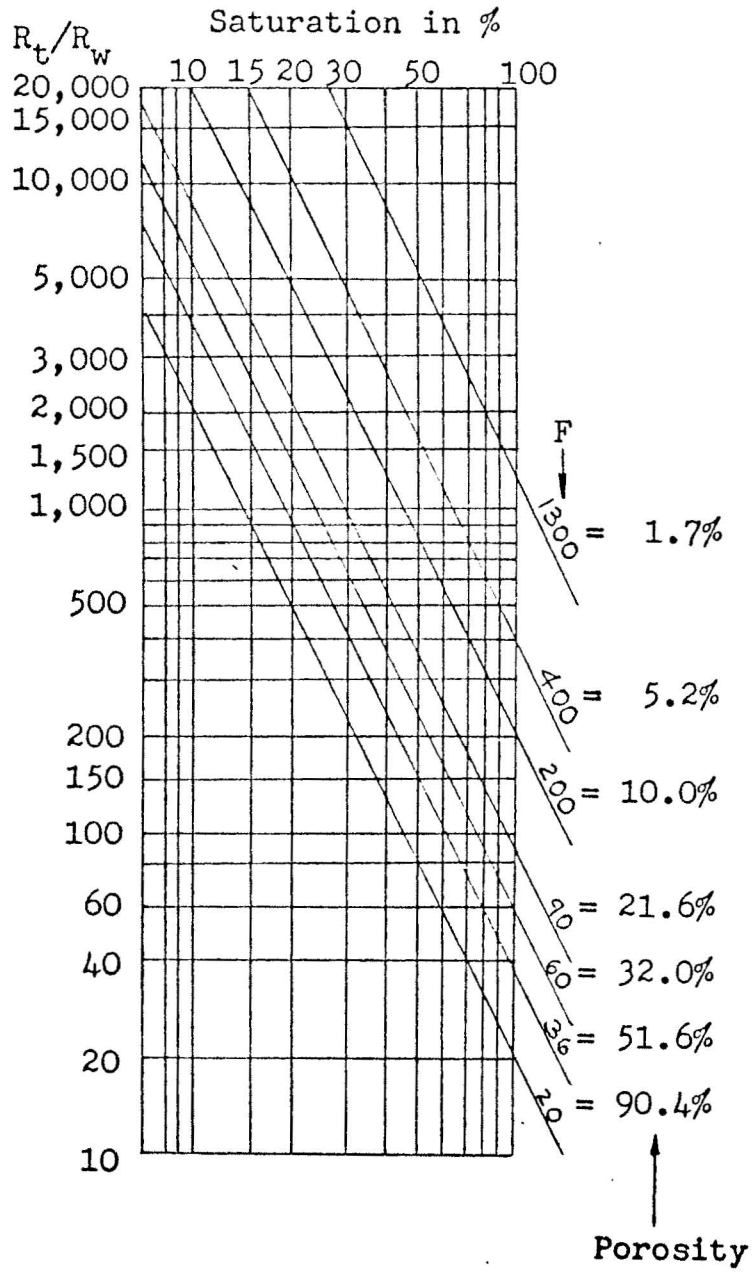

FIG. 3.1-33 POROSITY DETERMINATION FROM EMPIRICAL RELATIONS

This porosity can then be used in the following relation to obtain permeability

$$K = C\frac{\phi^x}{\left(\frac{c'}{\phi}\right)^y} \tag{3}$$

In formations composed of sand, x and y are generally equal to 3.0 and 2.0, respectively. C is equal to 79 for gases and 250 for oils. Typically, the quantity $\left(\frac{c'}{\phi}\right)$ has a range of values from 1.0 to 0.50 depending upon c' at any given value of ϕ. This constant is influenced by the rock type and its grain size. Although permeabilities can be calculated by this relation, a greater accuracy is possible by performing a pressure drawdown test analysis during well production conditions.

Formation porosities are also obtainable by sonic and radioactive devices. For the sonic log the Wyllie formula [20] is

$$\phi_s = \frac{\Delta t_{log} - \Delta t_{ma}}{\Delta t_f - \Delta t_{ma}} \quad . \tag{4}$$

The values of Δt_{ma} range from 40 to 70 sec/ft depending upon the type of formation. A typical value of Δt_f is 70 sec/ft while brines exhibit values in the neighborhood of 190 sec/ft. Since sonic logs measure primary porosities only, its range of values is usually low, between 2 to 10%.

The radioactive density log relation is similar to the sonic log. The empirical relation is

$$\phi_D = \frac{\rho_{ma} - \rho_b}{\rho_{ma} - \rho_f}$$

The density of matrix rocks, ρ_{ma}, is typically about 2.65 gms/cc and the fluid density ρ_f, for water is approximately 1.0. The measured density, ρ_b, then gives the value for total porosity ϕ_D. The difference in values between total porosity and primary porosity is secondary porosity or fracture porosity. However, the commonly used parameter in reservoir analysis is total porosity.

In the Imperial Valley, porosities are greater than 25% in the production zone. Porosities at Kilauea Summit fluctuate from a low value of 2% to a high of 30% over the depth of the borehole. Well specialists suggest that porosities in the range of 20% to 30% are desirable in the production zone for adequate flow rates.

In early logging the previously described analytical methods were done manually to obtain the desired subsurface information. However, with significant advances by well service companies, the process is now performed by applying computer programs for specific types of formations. The two common types of complete open-hole interpretation programs are the SARABAND and the CORIBAND techniques, both developed by the Schlumberger Company. SARABAND is applicable for shaley sands while CORIBAND is used primarily for complex lithologies.

b. Well Test Analysis

In order to evaluate a geothermal reservoir, whether it be drilling, development or production, various data on certain parameters are needed. These include formation thickness, permeability, porosity, viscosity, compressibility, thermal conductivity, fluid and rock density, temperature and formation average pressure.

Pressure is a particularly important parameter for use in materials heat balance calculations of geothermal liquid in place and determination of reservoir characteristics: compressed liquid, saturated liquid and steam or superheated steam. Finally, extrapolation into the future is best made by using the method which relates future production to future average pressure.

1) Mass Balance

$$W_c = W - W_P - W_L + W_e \qquad (5)$$

where W_c = current mass in reservoir, lbs.

W = initial mass in reservoir at the start of production, lbs.

W_P = mass produced, lbs.

W_L = mass lost via springs, wild wells, etc., lbs.

W_e = mass influx through aquifer, lbs.

2) Volumetric Balance

$$V\phi = (W - W_p - W_L + W_e)\ \left(x(v_g - v_f) + v_f\right) \qquad (6)$$

where V = reservoir bulk volume, ft^3

ϕ = porosity, fraction of bulk volume

x = steam quality in reservoir, mass fraction of fluid which is steam

v_g = specific volume of steam, ft^3/lb

v_f = specific volume of liquid water, ft^3/lb

3) Heat Balance

$$W_c h_c + (1 - \phi)\, V\rho_r C_r\, (T - T_o) = Wh_i + (1 - \phi)\, V\rho_r C_r\, (T_i - T_o)$$

$$- W_p h_p - W_L h_L + W_e h_e + Q_s \qquad (7)$$

where h_c = average enthalpy of total fluids in reservoir, btu/lb

h_i = average enthalpy of initial fluids in reservoir, btu/lb

h_p = average enthalpy of produced fluids, btu/lb

h_L = average enthalpy of lost fluids, btu/lb

h_e = average enthalpy of liquid water influx, btu/lb

ρ_r = formation density, lb/ft^3

C_r = specific heat of formation, btu/lb-F

T = current reservoir temperature, F

T_i = initial reservoir temperature, F

T_o = some reference temperature, F

Q_s = net heat conducted into reservoir, btu

The average enthalpy of any liquid-steam combination can be expressed by:

$$h = x(h_g - h_f) + h_f$$

where h = enthalpy of steam quality x, btu/lb

h_g = enthalpy of saturated steam, btu/lb

h_f = enthalpy of saturated liquid, btu/lb

Then with equations (5), (6), and (7) it is possible to solve for a set of unknowns (i.e., W--initial mass, T_i--initial temperature). The other parameters can be obtained through the production data or by estimations based on other geothermal wells.

In general, the well measurement program will obtain the average pressure of the reservoir vs. cummulative production in order to predict any future performance.

4) Background Material

a) Dimensionless Equations

$$t_D = \frac{kt}{\phi\mu C_t r_w^2} \tag{8}$$

$$r_D = \frac{r}{r_w} \tag{9}$$

$$P_D = \frac{2\pi kh}{g\mu} (P_i - P_{r,t}) \tag{10}$$

where k = permeability, md
t = time, hr
ϕ = fractional porosity
μ = viscosity, cp
C_t = total system effective total isothermal compressibility, psi^{-1}
r_w = well radius, ft
r = distance from well, ft
h = formation net thickness, ft
g = production, std bbl/day
P_i = initial pressure, psi
$P_{r,t}$ = pressure @ r ft, time t hrs, psi

b) Line Source Solution with Infinite Reservoir

Fluid flow through porous media is generally considered to be laminar with the exception of flow near the well. The basic equations used are the law of conservation of mass, Darcy's Law and equation(s) of state. With the following assumptions: 1) small pressure gradient, 2) small and constant fluid compressibility, 3) isometric rock properties, the governing equation is

$$\frac{1}{r}\frac{\partial}{\partial r}\left(r\frac{\partial p}{\partial r}\right) = \frac{\phi\mu}{k} c_t \frac{\partial p}{\partial t} \tag{11}$$

Solving with

initial condition: $p = p_D$ @ $t_D = 0$ for all r_D

boundary condition: $\lim_{r_D \to \infty} P_D(r_D, t_D) = 0$

$$\lim_{r_D \to 0} \left(r_D \frac{dp_D}{dr_D}\right) = -1$$

$$P_D(r_D t_D) \approx \frac{1}{2}\left[\ln \frac{t_D}{r_D{}^2} + 0.80907\right] \tag{12}$$

where $\frac{t_D}{r_D{}^2} > 70$

Once we have the relationship between P_D and t_D/r_D2, we can obtain the real pressure term $p_{r,t}$ @ any location and time.

c) Interference Test

"Interference" means the production of one well causing a detectable pressure drop at an adjacent well. The most simple case of interference is when pressure drop is measured at a shut-in well.

To perform the interference test data analysis, the technique of type curve matching is developed.

$$\log_{10} p_D = \log_{10} \frac{2\pi kh}{9\mu}(p_i - p_{r,t})$$

$$= \log_{10}\left(\frac{2\pi kh}{9\mu}\right) + \log_{10}(p_i - p_{r,t}) \tag{13}$$

Then, the plot of p_D and $(p_i - p_{r,t})$ will be the same on log-log paper with the difference using a constant term. A plot of the logarithm of the real pressure differences must look exactly like a graph of the logarithm of p_D as long as the same size log cycle is used.

The procedure for the interference data analysis is as follows:

(1) Graph the pressure drop at the observation well vs. time.

(2) Position the field data curve over the type curve and move it keeping axes parallel until the field data matches the line source solution.

(3) Read a "match point" as the corresponding coordinates of any point common to both graphs, while aligned.

(4) From the pressure and time match we will be able to determine the values of two reservoir parameters (i.e., permeability and porosity).

d) Skin Effect

Physically, the skin effect is a combination of invasion by drilling fluids, dispersion of clays, presence of a mud cake and of cement, presence of condensation near a steam well, partial well penetration, limited perforation and even stimulation treatment such as acidization or hydraulic fracturing.

The skin effect may be positive, negative, or zero. If the well is damaged, s(skin effect) will be positive. If the well is stimulated, s will be negative. However, if the permeability in the skin zone is the same as in the rest of the formation, then s will be zero. Also note that skin effect comes into play only if one wants the pressure measured at or near a well.

e) Bounded Reservoir

Unfortunately no reservoirs are infinite in size and most large reservoirs have more than one well. Therefore, all wells more or less have a finite reservoir volume from which fluids are drained.

The drainage area of many wells tends to be more of a square or rectangular shape than circular.

Equation (12) can be expressed as

$$p_D(t_{DA}) = \frac{1}{2}\left[\ln\frac{4At_{DA}}{\gamma r_w^2}\right] \qquad (14)$$

$$t_{DA} = \frac{0.000264\ kt}{\phi\mu c_t A} = t_D\,\frac{r_w^2}{A}$$

γ = exponential of Euler's constant $\cong$ 1.781

@ $t_{DA} \leq 0.05$, the effect of the boundaries is not felt at the well which behaves like a well in an infinite reservoir.

One notices that for a bounded reservoir, i.e., where no fluids cross the boundary, the dimensionless pressure increases rapidly as $t_{DA} \geq 0.1$. This obviously is due to the depletion of fluids throughout the reservoir. On the other hand for a constant pressure reservoir,

the dimensionless pressure approaches a constant which is due to the replenishment of fluids through the boundary.

At steady-state, the dimensionless pressure at the well in the water of a constant pressure square is

$$p_D = \frac{1}{2} \ln \frac{16A}{\gamma C_A r_w^2} \quad , \quad t_{DA} \geq 0.25 \tag{15}$$

C_A = shape factor for a well in a closed square, 30.88

At pseudo steady-state, the linear equation for dimensionless pressure at the well in the center of a bounded square is

$$p_D = \frac{1}{2} \ln \left[\frac{4A}{\gamma C_A r_w^2} \right] + 2\pi t_{DA} \quad , \quad t_{DA} \geq 0.1 \tag{16}$$

Equations (15) and (16) are perfectly general equations for all different shapes of reservoirs and well locations, if the shape factor C_A can be determined.

f) Pressure Drawdown Test

A pressure drawdown test is a series of bottom-hole pressure measurements made during a period of constant producing rate flow. Prior to the flow test, the well is usually shut-in to allow the pressure to be equalized throughout the formation. Drawdown tests are normally run on new wells or after a well has been shut-in for a long period.

The following is a summary of the drawdown test analysis procedure.

(1) Plot p_{wf} (bottom-hole flowing pressure) vs. $\log_{10} t$, find correct semilog straight line, slope, m and p_{1hr}. It may at times appear to have more than one possibility for a straight line. Suggested procedure is to plot $(p_i - p_{wf})$ vs. t on log-log type paper and compare with the line source solution type curve to determine the onset of the correct straight line.

(2) Find k, s, Δp_{skin} (real pressure drop due to skin effect) and FE (flow efficiency) with the appropriate equations.

g) Pressure Buildup Test

The pressure buildup test is the most important well test in reservoir engineering because it yields a great deal of information, such as, permeability, skin effect, and, perhaps most important of all,

the static average pressure in the drainage area with respect to the Matthew-Brons-Hazebroek function.

$$p_{D_{MBH}} = \frac{bh}{70.65g\mu\beta}(p^* - \bar{p})$$

$$= 4\pi t_{DA} - 2p_D(t_D) + \left[\ln t_D + 0.80907\right] \qquad (17)$$

p* (false pressure) is the pressure extrapolated to infinite shut-in time.

$$p_{D_{MBH}} = \ln\left(\frac{t + \Delta t}{\Delta t}\right) p_{ws} = \bar{p} \qquad (18)$$

Then from plots of $p_{D_{MBH}}$ vs.Δt_{DA} (Mathew-Brons-Hazebroek Function) for various drainage shapes one can get the average pressure.

The following is a summary of pressure buildup analysis by the Horner graph method:

(1) Plot p_{ws} (downhole well static pressure) vs. $\log_{10}\left(\frac{t+\Delta t}{\Delta t}\right)$, find m (slope), p_{1hr}, p* at $\frac{t+\Delta t}{\Delta t} = 1$. At times it may seem to have more than one possibility for a straight line. The suggested procedure is to plot $(p_{ws} - p_{wf})$ vs. Δt on log-log type paper and compare with the line source solution type curve to determine the onset of the correct straight line.

(2) Calculate k, s, Δp_{skin}, and FE with the appropriate equations.

(3) For $\bar{p}$:

  (a) Calculate t_{DA}, the dimensionless produced time.

  (b) Determine the drainage shape and well location.

  (c) Find $\bar{p}$ by going to a MBH pressure function plot.

In the general sense, software encompasses both computer programs and the standard type curve analysis. It appears that the methods of analysis used in the petroleum and gas industries cannot be naively applied to geothermal systems. A geothermal reservoir has temperature as the dominant parameter. Most petroleum reservoir analyses are based on isothermal conditions. Whiting [5] and Ramey [16] have successfully demonstrated that the regular volumetric balance method in petroleum engineering does not apply to geothermal reservoirs, but rather a material and energy balance method is needed. However, in most cases, the principles of

petroleum reservoir engineering for single-phase liquid flow can be applied with certain modifications to hot water reservoirs [22]. In the same manner, there is a kind of one-to-one analogy for the gas industry and vapor-dominated wells. Alas, nature is unprovidential, as the majority of reservoirs are steam-flashed, or two-phase. Two-phase well prediction is an extremely challenging and fruitful area for research.

Well test analysis, though rapidly developing, can perhaps best be summarized by quoting Alex Muraszew, writing on "Geothermal Resources and the Environment," in the 1972 *Geothermal World Directory* [23],

> "....with the present state-of-the-art, neither the capacity of the reservoir nor its longevity can be accurately predicted...."

III. Physical Modelling

Investigators: P. Takahashi & B. Chen

The physical model is a necessary balance to the ongoing software investigations. The physical model will not only serve as a convenient check on the math model, but will simulate conditions not easily attempted by software. The obejctives of the initial physical model studies will be to bring together known information about related laboratory studies, analyze the state-of-the-art, design the hardware system required for simulation, and initiate fabrication and preliminary tests.

Very little physical modelling work has been reported in the literature. The significant studies related to geothermal reservoirs include those of G. Cady [24], F.G. Miller [25], H. Henry and F. Kahout [26], and the remotely related work of J. Bear [27]. However, none of the reported investigations approached the problem on a total systems basis while considering the high [2012°F (1100°C) for magma, 527°F (275°C) at wellhead] temperatures expected.

In movement of fluid through a geothermal reservoir, the driving force is primarily the buoyant force. This force is created by heat within the geothermal system which decreases the fluid density. The dimensionless number determined to be of prime interest to the study is the Rayleigh Number (N_{Ra}). The Rayleigh Number is the product of the Grashof (N_{Gr}) and Prandtl (N_{Pr}) Numbers, where

$$N_{Gr} = \frac{\text{buoyant force}}{\text{viscous force}} \qquad (19)$$

To insure similarity between the physical and mathematical models and the actual reservoir, a modified Rayleigh number will be used. This dimensionless number is defined as follows:

$$\text{mod Ra} = \text{Ra}\,\frac{k}{L^2} \tag{20}$$

where Ra = Rayleigh No.
k = permeability (units of length squared)
L = characteristic length

since

$$\text{Ra} = \frac{\beta g \Delta T L^3}{\alpha \nu} \quad , \tag{21}$$

$$\text{mod Ra} = \frac{\beta g \Delta T L K}{\alpha \nu} \tag{22}$$

where β = coefficient of thermal expansion
α = thermal diffusivity
ν = kinematic viscosity
g = gravitational constant
ΔT = difference in temperature between the reservoir and ocean
L = height of aquifer

Convection is initiated at a modified Rayleigh number of 40; mod Ra's up to 1,000,000 can be expected for actual conditions in Hawaii. Calculations showed that it is possible to obtain mod Ra's up to 1,000 using the full scale unpressurized model (see Table 3.1-5). This model is tentatively planned to have a seawater capacity of 450 gallons, a variable (in size and temperature) heat source and glass bead permeable medium. As the model will be two dimensional, one face will be used to insert temperature measurement devices to obtain the temperature profile.

Three glass bead mesh sizes will be used to vary permeability (see Table 3.1-6). Various researchers have speculated that macroscopic fractures will result in aquifer permeabilities in the order of several hundred darcies. It was fortuitous that glass bead permeabilities were available to straddle this range and yet provide for reasonably high modified Ra numbers. Glass beads having mesh size/permeability of 12-14/1490, 20-30/319, and 40-50/80 were selected. Lower permeabilities can be obtained by using higher mesh sizes, consolidation, or artificial dike formation.

TABLE 3.1-5

MODIFIED RAYLEIGH NUMBERS FOR
VARIOUS MODEL SIZES AT
DIFFERENT EXPERIMENTAL ΔT's

ΔT, °F	Full Size	1/2 Size	1/3 Size	1/4 Size
10	46.9	23.5	15.6	11.7
20	93.8	46.9	31.2	23.5
30	140.7	70.4	46.8	35.2
40	187.6	93.9	62.4	46.9
50	234.5	117.4	78.0	58.7
60	281.4	140.9	94.0	70.4
70	328.3	164.4	109.0	82.1
80	375.2	187.9	125.0	93.8
90	422.1	211.4	140.0	106.0
100	469.0	234.9	156.0	117.0
200	938.0	469.0	312.0	234.0
300	1407.0	704.0	468.0	351.0
400	1876.0	938.0	624.0	468.0

Porous medium: 12-14 mesh glass beads

Fluid medium: seawater

TABLE 3.1-6

CALCULATED PERMEABILITIES OF GLASS BEADS

Mesh Size	Size Range (inches)	Size Range (microns)	Average Size (microns)	Permeability (cm^2)	Darcy
12 - 14	0.0661 - 0.0555	1680 - 1410	1545.0	1.47×10^{-5}	1490
14 - 20	0.0555 - 0.0331	1410 - 840	1125.0	7.81×10^{-6}	792
20 - 30	0.0331 - 0.0232	840 - 590	715.0	3.15×10^{-6}	319
30 - 40	0.0232 - 0.0165	590 - 420	505.0	1.57×10^{-6}	159
40 - 50	0.0165 - 0.0177	420 - 297	358.5	7.93×10^{-7}	80
50 - 70	0.0177 - 0.0083	297 - 210	253.5	3.97×10^{-7}	40
140 - 230	0.0041 - 0.0024	105 - 62	83.5	4.30×10^{-8}	4

A preliminary 50-gallon (1/3 size) model will be initially built. This smaller tank will give an economical means of testing construction and operational costs. Certain design questions such as to pressurize or unpressurize will also be answered. The heat source and temperature measurement and recording instruments will be the same for both the preliminary and final models. Materials and equipment for the preliminary model have been ordered and fabrication has commenced.

CONCLUSIONS

A comprehensive survey into the "state-of-the-art" of geothermal reservoir engineering has found a lack of hard quantitative information available. In-depth analyses were made on topics treating the nature of a geothermal reservoir, parameters requiring measurement in a geothermal well, and hardware and software required for well test and analysis. Two sections were included which make quick orientation to the field of geothermal reservoir engineering possible.

The field of geothermal reservoir engineering, although relatively undeveloped today, will show significant progress during the next few years. The progress will be an accelerated one because of improved international communications, the availability of computers, and the threat of another energy crisis, which has resulted in the release of funds for research and development in this area.

REFERENCES

1. Cheng, P. and K. H. Lau, "Steady State Free Convection in an Unconfined Geothermal Reservoir," *J. of GEOPHYSICAL RESEARCH*, Vol. 79, No. 29, 1974, pp. 4425-4431.

2. Lau, K. H. and P. Cheng, "The Effect of Dike Intrusion on Free Convection in a Geothermal Reservoir," *TECH. REPORT NO. 7*, Hawaii Geothermal Project, December 1, 1974.

3. Keller, George V., "Drilling at the Summit of Kilauea Volcano," Prepared for NSF, Colorado School of Mines, March, 1974.

4. Greenspan, D., "Numerical Studies of Viscous, Incompressible Flow Through an Orifice for Arbitrary Reynolds Number," *INT. J. FOR NUMERICAL METHODS IN ENGINEERING*, Vol. 6, 1973, pp. 489-496.

5. Whiting, Robert L., "A Reservoir Engineering Study of the Wairakei Geothermal Steam Field," *PRIVATE COMMUNICATION*.

6. Muffler, L.J.P. and White, D.E., "Geothermal Energy," *THE SCIENCE TEACHER*, Vol. 39, No. 3, March 1972.

7. Facca, Giancarlo, "Structure and Behavior of Geothermal Fields," *GEOTHERMAL ENERGY*, UNESCO, 1973, pp. 61-69.

8. Elder, John W., "Physical Processes in Geothermal Areas," *TERRESTIAL HEAT FLOW*, W.H.K. Lee, Editor, No. 8, 1965, pp. 211-239.

9. Hayashida, T., Ezima, Y., "Development of Otake Geothermal Field," *U.N. SYMPOSIUM ON THE DEVELOPMENT AND UTILIZATION OF GEOTHERMAL RESOURCES*, Pisa, 1970.

10. MacDonald, G.A., *VOLCANOES*, Prentice-Hall, Englewood Cliffs, 1972.

11. Steinberg, G.S. and Rivosh, L.A., "Geophysical Study of the Kamchatka Volcanoes," *J. of GEOPHYSICAL RESEARCH*, Vol. 70, 1970, pp. 3341-3369.

12. Keller, George V., "Drilling at the Summit of Kilauea Volcano," prepared for the National Science Foundation, March 15, 1974, p. 42.

13. White, D.E., "Geochemistry Applied to the Discovery Evaluation and Exploitation of Geothermal Energy Resource," Raporteur's Report, *UNITED NATIONS SYMPOSIUM ON THE DEVELOPMENT AND UTILIZATION OF GEOTHERMAL RESOURCES*, Pisa, 1970.

14. Kennedy, George C. and Griggs, David T., *POWER RECOVERY FROM THE KILAUEA IKI LAVA POOL*, RM - 2696 - AEC, December 12, 1960.

15. Colp, John L. and Furumoto, A.S., *THE UTILIZATION OF VOLCANO ENERGY*, proceedings of a conference held at Hilo, Hawaii, February 4-8, 1974.

16. Ramey, Henry, "A Reservoir Engineering Study of the Geysers Geothermal Field," *PRIVATE CORRESPONDENCE*, 1973.

17. Fournier, R.O. and Morgenstern, J.C., *A DEVICE FOR COLLECTING DOWNHOLE WATER AND GAS SAMPLES IN GEOTHERMAL WELLS*, U.S.G.S. Paper 750-C, 1971, PC151 - C155.

18. Fournier, R.O. and Truesdell, A.H., *A DEVICE FOR MEASURING DOWNHOLE PRESSURES AND SAMPLING FLUIDS IN GEOTHERMAL WELLS*, U.S.G.S. Paper 750-C, 1971, PC146 -C150.

19. Marshall, G.S. and Henderson, R.H., "Recording Temperature in Deep Boreholes," *ENGINEERING*, October 25, 1963, p. 540.

20. Schlumberger, *LOG INTERPRETATION VOLUME I AND V*, Schlumberger Ltd., New York, 1972 and 1974.

21. Schlumberger, *PRODUCTION LOG INTERPRETATION*, Schlumberger Ltd., New York, 1970.

22. Boldizsar, T., "Geothermal Energy Production from Porous Sediments in Hungary," *GEOTHERMICS*, U.N. (Pisa), Vol. 2, Pt. 1, pp. 99 - 109.

23. Meadows, Katherine F., *GEOTHERMAL WORLD DIRECTORY*, 1972.

24. Cady, G.V., "Model Studies of Geothermal Fluid Production," *THESIS PRESENTED TO STANFORD UNIVERSITY*, 1969, In Partial Fulfillment of the Requirements for the Degree of Doctor of Philosophy.

25. Miller, Frank G., "Steady Flow of Two-Phase Single-Component Fluids through Porous Media," *PETROLEUM TRANSACTIONS*, AIME, Vol. 192, 1951, pp. 205 - 216.

26. Henry, H. and Kahout, F., "Circulation Patterns of Saline Groundwater Effected by Geothermal Heating--as Related to Waste Disposal," *UNDERGROUND WASTEWATER MANAGEMENT AND ENVIRONMENTAL IMPLICATIONS*, Vol. 18, 1973, pp. 202 - 221.

27. Bear, Jacob, *DYNAMICS OF FLUIDS IN POROUS MEDIA*, American Elsevier Publishing Company, 1972.

28. Banwell, C.J., *GEOTHERMAL DRILLHOLES: PHYSICAL INVESTIGATIONS*, United Nations (Rome), 1961, pp. 60 - 71.

29. Hunt, A.M., *MEASUREMENT OF BOREHOLE DISCHARGES, DOWNHOLE TEMPERATURES AND PRESSURES, AND SURFACE HEAT FLOWS AT WAIRAKEI*, United Nations (Rome), 1961, pp. 196 - 207.

30. James, Russell, "Metering of Steam-water Two-phase Flow by Sharp-edged Orifices," *PROCEEDINGS: INSTITUTION OF MECHANICAL ENGINEERS*, Vol. 180, Pt. 1, 1965-66, pp. 549 - 566.

31. Smith, J.H., "Collection and Transmission of Geothermal Fluids," *GEOTHERMAL ENERGY (EARTH SCIENCES, 12)*, UNESCO, 1973, pp. 97 - 106.

32. Bolton, R.S., "Computer Analysis for the Wairakei Geothermal Field," *NEW ZEALAND ENGINEERING*, September 15, 1964, p. 348.

33. Bengma, P., *THE DEVELOPMENT AND PERFORMANCE OF A STEAM-WATER SEPARATOR FOR USE ON GEOTHERMAL BORES*, United Nations, (Rome), 1961, pp. 60 - 77.

34. Mahon, W.A.J., *SAMPLING OF GEOTHERMAL DRILLHOLE DISCHARGES*, United Nations (Rome), 1961, pp. 269 - 277.

35. Armstrong, E.L. and Lundberg, E.A., *GEOTHERMAL RESOURCE INVESTIGATIONS TEST WELL MESA 6-1*, February 1973.

36. Wainwright, D.K., "Subsurface and Output Measurements on Geothermal Bores in New Zealand," *GEOTHERMICS*, U.N. (Pisa), 1970, Vol. 2, Pt. 1, pp. 764 - 767.

37. James, Russell, *ALTERNATIVE METHODS OF DETERMINING ENTHALPY AND MASS FLOW*, United Nations (Rome), 1961, pp. 265 - 267.

38. Banwell, C.J., "Thermal Energy from the Earth's Crust--Parts 1 & 2--The Efficient Extraction of Energy from Heated Rock," *NEW ZEALAND JOURNAL OF GEOLOGICAL GEOPHYSICS*, Vol. 6 & 7, 1964, pp. 52 - 69 (6), pp. 535 - 593. (7).

TASK 3.6 OPTIMAL GEOTHERMAL PLANT DESIGN

Investigators: H. C. Chai, J. Chou & D. Kihara

INTRODUCTION

The efforts of Task 3.6 have been concentrated on studies of geothermal power plant configurations which might be considered for use in moderate temperature, low salinity fields. Emphasis has been placed on vapor flashing plants and binary fluid, vapor turbine cycles--focusing on the major parameters and criteria for selecting the particular configuration once the geothermal source is located and tested.

I. Survey of Geothermal Plants in Operation

The convecting fluids which carry the heat from reservoirs to the surface usually consist of steam, liquid water, various dissolved solids, and gases in a wide range of temperatures and pressures. Because of non-uniformity of the fluid, the methods of using geothermal energy for power production differ from one plant to another. The current methods have been surveyed and are summarized as follows:

1. Non-condensing steam plant (Fig. 3.6-1). Steam from wells is sent through a cyclone separator and admitted to the turbines which exhaust to the atmosphere. The non-condensing plant requires a minimum amount of auxiliary equipment and is readily adaptable as a portable unit. These units permit their use at varying inlet pressures without excessive sacrifice of efficiency, enabling accommodation to changing output characteristics of wells, or a study of the steam field while under exploitation. The units, as used in Italy, range from 500 to 6,000 kw. At the Bagnores area in Lardarello in 1958, the steam contained more than 90 percent of carbon dioxide. The power required to remove the carbon dioxide from the condensing steam would be larger than the gain in power output by using condensers. In two years the gas content was down to 30 percent, but the additional cost of a condensing unit still cannot be justified.

2. Condensing steam plant (Fig. 3.6-2). This type of plant is suitable for steam with gas content up to 8 to 10 percent. At the Geysers, California, the natural steam contains about 1 percent gases. There is an optimum operating pressure for each plant since the wellhead pressures decrease with increased rate of steam production while the available energy of steam decreases with the decreased pressure of steam. The Geyser's plants operate at 100 psia at the inlets of turbines, and the shut-off pressure of wells is around 475 psia. The power output per pound of steam increases with the degree of vacuum to which steam can exhaust. Higher vacuum requires larger condensers, larger gas removers for condensers, lower temperature of cooling water, and a larger quantity of cooling water circulated through the condenser. For each installation, there is an optimum pressure of condenser; for example, 1.5 in. Hg at Wairakei, New Zealand, 2-1/2 in. Hg for some Italian plants, and 4 in. Hg at the Geysers. Since the problem of contamination of condensate in a conventional steam plant does not exist in a geothermal plant, surface type condensers are not required. If the

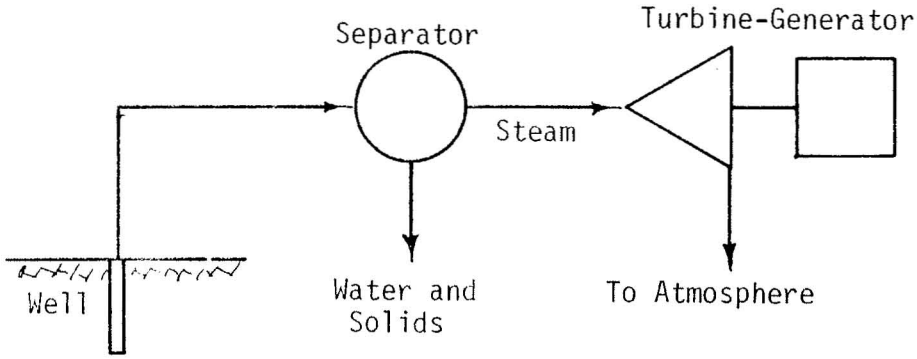

FIG. 3.6-1 NON-CONDENSING PLANT

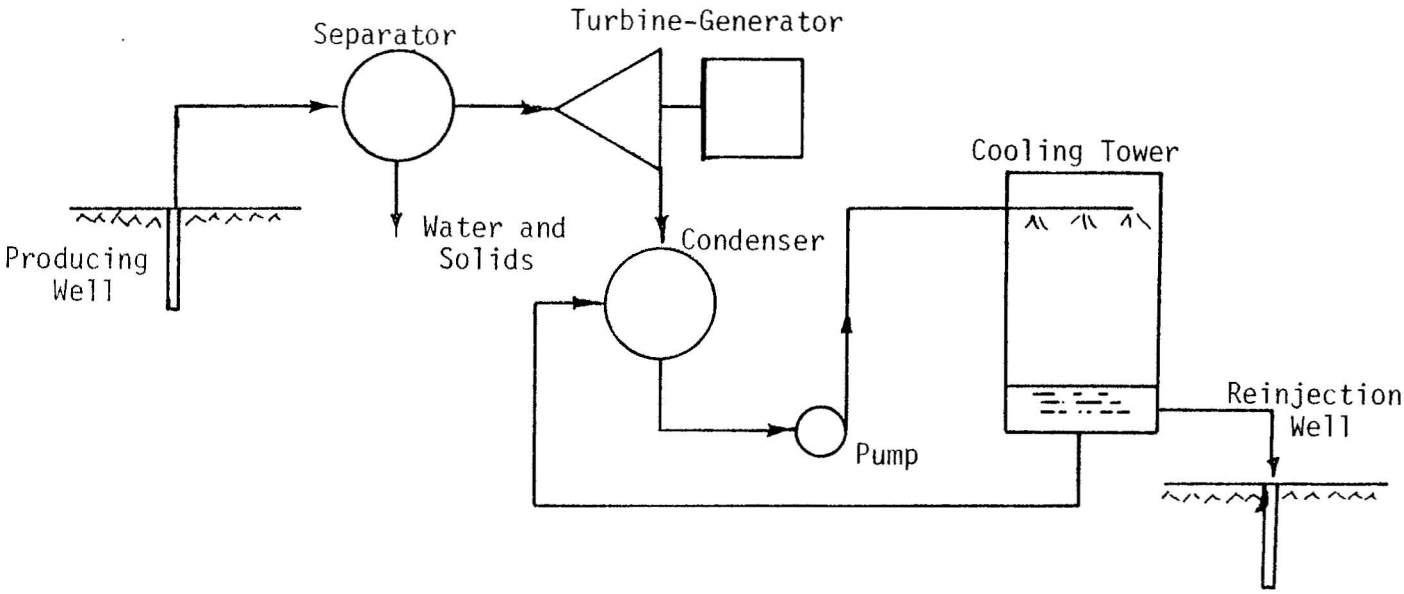

FIG. 3.6-2 CONDENSING PLANT

natural source of cold water is not available, a cooling tower may be installed for the conservation of cooling water. In Hawaii, if the site of the plant is located near the beach, there should be a considerable economic advantage by using sea water as cooling water.

3. Condensing plant using secondary steam (Fig. 3.6-3). The steam is used to heat the secondary steam in a heat exchanger, and the secondary steam operates in a closed cycle for power generation. This type of plant can be economical in power production for steam with 10 to 15 percent of gas content, and provides an opportunity for the recovery of chemicals from the non-condensable gases.

4. Condensing turbines using flash steam (Fig. 3.6-4). The liquid-dominated field is filled with compressed hot water that does not become steam until the pressure is released. A general belief is that liquid-dominated fields may be 20 times more abundant than vapor-dominated fields. In hot and shallow reservoirs such as those in Wairakei, the well is self-producing and a mixture of hot steam and liquid water emerges from wells by natural forces. The steam can be fed directly to the turbines, and the liquid water may be used to produce flash steam. The number of liquid-vapor separation stages can be more than two, depending upon the economical justification. The mixed-pressure turbines are built with separate inlets for steam at two or more different pressures and with suitable control mechanisms for each inlet. The thermal efficiency of the multi-stage plant can be as good as the binary cycle plant described in the following paragraph. Through the research efforts of engineers with the Ministry of Works, New Zealand, sufficient information is now available for the efficient design of this type of plant [17].

5. Binary cycle plant (Fig. 3.6-5). The possibility of using a fluid such as Freon or isobutane as the working fluid has been well explored [16]. Small Freon plants have been built in Japan. San Diego Gas and Electric Company is testing a 9 mw isobutane plant at Imperial Valley, California. Owing to the properties of Freon or isobutane, the cycle operates at supercritical pressure even at a temperature of 350°F or above, and thus the Rankine efficiency can be very satisfactory. The efficiency of isobutane turbines has been claimed to be about 10 percent higher than that of steam turbines at the same rating. One of the great advantages of isobutane or Freon systems over steam systems is that the construction of the turbines is light and simple. The capital cost of an isobutane plant excluding the wells, field piping and electric transmission lines is estimated to be $200 to $300 per kw of capacity, which is very close to the cost of large

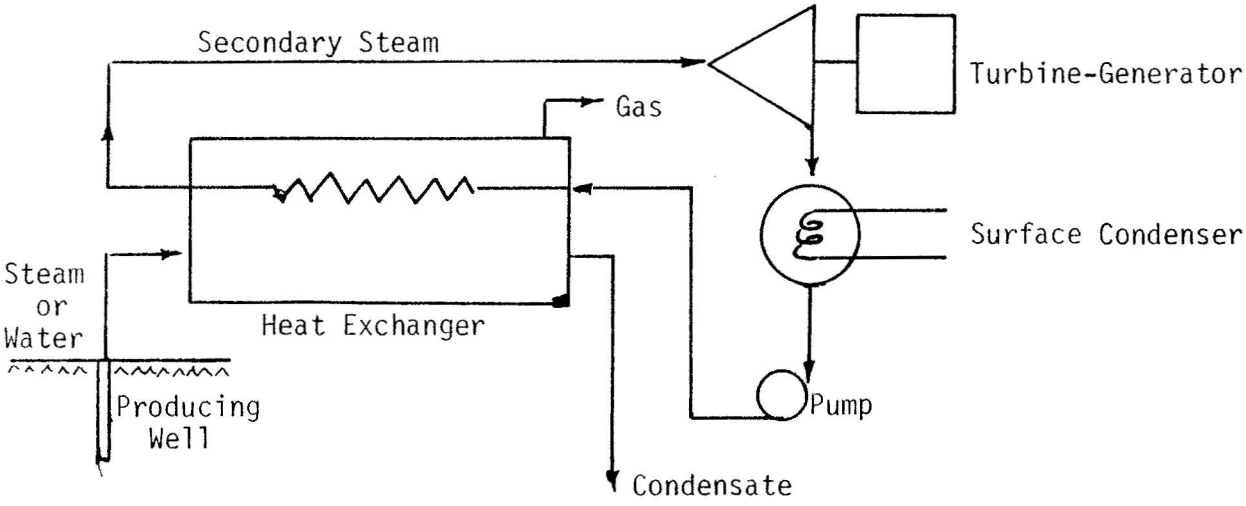

FIG. 3.6-3 CONDENSING PLANT USING SECONDARY STEAM

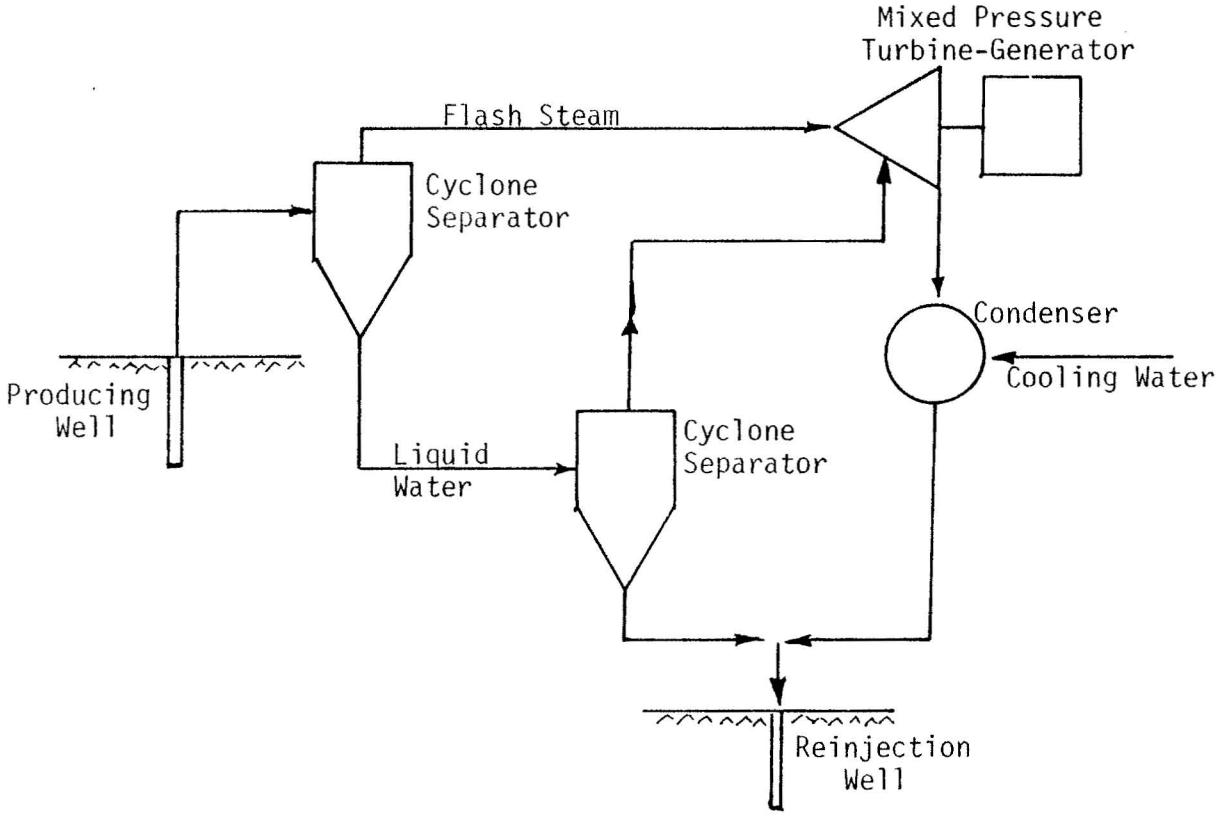

FIG. 3.6-4 CONDENSING TURBINES USING FLASH STEAM

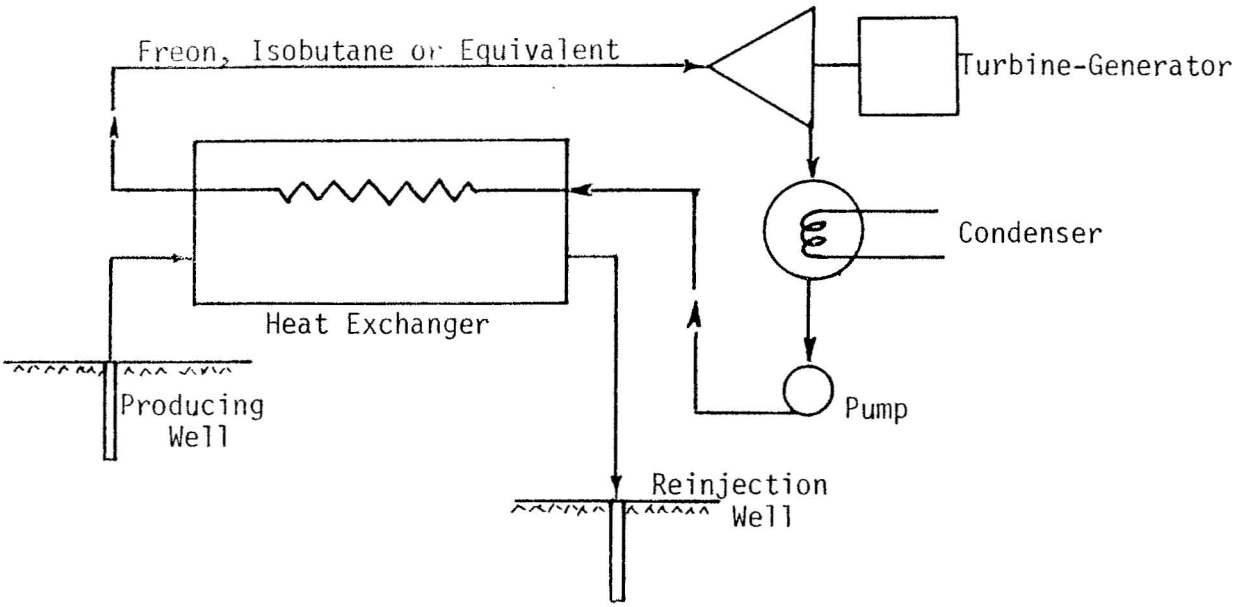

FIG. 3.6-5 BINARY CYCLE PLANT

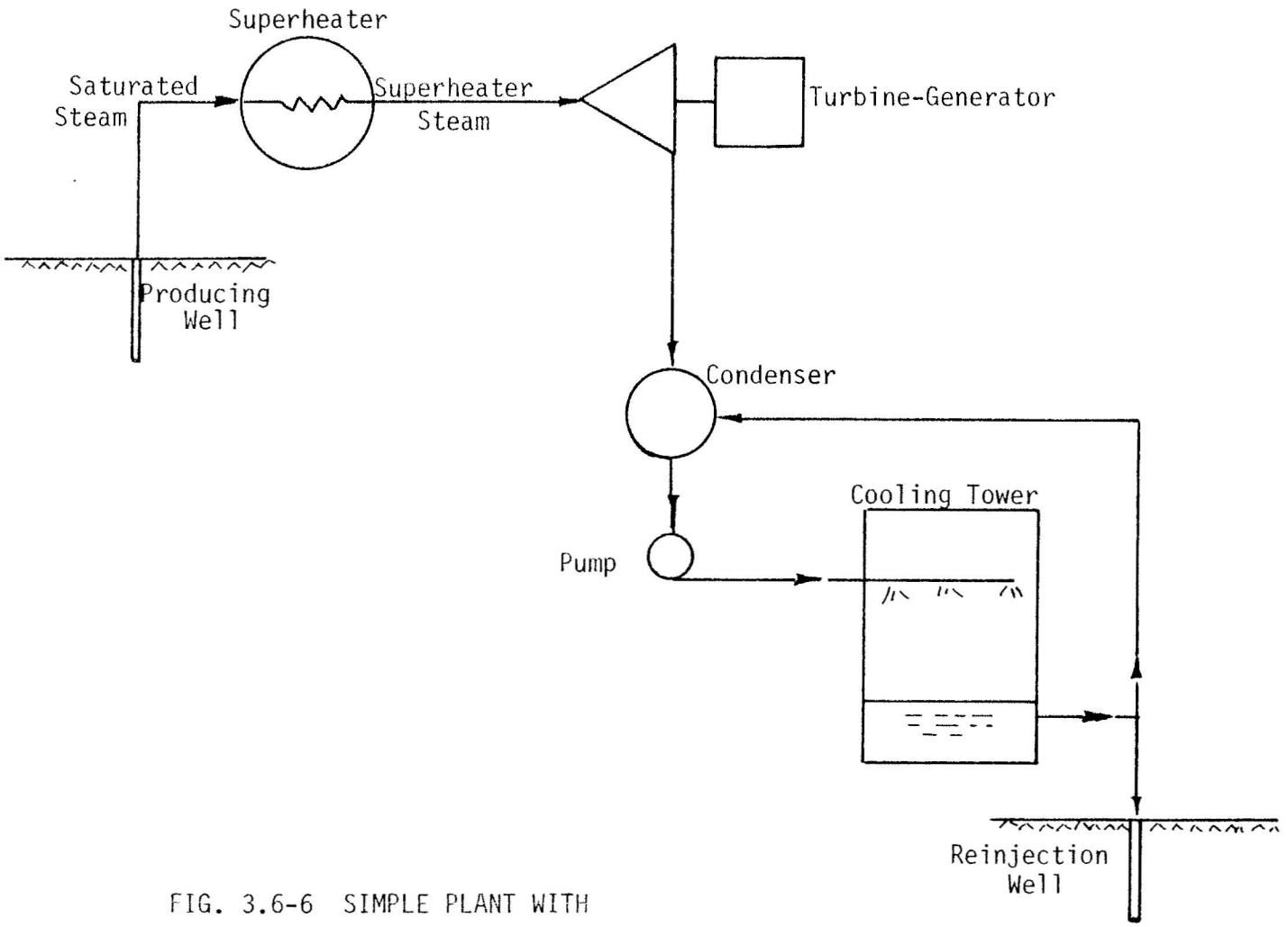

FIG. 3.6-6 SIMPLE PLANT WITH FOSSIL-FUEL SUPERHEATER

fossil fuel plants. The capital cost of the plants using natural steam at the Geysers is about one half of that of isobutane plants. Since the heat from reservoirs is free, the geothermal plant can afford a budget of $250 to $300 per kw capacity for field development cost. San Diego Gas and Electric Company is not sure yet how much the geothermal power produced by the isobutane system will cost. At present, it might be higher than power from fossil or nuclear plants. Since the geothermal plants are still in the early developmental stage, research will present great potential for cost reduction.

Superheating Geothermal Steam

In a conventional plant, good practice requires that the maximum moisture content of the exhaust steam from a turbine be limited to about 10 to 12 percent. The presence of moisture reduces the engine efficiency and causes the erosion of turbine blading. Because of the corrosive nature of geothermal fluids, the problems of moisture in turbines become even more serious in a geothermal plant, in which all the wetted parts are always made of stainless steel or other corrosive-resistant materials while the dry parts may be made of carbon steel which is not appreciably corroded by the dry geothermal steam. By superheating the steam with a conventional fossil-fuel superheater as shown in Fig. 3.6-6, it is possible to have dry exhaust steam.

Heat balances indicate that the overall thermal performance can be much improved for simple plants with nearly saturated steam from the wells, for illustration, the heat rate of fossil power and the quality of exhaust steam for a 15 mw simple plant as shown in Fig. 3.6-6, have been calculated and plotted in Fig. 3.6-7. It shows at 400°F superheat that the heat rates of fossil power are comparable to the heat rates of modern central power plants and that the moisture contents are less than 3 percent. Both the heat rate and the quality of exhaust steam can be further improved by increasing the degree of superheat to more than 400°F; however, the price of the turbines will increase by another step if the throttle temperature is over 750°F because of the materials of construction. The fixed charge of fossil power from a geothermal plant should be much lower than that from a conventional power plant since the superheater is the only additional equipment.

For the sample calculations, the combined turbine-mechanical and generator efficiency was assumed to be 97%. The turbine efficiencies were estimated according to the information given by Pollard and Drewry of General Electric Company [25]. The basic efficiencies are given in Fig. 3.6-8, based on 1.5 in. Hg

Boiler Efficiency of Superheater = 85%
Turbine Efficiency = 73 to 79%
Combined Mechanical and Generator Efficiency = 97%
Back Pressure = 2.5" Hg abs
Generator Rating = 15 mw

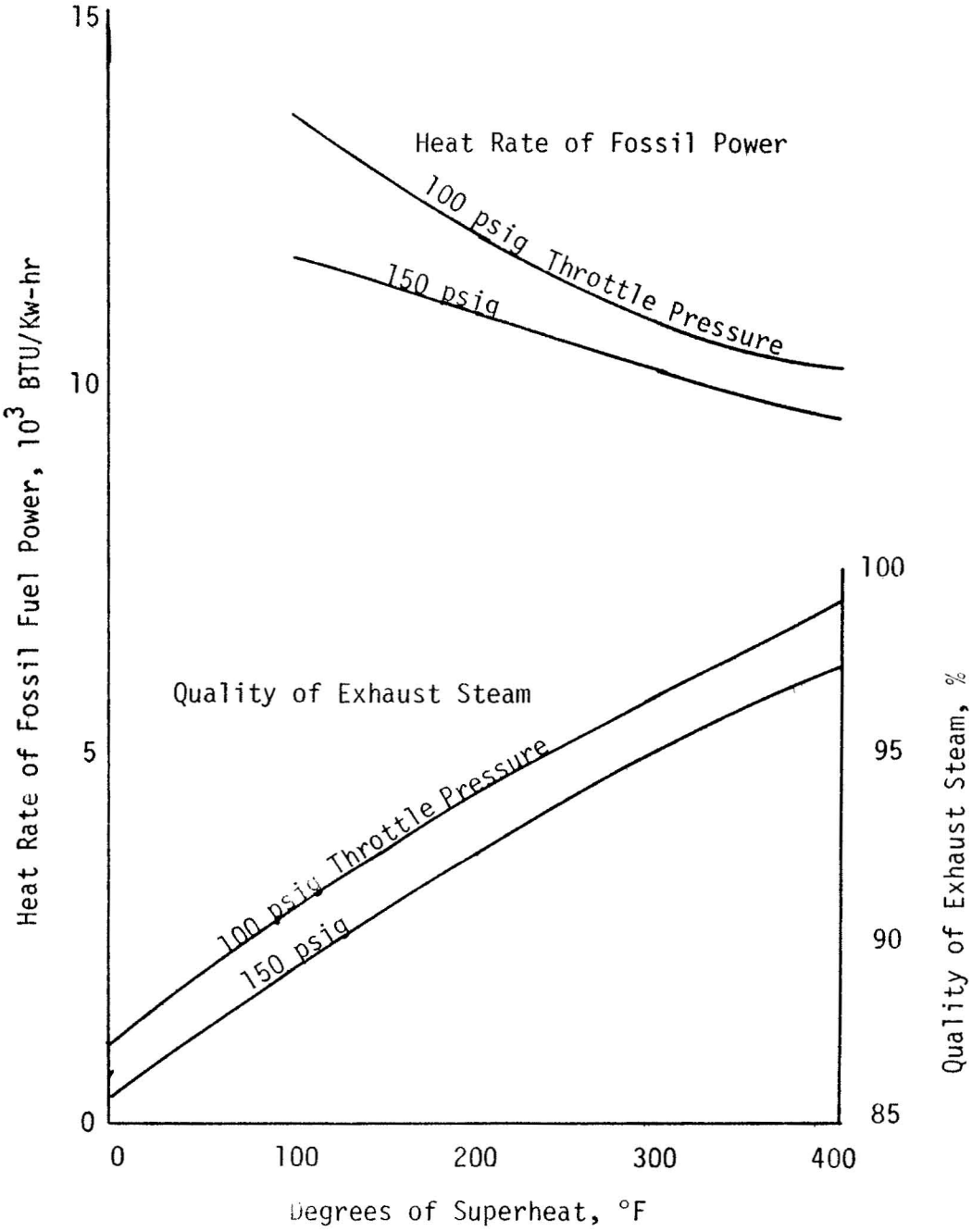

FIG. 3.6-7 HEAT RATE OF FOSSIL POWER AND QUALITY OF EXHAUST STEAM FOR SIMPLE PLANT WITH FOSSIL-FUEL SUPERHEATER

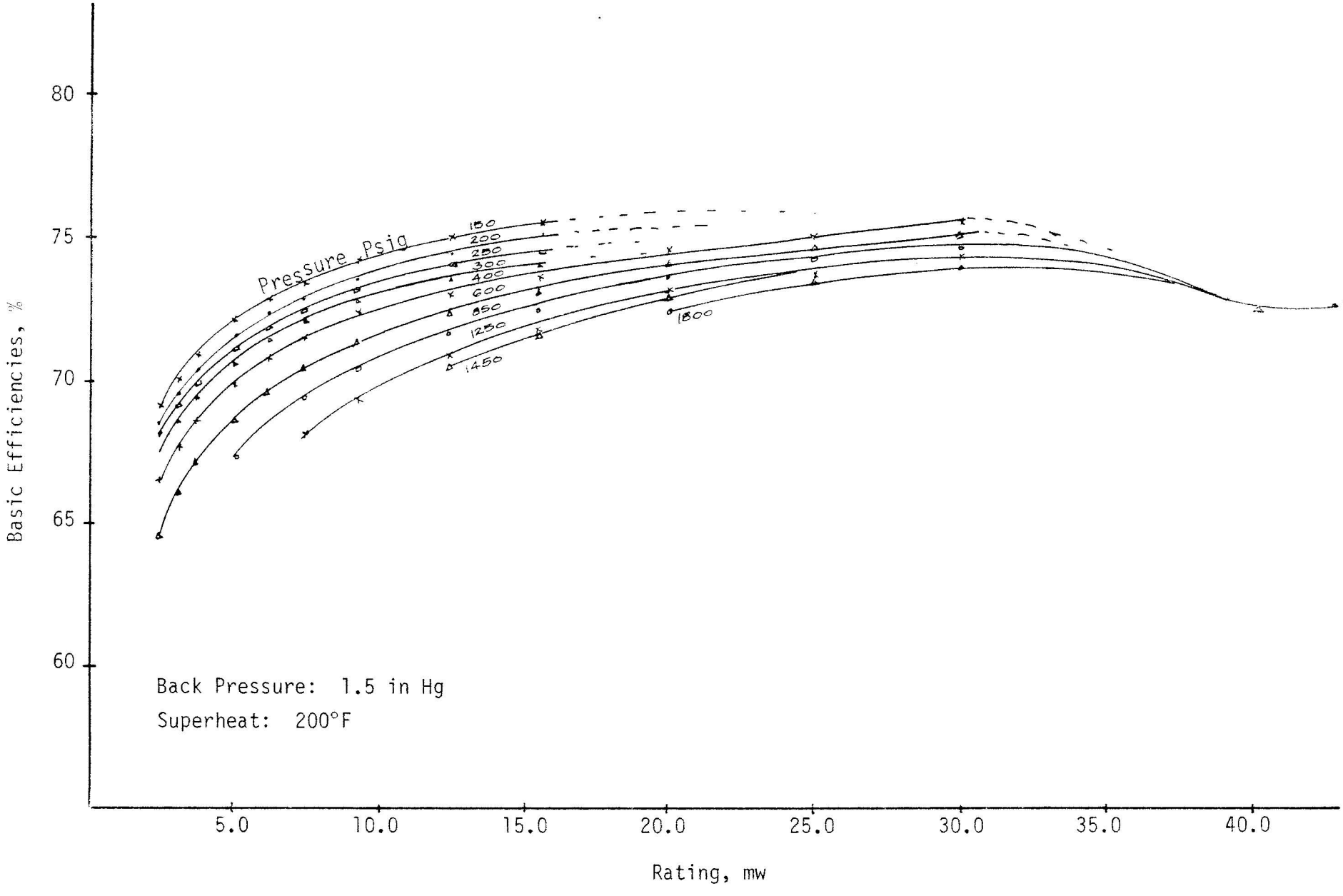

FIG. 3.6-8 BASIC EFFICIENCIES OF STEAM TURBINE [25]

back pressure and 200°F superheat. For a 15 mw plant that operates at 100 psig throttle pressure and 2.5 in. Hg back pressure, the turbine efficiencies and the steam rates are as follows:

Degree of superheat, °F	0	50	100	200	300	400
Turbine efficiency, %	0.737	0.746	0.752	0.768	0.780	0.791
Steam rate, lb/kwh	17.00	16.43	15.76	14.48	13.26	12.18

The heat rate of fossil power and the enthalpy of exhaust steam were determined by the following equations:

Heat rate of fossil power Btu/KwH = (power produced per lb saturated steam - power produced per lb superheated steam) ÷ $\left(\frac{h_2 - h_1}{\text{boiler efficiency}}\right)$ =

1/3413 (turbine efficiency x isentropic work per lb saturated steam - turbine efficiency x isentropic work per lb superheated steam) $\left(\frac{h_2 - h_1}{\text{boiler efficiency}}\right)$

where h_1 and h_2 are enthalpies of steam entering and leaving the superheater.

Enthalpy of exhaust steam = h_2 - turbine efficiency x isentropic work ÷ combined turbine - mechanical and generator efficiency.

Applying Fossil Energy to Condensing Plants which use Secondary Fluid

The efficiency of an engine may be increased by supplying heat at a higher temperature, and the maximum operating temperature is usually limited by the materials used for the construction of the engine. Since the geothermal fluids from wells exist at a temperature much below the maximum permissible temperature (around 1,200°F) of steam for a conventional plant, it is of interest to investigate the effect of heating the geothermal fluids with fossil fuel upon the efficiency of a geothermal plant. The preliminary calculations indicate there could be an economical gain in some cases. For example, Fig. 3.6-9 is a condensing plant using secondary steam at 2 in. Hg back pressure. Assuming the turbine efficiency to be 75 per cent, the work per lb of steam is 225 BTU. If the working pressure and the temperature are increased to 680 psia and 600°F respectively, by using fossil fuel as shown in Fig. 3.6-10, the work per lb of steam is increased to 295 BTU. Assuming the boiler efficiency to be 70%, the heat input from the fossil fuel is 133 BTU per lb of steam. Thus, the efficiency of converting fossil energy to power is (295-225)/133 = 52.6%, which is far above the thermal efficiency of modern power plants. Some calculations have been done for binary cycle plants with fossil heaters. Since the secondary fluid such as isobutane in a binary cycle operated at supercritical pressures, the efficiency of converting fossil energy to power is much lower

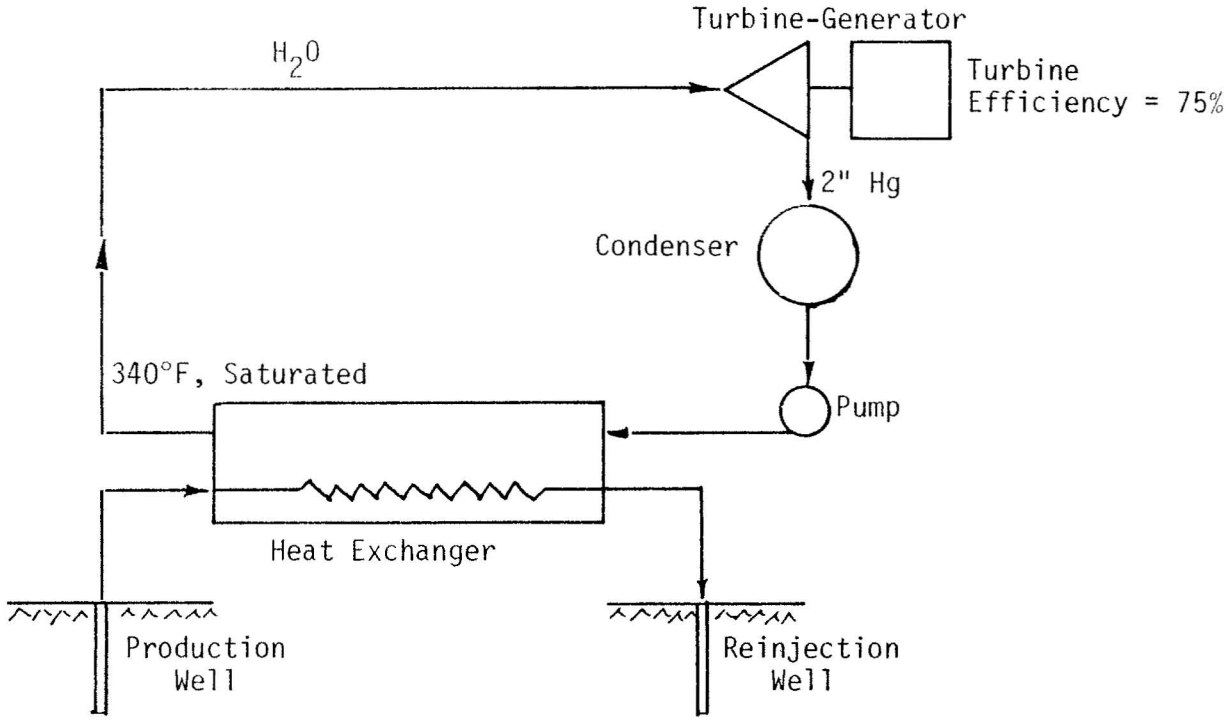

FIG. 3.6-9 A CONDENSING PLANT USING SECONDARY STEAM

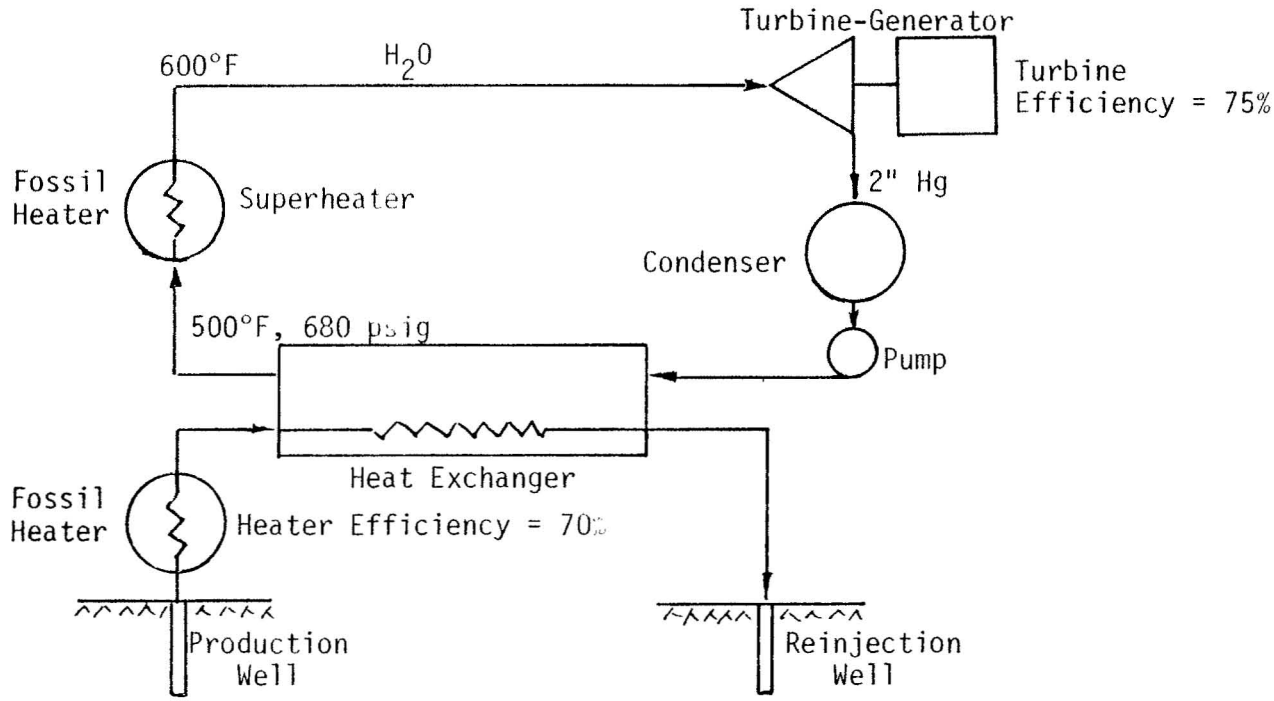

FIG. 3.6-10 A CONDENSING PLANT USING SECONDARY STEAM WITH FOSSIL HEATERS

than that for a condensing plant using secondary steam. Investigations in using fossil fuels to upgrade the overall plant efficiency will continue.

Using Deep Ocean Water as Cooling Water

In Hawaii, the average temperature of seawater is 81°F at the surface, and 41°F at a depth of 1,600 ft. For a geothermal plant near the sea, the cost of using sea water as cooling water in a condenser is likely to be lower than the cost of recycling the cooling water through a cooling tower. Assuming the back pressure of a steam turbine is 2.0 in. Hg for a plant using the surface sea water as cooling water, the back pressure could be lowered to 0.5 in. Hg with the same design of the condenser if the cooling water is taken from the deep ocean. The effect of temperature on cooling water on turbine output is illustrated in Fig. 3.6-11. Since the isobutane turbines have higher efficiencies than the steam turbines, the gain in power output of an isobutane plant should be more impressive than that of a steam plant. It is intended to expand the study on extracting more energy from geothermal fluids by taking advantage of deep ocean water.

II. Characteristics of Vapor Flashing Plants

1. Pressure Drop of Two-Phase Flow in Pipe

If the geothermal fluid flows out freely through a well in a liquid-dominated field, a part of the liquid will become vapor because of the pressure drop caused by friction and the potential energy change. The amount of vapor separated depends on the heat content of the fluid and the pressure drop. There are two options to treat the two-phase fluid at the wellhead. The first is to separate steam from brine at the wellhead, using a centrifugal cyclone separator. Thereafter, steam and brine are piped separately to the power plant where the flashed steam is produced from the brine at a lowered pressure, and is fed to the turbine in an intermediate-stage. This option was adopted at Wairakei under the fear of water-hammer, cavitation, surging flow and excessive vibrations which might occur in the transportation of the two-phase fluid through a pipe. To prevent flashing, the hot brine was pressurized by pumps and cooled by the injection of cold water. The second option is to transport the liquid-vapor mixture from the wellhead to the plant through a single pipe. The separation of vapor from liquid takes place

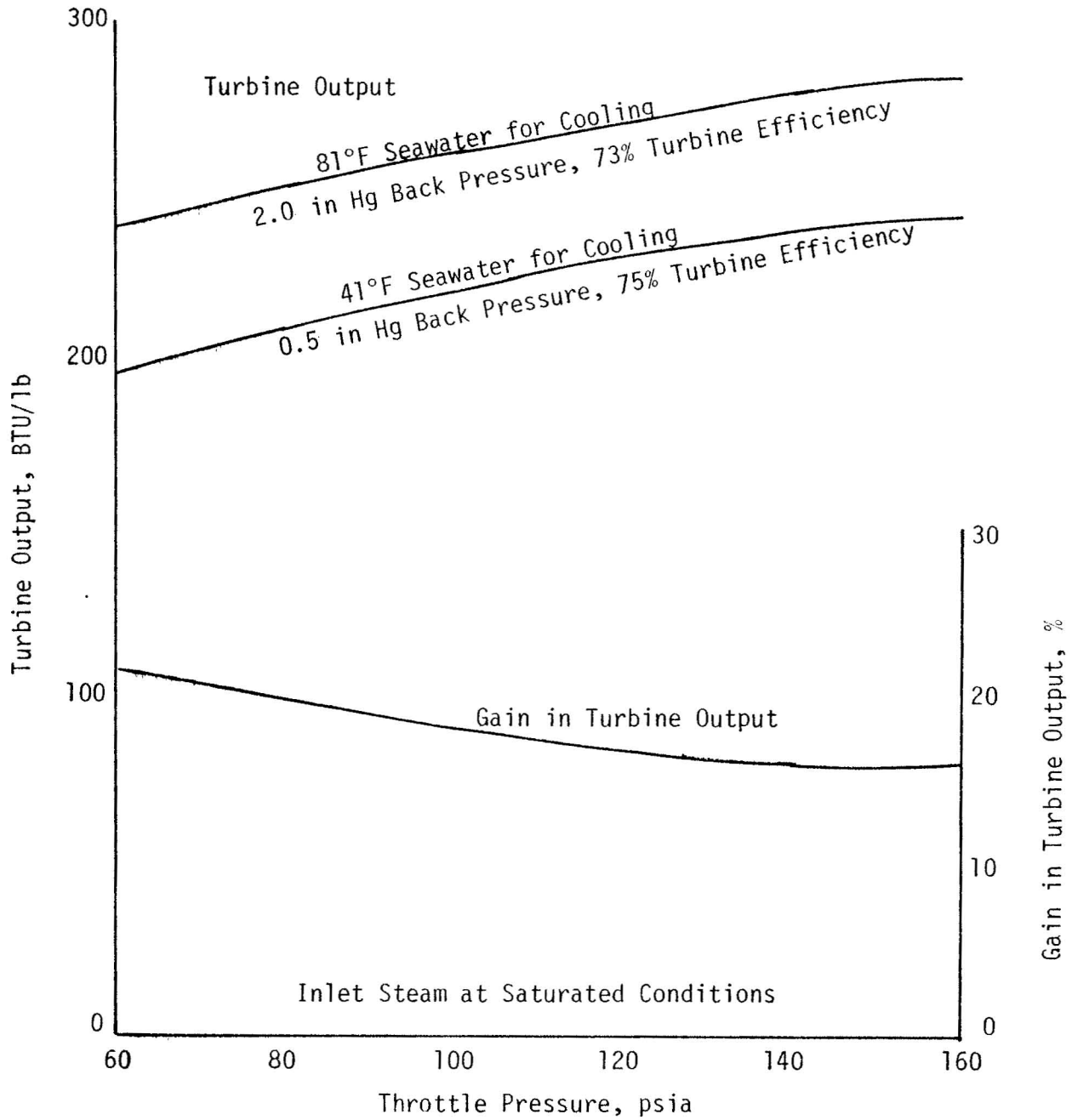

FIG. 3.6-11 EFFECT OF TEMPERATURE OF COOLING WATER ON TURBINE OUTPUT

in the plant. The advantages of the second option are the reduction in pipeline cost and the increase of power output.

Through a series of experiments James [19] and Takahashi, et al. [33] demonstrated that there was no serious difficulty, previously suspected, in the transportation of steam-water mixture. From experimental results and analytical considerations of flow patterns, they concluded that when the flow pattern is in the annular flow region, the flow is stable even in pipes of large diameters. Even flow regimes described as slug and stratified are not dangerous for a pipe filled with flowing water, since a slug or wave will not be able to attain high velocities with water and steam in its path. Cavitation cannot be a problem for a pipeline carrying steam-water mixture because of the presence of water vapor, carbon dioxide, hydrogen sulfide and other non-condensable gases. These gaseous compounds provide a buffer to the impact forces [22]. However, care should be taken in starting up, and the line should be initially heated and pressurized with steam to avoid pressure fluctuations and local water accelerations. There has been only one incident of water hammer at Wairakei when steam entered a closed pipe containing a large quantity of cold condensate. In James' experiment, a mixture of flashing steam and water flowed into a cold pipe which contained cold water in the upper leg of expansion bend; no water hammer was detected and only slight vibrations were noticed. The conclusion of the experiment was that the transportation of steam-water mixture in pipes can be as acceptable as that of steam alone and is perhaps preferable when there is residual water in the line.

There are three methods being suggested for calculating the pressure drop of a two-phase flow. The first method, introduced by Benjamin and Miller [5], involves the direct solution of the continuity and energy equations. They assumed isentropic expansion for determining the density of the liquid water mixture. Although the expansion of the fluid is not isentropic due to the friction loss, the results of their calculations fit the experimental data very well, due to the fact that the density of the mixture varies in nearly the same manner whether an isentropic or isenthalpic expansion is assumed. For clean steel pipes, they found the friction factor to be 0.012. The second method was initiated by James [19] who suggested that the pressure drop ΔP of a two-phase flow can be determined by first calculating the pressure drop ΔP_{sf} of steam flow in the mixture alone and then dividing it by $x^{0.5}$,

$$\Delta P = \Delta P_{sf} / x^{0.5} \tag{B.1}$$

where x is the dryness fraction. This equation was for moderate flows through the pipe, where the speed of the steam fraction is of the same order of normally recommended speed of steam alone. The calculated results by this equation were found to be inconsistent with the experimental data. The third method was originated by Lockhart and Martinelli. James [18] and Takahashi, et al. [33] found that Lockhart and Martinelli's correlation gave calculated values of pressure drop in excellent agreement with experimental results for horizontal loops and that the pressure drop for vertical expansion loop could also be predicted quite accurately with an additional factor. The first step is to calculate the dimensionless number χ as follows:

$$\chi = \frac{\Delta P_{lf}}{\Delta P_{sf}} = \sqrt{\left(\frac{W_{lf}}{W_{sf}}\right)^{1.8} \cdot \left(\frac{\rho_{sf}}{\rho_{lf}}\right) \cdot \left(\frac{\mu_{lf}}{\mu_{sf}}\right)^{0.2}} \tag{B.2}$$

where ρ, μ, P and W are the density, viscosity, pressure and mass flow rates, and the subscripts lf and sf refer to the liquid and steam fractions respectively. Figure 3.6-12 gives the non-dimensional pressure loss factor ϕ as a function of χ and the total pressure drop is

$$\Delta P = \phi^2_{sf} \ \Delta P_{sf} = \phi^2_{lf} \ \Delta P_{lf} \tag{B.3}$$

James stated that the Lockhart and Martinelli correlation is applicable to the flows with steam fraction velocity not less than about 60 ft/sec. At lower velocities, slug flow appears and the correlation becomes less accurate. Pressure drop increases exponentially with the increase of velocity. The optimum pipe diameter D for reasonable pressure drop was recommended by him as follows:

$$D = 0.1365 \left(\frac{W \cdot x}{p^{0.47}}\right)^{0.5} \tag{B.4}$$

Equation (B.4) can merely serve as a very rough guide. The optimum size

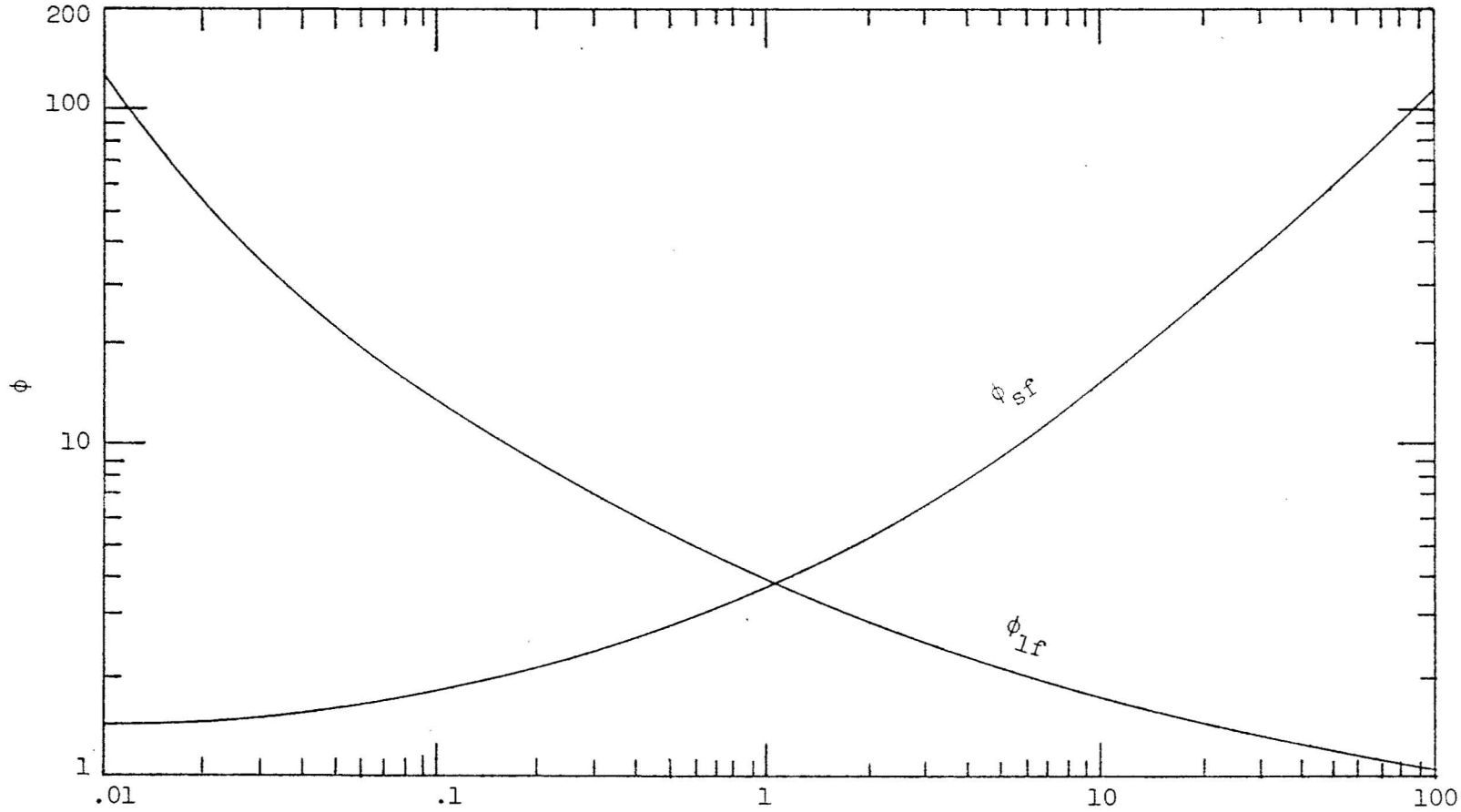

FIG. 3.6-12 LOCKHART MARTINELLI CORRELATION FOR TURBULENT LIQUID, TURBULENT VAPOR CASE

of pipe can be determined only after the cost of piping and cost of power loss due to pressure drop are carefully appraised.

Total annual piping cost = annual capital cost of piping + annual cost of power loss. The annual capital cost of piping is a function of the diameter D of pipe; the annual cost of power loss is affected by the pressure drop, which is inversely proportional to the fifth power of diameter.

$$\Delta P = \phi_{lf}^2 \cdot f \cdot \frac{L}{D} \cdot \left[\frac{(1-x)\cdot W}{\pi D^2 \cdot \rho_{lf}}\right]^2 \cdot \frac{1}{2gc} \cdot \rho_{lf} = C \cdot \frac{(1-x)^2 \cdot W^2}{D^5 \cdot \rho_{lf}} \qquad (B.5)$$

In summary, investigations by Takahashi [33] and James [19,22] have shown that two-phase geothermal fluids can be transported through pipes without suspected troubles of water hammer, cavitation and excessive vibrations. The Lockhart and Martinelli correlation is recommended for the determination of pressure drop.

2. Flashing Pressures

In a vapor flashing system hot water is flashed to steam at a pressure lower than the wellhead pressure. The vapors thus generated may be used to drive a mixed pressure turbine. Flashing may be done in a centrifugal cyclone separator. Bengma [4] discusses the development and selection of a steam water separator. Chierici [8] draws some important conclusions about the feasibility of using a condensing plant.

Work output from the turbine is the product of steam flow rate and the available energy. In a simple flashing system, the lower the flashing pressure, the higher the steam production rate. However, available energy associated with each pound of steam decreases with the lowering of the separator pressure. Therefore, there exists an optimum flashing pressure for obtaining maximum power from the hot water. At a pressure higher than the optimum, work output is small due to minimal available energy. At a pressure lower than the optimum, low turbine work results because of the diminished steam flow rate.

By employing multi-stage flashing, the temperature of discharged water is lowered and thus the work output of the plant can be greatly increased. The number of stages of flashing is a matter of economic justification. Power contribution of an additional stage decreases as the number of stages

increases, and specific volume of steam increases rapidly at low pressure to cause high cost of the multi-stage arrangement. An advantage of multiple admission of steam to a mixed pressure turbine is to improve the quality of the exhaust steam, thereby reducing erosion of the turbine blades. Also, steam flashed from separated water is practically free of gases. The percentage of gas content in the exhaust steam can be lowered by blending the flashed steam with the steam directly from the well. In a mixed-pressure turbine, there are separate inlets for steam at different pressures, and each inlet is equipped with its own control valve.

Hansen [15] stated that for a simple flashing cycle, optimum flashing pressure corresponds to a saturation temperature halfway between the well water temperature and saturation temperature of the condensate in the condenser. For example, for 400°F well water and 120°F condensate, the optimum flashing temperature should be 260°F. He extended the rule to the multi-stage flashing plant. For well water at 400°F, condensate at 120°F, and three-stage flashing, optimum intermediate pressures should correspond to saturation temperatures of 330°F, 260°F, and 190°F, resepctively. A procedure, described in the next paragraph, has been worked out to determine the exact optimum flashing pressure with numerical methods; the results confirm Hansen's rule of approximation.

Using a three-stage plant as an example, as indicated in Figure 3.6-13, we have the following equations from the consideration of mass and heat balance:

$$m_1 + m_4 = 1, \tag{B.6}$$

$$m_2 + m_5 = m_4, \tag{B.7}$$

$$m_3 + m_6 = m_5, \tag{B.8}$$

$$m_1 h_1 + m_4 h_4 + q_1 = h_0, \tag{B.9}$$

$$m_2 h_2 + m_5 h_5 + q_2 = m_4 h_4, \tag{B.10}$$

$$m_3 h_3 + m_6 h_6 + q_3 = m_5 h_5, \tag{B.11}$$

where q is the heat loss from the flashing tank per pound of fluid at wellhead, h is the specific enthalpy, m is the mass of the fluid, and the subscripts refer to the locations of points given in Figure 3.6-13. The conditions of steam and liquid water are not exactly saturated. Assume:

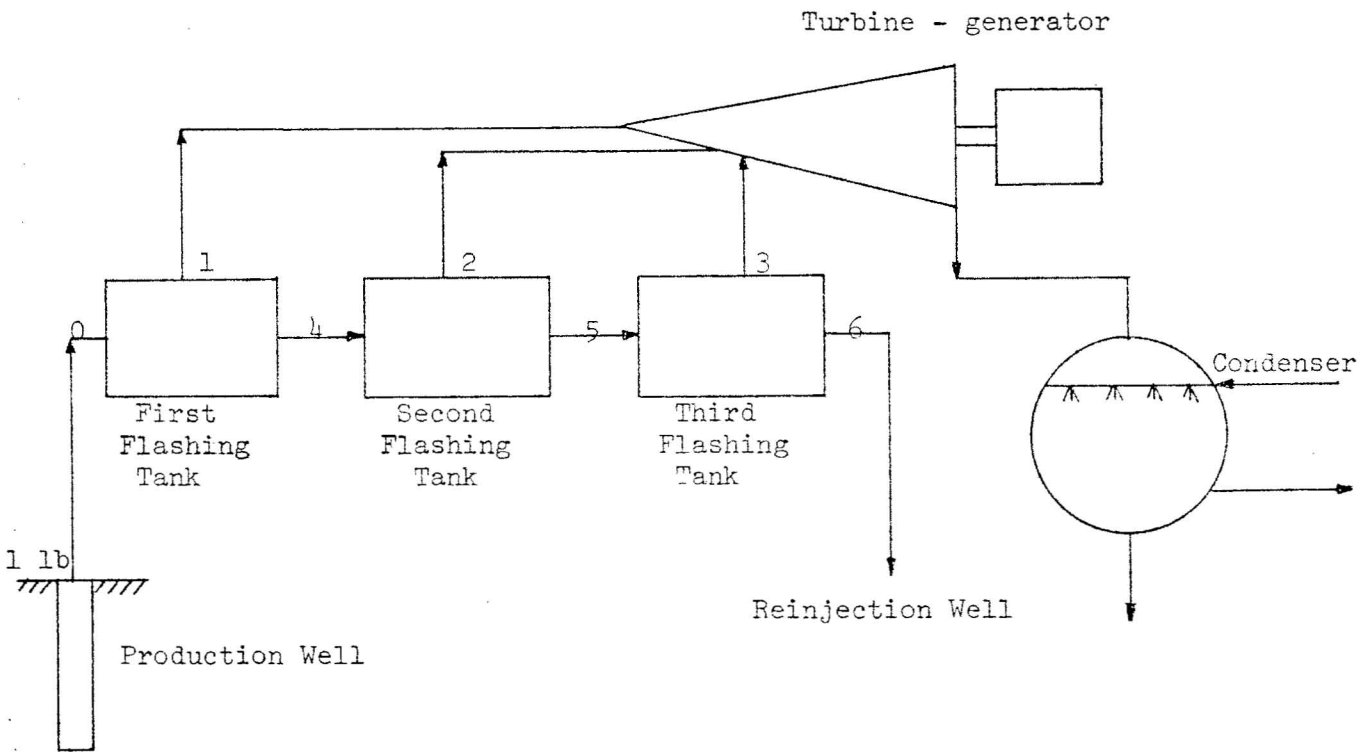

FIG. 3.6-13 THREE STAGE VAPOR FLASHING PLANT

$$h_1 = hf_1 + [1 - x(1)]\, hfg_1, \tag{B.12}$$

$$h_2 = hf_2 + [1 - x(2)]\, hfg_2, \tag{B.13}$$

$$h_3 = hf_3 + [1 - x(3)]\, hfg_3, \tag{B.14}$$

$$h_4 = [1 + z(1)]\, hf_1, \tag{B.15}$$

$$h_5 = [1 + z(2)]\, hf_2, \tag{B.16}$$

$$h_{6m} = [1 + z(3)]\, hf_3, \tag{B.17}$$

in which x is the moisture content and z is a parameter used to modify the heat content of liquid water, depending upon the efficiency of the flashing tank. Upon solving the above equations, we have

$$m_1 = \frac{y(1)\, h_o - [1 + z(1)]\, hf_1}{[1 - x(1)]\, hfg_1 - z(1)\, hf_1} \tag{B.18}$$

$$\frac{m_2}{m_4} = \frac{y(2)\, [1 + z(1)]\, hf_1 - [1 + z(2)]\, hf_2}{[1 - x(2)]\, hfg_2 - z(2)\, hf_2} \tag{B.19}$$

$$\frac{m_3}{m_5} = \frac{y(3)\, [1 + z(2)]\, hf_2 - [1 + z(3)]\, hf_3}{[1 - x(3)]\, hfg_3 - z(3)\, hf_3} \tag{B.20}$$

where

$$y(1) = \frac{h_o - q_1}{h_o} \tag{B.21}$$

$$y(2) = \frac{[1 + z(1)]\, hf_1 - q_2}{[1 + z(1)]\, hf_1} \tag{B.22}$$

$$y(3) = \frac{[1 + z(2)]\, hf_2 - q_3}{[1 + z(2)]\, hf_2} \tag{B.23}$$

The total work done per pound of well water is the sum of the products of turbine efficiency η, mass flow rate m and isentropic work Δhs,

$$\text{Total work} = \Sigma\, \eta\, m\, (\Delta hs). \tag{B.24}$$

The values of the enthalpies of saturated water are functions of temperature. In the range of 150°F to 380°F, the following two interpolation equations were found by the least squares method:

$$hf,\ Btu/lb = -430.622108 + 0.8109447839T + 0.146245395 \times 10^{-3}T^2, \quad (B.25)$$

$$hfg,\ Btu/lb = 1183.89061 + 0.529042078 \times 10^{-2}T - 0.4812738654 \times 10^{-2}T^2 \quad (B.26)$$

where T is the absolute temperature in degrees Rankine. The corresponding standard errors of estimate are 0.095818758 and 1.3655710 Btu/lb respectively. The isentropic work can also be expressed in terms of flashing temperatures if the condensing temperatures of turbine and the moisture content of the flashed vapor are given; for example, at 120°F condensing temperature, the following two emperical equations were determined as functions of absolute temperature for flashed vapors at a saturated condition and at 3% moisture content respectively:

$$\Delta hs,\ Btu/lb = -2171.27186 + 6.3073419T - 0.05344237355T^2 + 0.1602543655 \times 10^{-5}T^3, \quad (B.27)$$

$$\Delta hs,\ Btu/lb = -1657.42887 + 4.211654994T - 0.2512764913 \times 10^{-2}T^2 + 0.322149585l \times 10^{-6}T^3. \quad (B.28)$$

The respective standard errors of estimate are 1.4406118 Btu/lb and 1.539438 Btu/lb. With the hf, hfg and Δhs represented as functions of temperature, the total work became a function of three independent variables T_1, T_2, and T_3. The process of determining the optimum flashing temperatures involves cumbersome calculations. The steepest ascent method was applied to the calculations with the aid of a digital computer.

For saturated well water at 400°F and condensing temperature of 120°F, the total turbine work per pound of well water is tabulated in Table 3.6-1 for one- to four-stage plants. With reasonable amounts of heat losses through the flashing tanks, Hansen's rule of approximation yields nearly the same amount of work as obtained by the exact method. As expected, the power contribution of an additional stage diminishes as the number of stages increases. The extra work outputs due to second, third, and fourth stages are 29.33, 9.39, and 5.01 percents of the work of a single stage plant respectively. Also, the specific volume of steam increases rapidly to cause difficulty in turbine design. Thus, the number of flashing stages is likely to be limited to two. Because of the pressure drops through pipes and the high cost of low pressure equipment, the most economic flashing temperatures should be slightly higher than the calculated optimum temperatures.

TABLE 3.6-1 FLASHING TEMPERATURES AND TOTAL WORK FOR SATURATED WATER AT 400°F AND CONDENSING TEMPERATURE AT 120°F.

Index	t_1 °F	t_2 °F	t_3 °F	t_4 °F	Work, Btu Per Pound of Well Water
1	280	-	-	-	22.377
	260	-	-	-	23.085°
	240	-	-	-	22.89
	220	-	-	-	21.743
2	307	213	-	-	29.33°
3	330	260	190	-	32.034°
	326.6	257.1	186.04	-	32.068
	322.91	255.23	183.31	-	32.084*
	313.94	248.04	173.94	-	31.979
4	344	288	232	176	33.173°
	335.24	276.37	216.02	170.93	33.681
	332.56	275.0	218.71	167.80	33.713*
	334	168.65	221.46	161.67	33.615
5	330	260	190	-	31.193°
	322.02	253.57	185.33	-	31.267
	316.83	247.10	180.75	-	31.271*
	304.92	224.22	172.18	-	30.962
6	330	260	190	-	27.035°
	315.12	247.25	181.36	-	27.513
	300	228	169	-	27.7 *
	287.6	173.8	132.64	-	20.563
7	330	260	190	-	17.088°
	301.67	253.3	174.09	-	19.571
	267	192.29	146.39	-	20.892*
	254.62	173.8	132.64	-	20.562

° **Equal** distribution of temperature difference.

* **Optimal** flashing temperatures.

1 **1-stage** flashing, no heat loss, zero moisture content of **flashing** vapor, saturated water leaving tank.

TABLE 3.6-1 (Continued) FLASHING TEMPERATURES AND TOTAL WORK FOR SATURATED WATER AT 400°F AND CONDENSING TEMPERATURE AT 120°F.

---

2 2-stage flashing, no heat loss, zero moisture content of flashing vapor, saturated water leaving tank.

3 3-stage flashing, no heat loss, zero moisture content of flashing vapor, saturated water leaving tank.

4 4-stage flashing, no heat loss, zero moisture content of flashing vapor, saturated water leaving tank.

5 3-stage flashing, no heat loss, 3% moisture content of flashing vapor, superheated water leaving tank ($z = 0.015$).

6 3-stage flashing, with heat loss ($y = 0.97$), 3% moisture content of flashing vapor, superheated water leaving tank ($z = .015$).

7 3-stage flashing, with heat loss ($y = 0.90$), 3% moisture content of flashing vapor, superheated water leaving tank ($z = 0.015$).

Turbine efficiency is assumed to be 75%.

3. Wellhead Pressure

The wellhead pressure affects the sizes of pipeline and plant components, the total flow rate of fluid from the well, and the specific steam consumption for power production. Table 3.6-2 gives some typical values of wellhead pressures at various geothermal plants. The range of pressures is 60 to 210 psig. Contini [9] stated that the wellhead pressure should be 50 percent of the closed-in pressure; however, this rule is not followed usually. James [20] showed that no such relationship exists. Bruce [6] proposed that for vapor dominated fields, if the shut-off pressure is around 450 - 480 psig, the wellhead pressure should be about 120 psig. He also showed that for a shut-off pressure of 180 psig, the turbine inlet pressure should be 65 psig. As to vapor flashing plants using two cyclone separators, he suggested the inlet pressures of a mixed pressure turbine to be 75 and 2 psig respectively. For a plant using primary steam alone, Einarsson [11] concluded that the production of power increases with decreasing wellhead pressure and that the lower limit of the wellhead pressure depends upon the sizes and costs of the wellhead equipment, steam pipe and turbine. The upper limit of turbine inlet pressure is set by the requirement that the wetness in the turbine exhaust should not be greater than 14 percent unless a special moisture removal device is provided.

The advantages of applying high wellhead pressures are: 1) low specific steam consumption; 2) small borehole diameter; 3) small diameter of the main pipeline; 4) small size of the turbine for the same power output; 5) low rate of scale formation in the well. Geothermal wells are subjected to scaling mainly due to the precipitation of silica compound and calcium carbonate. The rate of precipitation is related to pressure, temperature, rate of flow, chemical composition of the solution, and gas content in the vapor. One of the methods of reducing the precipitation in wells is to operate the well at an adequately high pressure at the expense of lowering the flow rate and power output.

Wellhead pressures most commonly used now are in the range of 70 to 100 psig. In some plants at Geysers, the wellhead pressures have been lowered from 100 to 70 psig to improve plant efficiencies. At Wairakei, a

TABLE 3.6-2 WELLHEAD PRESSURES OF GEOTHERMAL PLANTS

	Field	Location	Wellhead Pressure psig
1	Vapor Dominated	Larderello, Italy	60
2	" "	Matsuda, Japan	65
3	" "	Geysers, U.S.A.	110 - 70
4	Liquid Dominated	Kamchatka, U.S.S.R.	37
5	" "	Otake, Japan	70
6	" "	Reykjavik, Iceland	75
7	" "	Wairakei, New Zealand	80, 140, 170, 210
8	" "	Cerro Prieto, Mexico	120

number of high pressure wells which originally discharged at pressures of about 220 psig are operating at 80 or 170 psig.

James [20] studied the problem of wellhead pressures by assuming three different cases. The first case is for vapor flashing plants using a single cyclone separator. For typical boreholes with the enthalpies of liquid-vapor mixture from 420 to 1200 Btu/lb, the optimum wellhead pressure varies from 70 to 100 psig if the pressure drop in the pipeline from the well to the plant is 25 psi. The second case is for steam filled aquifers where steam exists within a finite volume without an associated water phase, and the porosity of the volcanic rock varies from 0.1 to 1.0 [21]. The optimum wellhead pressure is calculated to be 70 psig, and it does not depend upon the initial closed-in pressure or the amount of volcanic rock associated with the steam. The third case is for a hot water aquifer, for which two possibilities exist. The steam may be drawn off from the top, or the pressurized hot water may be tapped from the bottom. The pressures that give the maximum operational life of the reservoir are 50 psig for the extraction of steam and 70 psig for the removal of hot water. Next he considered capital cost factor as a function of the wellhead pressure. The minimum cost occurs at the operating pressure in the range of 80 to 100 psig.

The power output can be enhanced by employing a multi-stage flashing plant. To evaluate the effect of wellhead pressure and number of stages on power output, the optimum wellhead pressures have been calculated in this study for different arrangements as shown in Figure 3.6-14. In the arrangement A, the steam is separated in a cyclone separator at the wellhead and the remaining liquid is rejected. In the other arrangements, the liquid vapor mixture is transported in a single pipe to the plant, where the steam is separated and flashed out in two or more stages. The typical flow rates of wells for the purpose of calculations are given in Figure 3.6-15, which shows that the well flow rate decreases as the wellhead pressure increases. The power output is the product of the flow rate and the work per pound of fluid, whose available energy decreases with the decrease of wellhead pressure. There exists an optimum wellhead pressure for the maximum power output of each arrangement. The optimum flashing pressures can be determined by using the rule discussed in Section 2. The enthalpy of the mixture is assumed to be

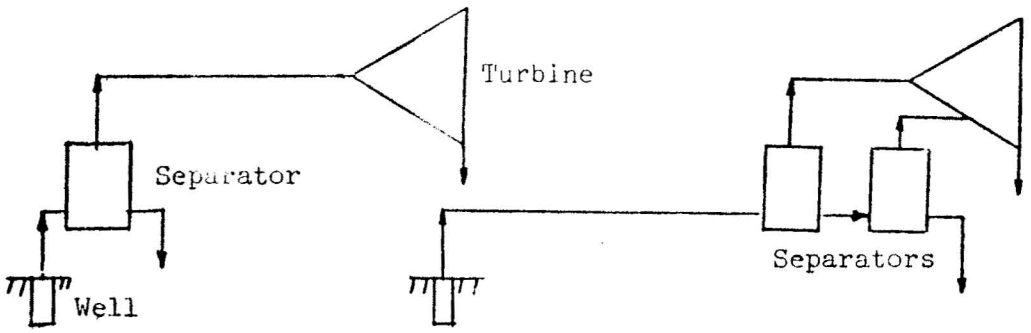

(A) Single-Stage Plant (B) Two-Stage Plant

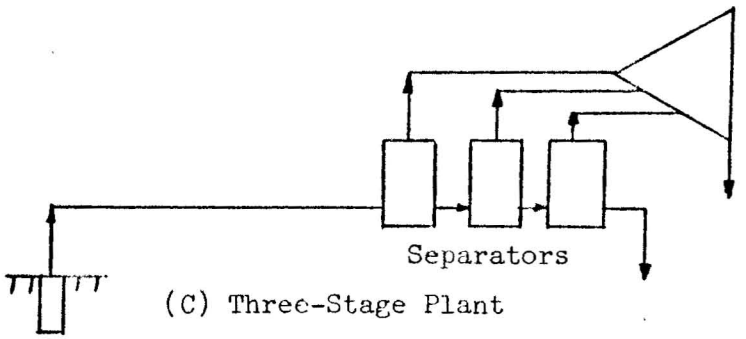

(C) Three-Stage Plant

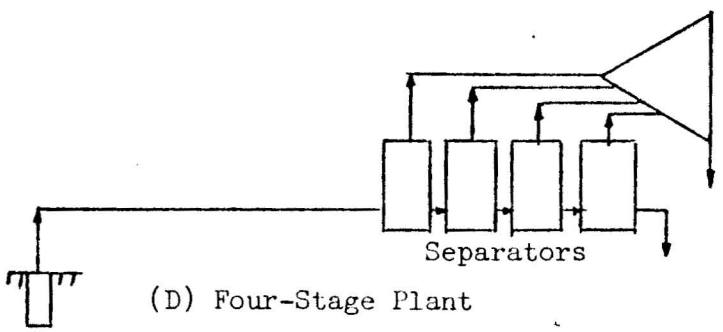

(D) Four-Stage Plant

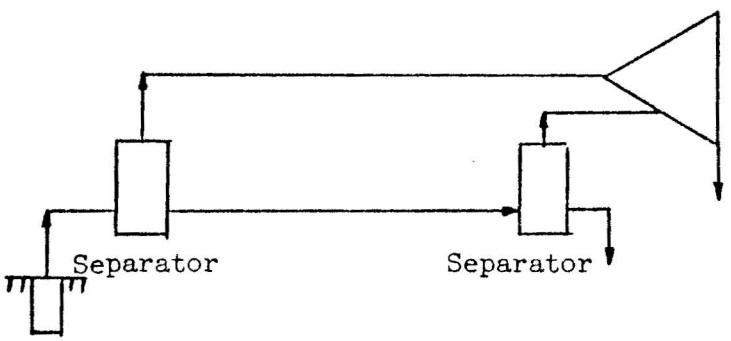

(E) Two-Stage Plant with Separate Pipelines for Steam and Water

FIG. 3.6-14 ARRANGEMENTS OF VAPOR FLASHING PLANTS

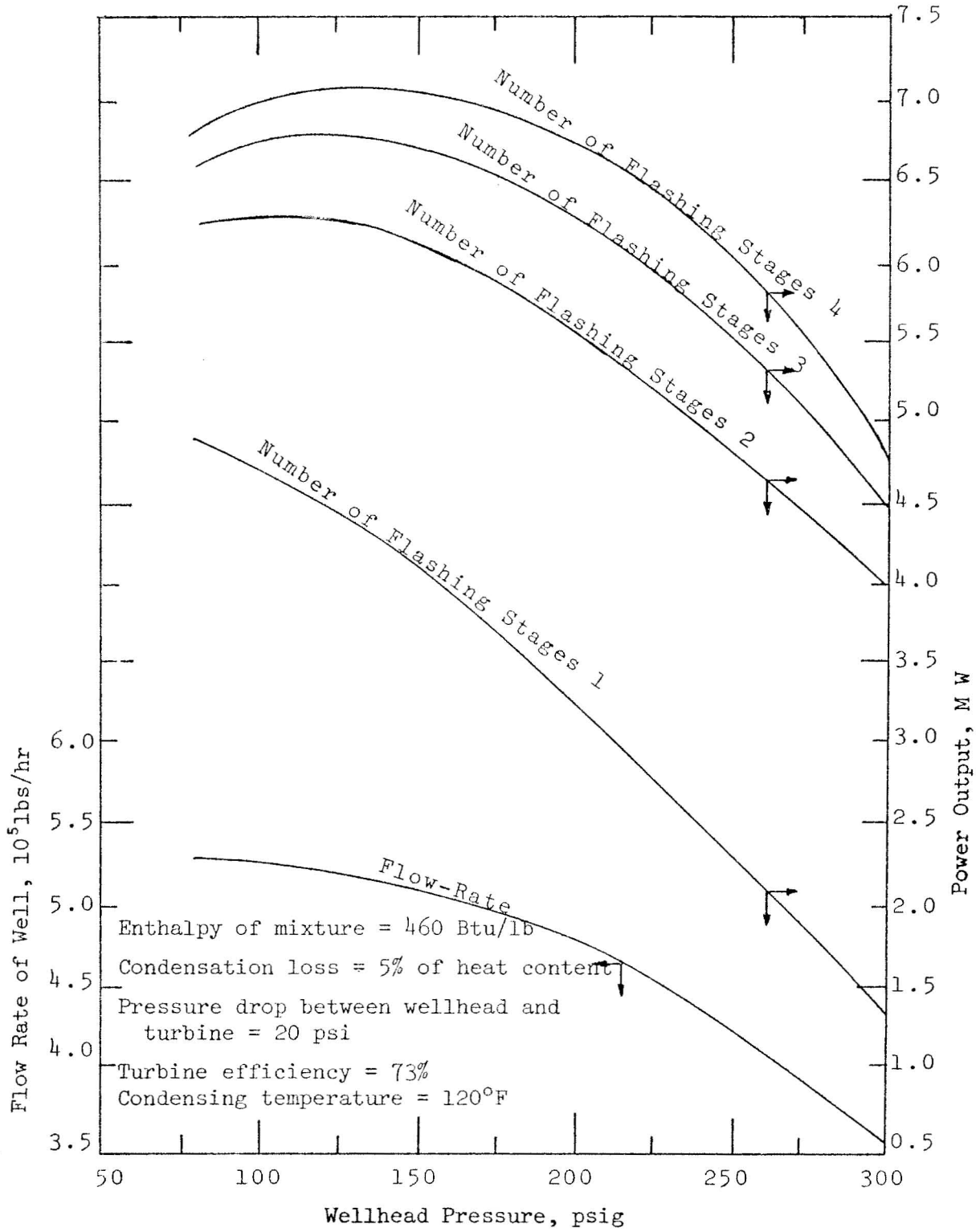

FIG. 3.6-15 WELL FLOW RATE AND POWER OUTPUT VERSUS WELLHEAD PRESSURE

460 Btu/lb. To account for the pressure drop and the condensation loss in the main pipeline, a pressure drop of 20 psi and a condensation loss of 5 percent of the fluid heat content are assumed. A combined turbine-generator efficiency of 73 percent has been used in this example. Under these assumptions, the variations of the gross power output for the four arrangements shown in Figure 3.6-14 are determined, and the results are given in Figure 3.6-15 in terms of wellhead pressure. The maximum power output of the arrangement A shown in Figure 3.6-14 is at the wellhead pressure of 80 psig, which is also the optimum pressure suggested by James [20]. By adding a flashing stage to the basic arrangement, the gain in power output is about 28.2% as shown in Figure 4. As the number of stages increases, the optimum wellhead pressure also increases and the rate of power gain diminishes. The second and third additional stages contribute relatively small gain in power output, 8.2 and 3.9% of the power output of the single stage plant respectively. The specific volume of the flashed steam and the size and cost of turbine increase rapidly with the number of stages. However, the moisture of exhaust steam in a multi-stage arrangement is lower than that in the single stage arrangement. The moisture contents and the specific volumes of the steam in the last flashing stages of the four arrangements of the example are as follows:

	Single Stage	2-Stage	3-Stage	4-Stage
v of steam ft^3/lb	4.6	22.2	36.4	53.5
x, $\frac{\text{lb. water}}{\text{lb. mixture}}$	18.5%	16.5%	16.1%	15.8%

In consideration of the overall costs, the optimal number of stages might be two for the majority of the plants.

In the arrangement E shown in Figure 3.6-14, steam and water are separated at the wellhead and transported separately to the plant, where water is flashed to steam. Takahashi [33] and James [22] carried out their studies independently and concluded that the arrangement E is not as economical as the arrangement B, which can yield the additional power at the least cost.

Generally, a turbine is driven by steams from several wells. Each well has its own flow characteristic. The characteristic curves of the flow rate versus wellhead pressure for the individual wells may be superimposed to

obtain the combined characteristic curve in the same manner as dealing with the overall performance of pumps in parallel. The pressure drops in the branches and the main line are directly related to the power loss, the design, and the cost of the piping system. In some existing systems, the pressure drop amounts to about 15-20 psi. When selecting the wellhead pressure, the effect of pressure drop on the system performance must not be neglected.

In Fig. 3.6-15, the curves near the points of maximum power output are flat. It appears desirable to select a wellhead pressure higher than the optimum pressure since the sizes of pipes and equipment can be lowered by increasing the working pressure. However, Usui et al. [34] argued that it is not advisable to select a wellhead pressure higher than the pressure which gives the maximum power because (1) such a design is apt to suffer power decrease by scale deposition on the nozzles and blades of the turbine, and (2) the well flow rate does not remain constant with time. At low wellhead pressure, the drop of flow rate may be retarded, and the underground paths of water are less likely to be blocked.

4. Cyclone Separator

The main function of a cyclone separator in a geothermal plant is to separate the steam fraction from the steam-water mixture. A tangential inlet of the separator creates the spinning vortices in the fluid. The liquid water is centrifuged to the walls while the steam fraction is removed from a concentric outlet.

In the bottom outlet cyclone (BOC) separator shown in Fig. 3.6-16, steam is removed from the bottom. At present, the BOC type of separator is very popular in vapor flashing plants. It can produce steam at a quality of 99.9 percent or better. A spiral inlet is better than a tangential inlet (Fig. 3.6-16) because it can streamline the flow so that the erosion of the wall can be reduced. Bengma [4] conducted tests on a BOC separator to evaluate the performance and determine the optimum dimensions. He analyzed his results with inlet mass wetness, outlet mass wetness, inlet volumetric wetness, inlet velocity, and breakdown point as the important parameters. The inlet and outlet mass wetness were defined as the ratio of mass flow of liquid water to the total mass flow of liquid water and steam. The inlet velocity was taken as the inlet mass flow of steam fraction multiplied by the specific volume of

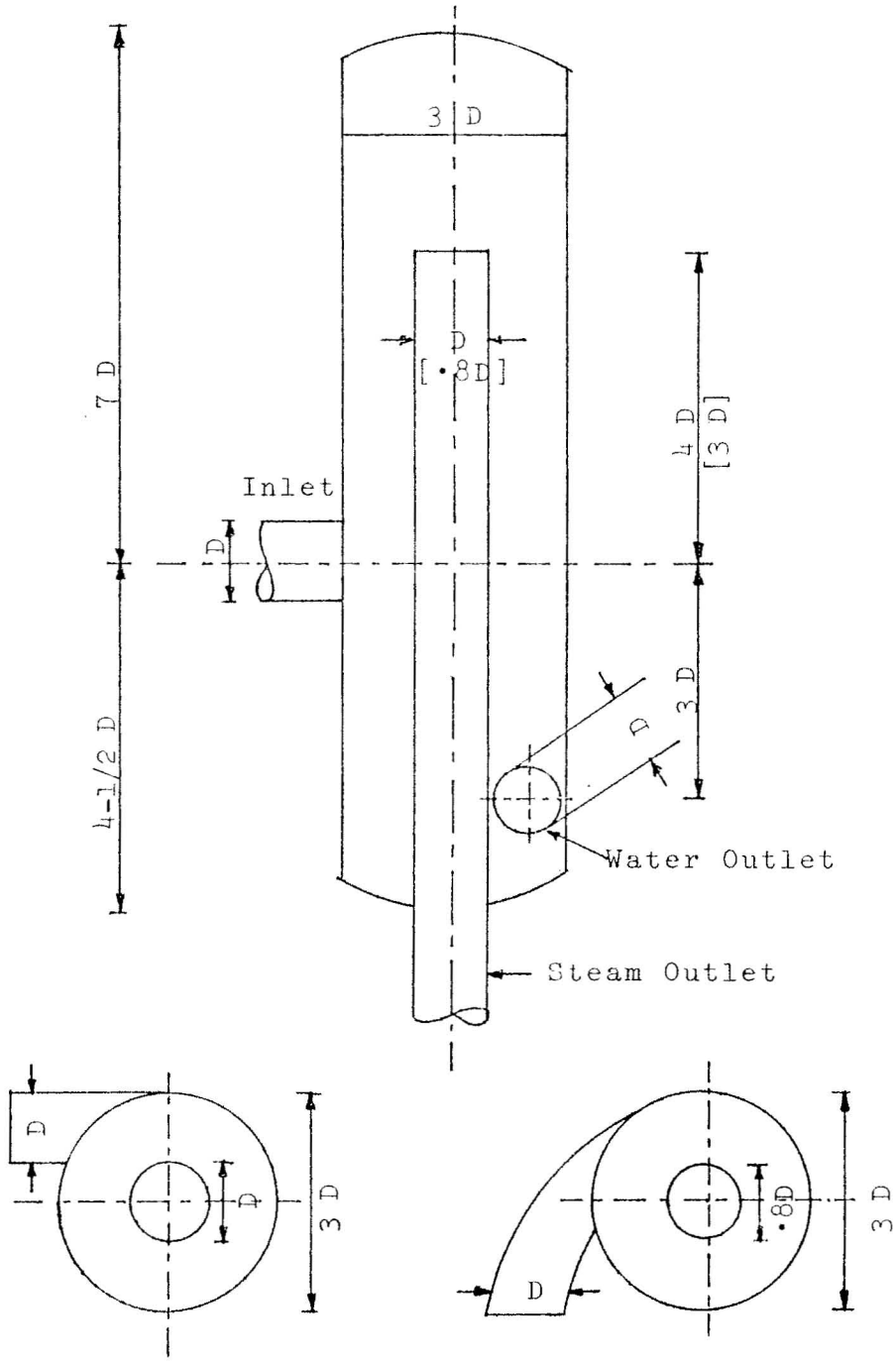

FIG. 3.6-16 BOTTOM OUTLET CYCLONE SEPARATOR WITH TANGENTIAL AND SPIRAL INLETS [4]

steam and then divided by the area of inlet. The breakdown point refers to the condition at which the mass wetness of separated steam is 0.5 percent. The following conclusions can be drawn from his investigation: (1) Separation is quite satisfactory at low inlet velocities regardless of the inlet wetness of steam. (2) The lower the separator pressure, the lower the inlet velocity at which breakdown occurs. (3) For a given separator inlet pressure, the drier the mixture, the greater the flow the separator can handle. (4) The pressure drop increases as the inlet velocity or the inlet volumetric wetness increases. Figure 3.6-17 shows the pressure drop between separator inlet and steam outlet plotted against the inlet velocity for different volumetric wetnesses. The variations of wetness of outlet steam with inlet velocity for different volumetric wetnesses are plotted in Figure 3.6-18.

To determine the most efficient separator configuration, the tests were made by Bengma [4] to experimentally find the optimum dimensions of the cyclone body, inlet, water outlet and steam outlet. In Figure 3.6-16 are the recommended dimensions, with the dimensions for tangential inlet in brackets. The dimensions are expressed in terms of the inlet diameter D since the inlet velocity governs the separator performance. From the rate of mass flow, the inlet mass wetness and the flashing pressure, the steam inlet velocity can be calculated for given values of pressure drop and separating efficiency by using Figures 3.6-17 and 3.6-18. The inlet pipe diameter and hence other dimensions can be determined from the steam inlet velocity and the recommended proportions in Figure 3.6-16.

Figure 3.6-19 shows a possible arrangement of two cyclone separators. The liquid-vapor mixture from the wells is led to the main pipeline. To meet varying load demands in a narrow range, a pressure control valve is provided to regulate the flow rate. The operating pressures of the separators are controlled by two throttling orifices. The experiences of plant operation in New Zealand, Japan and Mexico show that a float controlled valve is not as reliable as a throttling orifice. If the pressure in the second separator is below atmospheric pressure, a steam ejector or vacuum pump should be used for maintaining the vacuum in the storage tank. The liquid trap in the diagram is a device which is used to check the flow of liquid in the steam line. Care must be taken to guard against any possibility of a slug of water entering the steam line [2, 14, 36]. The water is collected in a surging tank, in which

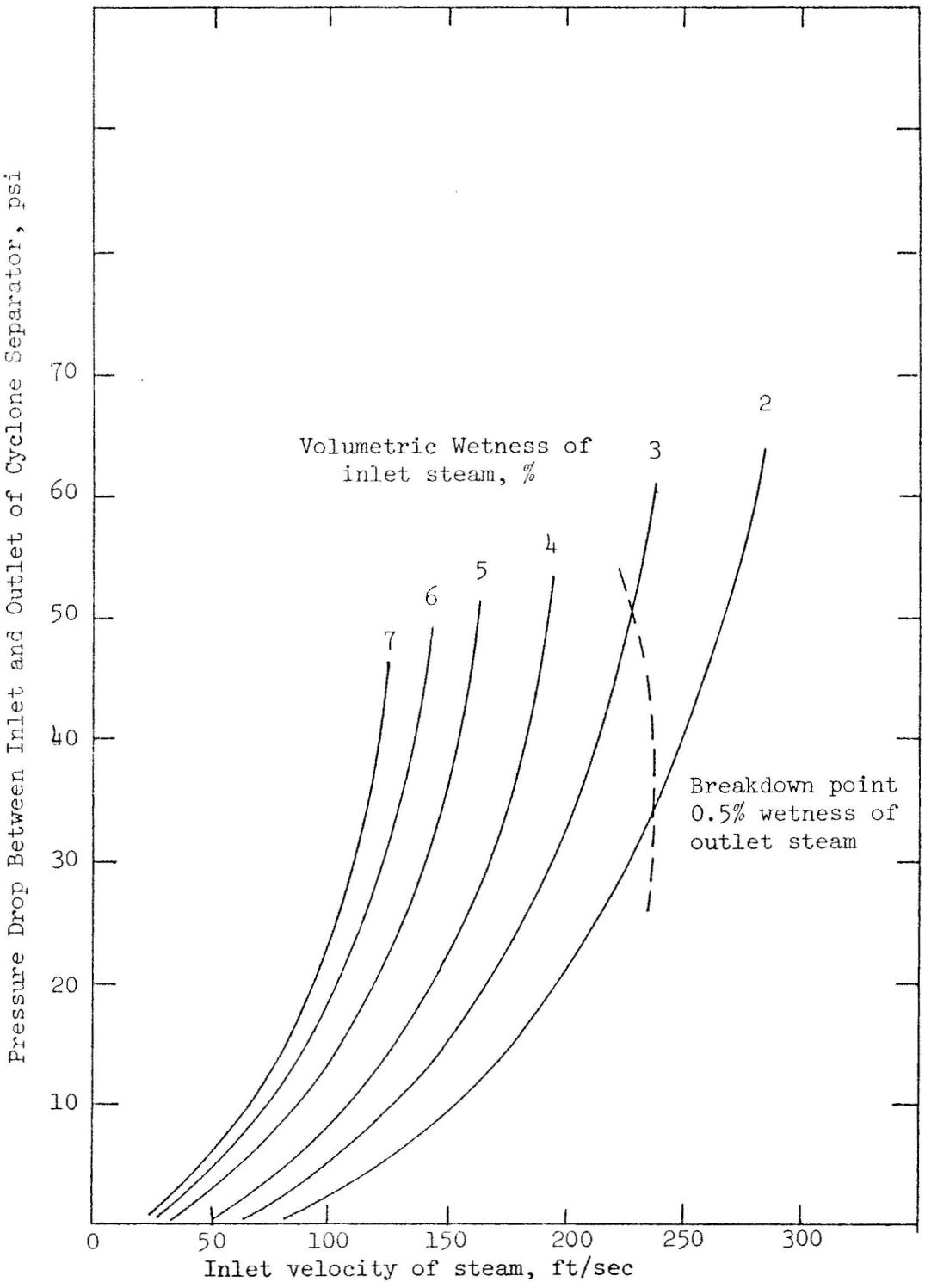

FIG. 3.6-17 EFFECT OF INLET WETNESS AND INLET VELOCITY ON PRESSURE DROP BETWEEN INLET AND OUTLET OF BOC SEPARATOR [4]

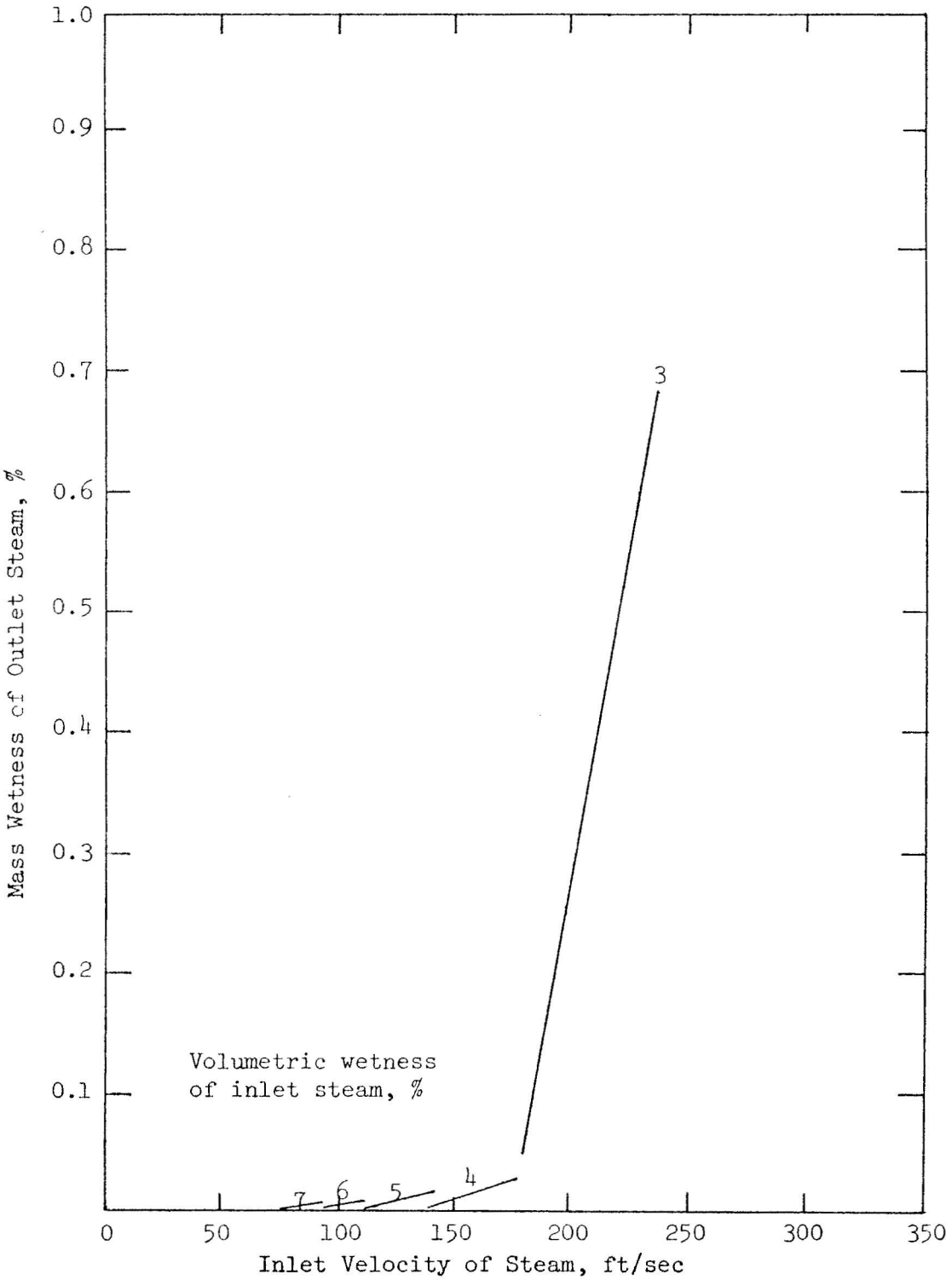

FIG. 3.6-18 EFFECT OF INLET WETNESS AND INLET VELOCITIES ON WETNESS OF OUTLET STEAM [4]

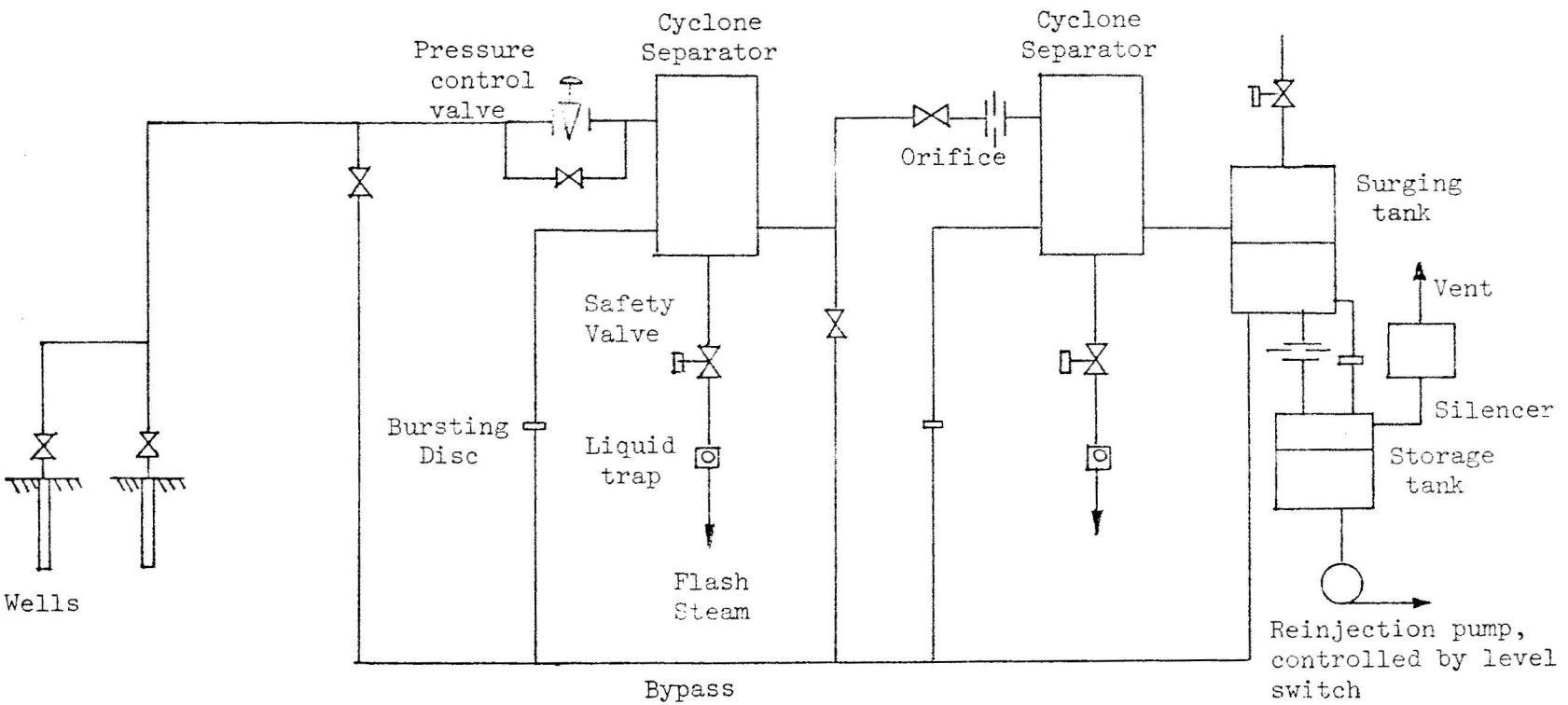

FIG. 3.6-19 FLOW DIAGRAM OF TWO LIQUID-VAPOR SEPARATORS

the level of liquid is effectively maintained by the throttling orifice. In the case of blockage of orifice or a large increase in water flow, the safety devices come into action for protection against the overflow in the surging tank.

5. Turbine

Estimates of turbine-performance are usually required in the preliminary stages of power plant design, and the estimation can often be made from the information available in manufacturer's publications and other literature. As an illustration, the performance curves have been estimated for the 10 MW turbine in a three-stage vapor flashing plant which generates power from saturated hot water at 400°F. The temperatures of the flash tanks are 330, 265 and 200°F and the turbine back pressure is 4 inches Hg absolute. According to the technical bulletins by General Electric Company [12, 25], the ratio of specific steam consumption at 20% to that at full load is 1.24. In Figure 3.6-20 is the estimated performance curve, and the basic steam rates can be found by extrapolation from the tables.

6. Heat Balance of a Hypothetical Plant

The design of a plant starts from the energy and mass balances, or called heat balances, from which the system performance and the requirements of the components may be determined. The first step of heat balance is to select basic parameters. By varying the values of the parameters, a number of heat balances can be worked out to form the basis for making decisions on the selection of the design. As an example, the heat balance of a two-stage vapor flashing plant is given in this section. Figure 3.6-21 shows the flow diagram of the plant, for which the basic assumptions are as follows:

Power output	=	8 MW
Number of cyclone separators	=	2
Wellhead pressure	=	100 psig
Number of wells	=	2
Water flow	=	10^6 lb/hr
Gas flow	=	3000 lb/hr
Enthalpy of water	=	400 Btu/lb
Pressure drop in main pipeline	=	10 psi
Condensation loss	=	3% of the heat content of water

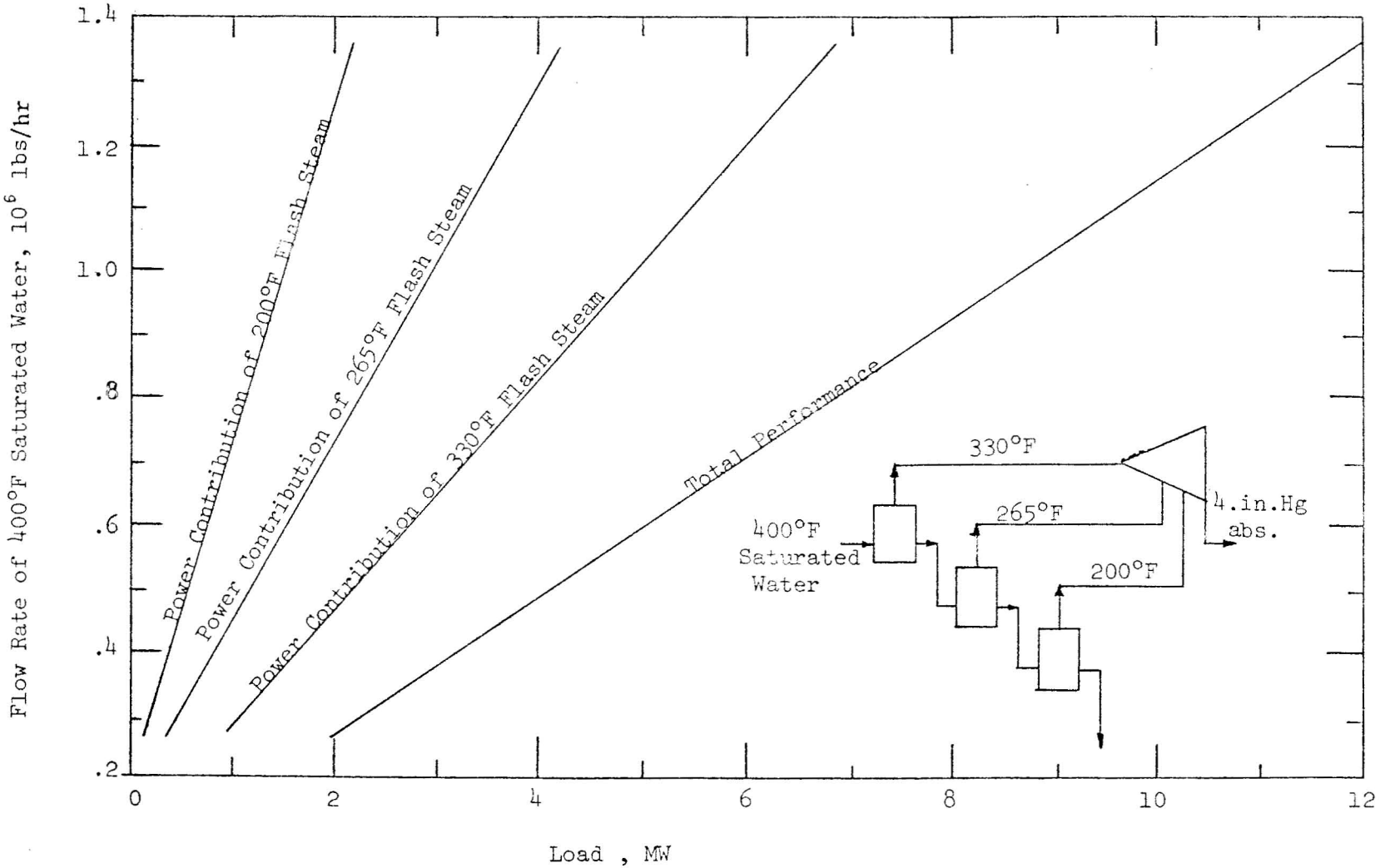

FIG. 3.6-20 ESTIMATED PERFORMANCE OF A 10 MW TURBINE FOR PLANT USING 400°F SATURATED WATER

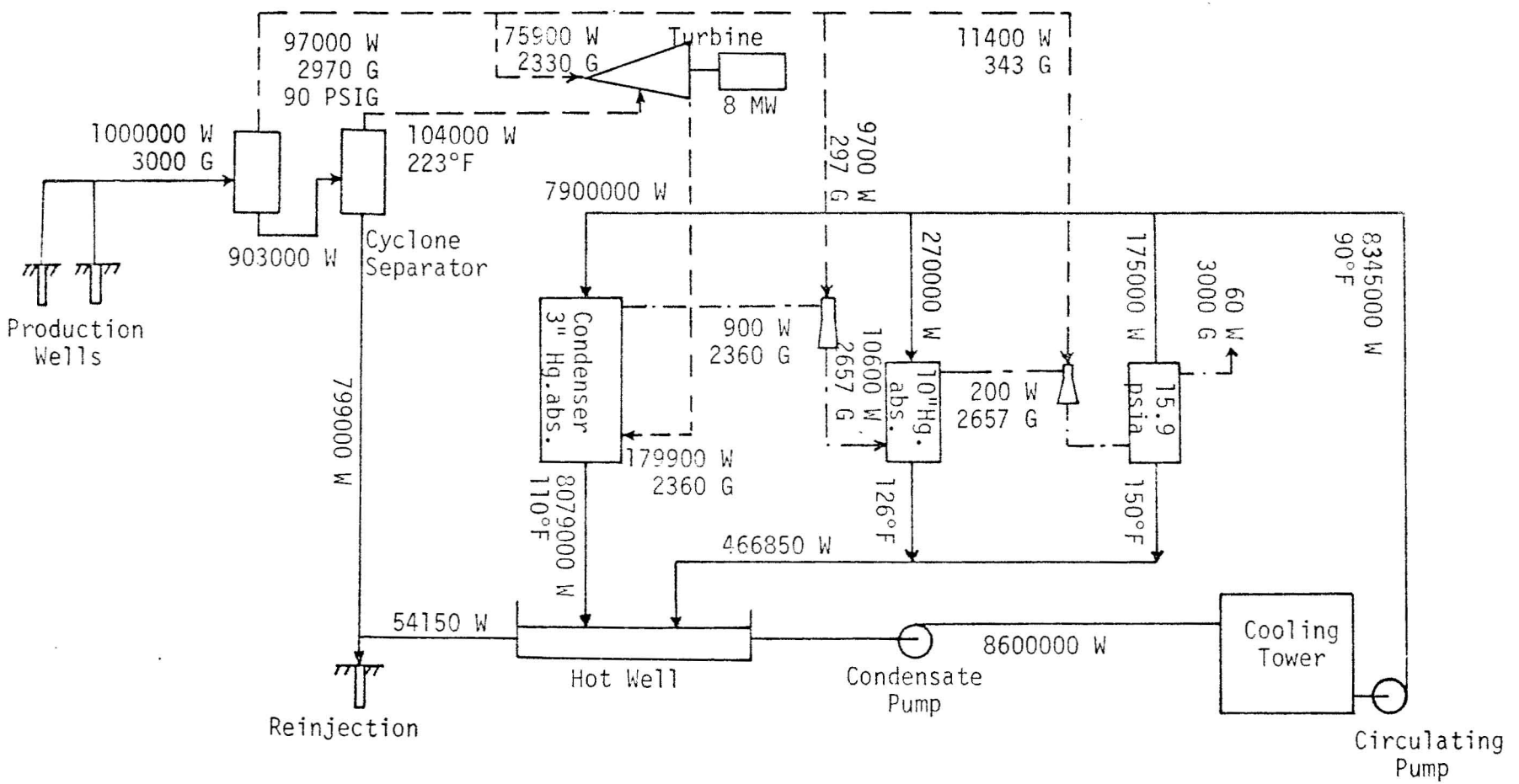

W = lb. water and steam per hr., G = lb. gas per hr.

FIG. 3.6-21 FLOW DIAGRAM OF A VAPOR FLASHING PLANT

Turbine-generator efficiency	=	73%
Pump efficiency	=	75%
Fan motor efficiency	=	90%
Ejector efficiency	=	5.6%
Condensing pressure	=	3 in. Hg. abs.
Wet bulb temperature	=	75°F
Approach of cooling tower	=	15°F

The process of heat balance involves the selection of the optimum flashing temperature, the energy and material balances of geothermal water, non-condensable gases and cooling water. The optimum flashing temperature of this example is 223°F, as determined by the rule stated in Section 2. After the temperature in the second cyclone separator is selected, the steam productions of the two separators can be determined. They are 97,000 lb/hr and 104,000 lb/hr respectively.

The wellhead pressure affects the flow rate of fluid from the well and the specific steam consumption for power production. To evaluate the effect of wellhead pressure on the specific steam consumption, Figure 3.6-22 has been constructed for different enthalpies of well water. The graph shows that the pressure which yields the highest power output per million pounds of water, i.e., the lowest specific steam consumption, increases as the enthalpy of well water increases.

7. Cooling Tower

Cooling towers can be either dry or wet type. The dry cooling towers are not suitable for a condensing geothermal plant because: (1) they can cool water only to the limit of dry bulk temperature, (2) due to the mineral content of the condensate, the surfaces of the tubes are subject to fouling, (3) they are costly. The draft of a wet cooling tower can be produced mechanically or naturally. As compared with mechanical draft towers, natural draft towers occupy less space, consume less power and require less piping. They do not have many problems of fogging, drift and internal recirculation, and have long service life. However, they are not economical for plants having ratings less than 150 MW [31]. A mechanical draft tower can operate on forced or induced draft fans. The forced draft tower has the disadvantages of nonuniform air distribution and partial recirculation of vapor. As to induced draft towers, the crossflow design has distinct advantages over the counterflow arrangement.

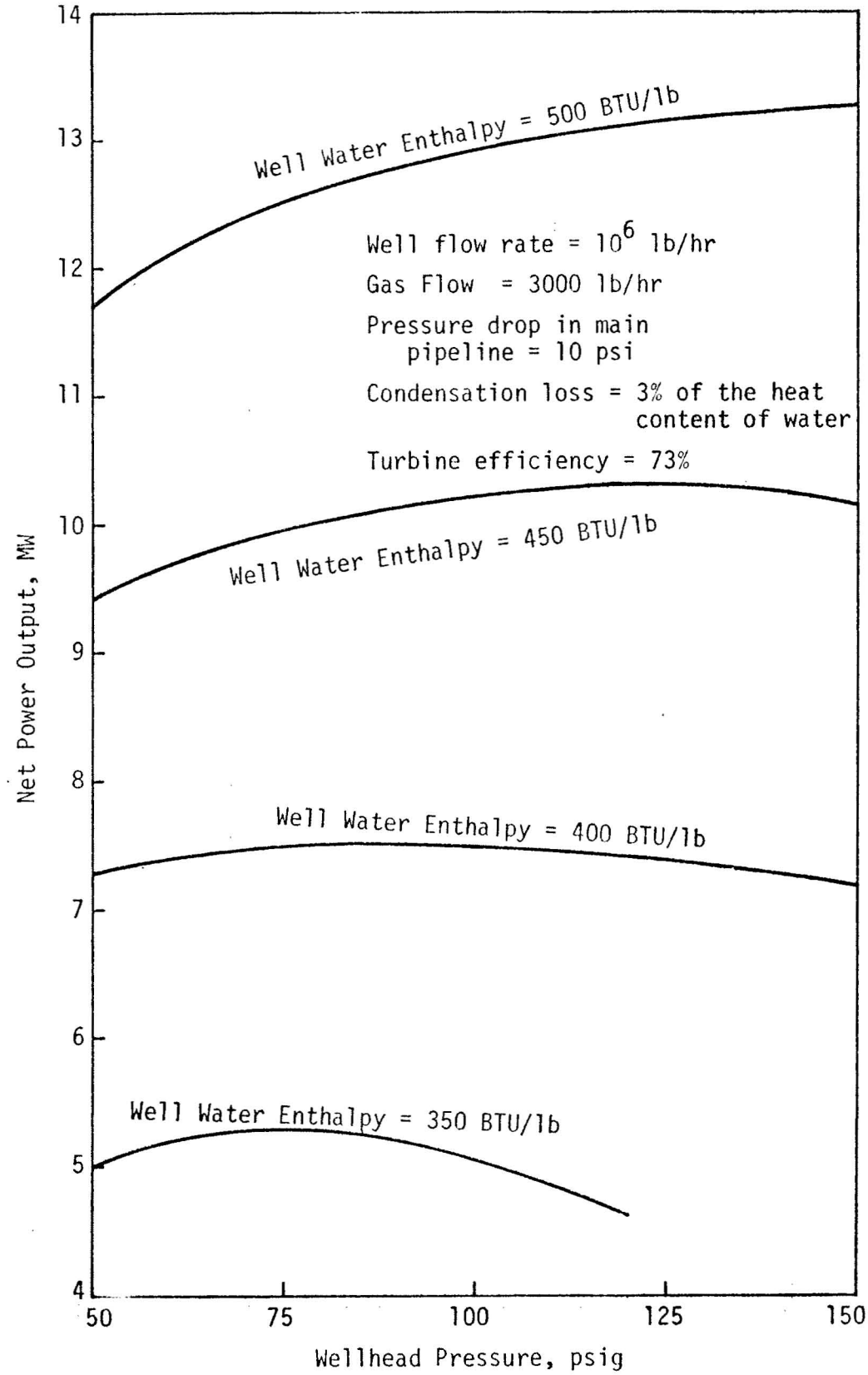

FIG. 3.6-22 VARIATION OF SPECIFIC POWER OUTPUT WITH WELLHEAD PRESSURE FOR A TWO-STAGE VAPOR FLASHING PLANT

The distance of air travel in a crossflow tower is independent of the fill height; thus, both the distance of air travel and the height of the fill can be adjusted to minimize the loss of draft. In a counterflow tower, the distance of air travel varies directly with the fill height, which can be increased only at the expense of increasing the horsepower of the fan to compensate for the loss of draft. Cooling range is the temperature difference between the hot water entering the tower and the cold water leaving the tower. The crossflow tower is better than the counterflow tower to handle a large cooling range and a small approach, which is the difference between the wet bulb temperature of air and the temperature of leaving water. Besides, the pumping head of crossflow tower is lower than that of counterflow tower. In conclusion, an induced-draft crossflow tower is recommended for a geothermal power plant.

The performance of a cooling tower is a function of the cooling range, the approach and the ratio of water flow to air flow. The usual range of cooling towers in power plants is 10 to 40°F while the approach may be around 15°F. The approach has a great influence on the size of tower. The closer the cold water temperature approaches the wet bulb temperature, the greater the size of tower. The usual range of water-air mass flow ratio (L/G) is around 1.2 - 2.0 for mechanical draft towers in steam power plants.

In a cooling tower, there are numerous tiny water droplets, from which heat is transferred to the air in the free stream. The quantity of heat lost by the water is equal to the amount of heat gained by air; and the net transfer of energy may be expressed in terms of enthalpy potential as follows [3, 37]:

$$-L\ Cpw = G \cdot dh = K \cdot a \cdot dV \cdot (h' - h) \tag{B.29}$$

or

$$-l \cdot (dx)\ (dy)\ Cpw \cdot dt = g \cdot (dz)(dy)\ dh = K \cdot a \cdot dx \cdot dy \cdot dz \cdot (h' - h) \tag{B.30}$$

where dx, dy and dz are the dimensions of an infinitesimal volume dv, L and G are the flow rates of water and air in lb/hr respectively, l and g are the water and air flow rates per unit cross-sectional area perpendicular to the respective direction of flow in $lb/hr/ft^2$, $h' - h$ is the enthalpy potential defined as the difference between the enthalpy h' of saturated air at temperature

t of water and the enthalpy of the unsaturated air in the free stream, a is the surface area of water per unit volume of tower in cu. ft./sq. ft., Cpw is the specific heat of water and K is the overall coefficient in lb/hr. sq. ft. which relates enthalpy potential to the heat transferred from water to air. For a small increment of tower with $\Delta x = \Delta z$, equation (B.30) may be revised as

$$\Delta h = \frac{-1}{g} \cdot \Delta t \qquad \text{(B.31)}$$

$$\left(\frac{\Delta t}{h^1 - h}\right)_{avg} \cdot \left(1 \cdot \frac{Btu}{lb\ °F}\right) = \frac{-K \cdot a}{1} \cdot \Delta z \qquad \text{(B.32)}$$

where Δz is the incremental height of tower in ft.

The dimensionless term in the right hand side of equation (B.32) is called number of transfer units (N T U). The dimensions of the tower can be related to NTU for a given design condition. To analyze a crossflow tower, the tower is divided into a series of incremental volumes, horizontally and vertically as shown in Figure 3.6-23. For the example, it is assumed: inlet water temperature 120°F, wet bulb temperature of air 75°F, ratio of water flow to air flow (1/g) 2.5 and NTU 0.2 for every increment. The calculations were started at the upper left corner, where the conditions of entering air and water are given. By trial and error, one finds in the first increment: $(h^1 - h)_{in}$ = 80.98 Btu/lb, $(h^1 - h)$ avg. + 53.23 Btu/lb, Δt = 10.65°F, Δh = 26.63 Btu/lb, $(h^1 - h)_{out}$ = 24.97 Btu/lb, and temperature of leaving water = 109.35°F. The calculations proceed progressively to the subsequent increments. There are five horizontal and nine vertical increments. The ratio of water flow in lb/hr to air flow in lb/hr is $(1/g)\cdot(5/9) = 1.39$.

The height and length of the tower are related to the total number of transfer units, designated as number of vertical transfer units (NVTU) in the vertical direction and number of horizontal transfer units (NHTU) in the horizontal direction. In Figure 3.6-23, NVTU = (no. of vertical increments) (NTU) = (9)(0.2) = 1.8, and NHTU = (5)(0.2) = 1.0. Since equations (B.31) and (B.32) are based on the condition that the height of an increment is equal to its width, $\Delta x = \Delta z$, the ratio NVTU/NHTU gives the proportion of the height to the width of tower.

Water
$t = 120^{\circ}F$
$h^1 = 119.59$ BTU/lb

AIR, Wet Bulb Temperature = 75°F
h = 38.61 Btu/lb

$\Delta t = 10.65$ $t = 109.35$ $h^1 = 90.91$ h=65.24	$\Delta t = 7.1$ $t = 112.9$ $h^1 = 99.68$ h=82.99	$\Delta t = 4.75$ $t = 115.71$ $h^1 = 105.71$ h=94.87	$\Delta t = 3.2$ $t = 116.8$ $h^1 = 110.22$ h=102.87	$\Delta t = 2.16$ $t = 117.84$ $h^1 = 113.24$ h=108.27
$\Delta t = 7.16$ $t = 102.19$ $h^1 = 75.78$ h=56.51	$\Delta t = 5.95$ $t = 106.95$ $h^1 = 85.63$ h=70.39	$\Delta t = 4.77$ $t = 110.94$ $h^1 = 94.72$ h=32.32	$\Delta t = 3.67$ $t = 113.15$ $h^1 = 100.31$ h=91.5	$\Delta t = 2.82$ $t = 115.02$ $h^1 = 105.04$ h=98.55
$\Delta t = 5.21$ $t = 96.98$ $h^1 = 66.52$ h=51.64	$\Delta t = 4.66$ $t = 102.29$ $h^1 = 75.98$ h=63.29	$\Delta t = 4.26$ $t = 106.68$ $h^1 = 85.04$ h=73.94	$\Delta t = 3.51$ $t = 109.64$ $h^1 = 91.55$ h=82.72	$\Delta t = 2.17$ $t = 112.85$ $h^1 = 99.55$ h=94.15
$\Delta t = 3.98$ $t = 93$ $h^1 = 60.25$ h=48.56	$\Delta t = 3.83$ $t = 98.46$ $h^1 = 69.03$ h=58.14	$\Delta t = 3.68$ $t = 103$ $h^1 = 77.34$ h=67.34	$\Delta t = 3.29$ $t = 106.35$ $h^1 = 84.31$ h=77.57	$\Delta t = 3.19$ $t = 109.66$ $h^1 = 91.59$ h=83.55
$\Delta t = 3.1$ $t = 89.9$ $h^1 = 55.79$ h=46.36	$\Delta t = 3.2$ $t = 95.26$ $h^1 = 63.74$ h=54.36	$\Delta t = 3.19$ $t = 99.81$ $h^1 = 71.39$ h=62.34	$\Delta t = 3.01$ $t = 103.34$ $h^1 = 78.01$ h=69.87	$\Delta t = 2.95$ $t = 106.71$ $h^1 = 85.10$ h=77.25
$\Delta t = 2.49$ $t = 87.41$ $h^1 = 52.46$ h=44.84	$\Delta t = 2.69$ $t = 92.57$ $h^1 = 59.62$ h=51.57	$\Delta t = 2.78$ $t = 97.03$ $h^1 = 66.6$ h=58.52	$\Delta t = 2.71$ $t = 100.63$ $h^1 = 72.88$ h=65.3	$\Delta t = 2.71$ $t = 104$ $h^1 = 79.31$ h=72.08
$\Delta t = 2.02$ $t = 85.39$ $h^1 = 49.91$ h=43.65	$\Delta t = 2.3$ $t = 90.27$ $h^1 = 56.31$ h=49.39	$\Delta t = 2.44$ $t = 94.59$ $h^1 = 62.68$ h=55.49	$\Delta t = 2.57$ $t = 98.06$ $h^1 = 68.33$ h=61.02	$\Delta t = 2.54$ $t = 101.46$ $h^1 = 74.41$ h=67.37
$\Delta t = 1.64$ $t = 83.75$ $h^1 = 47.93$ h=42.72	$\Delta t = 2.05$ $t = 88.22$ $h^1 = 53.52$ h=47.25	$\Delta t = 2.21$ $t = 92.38$ $h^1 = 59.34$ h=52.78	$\Delta t = 2.2$ $t = 95.86$ $h^1 = 64.7$ h=58.28	$\Delta t = 2.26$ $t = 99.2$ $h^1 = 70.31$ h=63.93
$\Delta t = 1.38$ $t = 82.38$ $h^1 = 46.33$ h=42.04	$\Delta t = 1.67$ $t = 86.55$ $h^1 = 51.33$ h=46.22	$\Delta t = 1.89$ $t = 90.49$ $h^1 = 56.62$ h=50.95	$\Delta t = 1.96$ $t = 93.9$ $h^1 = 61.62$ h=55.85	$\Delta t = 2.04$ $t = 97.16$ $h^1 = 66.82$ h=60.95

FIG. 3.6-23 DISTRIBUTION OF WATER TEMPERATURE AND AIR ENTHALPY IN A CROSS-FLOW COOLING TOWER

The resulting average temperature of the water is 90.1°F for the example given in Fig. 3.6-23. The variations of water temperature with different values of NHTU and NVTU for the typical example were calculated and are given in Table 3.6-3. To facilitate the application of the calculated results to the estimation of tower performance, Fig. 3.6-24 was constructed with water temperature as ordinate, and NHTU and NVTU as the other two variable parameters. For a given value of leaving temperature of water, there are various combinations of the L/G ratio, the number of horizontal increments and the number of vertical increments of tower. The volume of tower fill and the draft loss are affected by the height and the width. The recommended design point is at L/G ratio of about 1.6 [29].

The values of K•a have been experimentally determined in relation to air flow (g) for a splash filled tower by Snyder [30], as shown in Fig. 3.6-25. At g = 1000 lb/hr - ft^2, the value of K•a is 93 lb/hr - ft^3 from the diagram. Since the value of NVTU is equal to the product of the number of vertical increments and NTU, by equation (B.32) we have: tower height = (NVTU) (1/K•a); likewise tower width = (NHTU) (1/K•a). For the L/G ratio of 1.39, one finds NHTU = 1.0 and NVTU = 1.8 from Fig. 3.6-23; thus tower height = 45.9 ft. and tower width = 25.5 ft. Usually the air enters a tower from two opposite sides. If so, the width of the tower doubles to 2 x 25.5 = 51 ft. For 24,000 gpm of water flow (L), the dimensions of the tower are 48.4 ft high x 53.6 ft wide x 96 ft long. If the tower is divided into three cells, the length of each cell is 32 ft.

Special materials are needed to resist the chemical reaction of the impurities in the water. The condensate and cooling tower pipes can be made of stainless steel, aluminum, or a plastic-coated material. The casing is usually made of asbestos cement. For additional resistance to corrosion, the wetted surface may be coated with tar, epoxy compounds, or synthetic rubbers. The drift eliminators can be of treated wood, galvanized steel, stainless steel, plastic, or coated asbestos. The material of the tower filling can be of redwood, plastic, aluminum, stainless steel, or ceramics. The last three are expensive. Test results at Geysers showed polyvinyl chloride as a favorable material for the tower fill.

TABLE 3.6-3 TEMPERATURES OF WATER LEAVING A CROSS-FLOW COOLING TOWER

NHTU	NVTU								
	.2	.4	.6	.8	1.0	1.2	1.4	1.6	1.8
.2	109.35°F	102.19	96.98	93	89.9	87.41	85.39	83.75	82.38
.4	111.13	104.57	99.64	95.73	92.58	89.99	87.83	85.99	84.47
.6	112.65	106.69	101.98	98.15	94.94	92.34	90.08	88.12	86.47
.8	113.69	108.31	103.90	100.20	97.08	94.41	92.08	90.05	88.33
1.0	114.52	109.65	105.69	102.09	99	96.33	93.95	91.88	90.10

Flow Ratio l/g = 2.5

Wet Bulb Temperature = 75°F

Temperature of Leaving Water = 120°F

NTU = 0.2

NHTU = (No. of horizontal increments) (NTU)

NVTU = (No. of vertical increments) (NTU)

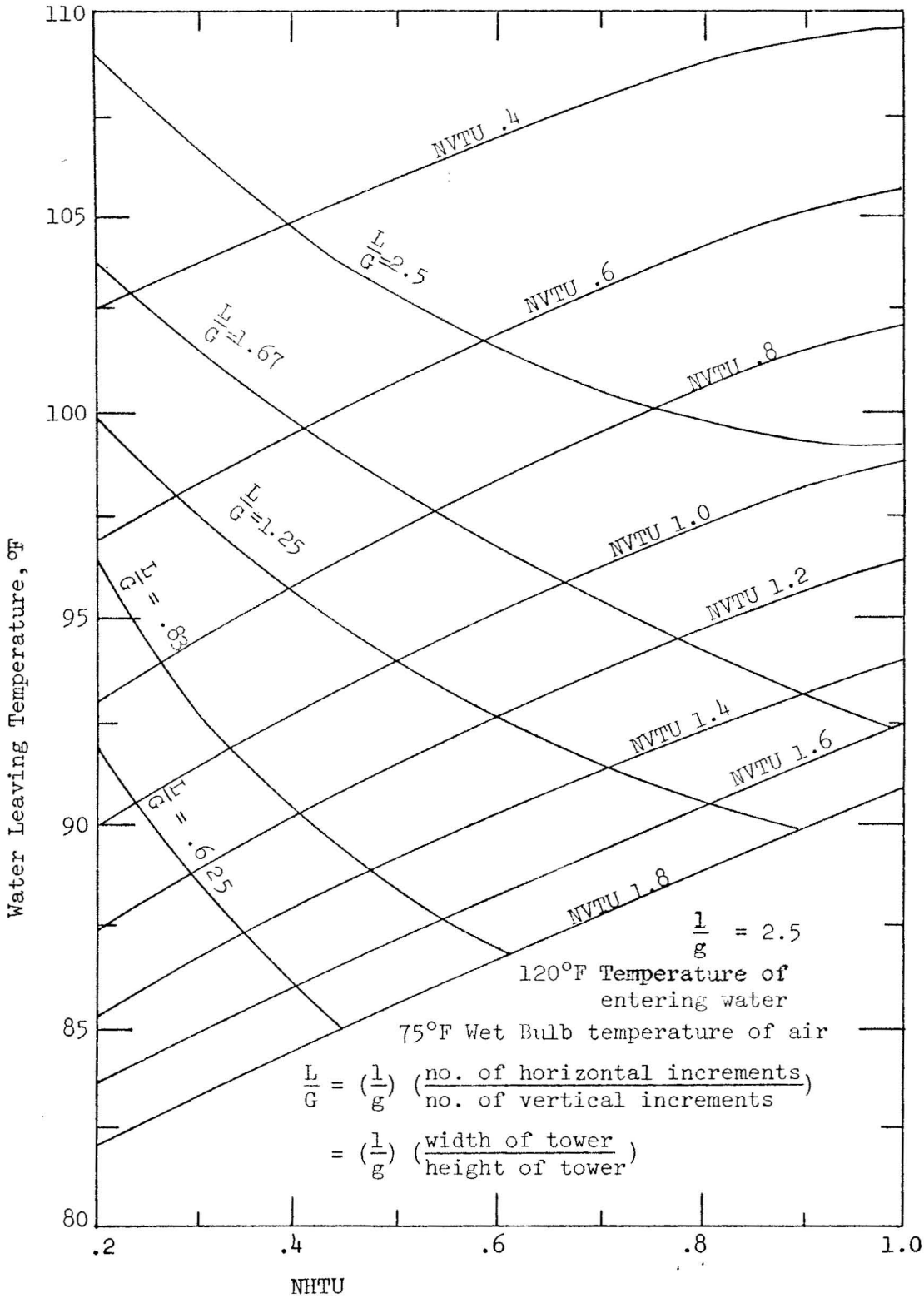

FIG. 3.6-24 PERFORMANCE OF A CROSS-FLOW COOLING TOWER

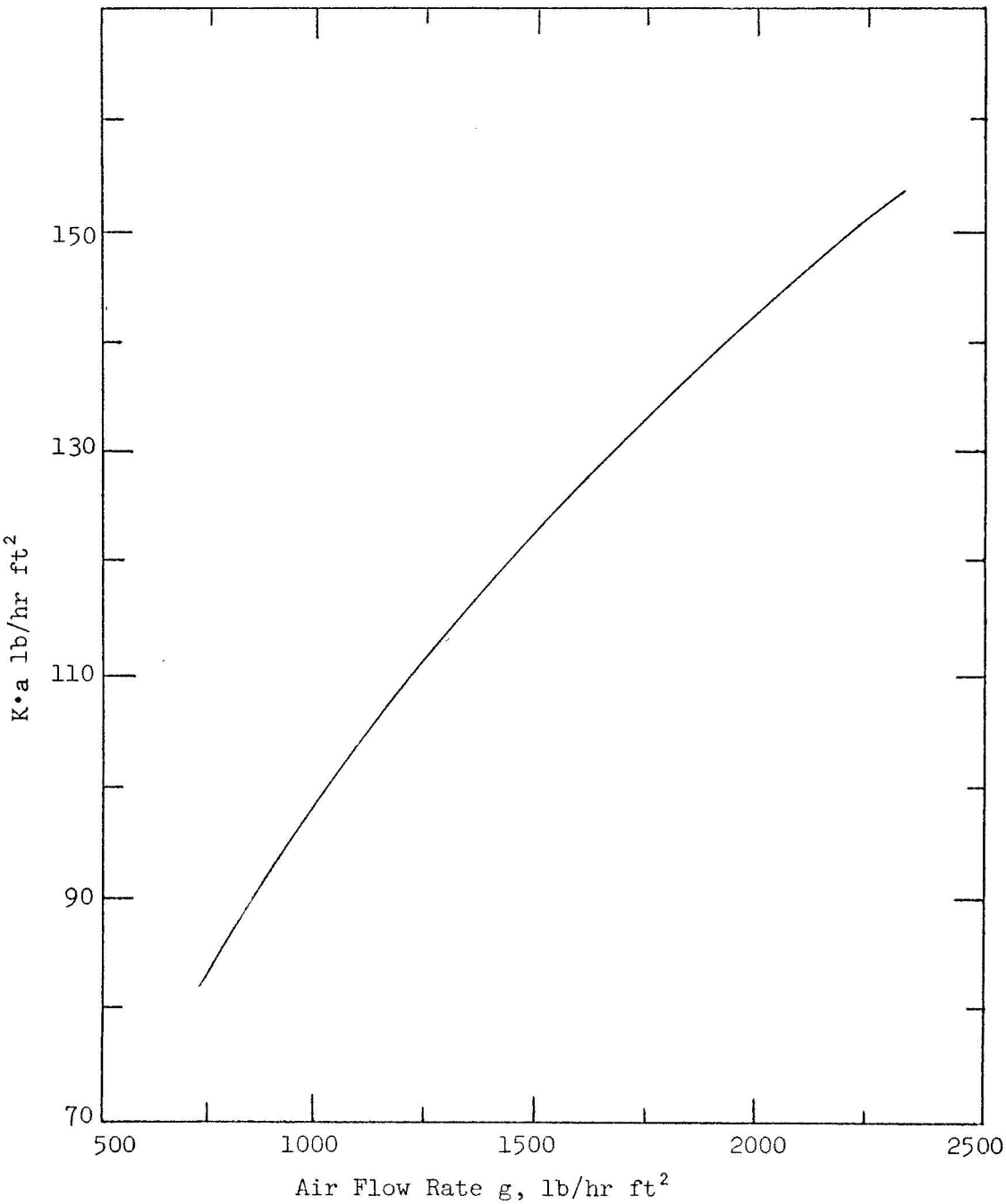

FIG. 3.6-25 TOWER COEFFICIENT K•a VERSUS AIR FLOW RATE g [30]

8. Arrangement of Equipment

Several arrangements of the power plant are possible, depending upon the topography of the site which can be hilly or flat. Saporiti [27] considered the arrangements of plants and found that 30 to 50 ft. difference in level is desirable. The plant arrangements can be classified into two categories: with underlying condensers and with overlying condensers.

In plants with underlying condensers, the condenser is placed directly beneath the turbine to make full use of the vacuum. Either the turbine is placed on an elevated level, or a deep excavation is necessary for the accommodation of the hot well. At Larderello, some of the turbines are placed at the ground level with the hot-wells in the excavated pits. The barometric pipes are lowered into the hot-wells till they reach the underground vessels which are connected to underground tunnels for the discharge of overflow. The condensate pumps push the hot water through the spray nozzles of the cooling tower. If the pump fails, the excess water is discharged to the tunnel to avoid the danger of overflow into the steam pipe. The major drawback of this scheme is the high costs of excavation and tunnels.

To reduce the depth of the excavated pit and to remove the necessity of laying underground tunnels, a modified arrangement is presented in Figure 3.6-26. The condenser is divided into two sections for the reduction of its height. To do away with the discharge tunnels, the level controls and interlocks are provided to avoid possible overflow in the case of sudden shutdown of the circulating water pump. If the pump fails, the interlock mechanism trips the turbine admission valve, breaks the vacuum in the condenser through a vacuum breaker and closes the quick-closing valve at the inlet of cooling water line. The level of cooling water should be slightly lower than that of the condenser spray nozzles so that the cooling water will not flow into the condenser after the vacuum breaker is released.

Plant arrangements with overlying condensers, as being adopted in some of the plants at Geysers, do not require excavation work. The barometric condenser must be installed above the turbine level. Due to the pressure drop in the exhaust duct, the back pressure of turbine increases. Figures 3.6-27, 3.6-28 and 3.6-29 illustrate three arrangements with overlying condensers: with upper cooling towers, with lower cooling towers and with cooling towers at the turbine level. If the turbine, hot well and cooling tower are located at the same

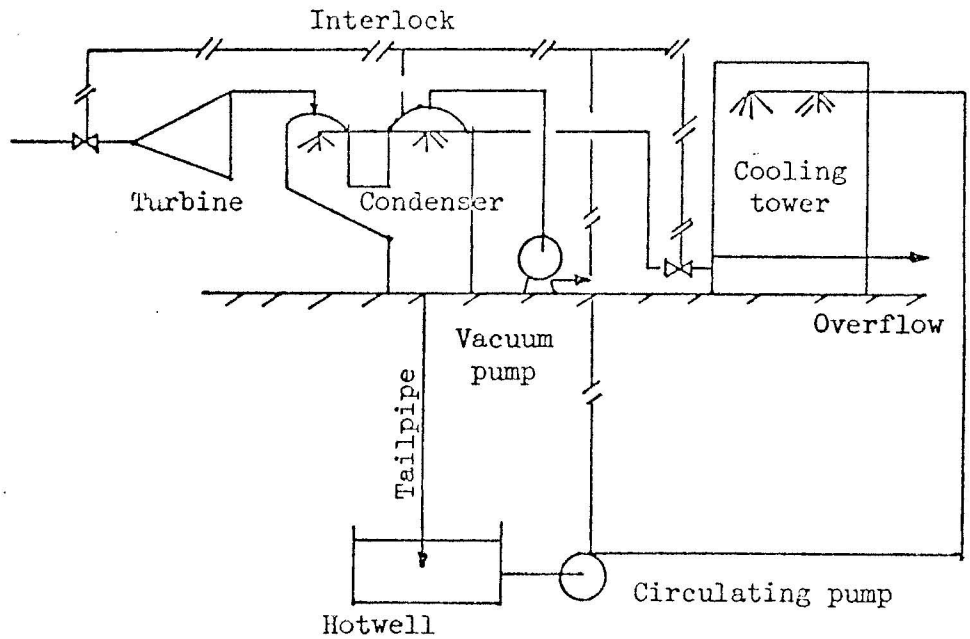

FIG. 3.6-26 PLANT ARRANGEMENT WITH UNDERLYING CONDENSER

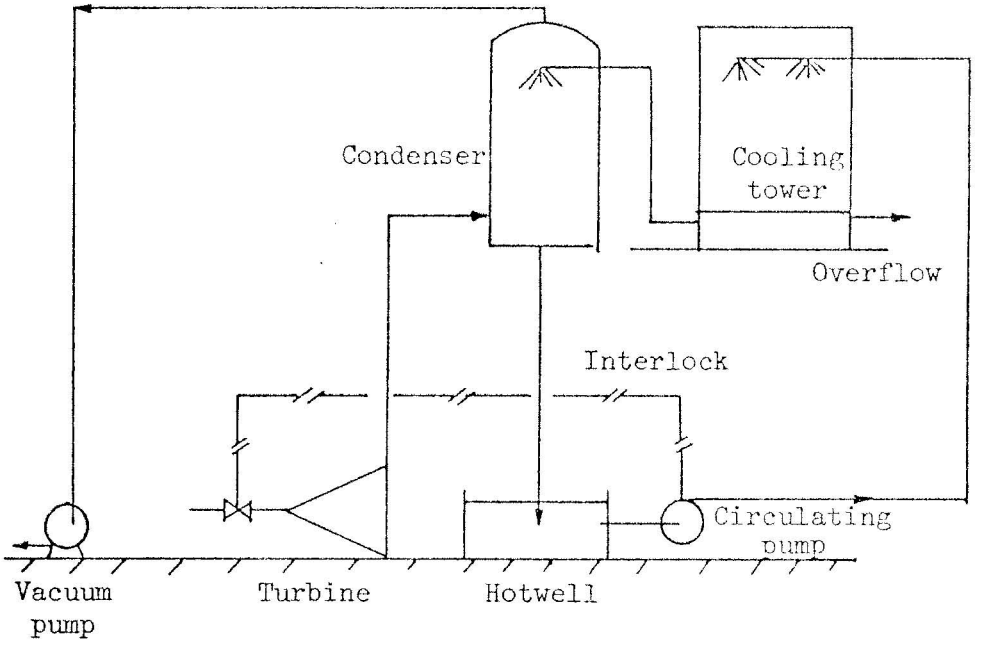

FIG. 3.6-27 PLANT ARRANGEMENT WITH OVERLYING CONDENSER AND UPPER COOLING TOWER

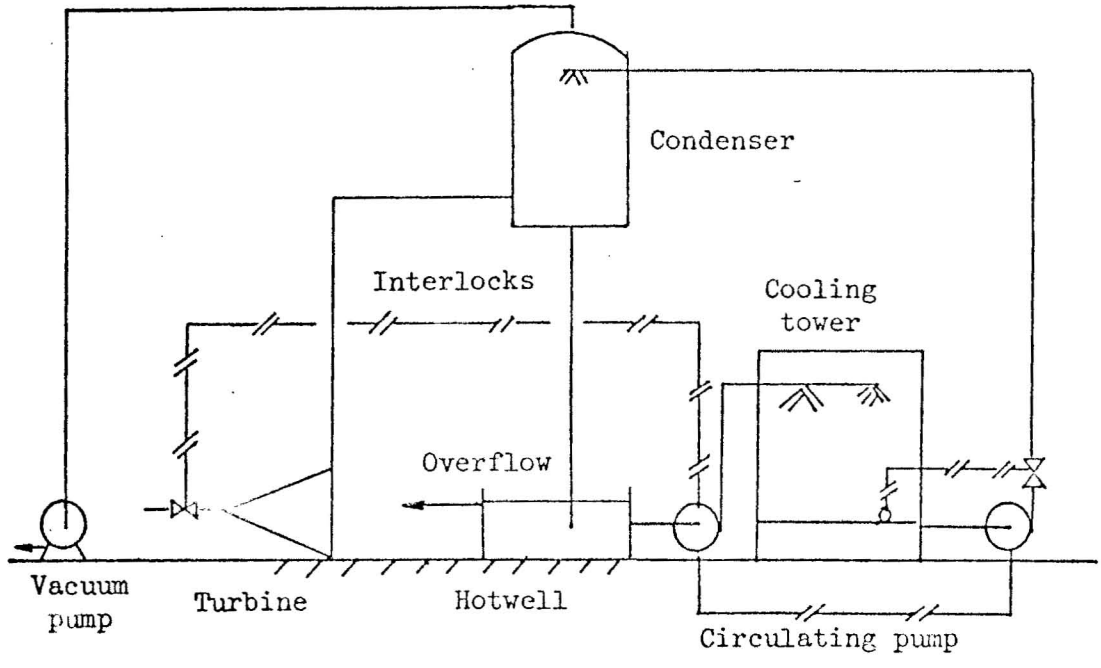

FIG. 3.6-28 PLANT ARRANGEMENT WITH OVERLYING CONDENSER FOR COOLING TOWER AT TURBINE LEVEL

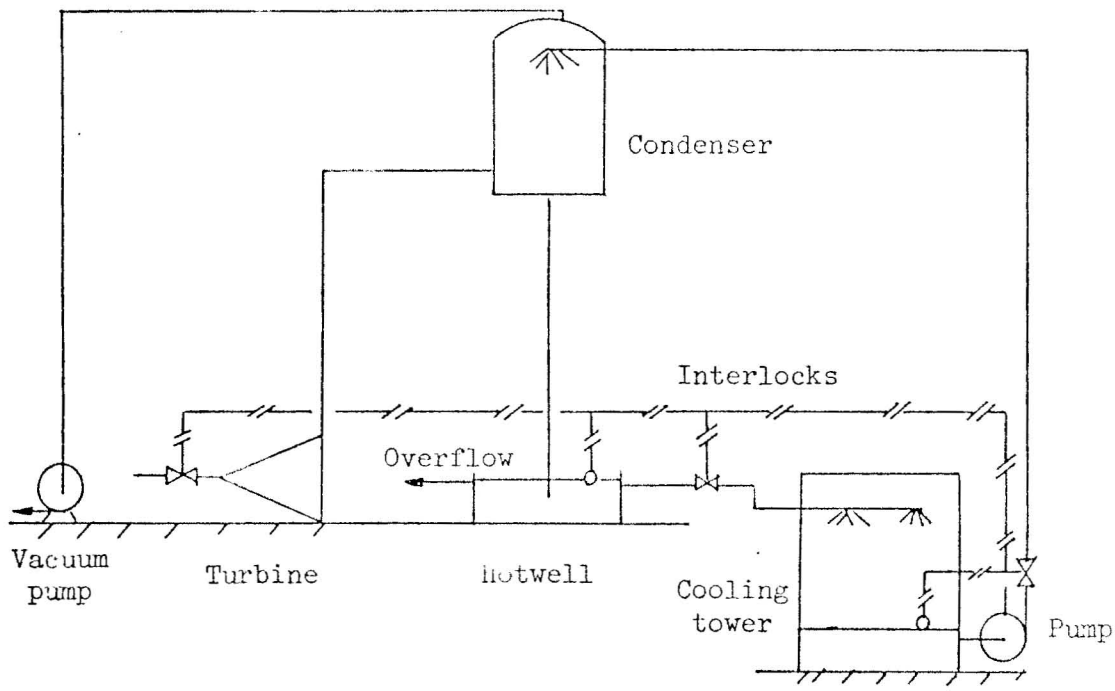

FIG. 3.6-29 PLANT ARRANGEMENT WITH OVERLYING CONDENSER AND LOWER COOLING TOWER

level, then two circulating water pumps are required. If there is 30 to 50 ft. difference in the ground level, the plant arrangement shown in Figures 3.6-27 or 3.6-29 may be adopted; one of the advantages is that only one circulating pump is required which simplifies controls and safety devices.

To avoid the high costs of the supporting structure of the condenser and the long turbine exhaust duct, a low-level type condenser may be used; however, a failure of the circulating pump can cause serious damage to the turbine, and the pumping power is very high. Since the barometric pipe, the cooling water-inlet pipe, and the noncondensable gas extraction pipe are nearly at the same temperature, they can be used together to support the condenser for reducing the cost of supporting structure.

If the site for power station is on a steep slope, the setup as shown in Figure 3.6-26 is an ideal arrangement with the tailpipe of the main condenser to follow the natural contour. It gives the advantage of low back pressure without incurring the cost of excavation, and only one circulating pump is required.

III. A Study of Simultaneous Fresh Water Production and Electrical Power Generation with a Regenerative Vapor-Turbine Cycle

The expected performances and the advantages of a closed cycle using isobutane as the working fluid have been discussed in detail by Anderson [1] and Holt et al. [16]. In a basic cycle described in the literature (Figure 3.6-30), geothermal fluid from wells is used as the heat source. Holt et al. evaluated the effects of isobutane pressures on the thermal efficiency of the basic cycle and found that the optimal working pressure largely depends on the temperature of available geothermal fluid. The optimal working pressure increases with the increase of brine temperature, and the isobutane vapor exiting the turbine has to be at highly superheated conditions in order to achieve high thermal efficiency.

To improve the thermal efficiency of a simple gas turbine cycle, a regenerator may be used to allow the interchange of energy between the turbine exhaust and the compressed air entering the combustion chamber. This principle can be applied profitably to the basic isobutane cycle for a geothermal power plant as shown in Figure 3.6-31. A sample calculation was made to evaluate the advantages of adding a regenerator to the basic cycle under the following assumed conditions:

a. The efficiency of the isobutane turbine-generator is 85%, and the efficiency of the feed pump is 80%.

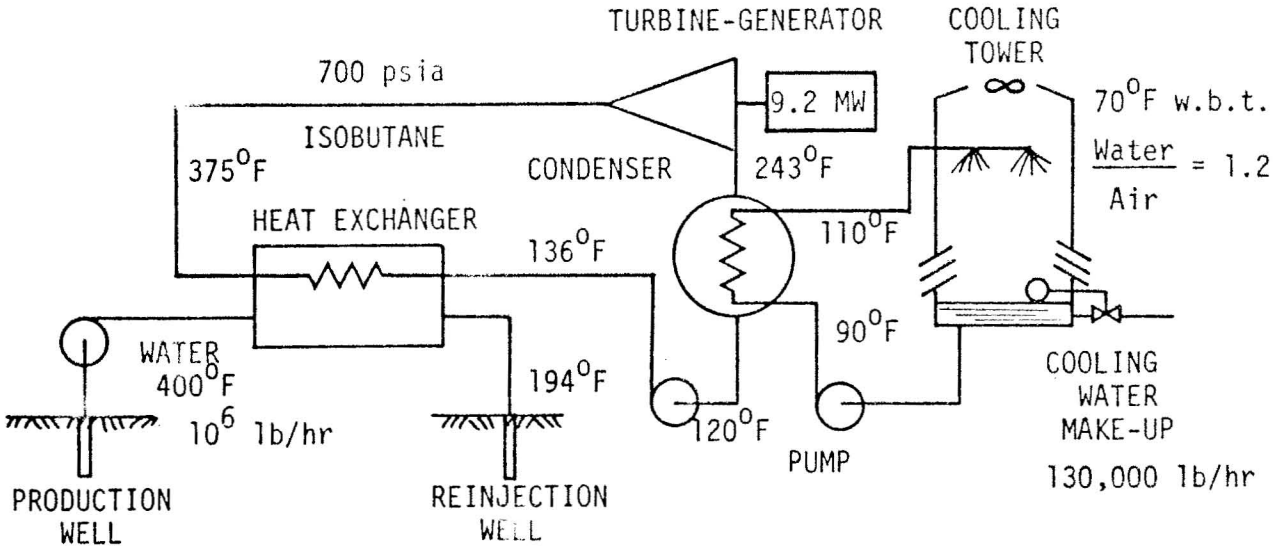

FIG. 3.6-30 BASIC ISOBUTANE CYCLE

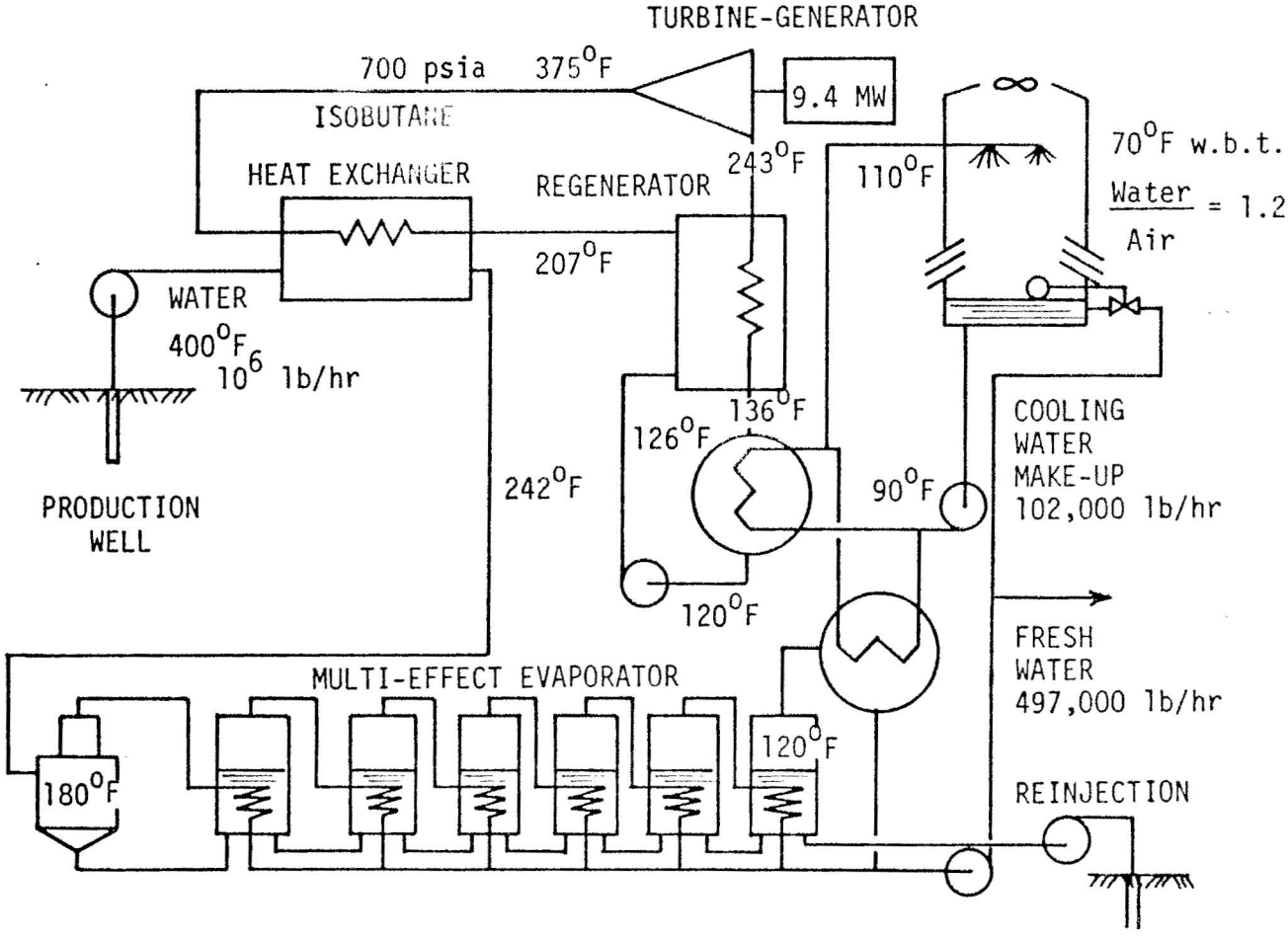

FIG. 3.6-31 REGENERATIVE VAPOR-TURBINE CYCLE
AND MULTI-EFFECT EVAPORATOR

b. One million lbs. of hot water flows into the power plant at 400°F with heat content of 375 BTU per lb.

c. The minimum temperature difference between the hot water and the isobutane is taken to be 10°F in a counter-flow heat exchanger. For example, the temperature differences between the two fluids is plotted in Fig. 3.6-32 for the operating pressure of isobutane at 700 psia.

d. The condensing temperature of isobutane is 120°F.

e. The terminal temperature difference of isobutane in the regenerator is 10°F. Pressure drops and heat losses of the fluids through pipes and heat exchangers are neglected.

The results of calculations are found to be interesting. In Table 3.6-4 are the mass flow rate of isobutane and the throttle temperature at various operating pressures. To illustrate the significance of the results, power production, heat rejection and temperature of water leaving the heat exchanger are plotted in Figures 3.6-33, 3.6-34, and 3.6-35 respectively. The increases in power production by using a regenerator are insignificant; the maximum gain is in the order of 2% of the power produced by the basic cycle at the optimum operating pressure of 700 psia. However, the rates of heat which must be rejected to the environment differ noticeably between the two cycles. At 700 psia, the rate of heat rejection of the regenerative cycle is reduced to 72% of the basic cycle. Since the heat rejection equipment is a major cost item in the geothermal power plant, the application of the regenerator should significantly affect the total cost of the plant. The capital cost of a regenerator could be offset by the reduction of the size of the main heat exchanger, and the heating surface of the regenerator is free from corrosion and scaling, which may adversely affect the primary heat exchanger dealing with water from the wells. The temperature of water leaving the heat exchanger of the regenerative cycle is much higher than that of the basic cycle, as shown in Figure 3.6-35. Thus, the heat can be economically extracted from the discharge of hot water for industrial applications. Many geothermal reservoirs are located in areas where the supply of fresh water is inadequate; if so, the regenerative cycle offers a great potential for the simultaneous production of fresh water and electrical power. As indicated in Figure 3.6-31, the discharge of hot water may be led to a multi-effect evaporator to convert a part of the water from a geothermal well to distilled water. The knowledge of designing such an evaporator is very well advanced from the research sponsored by the Office of Saline Water. Depending

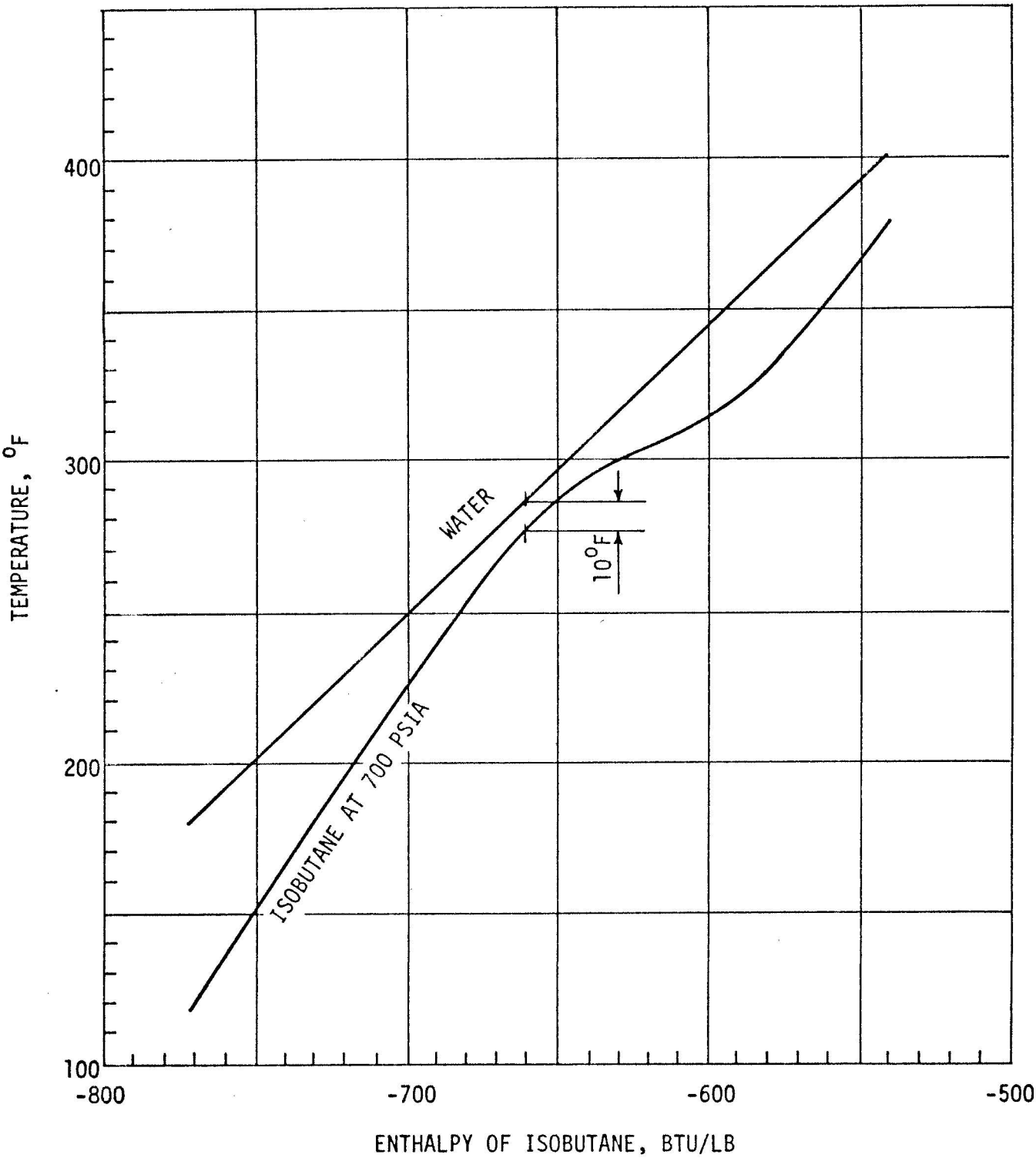

FIG. 3.6-32 TYPICAL TEMPERATURE DIFFERENCES BETWEEN WATER AND ISOBUTANE IN COUNTERFLOW HEAT EXCHANGER

TABLE 3.6-4 THROTTLE TEMPERATURE AND MASS FLOW RATE OF ISOBUTANE

OPERATING PRESSURE, PSIA	THROTTLE TEMPERATURE, ^{o}F	MASS FLOW RATE, 10^3 LB/HR	
		Basic Cycle	Regenerative Cycle
900	380	1000	1015
800	375	998	1006
700	375	919	933
600	390	913	925
500	380	914	916
400	390	855	856

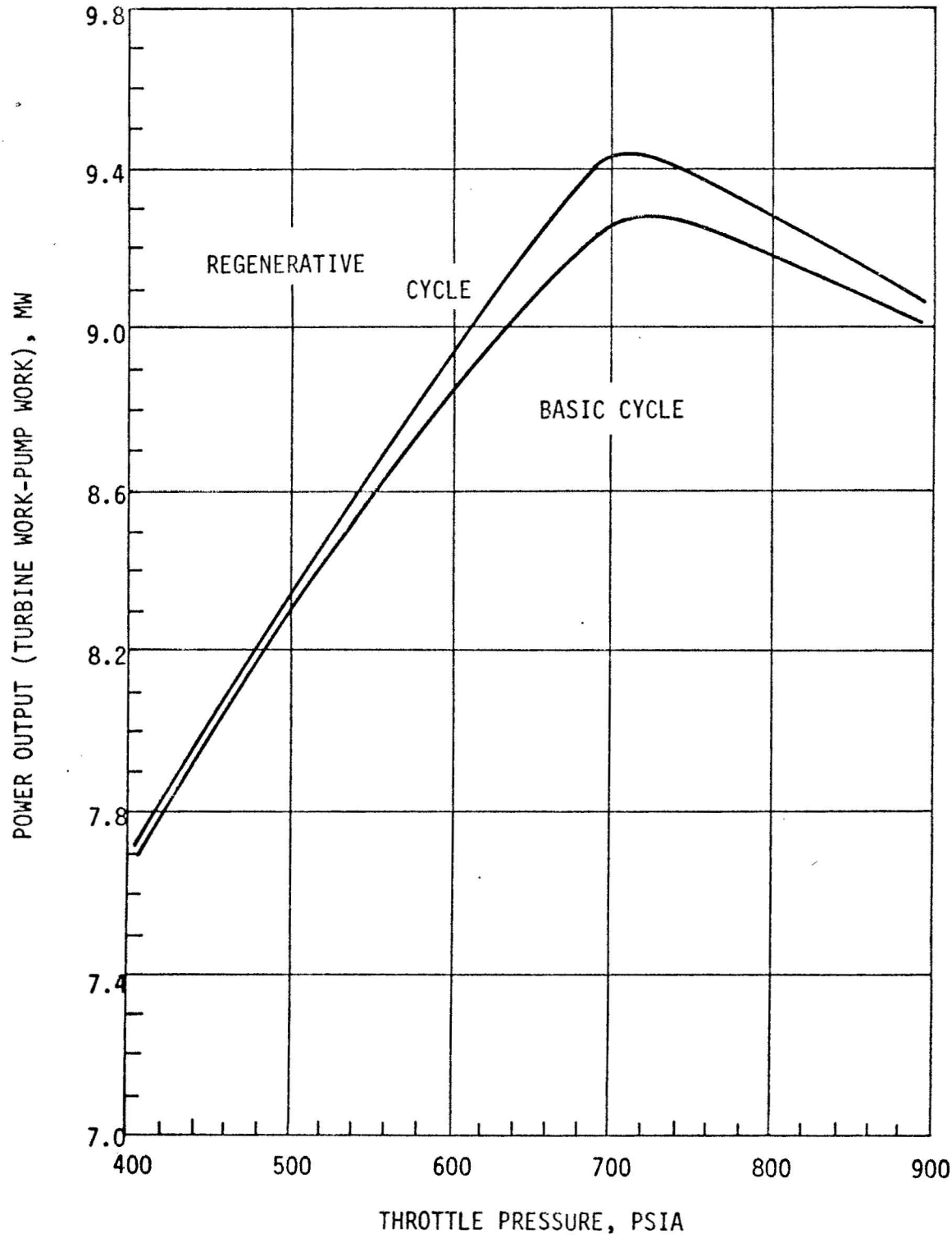

FIG. 3.6-33 POWER OUTPUT

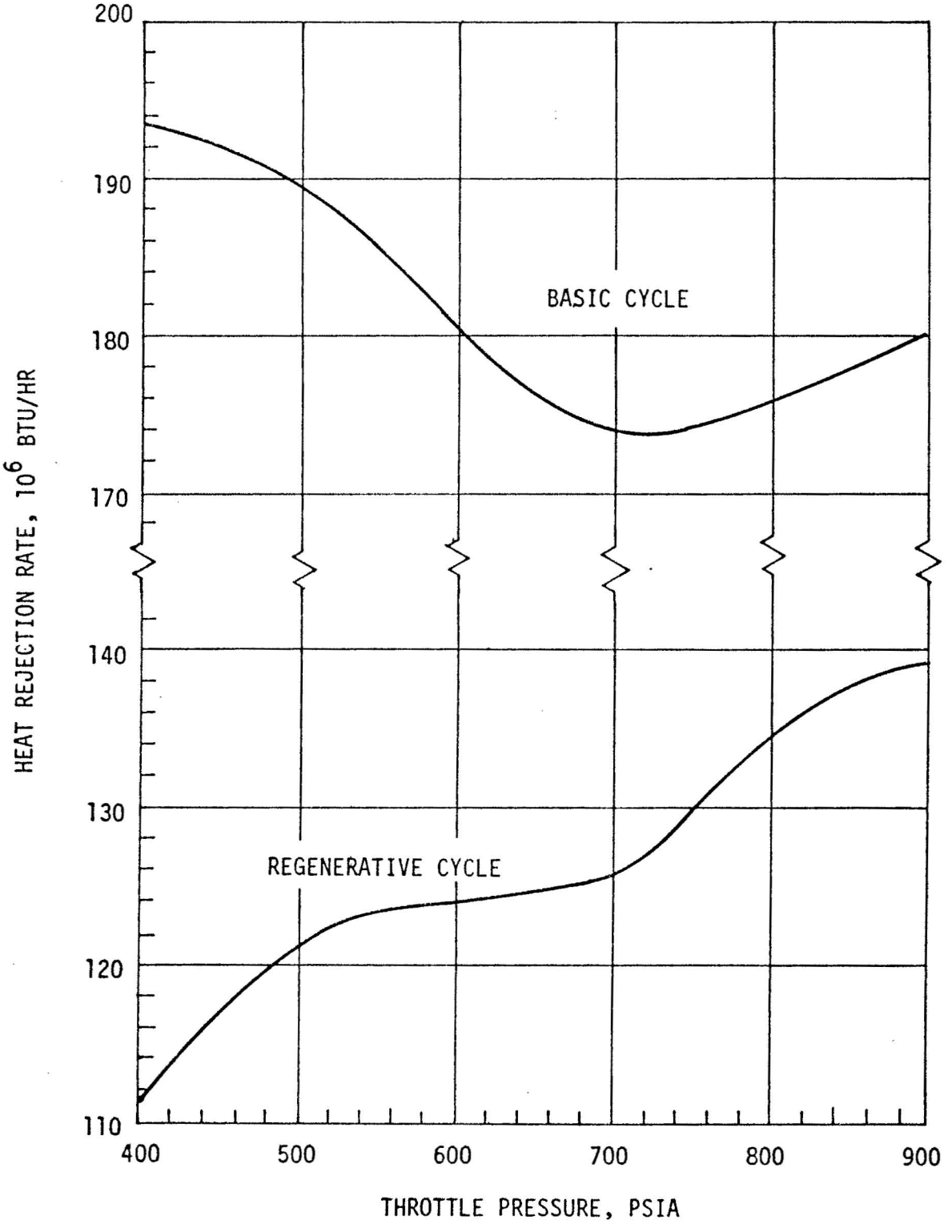

FIG. 3.6-34 HEAT REJECTION RATE

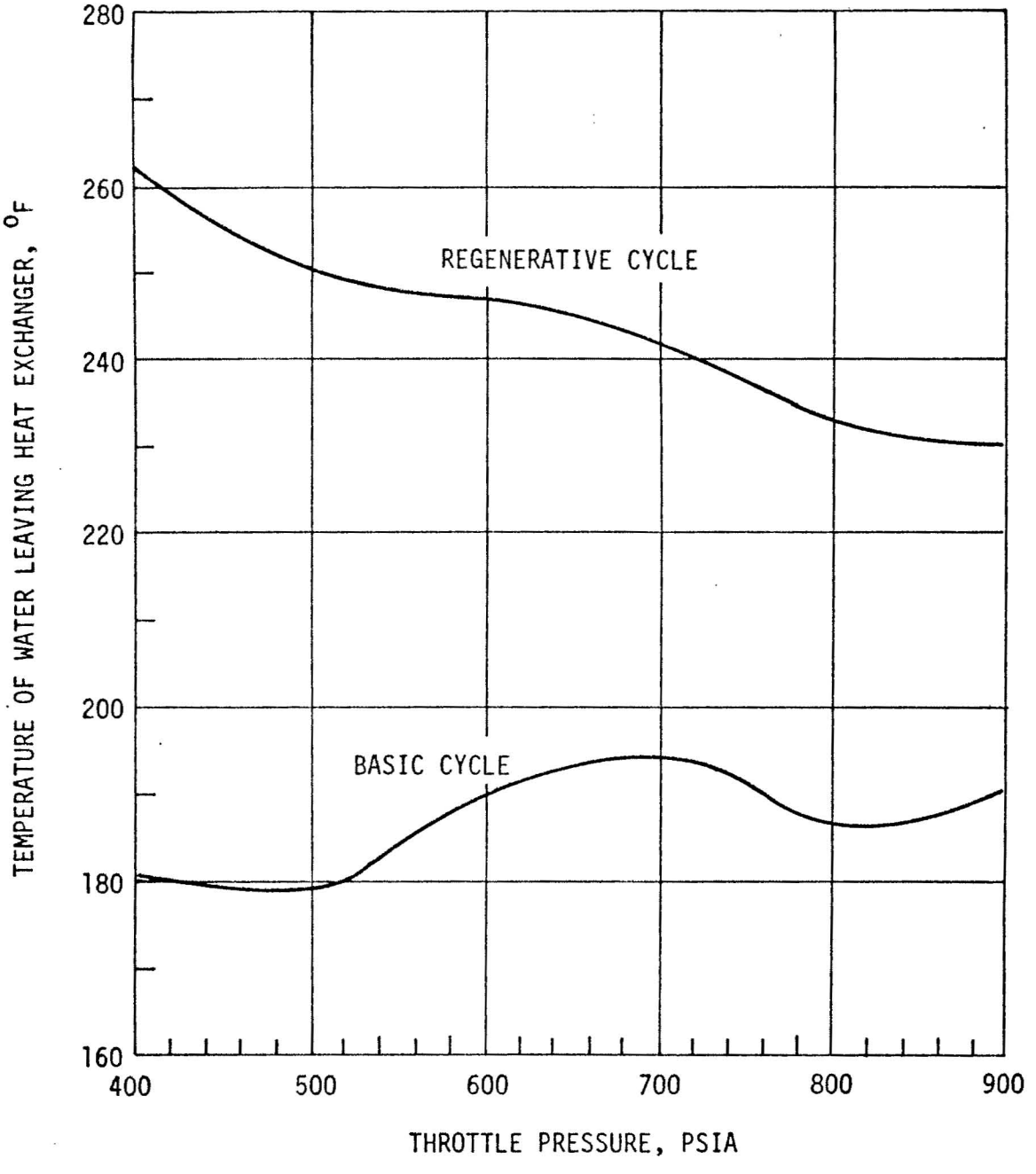

FIG. 3.6-35 TEMPERATURE OF WATER LEAVING THE HEAT EXCHANGER

upon the design of the heat rejection system and weather conditions, the water evaporated in cooling water is in the order of 102,000 lbs. per hour for a 10 MW regenerative isobutane plant operating at 700 psia. With a six-effect evaporator, it is possible to export 497,000 lbs/hr of fresh water for the arrangement shown in Figure 3.6-31. Should the seawater or brackish water be available from nearby sources for cooling, a multi-stage flashing evaporator might be more suitable for desalting water than a multi-effect evaporator. Detailed discussions of desalting plants are beyond the scope of this short section. Nevertheless, the possibility of combining a closed regenerative vapor plant with a desalting plant has been demonstrated. Conditions of geothermal reservoirs and regional requirements of power and water vary from one locality to another. For every locality, all the possible alternatives of plant designs must be carefully evaluated so that the most economically and technically feasible design can be determined. Addition of a regenerator to a closed vapor cycle for geothermal power plants could be an attractive alternative because it reduces the rate of heat rejection and supplies heat at intermediate temperatures for other uses.

IV. Characteristics of Binary Fluid, Vapor Turbine Cycles

Computer programs to study the effects of variations of system parameters were written and prooftested. The specific system considered is shown in Figure 3.6-36. A simple Rankine cycle with superheat (Figure 3.6-37) and heat input from a high temperature brine was the focus of our efforts.

Since a task objective would be to minimize the cost of net power output, i.e., well production rate per kilowatt electrical power output, primary attention was on the interaction between the heat input through a vertical counterflow boiler and superheater and on various parameters of the Rankine cycle.

The performance of the heat exchanger components is governed by the transport equations and can be determined by the use of correlation equations. The characteristics of the Rankine cycle are determined by the laws of thermodynamics and properties of the working fluid. The interface of these two systems occurs at the heat transfer surfaces -- the temperatures of the fluids of either side are shown in Figure 3.6-38. The shapes of the curves are functions of the fluid system pressure, and relative mass flow rates.

The computer programs modelling the system under consideration have the following characteristics:

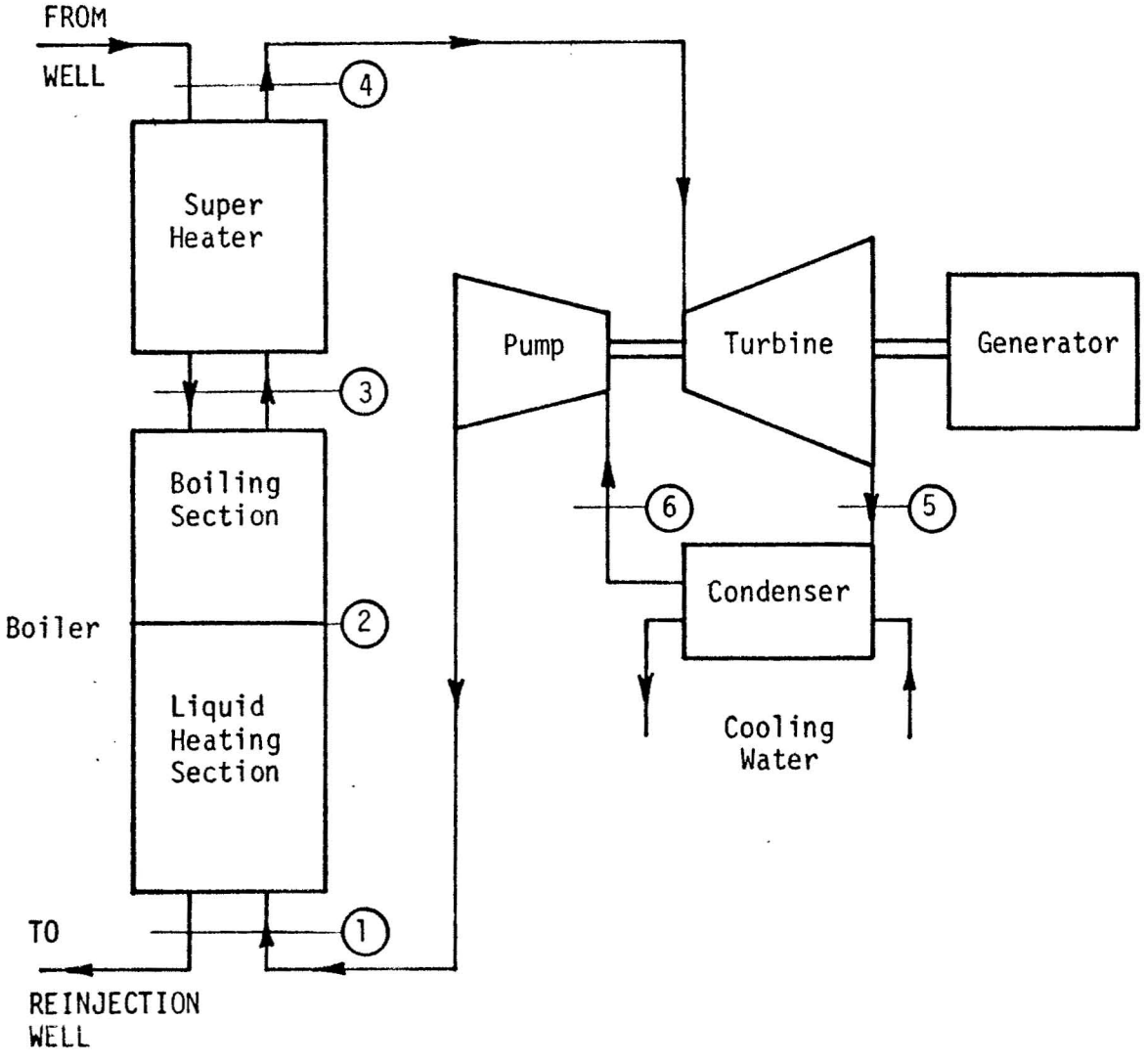

FIG. 3.6-36 SCHEMATIC OF RANKINE CYCLE WITH HEAT INPUT FROM HOT BRINE

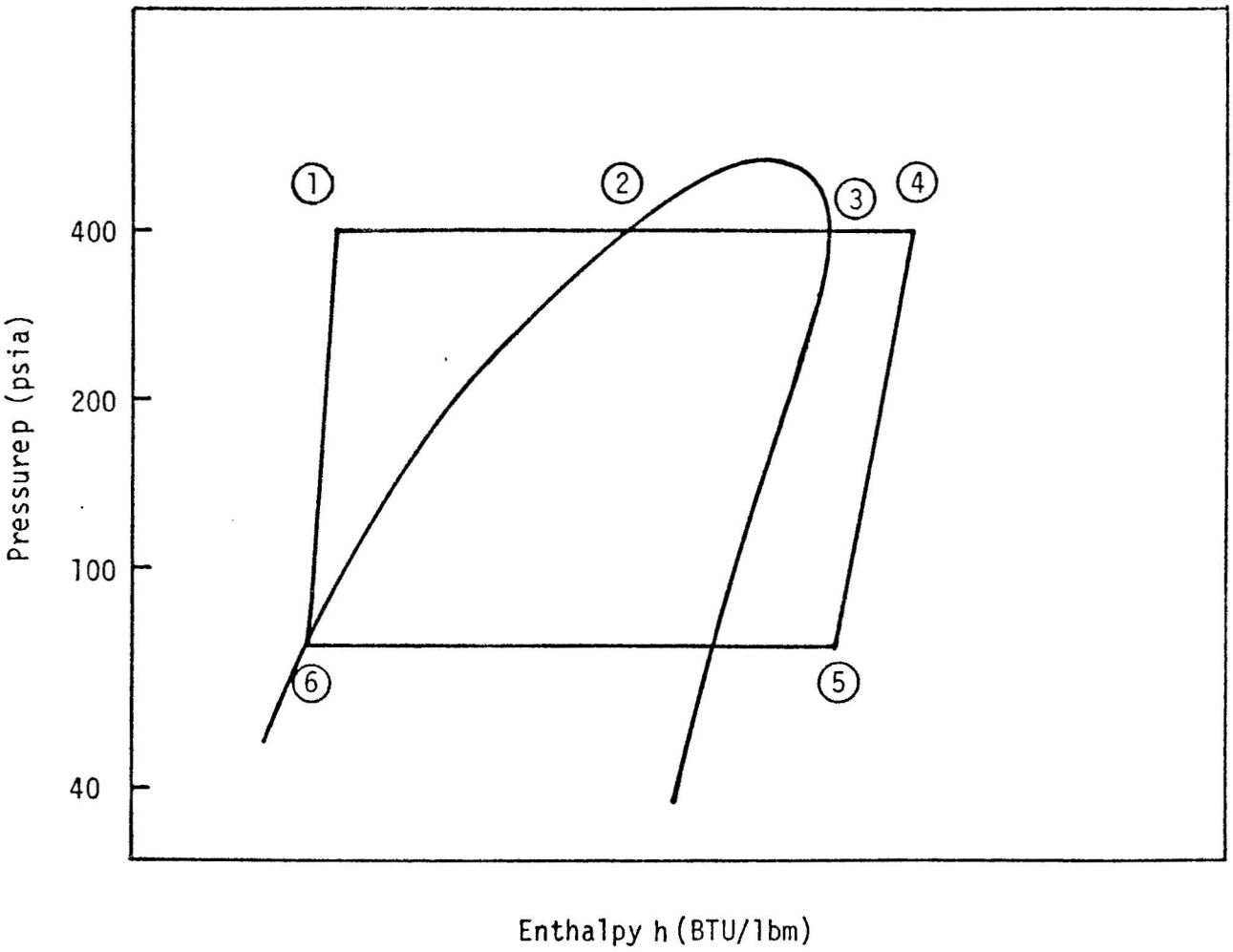

FIG. 3.6-37 RANKINE CYCLE WITH SUPERHEAT

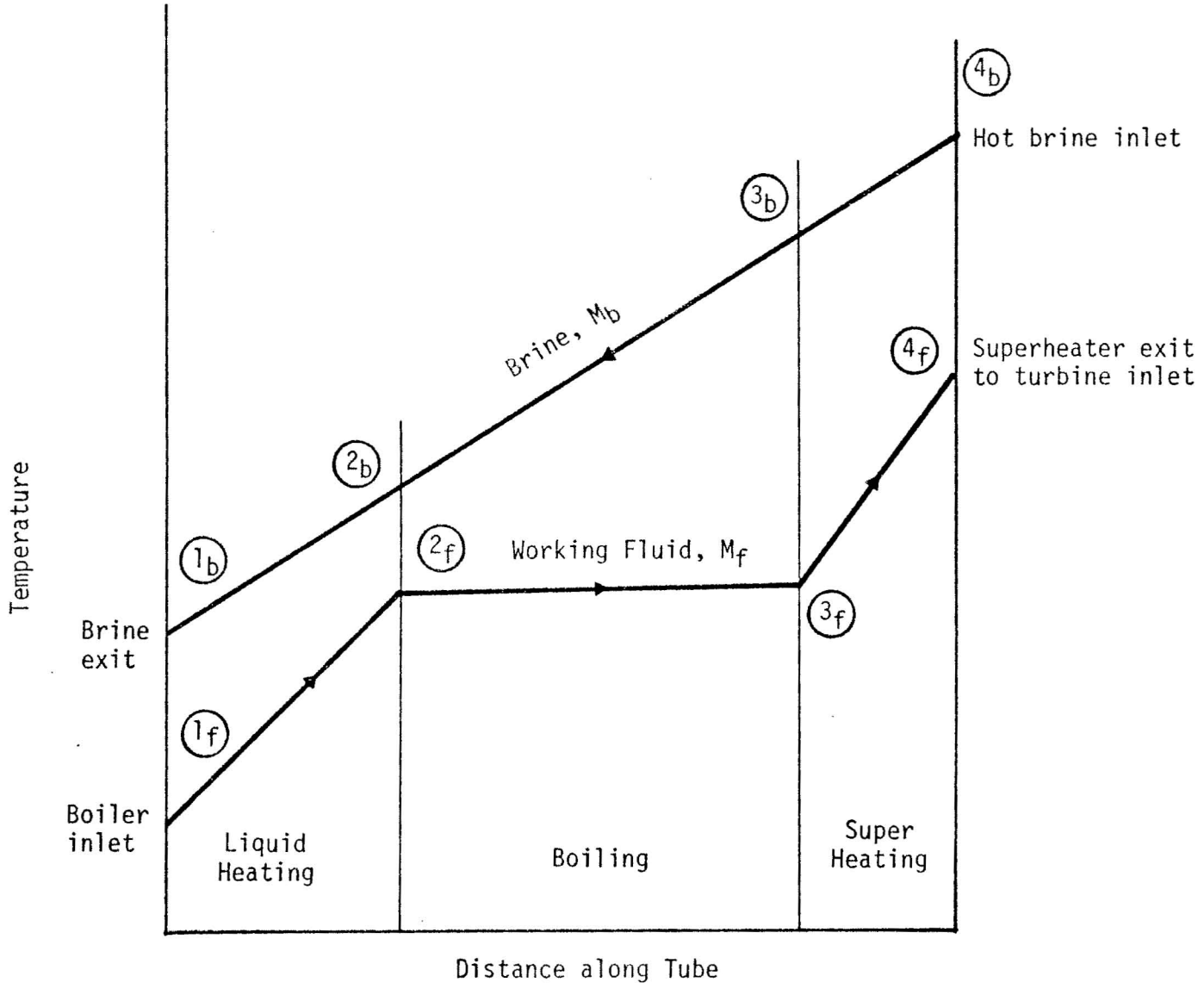

FIG. 3.6-38 FLUID CONDITIONS IN THE HEAT EXCHANGER

1. Rankine Cycle Computer Program
   a. Input
      1) Table of property values of working fluid
      2) Turbine inlet conditions, pressure and temperature (also superheater exit conditions)
      3) Condenser outlet conditions, pressure and temperature
      4) Component efficiencies
      5) Required net power output
   b. Output
      1) Property values of working fluid at all points in the cycle
      2) Cycle efficiency
      3) Mass flow rate for required power output
      4) Heat rejection rate
2. Boiler and Superheater Computer Program
   a. Input
      1) Properties of working fluid
      2) Properties of brine
      3) Brine inlet temperature and velocity
      4) Working fluid inlet temperature
      5) Pinch point temperature difference
      6) Tube material, diameter, spacing
      7) Fouling factors
   b. Output
      1) Convective heat transfer coefficients on both sides
      2) Number of tubes
      3) Length of tubes
      4) Total heat transfer rate across tube walls
      5) Ratio of mass flow rates -- brine to working fluid

The vertical configuration was first considered primarily because of the availability of suitable heat transfer equations for its design. Correlation equations for boiling heat transfer for a single tube are available for both vertical and horizontal tubes. However, the effect of tube spacing and number of tube rows on the average heat transfer coefficient for horizontal heat exchangers is not known. This was discussed by Palen et al. [24] but no quantitative results were presented.

In the design of these vertical heat exchangers, Chen's [7] correlation equation is used for the boiling section. The equation is not shown here because it is long and so many terms are included. Chen's correlation equation was used for the boiling section because (a) his experimental results seem to be accurate, (b) the equation applies to boiling heat transfer of fluid flowing in vertical tubes with quality ranging from 0 to 100%, and (c) his results agree very well with the experimental results of other investigators [10, 13, 26, 28]. For the nonboiling region, the equation recommended by Kays [23] is used.

Hot brine is circulated inside the tubes because of cleaning considerations. Use of finned tubes has not been considered because the inside and outside convective heat transfer coefficients are approximately the same magnitude and there is no need to artificially increase one or the other.

Currently no specific input data are available for the complete design of the heat exchanger equipment. The brine inlet temperature will be known only after a production well is drilled. The inside fouling factor will be determined by the brine temperature and the contents of minerals in the brine. Working fluid inlet temperature will be determined by whether a dry or wet cooling tower is going to be utilized. Because of this situation, a general computer program was written, and all the required terms are included in the program for the design of the heat exchanger. As soon as specific information becomes available, these data will be fed into the program, and the dimensions of the heat exchanger and other information such as mass flow rates, transfer coefficients, number of tubes required, etc., will be computed and printed.

The design procedure used to determine specifications for the boiler-superheater is based on an overall heat balance of the heat exchanger, and as a first approximation, heat losses are neglected. This procedure is outlined below:

1. Parameter values selected initially are
   a. system pressure
   b. inlet temperature of working fluid
   c. degree of superheat
   d. brine inlet temperature

   This completely determines the state of the working fluid as it travels through the heat exchanger (Figure 3.6-38).
2. From the analysis of the Rankine cycle, the required mass flow rate of the working fluid is computed.

3. On Figure 3.6-38, locate the likely pinch point (location where the temperature difference between brine and working fluid occurs) and assign a pinch point temperature difference of 20°F.
A heat balance of the liquid heating section yields

$$[Mc_p(T_2 - T_1)]_b = [Mc_p(T_2 - T_1)]_f$$

An overall heat balance of the entire heat exchanger yields

$$[Mc_p(T_4 - T_1)]_b = [M(h_4 - h_1)]_f$$

These equations allow the calculation of the temperature of the brine at all locations in the heat exchanger and the ratio of brine flow rate, M_b, to the working fluid flow rate, M_f. However, since the working fluid flow rate, M_f, is known from the analysis of the Rankine cycle, the brine flow rate, M_b, can be determined.

4. For any particular component (liquid heating, boiling, or superheating region) the brine bulk temperature, $T_{b,bulk}$, can be calculated. Using appropriate values of tube diameter, d_i, and brine velocity, V_b(7, 10, or 15 ft/sec), the mass flow rate for a single tube is calculated by

$$m_b = (\rho AV)_b = (\rho \tfrac{\pi}{4} d_i^2 V)_b$$

and the number of tubes by

$$N = \frac{\text{Total mass flow rate of brine}}{\text{Mass flow rate of brine in one tube}} = \frac{M_b}{m_b} .$$

The Reynolds number Re and the Prandtl number Pr are then calculated and based on the bulk temperature

$$Re = \frac{\rho V d_i}{\mu} \quad , \quad Pr = \frac{c_p \mu}{k}$$

The equation recommended by Kays [23]

$$Nu_i = \frac{h_i d_i}{k} = 0.0155\ Pr^{0.5}\ Re^{0.83}$$

is used to compute the inside convective heat transfer coefficient h_i.

5. Outside the tubes the bulk temperature of the working fluid is calculated. With the number of tubes known and the tube spacing assumed; e.g.,

$\frac{S}{d} = 1.25$, the equivalent diameter of the flow passage, $d_{o,eq}$, and the mass flow rate per unit flow passage, m_f, are determined. Use of Kay's equation

$$Nu_o = \frac{h_o d_{o,eq}}{k_f} = 0.0155\ Pr^{0.5}\ Re^{0.83}$$

yields the outside convective heat transfer coefficient, h_o.

6. The rate at which the working fluid is heated is set equal to the heat transferred through the tube walls

$$[M(h_2 - h_1)]_f = UA_o(T_{b,bulk} - T_{f,bulk})$$

where

$$U = \left[\frac{d_{o,eq}}{h_i d_i} + \frac{d_{o,eq}}{2k} \ln \frac{d_{o,eq}}{d_i} + \frac{1}{h_o} + R_i + R_o\right]^{-1}$$

= overall heat conductance

$A_o = Nd_o H_{NB}$ = total wall area of non-boiling sections.

The length of the tubes in the non-boiling section, H_{NB}, can then be calculated.

7. In the boiling region, a heat balance yields

$$Q_B = [M(h_3 - h_2)]_b = [M(h_3 - h_2)]_f$$

Further, properties of both brine and working fluid are known at the inlet and outlet of the tube; velocities can be calculated.

To find the boiling height, H_B, assume a value for H_B and calculate Q_B on the brine side

$$Q_{B,b} = h_i A_i (T_{bulk} - T_{wall})_b$$

to find T_{wall} on the brine side. With the tube material and wall thickness specified, T_{wall} on the working fluid side can be calculated. Then on the working fluid side, which is boiling

$$Q_{B,f} = h_o A_o (T_{bulk} - T_{wall})_f$$

where h_o is calculated using Chen's [7] correlation. This last calculated value of $Q_{B,f}$ is compared with the value Q_B calculated in the

first equation of this section. The assumed value of H_B is adjusted until the values of Q_B and $Q_{B,f}$ are within a prescribed tolerance.

8. In the superheater, the procedures of sections 5 and 6 are followed except the correlation equation [23] for gases

$$Nu_0 = 0.021\ Pr^{0.6}\ Re^{0.8}$$

is used for the vapor portion of the working fluid.

The pressure drop experienced by the working fluid as it flows through the heat exchanger was calculated according to the following expressions:

Two-phase frictional pressure drop [35]

$$\Delta P_{TP} = \phi_F^2\ \Delta P_F\ ,$$

$$\phi F^2 = \left[1 + x\left(\frac{\rho_F}{\rho_g} - 1\right)\right]\left[1 + x\left(\frac{\mu_F}{\mu_g} - 1\right)\right]^{-(1/4)},$$

where

x = quality,
ρ = density,
μ = viscosity,
subscript F = liquid,
subscript g = gas,
subscript TP = two phase.

Accelerational pressure drop:

$$\Delta P = \frac{W}{A}\Delta V,$$

$$W = \rho AV.$$

Gravitational pressure drop:

$$\Delta P = \rho_m g z \cos\theta,$$

where

ρ_m = average density,
z = tube length,
g = gravity.

Single phase frictional pressure drop [32]:

$$\Delta P = \gamma h_f,$$

$$h_f = f\frac{L}{D}\frac{V^2}{2g},$$

$$f = a + b\ Re^{-c}$$

$$a = 0.94K^{0.225} + 0.53K$$

$$b = 88K^{0.44}$$

$$c = 1.62K^{0.134}$$

where

K = relative roughness.

3. Selection of a Working Fluid for a Binary Fluid, Vapor Turbine Cycle

A short list of possible working fluids, with a wide range of properties, was initially studied for possible utilization in a simple Rankine cycle. The fluids considered and their relevant characteristics are given in Table 3.6-5.

The analysis of the power producing cycle was conducted for the following set of conditions:

Net Power output	10 MW
Condenser outlet conditions	Saturated liquid at 100°F
Heat source	Liquid brine at temperature indicated
Turbine efficiency	85%
Pump efficiency	75%
Pinch point temperature difference	20°F
Pressure losses and heat losses neglected	

The results of the analysis can be viewed from two perspectives. If the cycle is considered by itself, i.e., independent of the heat source, then the thermal efficiency, given by η = Net work output/Gross heat input, would be one of the primary factors to be selected. The variation of this parameter as a function of the turbine inlet temperature, i.e., the maximum temperature that the working fluid experiences, is shown in Figs. 3.6-39 to 3.6-41. The

TABLE 3.6-5 WORKING FLUIDS AND PROPERTIES

Fluid	Critical Point		Boiling temp. at atm press.	Liquid density at 100°F	Vapor spec. vol. at 100°F
	T_c °F	p_c psia	T_{sat} °F	ρ_f, lbm/ft^3	v_g ft^3/lbm
R-11 CCl_3F	338.4	640.0	74.9	90.21	1.765
R-113 CCl_2-$CClF_2$	417.4	498.9	117.6	95.79	2.976
R-114 $C_2Cl_2F_4$	294.3	473.0	38.8	88.40	0.696
R-C318 C_4F_4	239.6	403.6	21.5	90.33	0.382
R-600a iso-C_4H_{10} $CH(CH_3)_3$	275.0	529.2	10.9	33.30	1.262

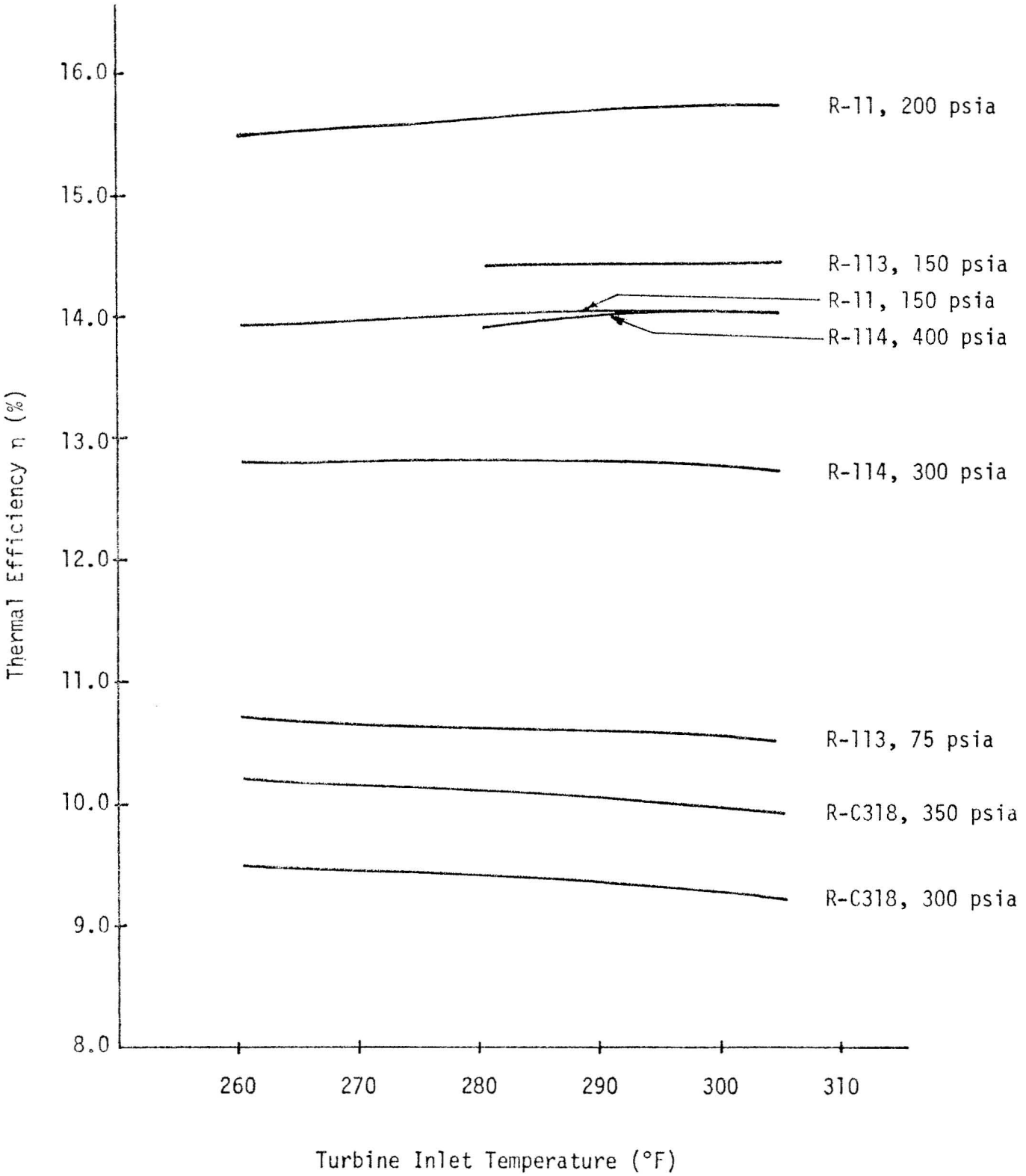

FIG. 3.6-39 THERMAL EFFICIENCIES USING VARIOUS WORKING FLUIDS WITH BRINE AT 325°F

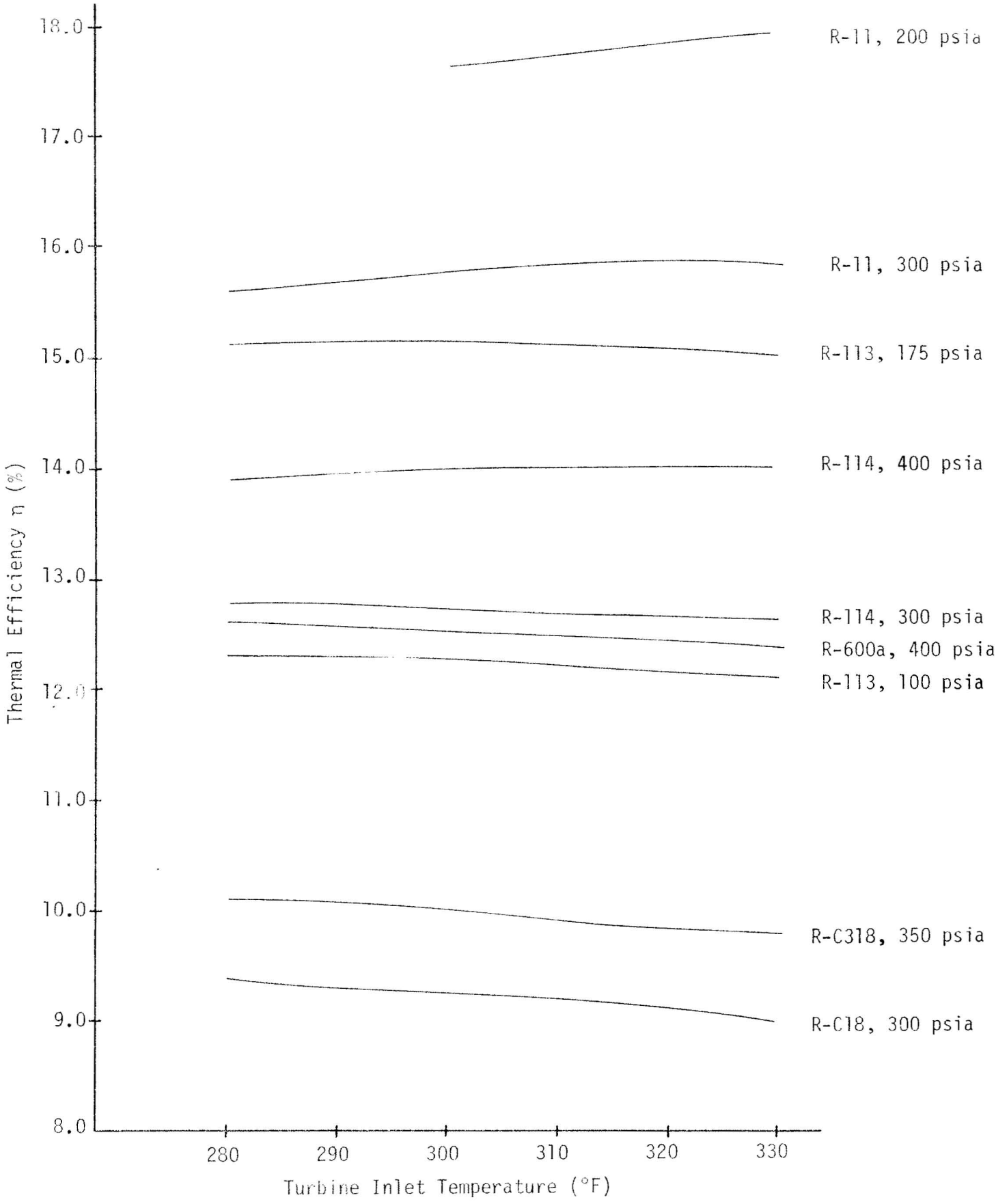

FIG. 3.6-40 THERMAL EFFICIENCIES USING VARIOUS WORKING FLUIDS WITH BRINE AT 350°F

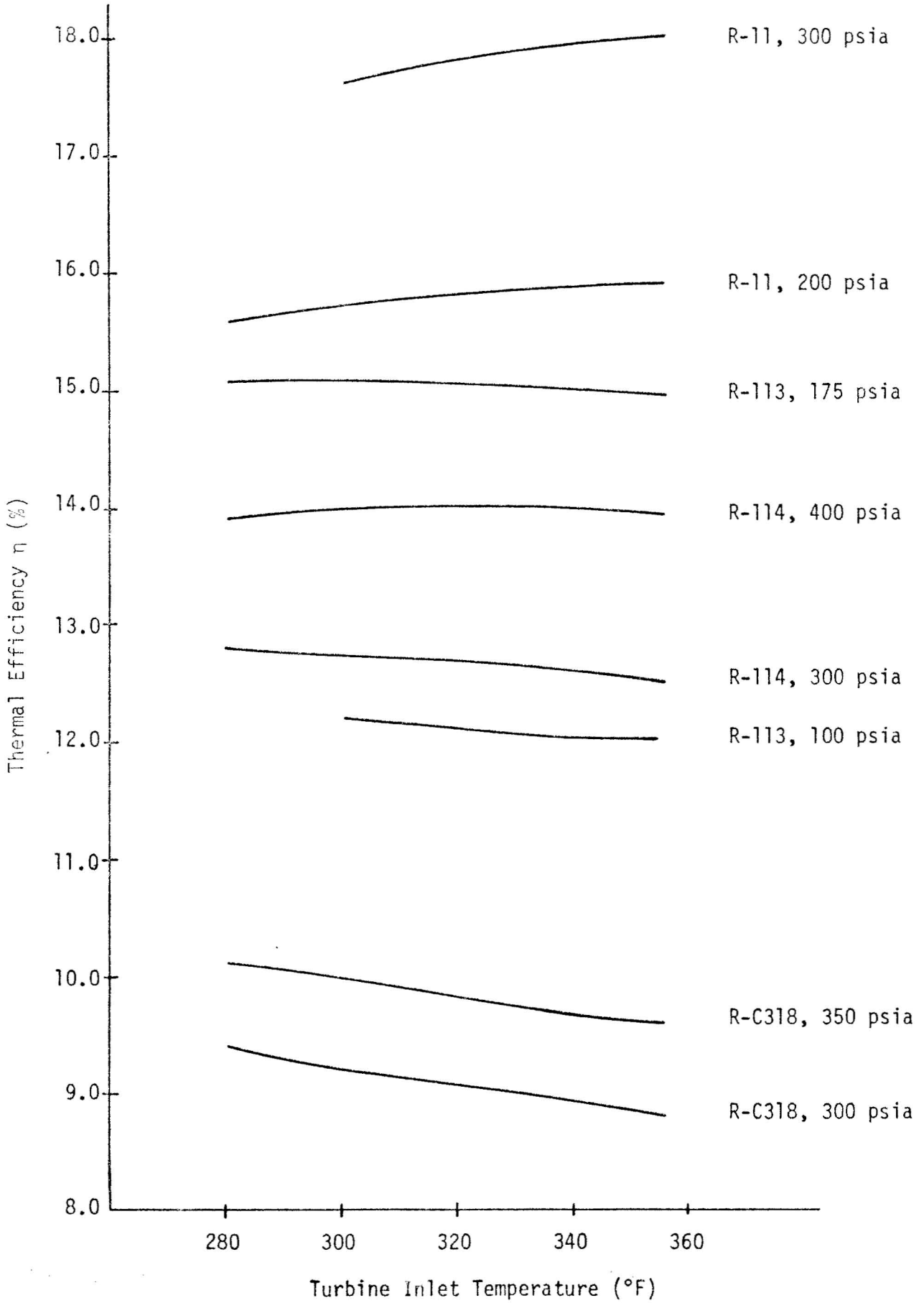

FIG. 3.6-41 THERMAL EFFICIENCIES USING VARIOUS WORKING FLUIDS WITH BRINE AT 375°F

performances of these fluids are shown for various working pressures and for brine inlet temperatures of 325°F, 350°F, 375°F. In almost all instances the curves are essentially flat, indicating that the efficiency is relatively insensitive to turbine inlet temperature. In a few cases, the curves have negative slopes, viz., thermal efficiency decreasing as turbine inlet temperature increases. This is due to the fact that the fluid exiting the turbine has increasingly higher degrees of superheat which must be rejected in the condenser.

If the consumption of hot brine is to be the governing factor, Figs. 3.6-42 to 3.6-44 which show the required brine flow rate as a function of turbine inlet temperature are essential. Again, these figures are for brine temperatures of 325°F, 350°F and 375°F.

There are some interesting observations to be made from Figs. 3.6-42 to 3.6-44. In general, all curves have positive slopes, which indicates that as turbine inlet temperature is increased, a greater flow rate of brine is required. This trend becomes more pronounced as the brine temperature increases.

Furthermore, by comparing the efficiency curves with the brine flow rate curves for the same brine temperature, it is seen that those working fluids which yield the highest efficiencies are not necessarily those which require the smallest brine flow rates.

The variation of required brine flow rate with brine inlet temperature is shown in Figs. 3.6-45 to 3.6-47. As would be expected, for a given power output, the higher the brine inlet temperature, the lower the flow rate required.

The effect of using system pressures greater than the critical pressure is shown in Figs. 3.6-48 to 3.6-50. Figs. 3.6-48 and 3.6-49 show the effect of system pressure and turbine inlet temperature on the thermal efficiency of the basic cycle and on the rate of consumption of the primary resource, brine. In general, higher system pressures lead to a reduced brine mass flow rate, although a minimum does appear to exist for a system pressure of 700 psia and turbine inlet temperature of 300°F (see Fig. 3.6-50).

In addition to this initial study, an exhaustive search of a broad range of possible working fluids is being conducted. The preliminary list of those candidate fluids being considered is listed in Table 3.6-6. To narrow this list to a workable number, a series of go-no go tests will be applied, e.g., thermal stability at 300°F. These will then be followed by a series of more detailed analyses related to the Rankine power cycle.

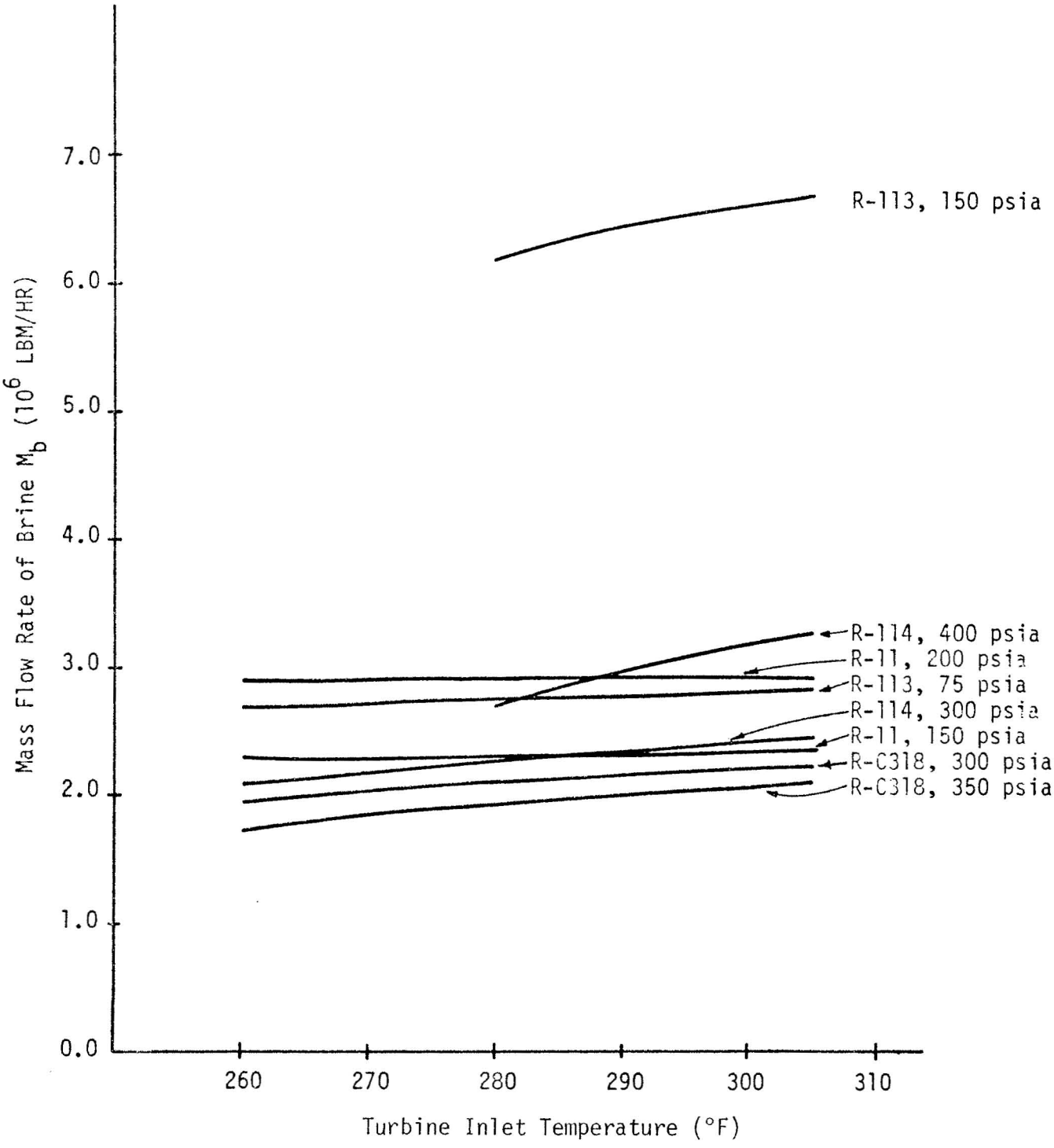

FIG. 3.6-42 BRINE FLOW RATES USING VARIOUS WORKING FLUIDS WITH BRINE AT 325°F

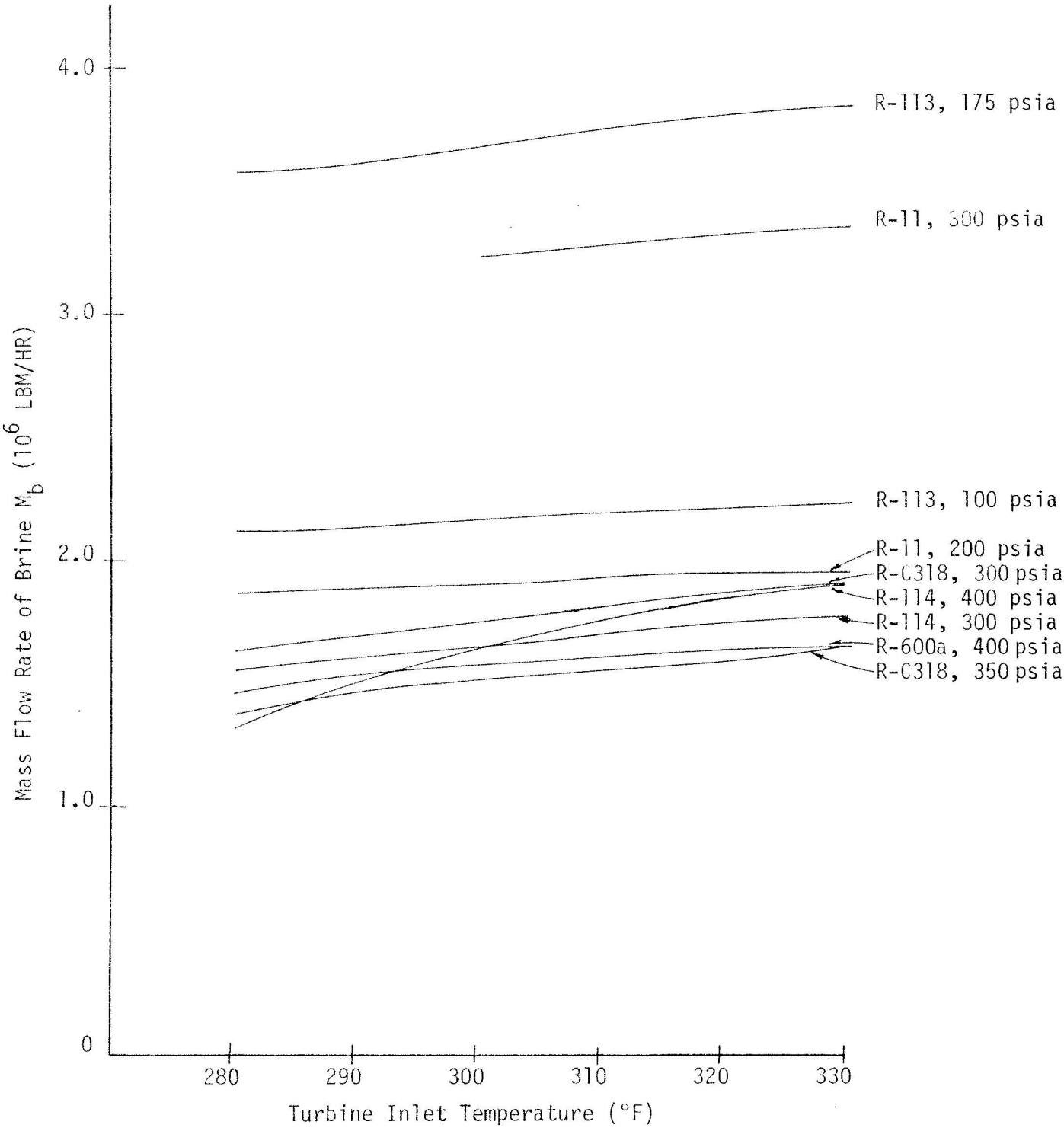

FIG. 3.6-43 BRINE FLOW RATES USING VARIOUS WORKING FLUIDS WITH BRINE AT 350°F

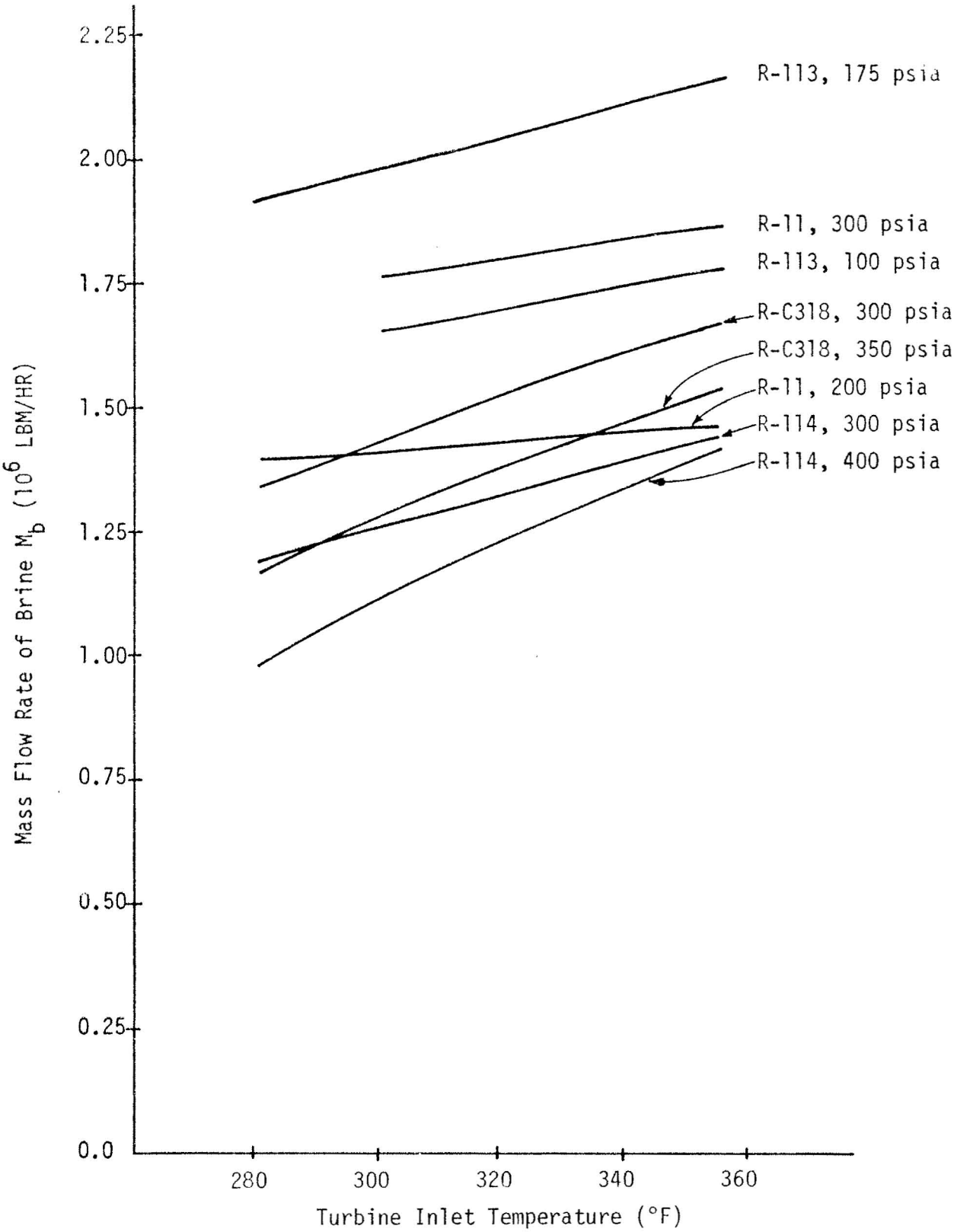

FIG. 3.6-44 BRINE FLOW RATES USING VARIOUS WORKING FLUIDS WITH BRINE AT 375°F

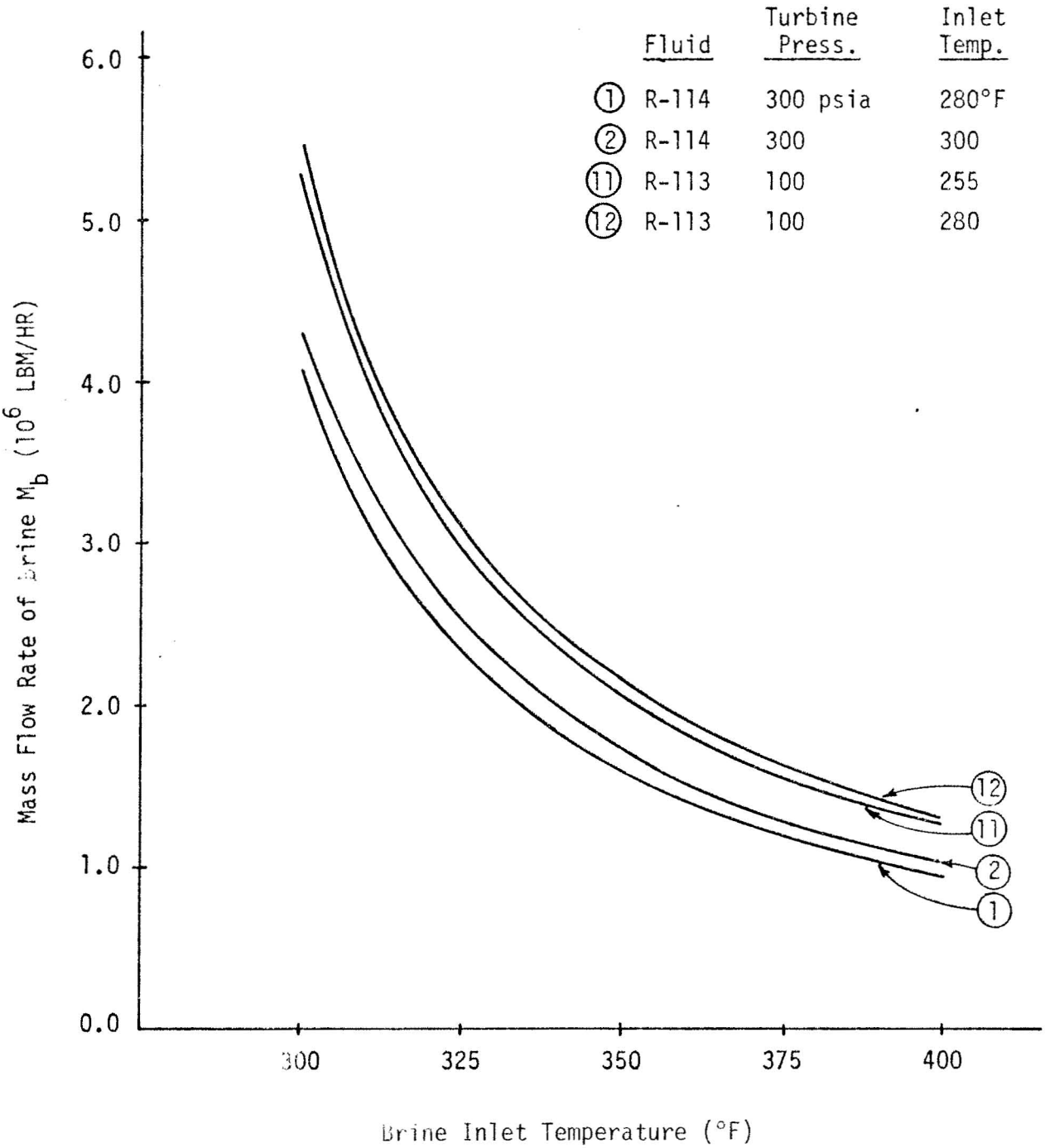

FIG. 3.6-45 BRINE FLOW RATES USING R-113 and R-114

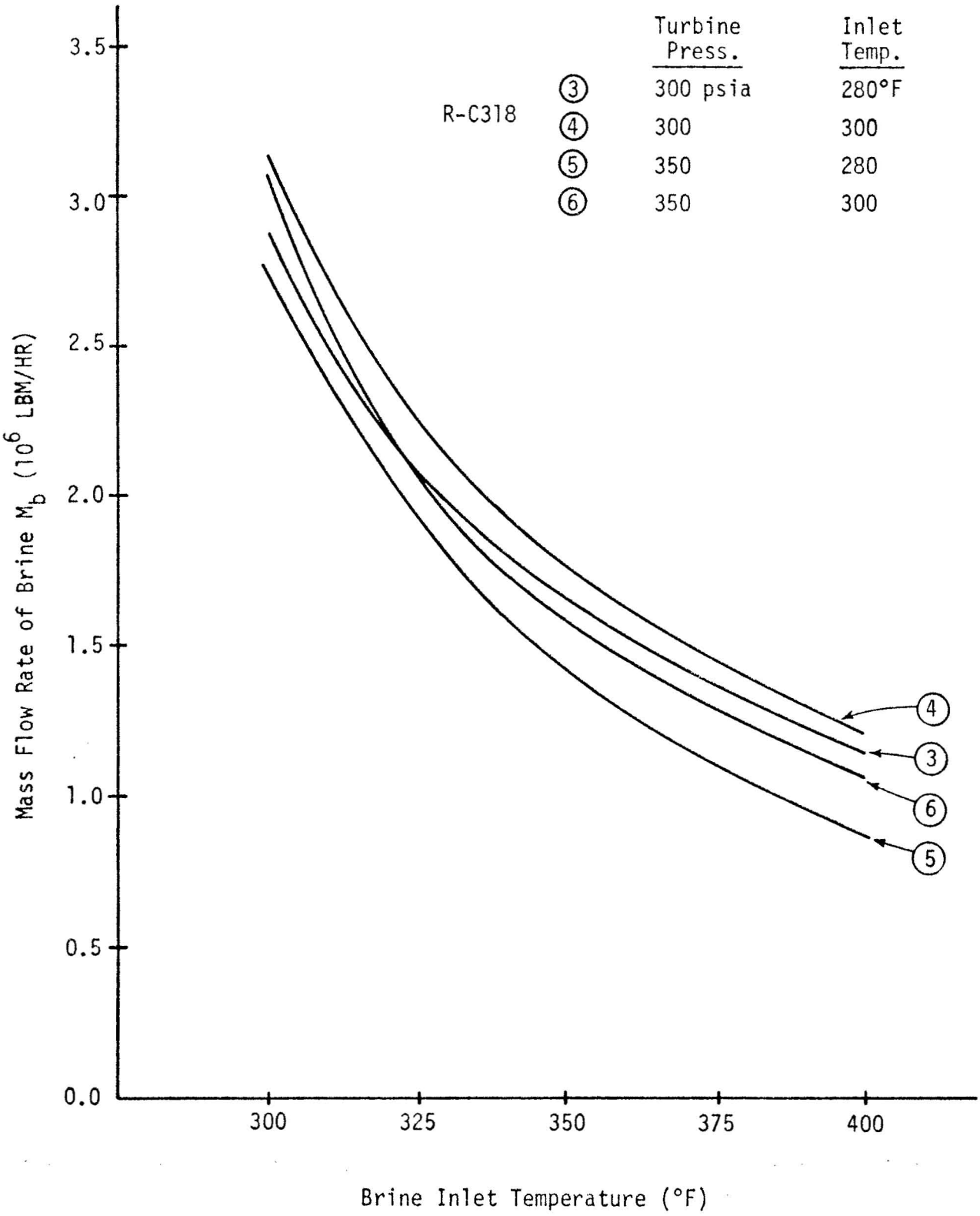

FIG. 3.6-46 BRINE FLOW RATES USING R-C318

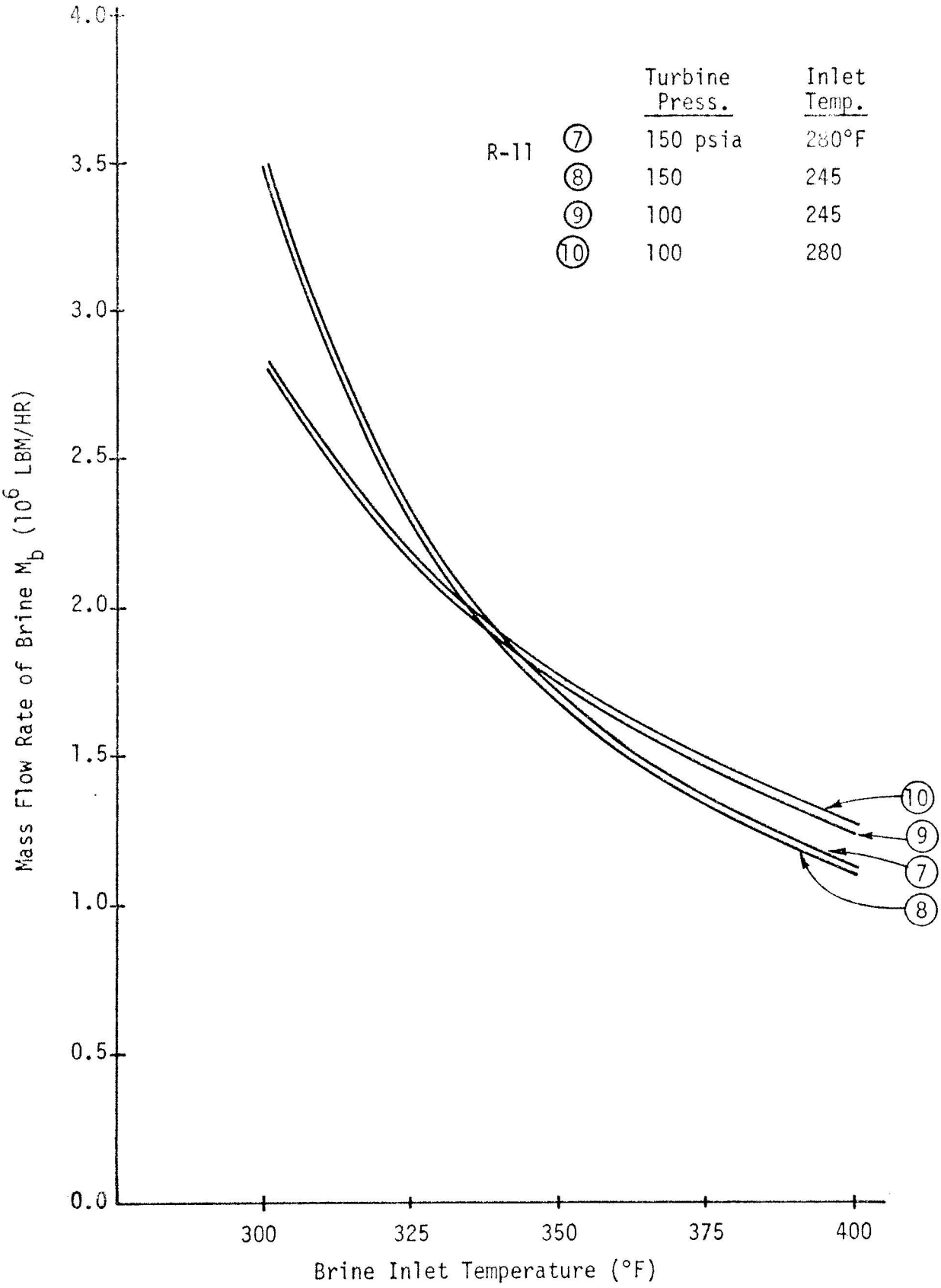

FIG. 3.6-47 BRINE FLOW RATES USING R-11

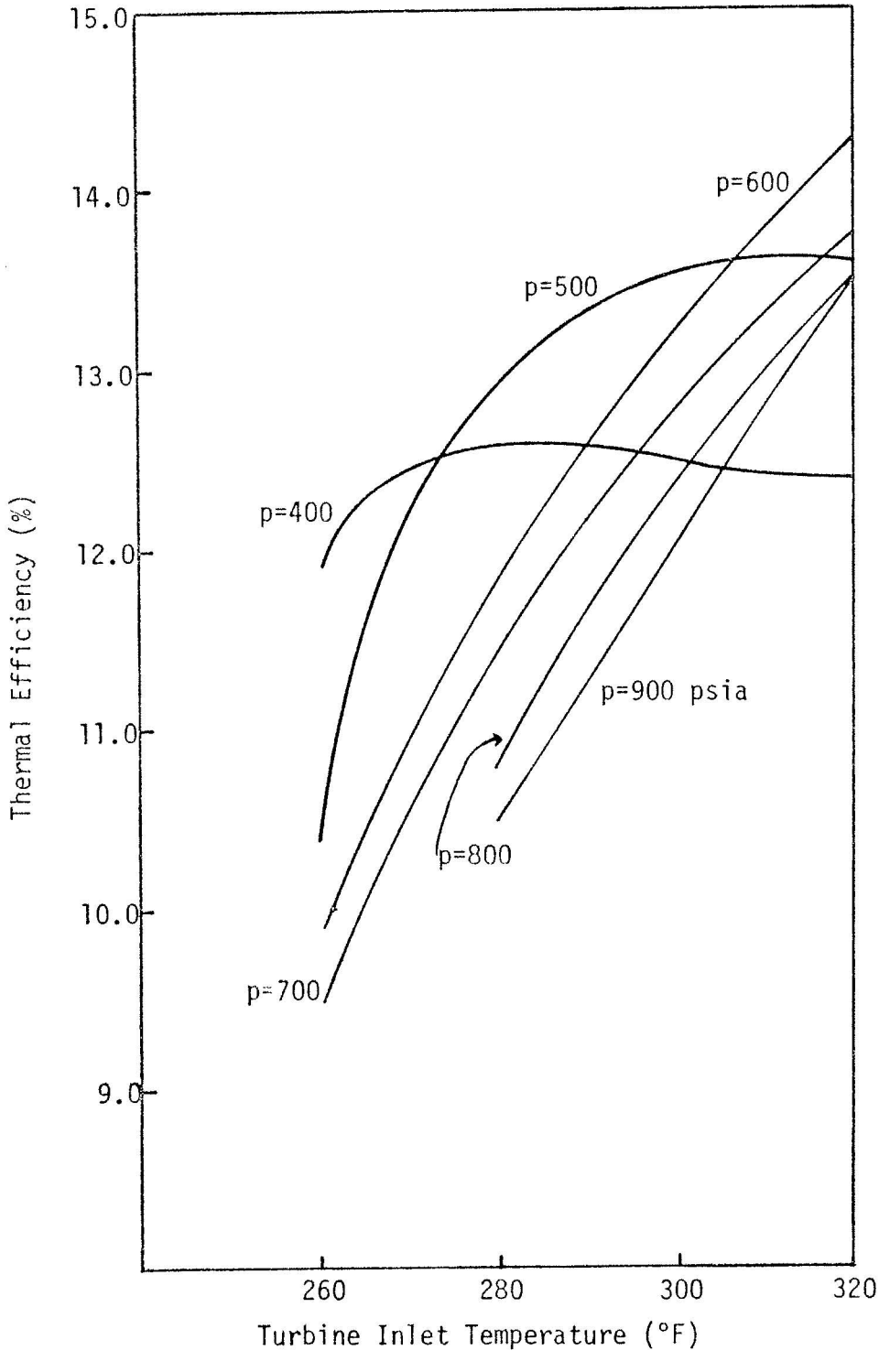

FIG. 3.6-48 THERMAL EFFICIENCY FOR ISOBUTANE CYCLE AS A FUNCTION OF TURBINE INLET TEMPERATURE AND SYSTEM PRESSURE

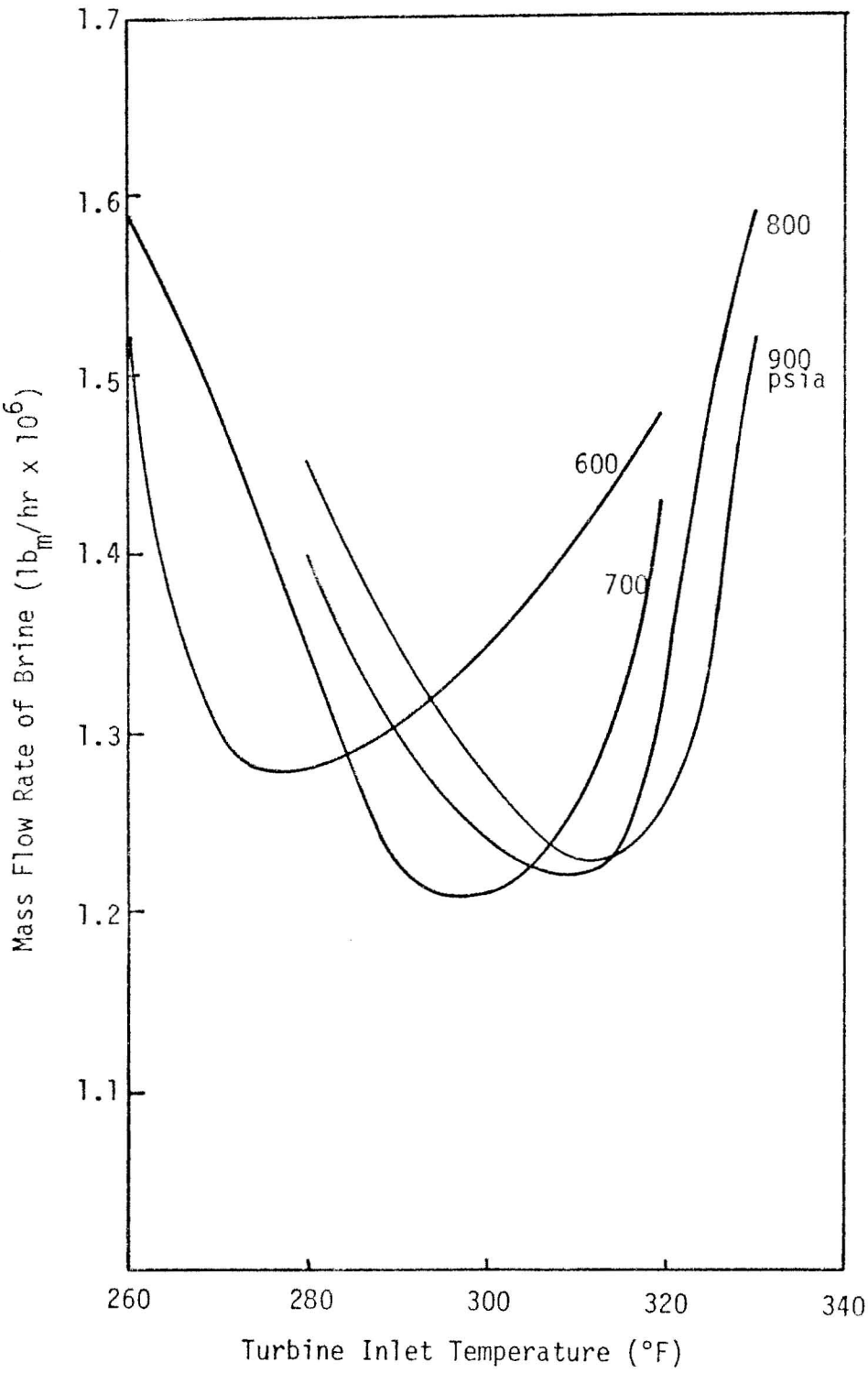

FIG. 3.6-49 BRINE FLOW RATE REQUIRED AS A FUNCTION OF TURBINE INLET TEMPERATURE FOR SUPERCRITICAL PRESSURES

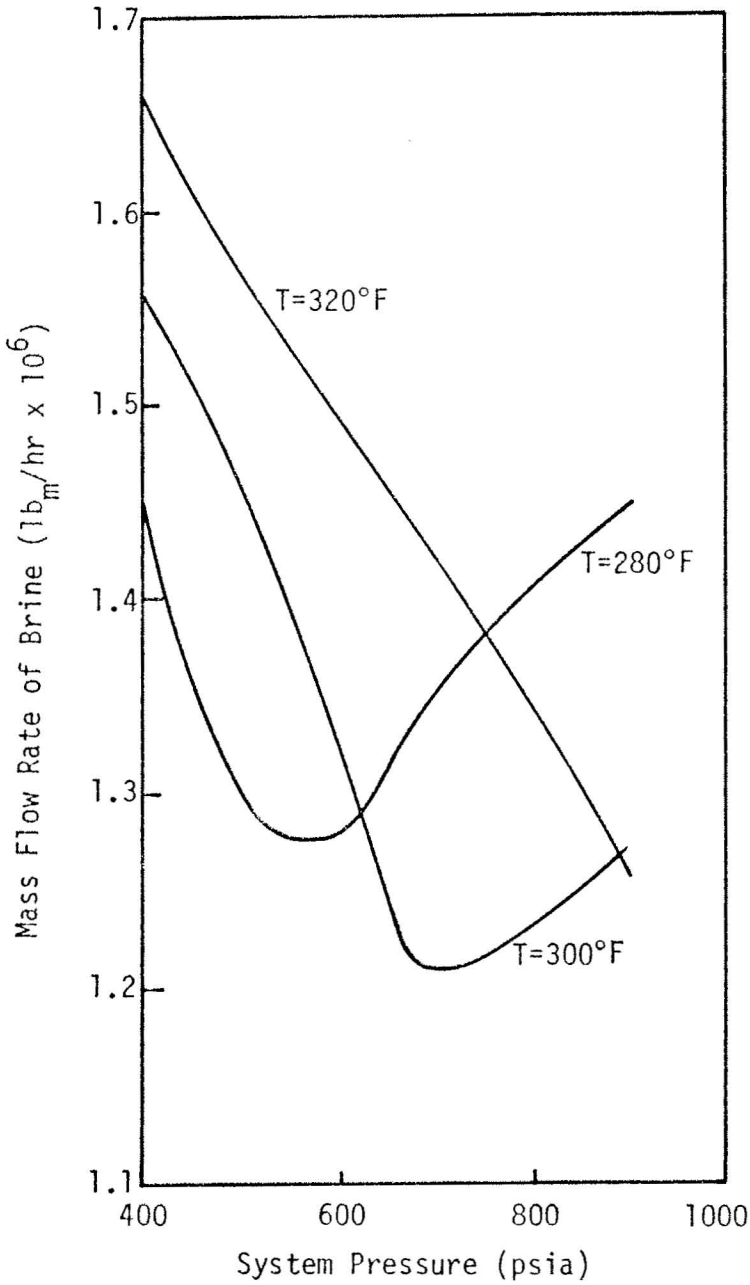

FIG. 3.6-50 BRINE FLOW RATE AS A FUNCTION OF SYSTEM PRESSURE

TABLE 3.6-6

WORKING FLUIDS AND PROPERTIES

	Fluid	Chemical Formula	Molecular Weight	Critical Point	
				T_c °F	P_c psia
1.	Methane	CH_4	16.04	-116.00	673.0
2.	Ethane	C_2H_6	30.07	90.32	709.8
3.	Propane	C_3H_8	44.09	206.00	617.0
4.	n-Butane	C_4H_{10}	58.10	305.62	550.7
5.	Ethylene	C_2H_4	28.05	49.82	742.1
6.	Propylene	C_3H_6	42.08	197.40	667.0
7.	1-Butene	C_4H_8	56.10	295.60	583.0
8.	Cis-2-Butene	C_4H_8	56.10	324.30	600.0
9.	Trans-2-Butene	C_4H_8	56.10	311.90	600.0
10.	Propadiene (Allene)	C_3H_4	40.06	248.00	793.0
11.	1,3 Butadiene	C_4H_6	54.09	306.00	628.0
12.	1,2 Butadiene	C_4H_6	54.09	339.00	653.0
13.	Methyl Chloride	CH_3Cl	50.50	290.20	964.0
14.	Methylene Chloride	CH_2Cl_2	84.90	472.40	893.0
15.	Chloroform	$CHCl_3$	119.40	499.40	805.0
16.	Carbon Tetrachloride	CCl_4	153.80	541.00	660.0
17.	Vinyl Chloride	C_2H_3Cl	62.50	313.10	809.0
18.	Vinylidene Chloride	CH_2CCl_2	96.95	429.20	758.0
19.	Trichloroethylene	C_2HCl_3	131.40	567.80	710.0
20.	Perchloroethylene	C_2Cl_4	165.00	643.40	650.0

TABLE 3.6-6 (continued)

	Fluid	Chemical Formula	Molecular Weight	Critical Point	
				T_c °F	P_c psia
21.	Ethyl Chloride	C_2H_5Cl	64.50	368.00	761.0
22.	Ethylene Dichloride	$C_2H_4Cl_2$	99.00	553.40	780.0
23.	Propyl Chloride	C_2H_7Cl	78.50	445.40	663.0
24.	Propylene Dichloride	$C_3H_6Cl_2$	113.00	578.60	641.0
25.	Methanol	CH_4O	32.04	463.40	1155.0
26.	Ethanol	C_2H_6O	46.07	469.00	924.0
27.	Propanol	C_3H_8O	60.10	506.00	749.0
28.	Butanol	$C_4H_{10}O$	74.1	553.00	640.0
29.	Isopropyl Alcohol	C_3H_8O	60.10	454.90	691.0
30.	Isobutyl Alcohol	$C_4H_{10}O$	74.10	530.00	623.0
31.	Sec-butyl Alcohol	$C_4H_{10}O$	74.10	504.80	608.0
32.	Tert-butyl Alcohol	$C_4H_{10}O$	74.10	454.40	614.0
33.	Allyl Alcohol	C_3H_6O	58.08	521.00	831.0
34.	1-Amyl Alcohol	$C_5H_{12}O$	88.10	590.70	557.0
35.	1-Hexyl Alcohol	$C_6H_{14}O$	102.20	595.70	490.0
36.	1-Heptyl Alcohol	$C_7H_{16}O$	116.20	630.80	436.0
37.	Ethylene Oxide	C_2H_4O	44.10	383.80	1043.0
38.	Propylene Oxide	C_3H_6O	58.10	407.60	714.0
39.	Epichlorohydrine	C_3H_5OCl	92.50	612.80	721.0
40.	1,2 Butylene Oxide	C_4H_8O	72.10	468.80	630.0
41.	Ethylene Glycol	$C_2H_6O_2$	62.1	704.60	1120.0
42.	Diethylene Glycol	$C_4H_{10}O_3$	106.10	764.00	680.0

TABLE 3.6-6 (continued)

	Fluid	Chemical Formula	Molecular Weight	Critical Point	
				T_c °F	P_c psia
43.	Triethylene Glycol	$C_6H_{14}O_4$	150.20	818.00	486.0
44.	n-Pentane	C_5H_{12}	72.20	385.50	489.5
45.	n-Hexane	C_6H_{14}	86.20	454.10	440.0
46.	n-Heptane	C_7H_{16}	100.20	512.62	396.8
47.	n-Octane	C_8H_{18}	114.20	563.70	362.1
48.	1-Pentene	C_5H_{10}	70.13	376.90	586.0
49.	1-Hexene	C_6H_{12}	84.20	460.00	471.7
50.	1-Heptene	C_7H_{14}	98.20	507.40	426.2
51.	1-Octene	C_8H_{16}	112.20	560.30	395.3
52.	Isobutane	C_4H_{10}	58.12	274.96	529.1
53.	Isobutylene	C_4H_8	56.10	291.90	580.0
54.	Isoprene	C_5H_8	68.11	412.00	558.4
55.	Isopentane	C_5H_{12}	72.20	369.00	483.0
56.	Isohexane	C_6H_{14}	86.17	435.10	440.0
57.	2-Methylhexane	C_7H_{16}	100.20	495.00	400.0
58.	Isooctane	C_8H_{18}	114.20	519.40	375.0
59.	2-Methylheptane	C_8H_{18}	114.20	547.50	364.0
60.	Formaldehyde	CH_2O	30.02	278.00	984.0
61.	Acetaldehyde	C_2H_4O	44.05	369.80	803.0
62.	Propionaldehyde	C_3H_6O	58.08	427.40	674.0
63.	Butylaldehyde	C_4H_8O	72.11	477.80	580.0
64.	Acetone	C_3H_6O	58.08	454.40	690.0

TABLE 3.6-6 (continued)

	Fluid	Chemical Formula	Molecular Weight	Critical Point	
				T_c °F	P_c psia
65.	2-Butanone	C_4H_8O	72.10	503.90	602.0
66.	3-Pentanone	$C_5H_{10}O$	86.13	599.40	542.0
67.	4-Methylpentanone-2	$C_6H_{12}O$	100.16	568.30	475.0
68.	Methyl Ether	C_2H_6O	46.07	259.80	763.0
69.	Ethyl Ether	$C_4H_{10}O$	74.12	380.20	522.0
70.	Propyl Ether	$C_6H_{14}O$	102.20	488.60	414.0
71.	Butyl Ether	$C_8H_{18}O$	130.20	584.00	345.0
72.	Methyl Acetate	$C_3H_6O_2$	74.08	452.10	666.0
73.	Ethyl Acetate	$C_4H_8O_2$	88.10	481.60	557.0
74.	Butyl Acetate	$C_6H_{12}O$	116.16	582.20	442.0
75.	Vinyl Acetate	$C_4H_6O_2$	86.10	485.00	609.0
76.	Acetic Anhydride	$C_4H_6O_3$	102.09	564.20	675.0
77.	Propionic Anhydride	$C_6H_{10}O_3$	130.15	594.80	478.0
78.	Ethyl Formate	$C_3H_6O_2$	74.09	454.90	686.0
79.	Isopropyl Acetate	$C_5H_{10}O_2$	102.15	468.80	507.0
80.	Benzene	C_6H_6	78.11	552.00	714.0
81.	Ethylbenzene	C_8H_{10}	106.16	651.20	540.0
82.	Propylbenzene	C_9H_{12}	120.19	689.40	460.0
83.	Cumene	C_9H_{12}	120.19	676.20	460.0
84.	Cyclopropane	C_3H_6	42.08	256.00	797.0
85.	Cyclobutane	C_4H_8	56.10	373.40	713.0
86.	Cyclopentane	C_5H_{10}	70.13	461.48	654.7

TABLE 3.6-6 (continued)

	Fluid	Chemical Formula	Molecular Weight	Critical Point	
				T_c °F	P_c psia
87.	Cyclohexane	C_6H_{12}	84.16	535.60	591.5
88.	Bromobenzene	C_6H_5Br	157.02	746.00	655.0
89.	Chlorobenzene	C_6H_5Cl	112.56	678.00	655.0
90.	Fluorobenzene	C_6H_5F	96.10	547.30	655.0
91.	R-11	CCl_3F	137.38	388.40	640.0
92.	R-12	CCl_2F_2	120.93	233.60	597.0
93.	R-22	$CHClF_2$	86.48	204.80	721.9
94.	R-113	$CCl_2F\text{-}CClF_2$	187.39	417.40	498.9
95.	R-114	$C_2Cl\ F_4$	170.94	294.30	473.0
96.	R-115	CF_3CF_2Cl	154.50	175.90	458.0
97.	R-502	$CHClF_2$ (48.8%) $CClF_2CF_3$ (51.2%)	111.60	194.00	619.0
98.	R-318	C_4F_8	200.04	239.60	403.6
99.	R-13B1	$CBrF_3$	148.93	152.60	575.0

4. Heat Exchanger Design

a. Parametric Study of a Vertical Counterflow Heat Exchanger

A vertical counterflow heat exchanger, which is to be the prime heat exchange unit between the hot brine and the working fluid in the power producing cycle, was designed assuming the following standard set of conditions:

Heat source	Liquid brine at 350°F
Net power output	10 MW
Working fluid	R-600a - isobutane
Condenser outlet conditions	Saturated liquid at 100°F
Tube diameter	1 inch
Pitch	1.1
Isobutane velocity	7 ft/sec
Pinch point temperature difference	20°F
System pressure	400 psia
Scale thickness	Zero

Pressure losses and heat losses neglected

The details of a parametric study just concluded are detailed in Hawaii Geothermal Project Engineering Program Technical Report No. 5. However, a summary of some of the results is presented here. In this parametric study, one parameter was varied while all of the others were kept constant. In this fashion significant trends could be more easily detected.

The variation of total length required as a function of turbine inlet temperature is shown in Fig. 3.6-51. This was part of the standard design but is shown here to give an indication of the lengths to be expected in a heat exchanger of this type. It is interesting that a minimum for the required tube length exists at a temperature of approximately 290°F.

In Fig. 3.6-52, the inside tube diameter is the parameter varied. As the diameter is decreased, the total tube length decreases but the number of tubes increases to compensate for the decrease in surface area per tube.

Fig. 3.6-53 shows the variations of tube length and pressure drop with isobutane velocity. As both tube length and pressure increase markedly with isobutane velocity, there is good reason to keep the velocity of the working fluid at a fairly low value. Of course, a lower velocity means that the flow cross-sectional area must be increased in order to permit the mass flow rate of the working fluid to remain constant.

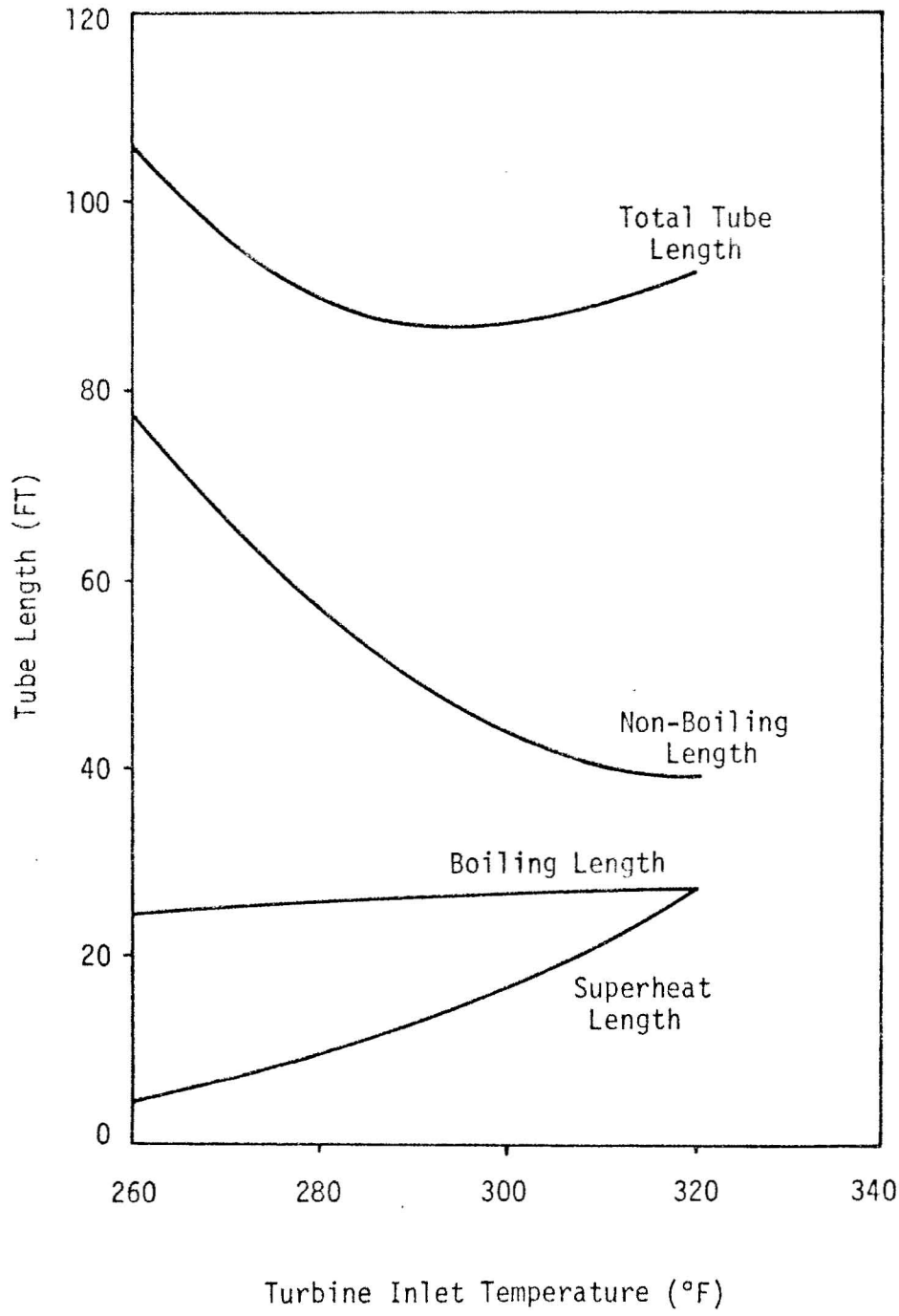

FIG. 3.6-51 THE EFFECT OF TURBINE INLET TEMPERATURE ON TUBE LENGTHS

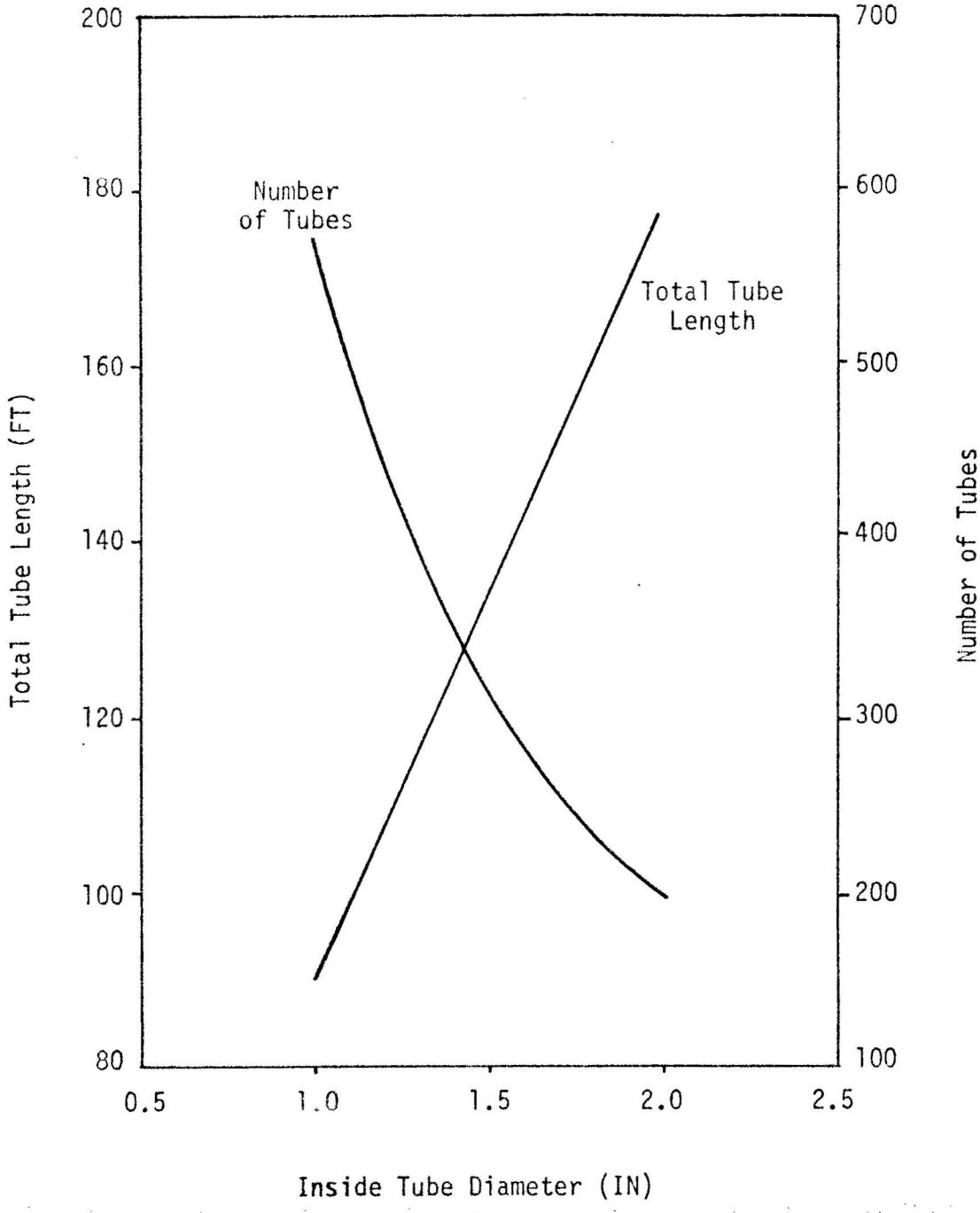

FIG. 3.6-52 THE EFFECT OF TUBE DIAMETER ON TUBE LENGTH AND NUMBER OF TUBES

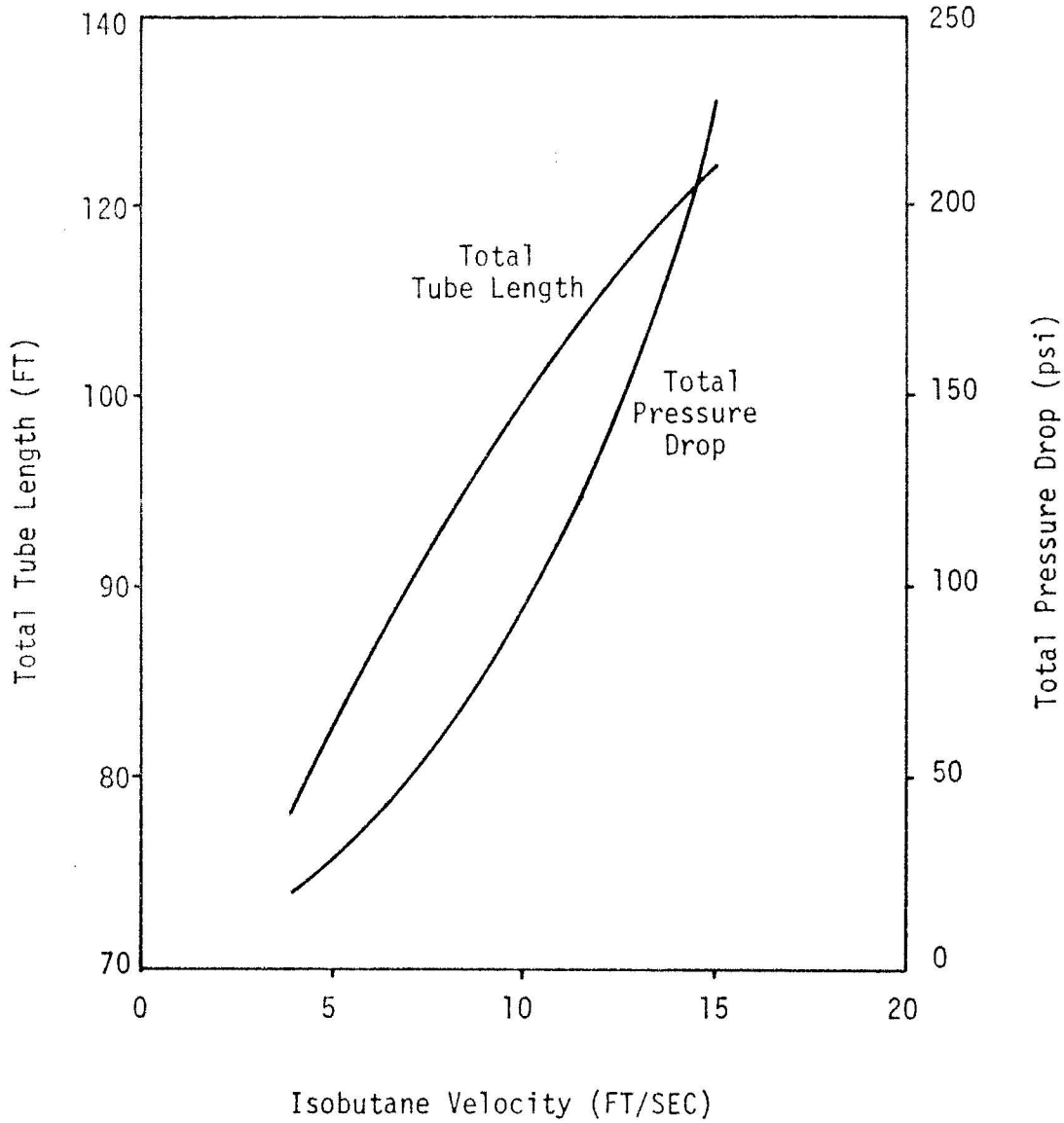

FIG. 3.6-53 EFFECT OF ISOBUTANE VELOCITY ON TUBE LENGTH AND PRESSURE DROP

The pinch point temperature difference is another important parameter to be considered. The effect of this parameter on tube length, pressure drop, brine flow rate, and brine exit temperature is depicted in Figs. 3.6-54 and 3.6-55. It is seen that while a larger pinch point temperature difference is advantageous in terms of shorter tube length and smaller pressure drop, it results in a greater flow rate of brine required and a higher brine exit temperature.

Probably the overriding factor in the design of heat exchangers for geothermal power is that of scale deposition. Because of its low thermal conductivity and roughness, failure to prevent the deposition of scale can be disastrous. As seen in Fig. 3.6-56 the presence of 0.030 inch of scale on a 1-inch diameter is sufficient to cause a doubling of the tube length required and the resulting pressure drop.

The effect of tube pitch, the ratio of distance between tubes to tube diameter, on tube length and number of tubes is shown in Fig. 3.6-57. Here the two curves have slopes of opposite signs so that some sort of trade off must be decided upon.

Effect of Pressure

The critical pressure of isobutane is 529 psia, so a system pressure of 600 psia was used in the computational procedure to determine the effect of supercritical pressure on heat exchanger design. In Fig. 3.6-58, the effect of pressure on cycle efficiency can be seen as the turbine inlet temperature is varied. The differences between the subcritical and supercritical efficiency curves will produce significant behavior differences in the respective tube length, tube material, and pressure drop curves. The aforementioned curves are shown in Figures 3.6-59 to 3.6-61.

The following conclusions were drawn from the results of the subcritical pressure and supercritical pressure cases:

1. Systems using supercritical pressures will require significantly more tube material than systems employing subcritical pressures.
2. Pumping requirements will generally be less for supercritical pressure conditions than for subcritical pressure conditions.

Under subcritical pressure conditions, variations in turbine inlet temperature will produce the following effects:

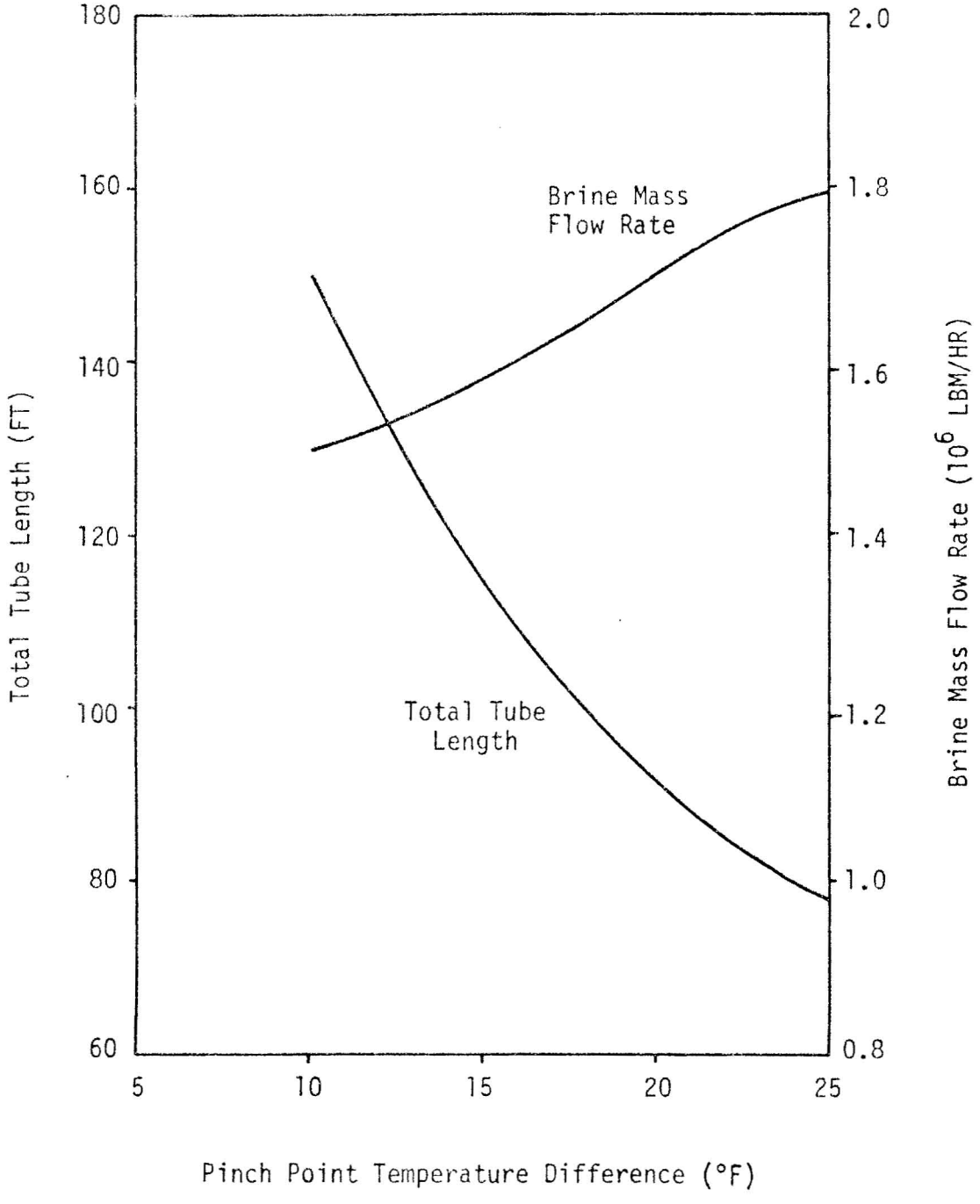

FIG. 3.6-54 THE EFFECT OF PINCH POINT TEMPERATURE DIFFERENCE ON TUBE LENGTH AND BRINE FLOW RATE

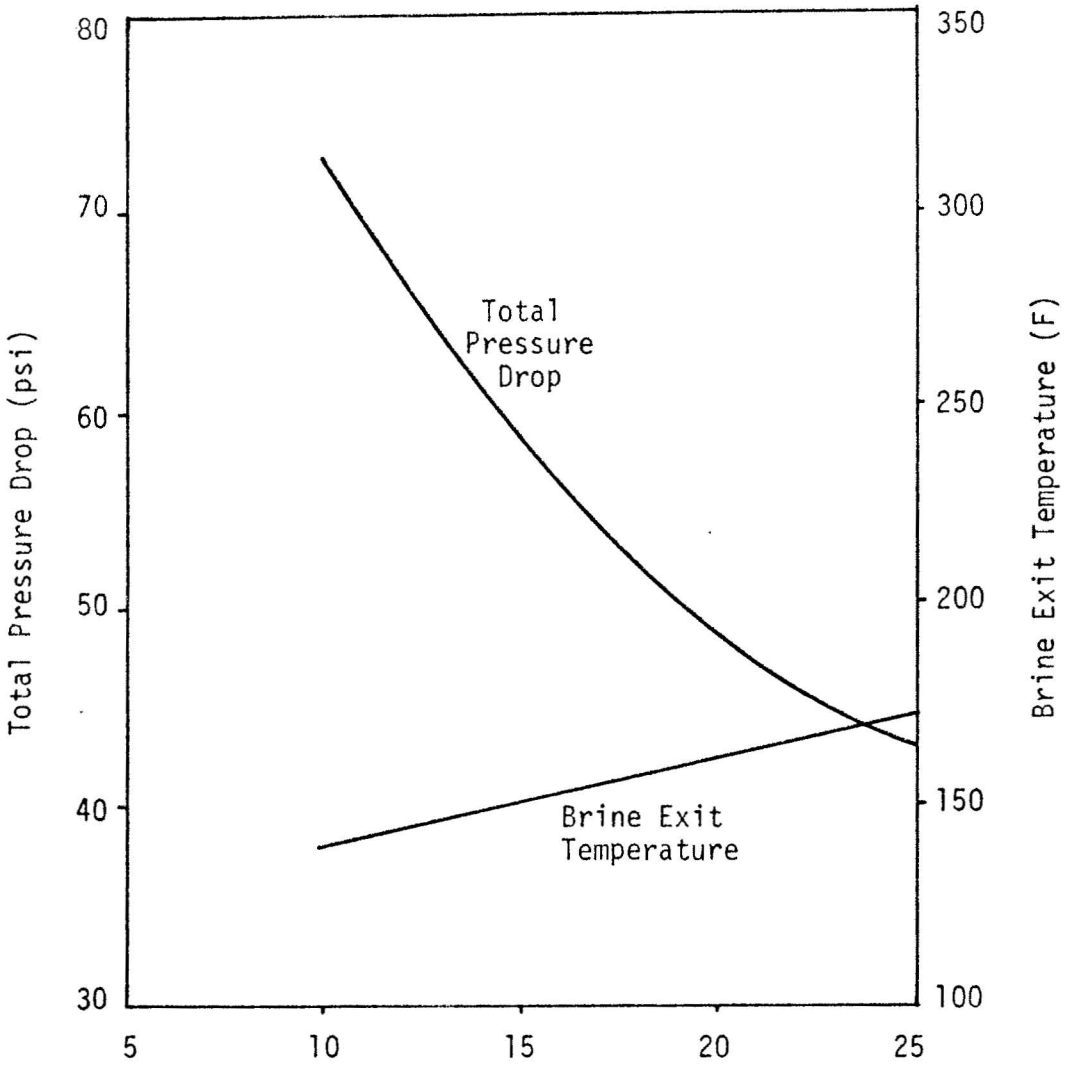

FIG. 3.6-55 THE EFFECT OF PINCH POINT TEMPERATURE DIFFERENCE ON PRESSURE DROP AND BRINE EXIT TEMPERATURE

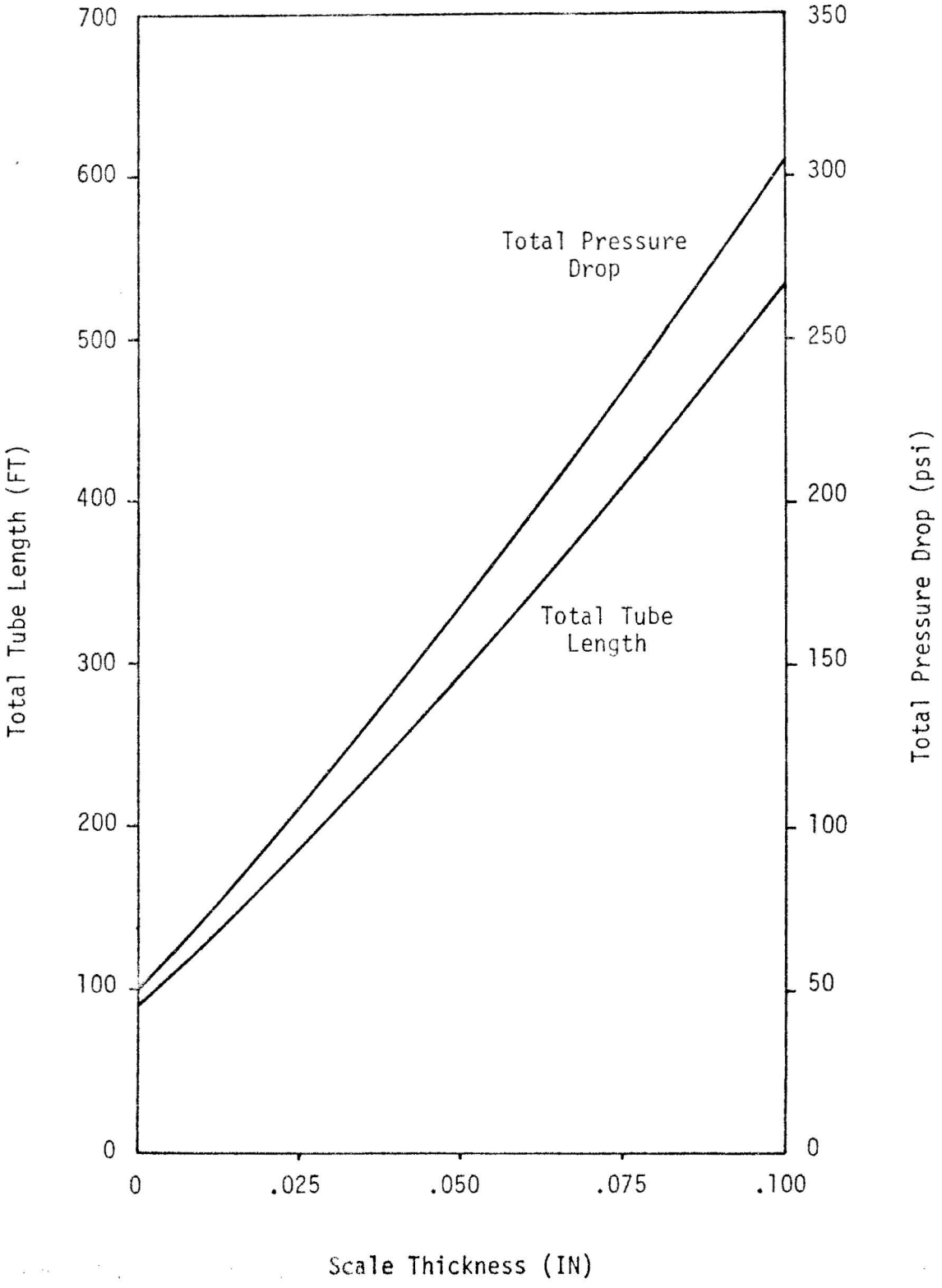

FIG. 3.6-56 THE EFFECT OF SCALE THICKNESS ON TUBE LENGTH AND PRESSURE DROP

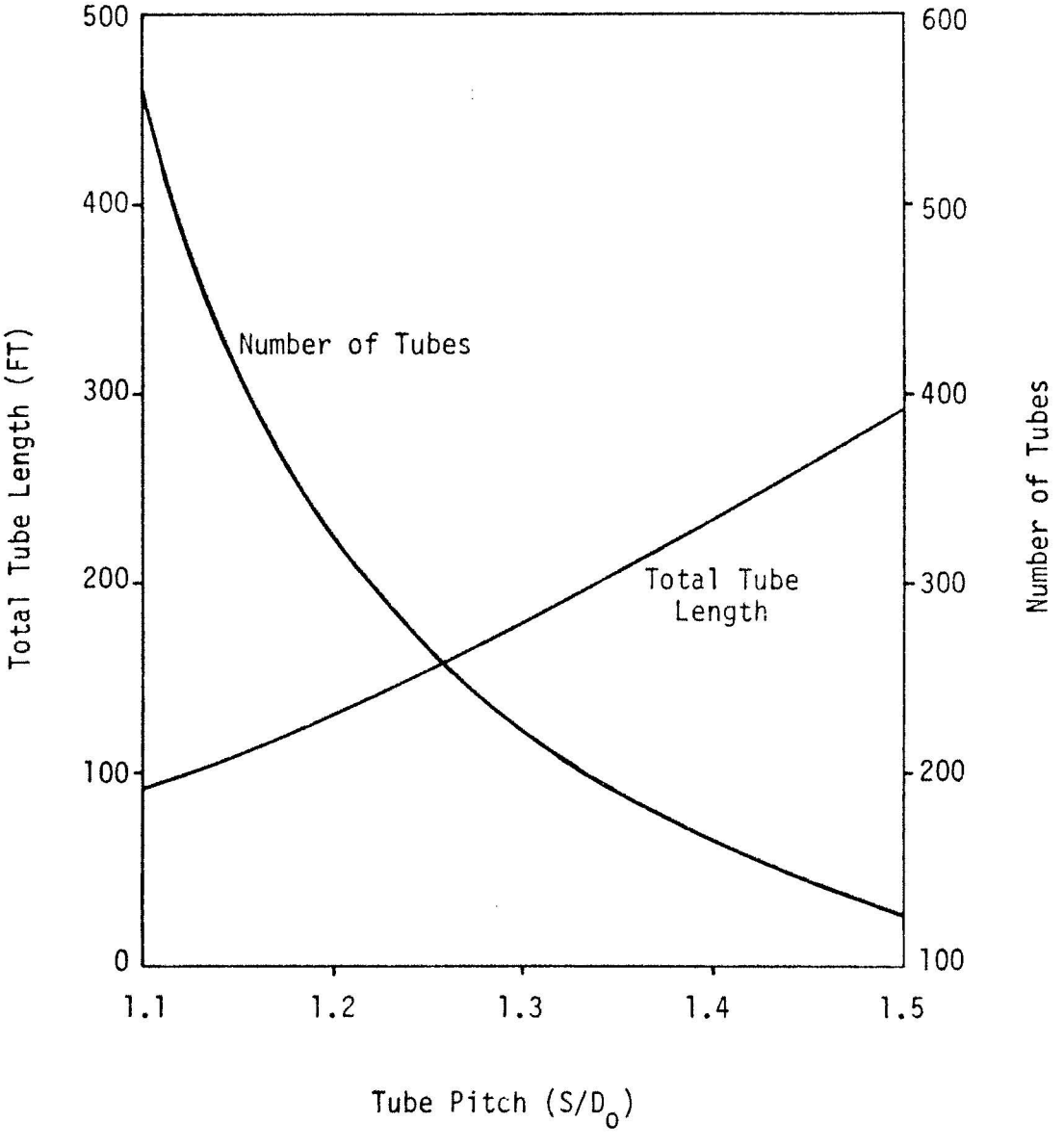

FIG. 3.6-57 THE EFFECT OF TUBE PITCH ON TUBE LENGTH AND NUMBER OF TUBES

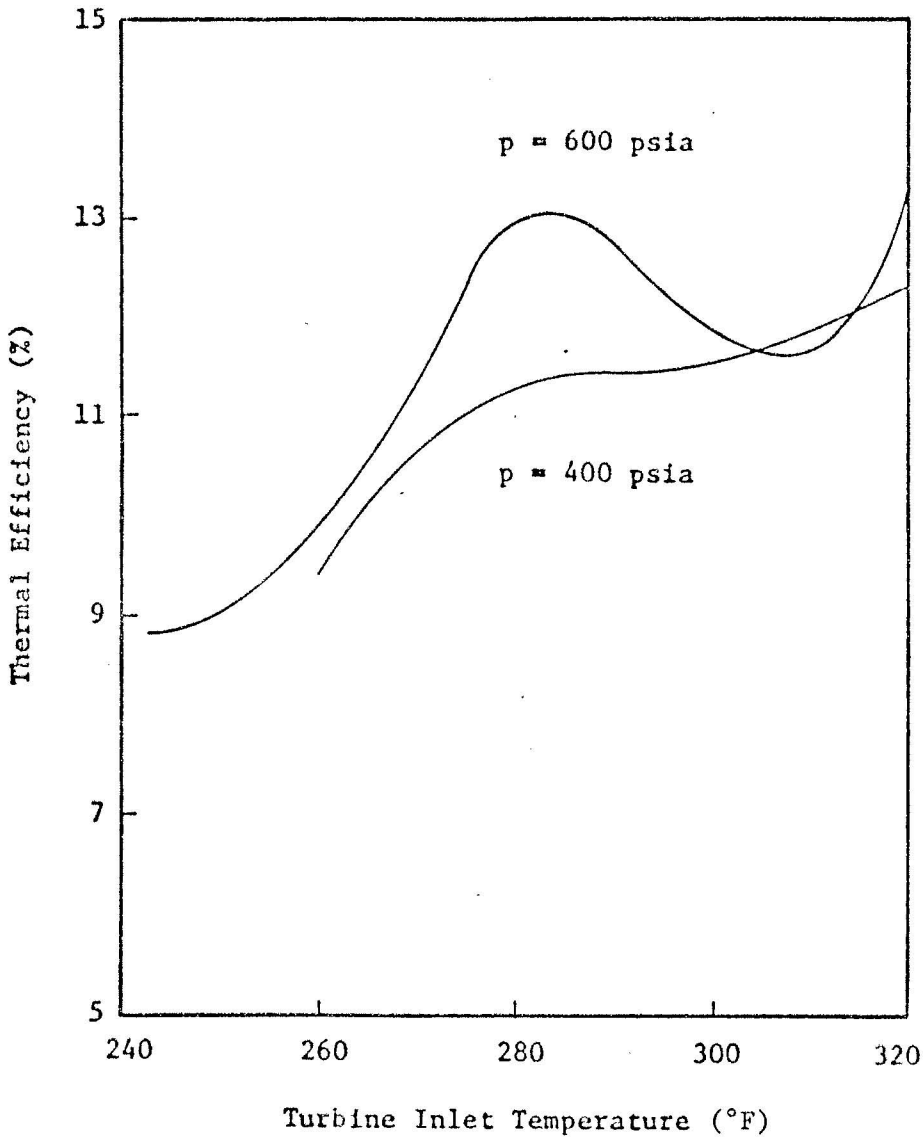

FIG. 3.6-58 THE EFFECT OF PRESSURE ON THERMAL EFFICIENCY

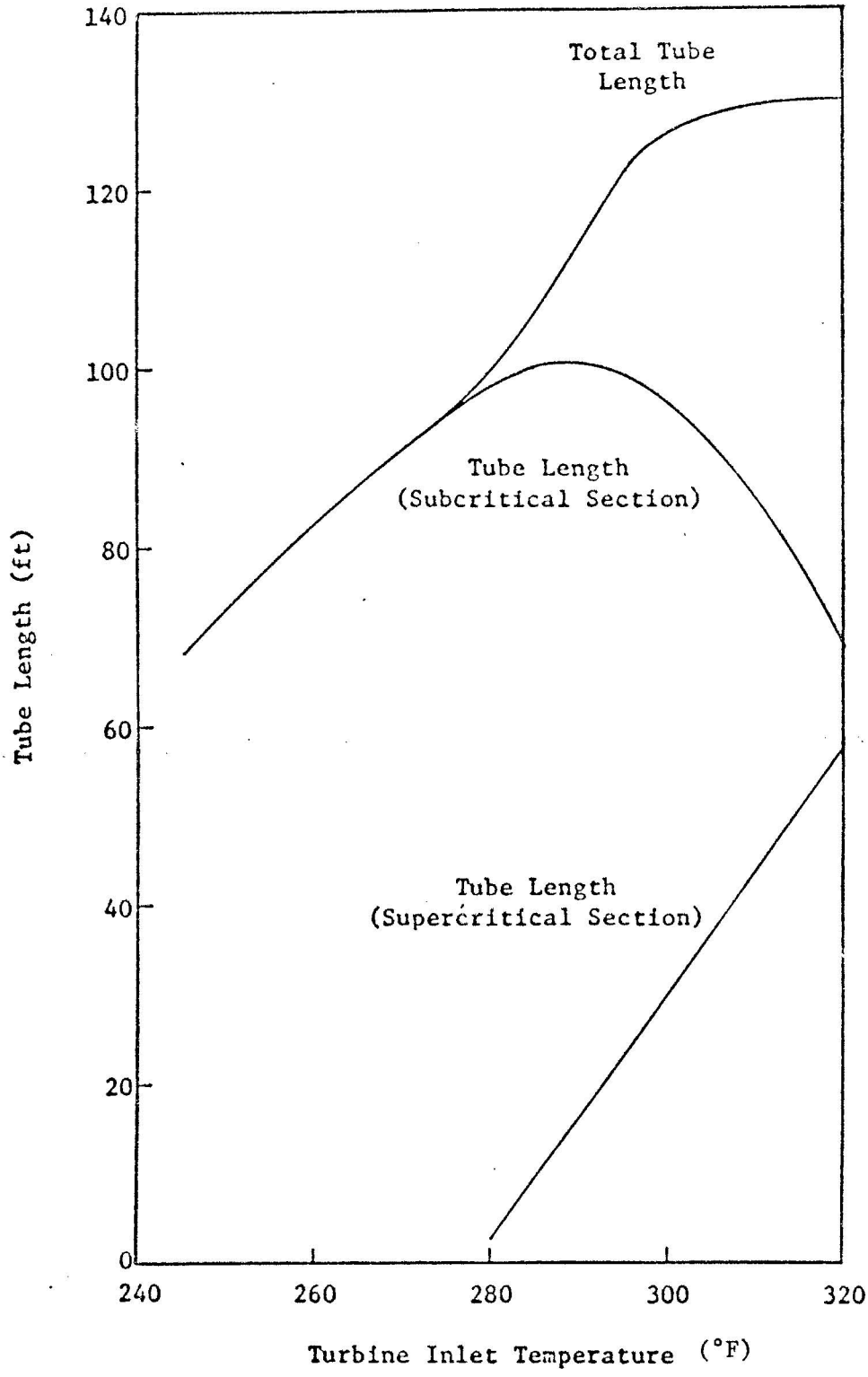

FIG. 3.6-5 RELATIONSHIP BETWEEN TUBE LENGTH AND TURBINE INLET TEMPERATURE

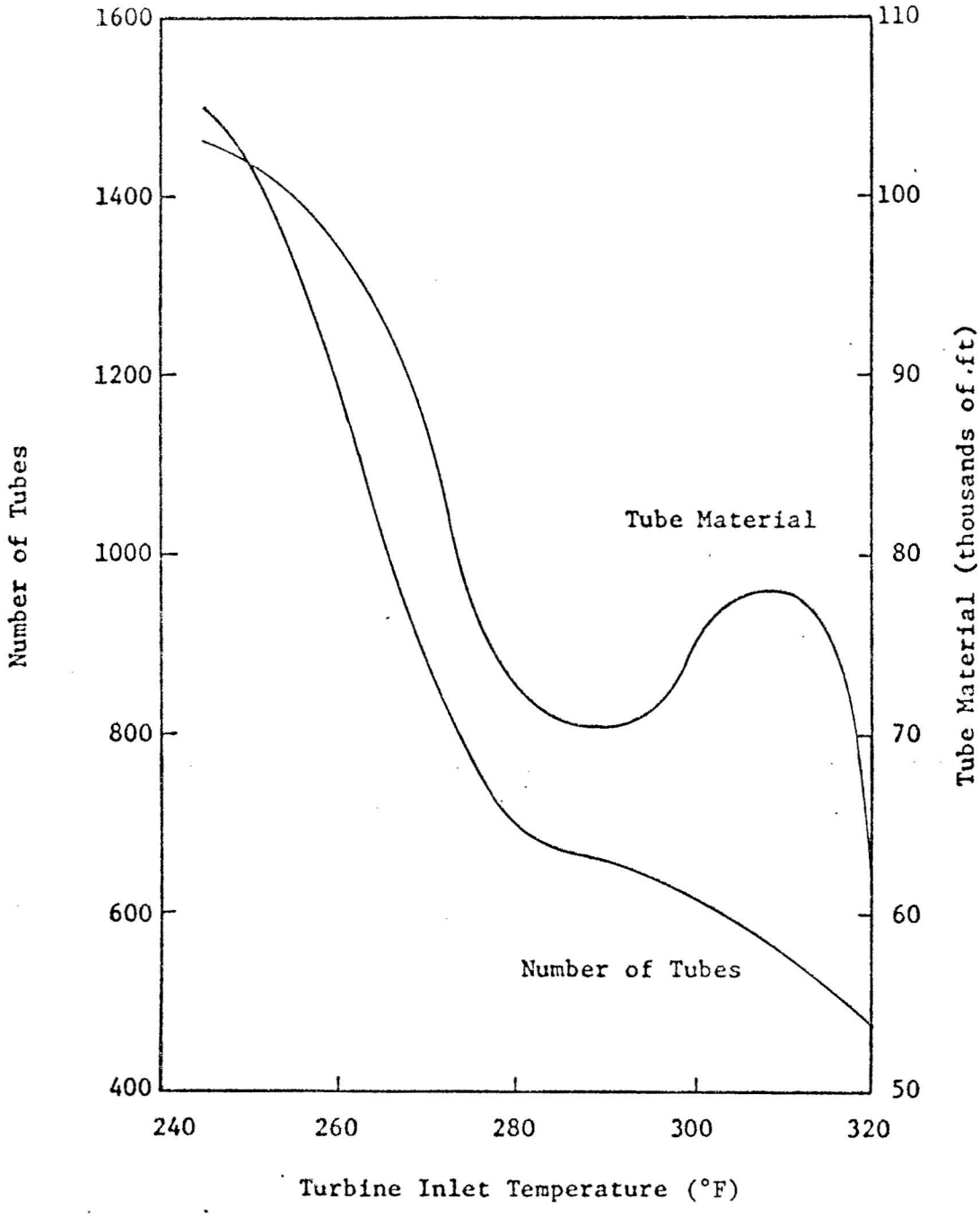

FIG. 3.6-60 THE EFFECT OF TURBINE INLET TEMPERATURE ON TUBE MATERIAL AND THE NUMBER OF TUBES

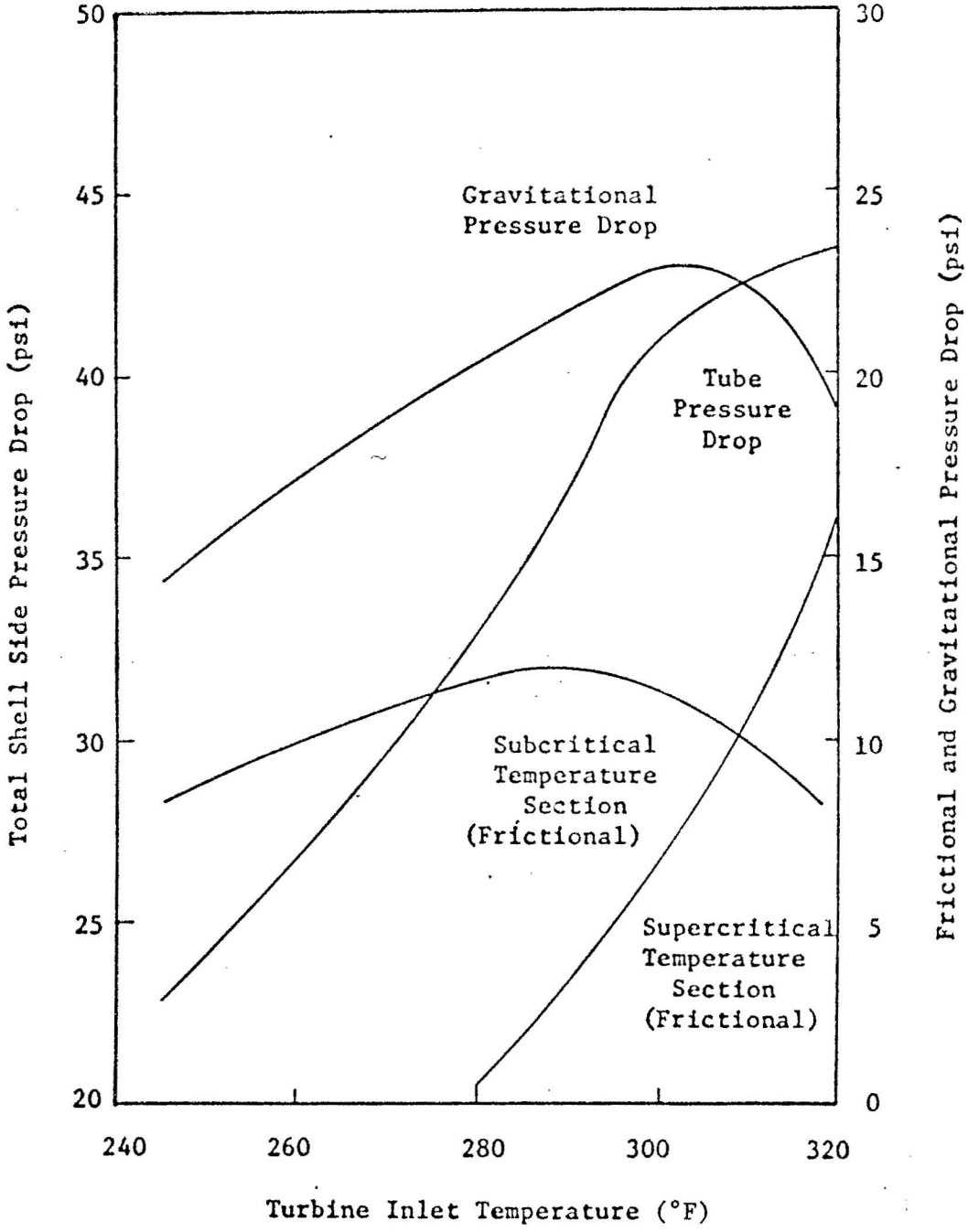

FIG. 3.6-61 THE EFFECT OF TURBINE INLET TEMPERATURE ON SHELL SIDE PRESSURE DROP

1. Tube lengths change significantly in the nonboiling and superheat sections, where they respectively decrease and increase as turbine inlet temperature increases.
2. The total shell side pressure drop will change significantly as turbine inlet temperature is varied.
3. An increase in the turbine inlet temperature will result in a decrease in the required quantity of tube material.

Conclusions concerning the effect of inside tube diameter are as follows:

1. Increasing the inside tube diameter will bring about nearly proportional increases in total tube length and total shell side pressure drop.
2. The quantity of tube material necessary will increase if tube diameter is increased.

The effect of pitch was considered and the following conclusions were drawn:

1. Total tube length will increase as pitch increases.
2. Frictional and gravitational pressure drops are similar in magnitude, but the relations between frictional pressure drop and pitch is the inverse of that associated with gravitational pressure drop and pitch.
3. The quantity of tube material required will decrease as pitch increases.

Consideration of the effect of scaling resulted in the following observations:

1. The presence of scale greatly increases the thermal resistance between the brine and isobutane.
2. Total tube length and total shell side pressure drop increase almost proportionately with scale thickness.
3. Since tube number is unaffected by the presence of scale, required tube material quantity is proportional to tube length.

Consideration of the effect of pinch point temperature difference led to the following conclusions:

1. Brine mass flow rate increases as the pinch point temperature difference increases.
2. An inverse relationship exists with pinch point temperature difference for both total tube length and total shell side pressure drop.
3. Since tube number is not a function of pinch point temperature difference, tube material quantity is proportional to tube length, and therefore has an inverse relationship with pinch point temperature difference.

V. Experimental Heat Transfer Loop

A test apparatus was designed to investigate the heat transfer and pressure drop characteristics of Freon-11 on the outside surfaces of a tube bundle. The schematic diagram of the test loop is shown in Fig. 3.6-62. The heat exchanger can be set up in either a horizontal or vertical configuration.

The purpose of this investigation is as follows:

Vertical Heat Exchanger

Compute the average heat transfer coefficient and the pressure drop from experimental data, and compare these results with those values predicted by the computer program which has been written for this purpose. If the difference between the experimental and predicted values is more than 15%, new correlation equations will be formulated.

Horizontal Heat Exchanger

Compute the average heat transfer coefficient and the pressure drop from the experimental data and formulate correlation equations for heat transfer and pressure drop. Comparison of the heat transfer and pressure drop correlation equations will be made between those for tube bundles and those for single horizontal tubes to obtain a correction factor which may be applied to the single tube equations to predict these values for tube bundles. The heat exchanger will be constructed with a pyrex glass cylinder in such a way that vapor generation and vapor passage can be observed. This information may be useful in selecting an optimum configuration for a horizontal heat exchanger.

Test Apparatus

Seven electrical tubular heaters (outside diameter = 0.496 inch, length = 51 5/8 inches, maximum power output per square inch = 40 watts) will be arranged with a triangular pitch of 0.744 inch in a pyrex cylinder (wall thickness = 0.25 inch, inside diameter = 2.25 inches) as shown in Fig. 3.6-63.

Power to the heaters will be supplied by the combination of a constant voltage transformer and a variable voltage transformer. Power input will be measured by a digital voltmeter and an ammeter.

A Consolidated Control analog-direct digital indicator will be used with the combination of copper-constantan thermocouples and turbine flow meter to measure the temperatures at various points and volumetric flow rate, respectively. Pressures will be measured by Bourden tube pressure gauges.

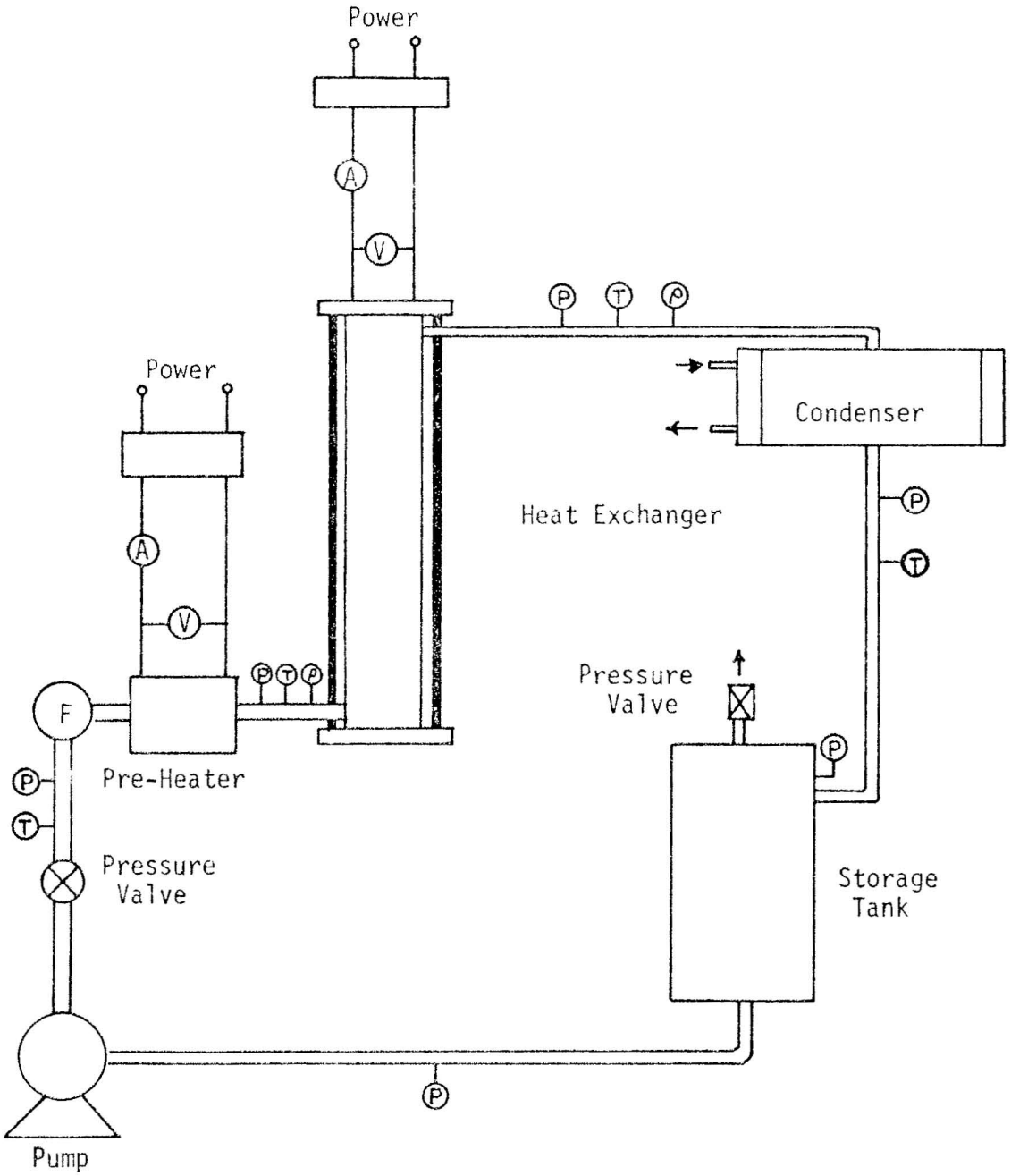

P - Pressure Meter
T - Temperature Meter
ρ - Density Meter
F - Flow Meter
A - Ammeter
V - Volt Meter

FIG. 3.6-62 SCHEMATIC OF EXPERIMENTAL TEST LOOP

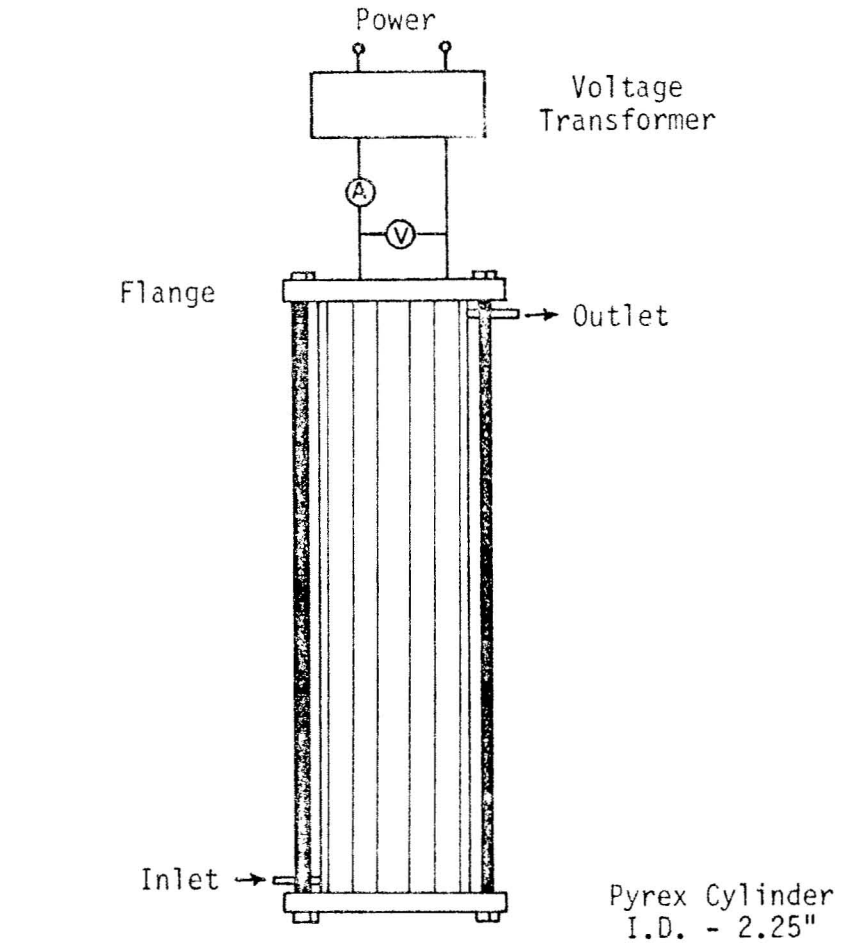

FIG. 3.6-63 LAYOUT OF HEAT EXCHANGER TEST SECTION

Investigations have been conducted to find a manufacturer of an instrument which will measure density or void fraction of vapor, but so far it has not been successful. In the event it is not possible to purchase the direct reading instrument, a throttling calorimeter will be used to measure the enthalpy of the vapor.

The condenser will be a single-shell two-tube pass type, and it will be constructed with 36 low finned tubes (outside diameter = 0.75 inch, fin height = 0.125 inch, length = 6 feet, number of fins per inch = 11) as depicted in Fig. 3.6-64. The tube side cooling water will be cooled by a five-ton water-cooled water chiller. Condensed Freon will be stored in a stainless steel or copper tank.

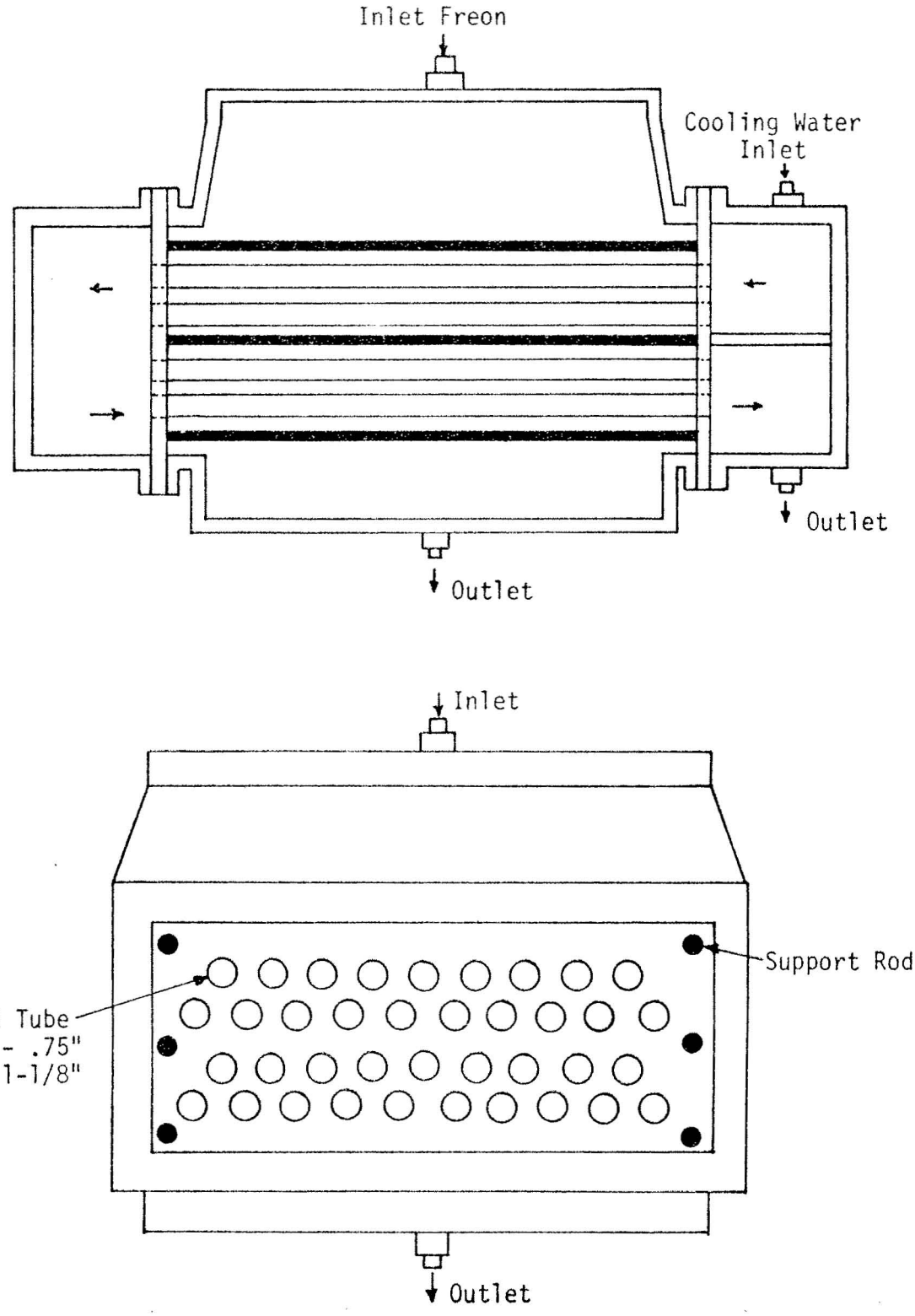

FIG. 3.6-64 LAYOUT OF CONDENSER

REPORTS AND PUBLICATIONS

1. Chou, J. C. S. and Ahluwalia, R. K., "Regenerative Vapor Cycle with Isobutane as Working Fluid," *Geothermics*, 3rd Issue, 1974 (in press).
2. Shimozono, G., Chai, H. C., and Kihara, D. "A Parametric Study of a Vertical Heat Exchanger Designed for Geothermal Power Plant Application," *Hawaii Geothermal Project Engineering Program Technical Report No. 5*, Sept., 1974.
3. Ahluwalia, R. K. and Chou, J. C. S., "Characteristics of Vapor Flashing Geothermal Plants," *Hawaii Geothermal Project Engineering Program Technical Report No. 6*, Nov., 1974.

REFERENCES

1. Anderson, J. H. "The Vapor-Turbine Cycle for Geothermal Power Generation," *Geothermal Energy*, Stanford University Press, 1973, Chapter 8, p. 163.

2. Armstead, H. C. H. and J. R. Shaw. "The Control and Safety of Geothermal Installations," *Geothermics* - Special Issue 2, Vol. 2, Part 1, 1970, p. 848.

3. Baker, D. R. and H. A. Shryock. "A Comprehensive Approach to the Analysis of Cooling Tower Performance," *Journal of Heat Transfer*, Vol. 83, 1961, p. 339.

4. Bengma, P. "The Development and Performance of Steam-Water Separator for Use on Geothermal Bores," *Proceedings of U. N. Conference on New Sources of Energy* (Rome), Vol. 3, 1961, p. 60.

5. Benjamin, M. W. and J. H. Miller. "The Flow of a Flashing Mixture of Water and Steam through Pipes," *Transactions of the American Society of Mechanical Engineers*, Vol. 64, 1942, p. 657.

6. Bruce, A. W. "Engineering Aspects of a Geothermal Power Plant," *Geothermics* - Special Issue 2, Vol. 2, Part 2, 1970, p. 1516.

7. Chen, J. C. "Correlation for Boiling Heat Transfer to Saturated Fluids in Convective Flow," *Industrial and Engineering Chemistry, Process, Design and Development*, Vol. 5, No. 3, July, 1966, p. 322-329.

8. Chierici, A. "Planning of a Geothermal Power Plant: Technical and Economic Principles," *Proceedings of U. N. Conference on New Sources of Energy* (Rome), Vol. 3, 1961, p. 229.

9. Contini, R. "Methods of Exploitation of Geothermal Energy and the Equipment Required," *Proceedings of U. N. Conference on New Sources of Energy* (Rome), Vol. 3, 1961, p. 111.

10. Dengler, C. E. and J. N. Addoms. "Heat Transfer Mechanism for Vaporization of Water in Vertical Tubes," *Chemical Engineering Progress Symposium Series*, Vol. 52, No. 18, 1956, p. 95-105.

11. Einarsson, S. S. "Proposed 15-Megawatt Geothermal Power Station at Hveragerdi, Iceland," *Proceedings of U. N. Conference on New Sources of Energy* (Rome), Vol. 3, 1961, p. 354.

12. General Electric Company, *Medium Turbine Generators, Condensing and Non-Condensing Application*, Publication No. GEA-3277D.

13. Guerrieri, S. A. and R. D. Talty. "A Study of Heat Transfer to Organic Liquids in Single-Tube, Natural Circulation, Vertical Tube Boilers," *Chemical Engineering Progress Symposium Series*, Vol. 52, No. 18, 1956, p. 69-77.

14. Haldane, T. G. N. and H. C. H. Armstead. "Geothermal Development at Wairakei, New Zealand," *Proceedings of Institution of Mechanical Engineers* (London), Vol. 176, No. 23, 1962, p. 603.

15. Hansen, A. "Thermal Cycles for Geothermal Sites and Turbine Installation at the Geysers Power Plant, California," *Proceedings of U.N. Conference on New Sources of Energy* (Rome), Vol. 3, 1961, p. 365.

16. Holt, B., A. J. L. Hutchinson, and D. H. Cortez. "Advanced Binary Cycles for Geothermal Power Generation," Tenth Annual Technical Meeting, American Institute of Chemical Engineers, Southern California Section, April 24, 1973.

17. James, R. "Second Generation Geothermal Power," *New Zealand Engineering*, Vol. 23, 1968, p. 230-236.

18. James, R., G. D. McDowell and M. D. Allen. "Flow of Steam-Water Mixtures through a 12-inch Diameter Pipeline: Test Results," *Geothermics* - Special Issue 2, Vol. 2, Part 2, 1970, p. 1581.

19. James, R. "Pipeline Transmission of Steam-Water Mixture for Geothermal Power," *New Zealand Engineering*, Vol. 23, 1968, p. 55.

20. James, R. "Optimum Wellhead Pressure for Geothermal Power," *New Zealand Engineering*, Vol. 22, 1967, p. 221.

21. James, R. "Power Life of a Hydrothermal System," *Proceedings of Second Australian Conference on Hydraulics and Fluid Mechanics* (Auckland, New Zealand), 1966, p. 211.

22. James, R. "Power Station Strategy," *Geothermics* - Special Issue 2, Vol. 2, Part 2, 1970, p. 1676.

23. Kays, W. M., *Convective Heat Transfer and Mass Transfer*, McGraw-Hill Book Co., Inc., 1966, p. 173.

24. Palen, J. W., V. A. Yarden, and J. Ta orek. "Characteristics of Boiling Outside Large Scale Horizontal Multitube Bundles," *Chemical Engineering Progress Symposium Series*, Vol. 68, No. 118, 1972, p. 50-61.

25. Pollard, E. V. and K. A. Drewry. *Estimating Performance of Automatic Extraction Turbines*, Publication No. 2685, General Electric Company.

26. Sani, R. L. "Downflow Boiling and Non-Boiling Heat Transfer in a Uniformly Heated Tube," *University of California Radiation Laboratory Report UCRL 9023*, 1960.

27. Saporiti, A. "Progress Realized in Installations with Endogeneous Steam Condensing Turbine Generator Units," *Proceedings of U. N. Conference on New Sources of Energy* (Rome), Vol. 3, 1961, p. 380.

28. Schrock, V. E. and L. M. Grossman. "Forced Convection Boiling in Tubes," *Nuclear Science and Engineering*, Vol. 12, 1962, p. 474-481.

29. Scotfield, F. C. *Power Plant Heat Rejection in an Arid Climate*, Engineering Experiment Station, College of Engineering, The University of Arizona, Tuscon, Arizona, 1971.

30. Snyder, N. W. "Effect of Air Rate, Water Rate, Temperature and Packing Density in a Crossflow Cooling Tower," *American Institute of Chemical Engineers, Heat Transfer Symposium*, Vol. 52, No. 18, 1955, p. 61.

31. Steur, W. R. "Cooling Tower on Cooling Pond -- An Appraisal," *Proceedings of the American Power Conference*, Vol. XXIV, 1961, p. 245.

32. Streeter, V. L., *Fluid Mechanics*, Fifth Edition, McGraw-Hill Book Co., Inc., 1971, p. 287-294.

33. Takahashi, Y., T. Hayashida, S. Soezima, S. Aramaki and M. Soda. "An Experiment on Pipeline Transportation of Steam Water Mixture at Otake Geothermal Field," *Geothermics* - Special Issue 2, Vol. 2, Part 1, 1970, p. 382.

34. Usui, T. and K. Aikawa. "Engineering and Design Features of the Otake Geothermal Power Plant," *Geothermics* - Special Issue 2, Vol. 2, Part 2, 1970, p. 1533.

35. Wallis, G. B. *One-Dimensional Two-Phase Flow*, McGraw-Hill Book Co., Inc., 1969, p. 18-35.

36. Wigley, D. M. "Recovery of Flash Steam from Hot Bore Water," *Geothermics* - Special Issue 2, Vol. 2, Part 2, 1970, p. 1588.

37. Zamuner, N. "Cross Flow Cooling Tower Analysis and Design," *American Society of Heating, Refrigerating and Air Conditioning Engineers Journal*, 1962, p. 50.